A Thesis for the Degree of Ph.D. in Engineering

An Accurate Removal of Eyeblink Artifact from Single-channel Electroencephalogram by Supervised Tensor Factorization

August 2016

Graduate School of Science and Technology
Keio University

Suguru Kanoga

CONTENTS

LIST OF FIGURES

LIST OF TABLES

LIST OF ABBREVIATIONS

A

AC	Alternating-Current
AV	AVerage reference recording

B

BCI	Brain-Computer Interface
BER	Balanced Error Rate
BP	BiPolar recording
BSS	Blind Source Separation

C

CEEMD	Complete Ensemble Empirical Mode Decomposition
CI	Confidence Interval
CN	Cranial Nerves
CV	Cross Validation

D

DC	Direct-Current
DFT	Discrete Fourier Transform
DOF	Degree Of Freedom
DWT	Discrete Wavelet Transform

E

ECG	ElectroCardioGram
ECoG	ElectroCorticoGram
EEG	ElectroEncephaloGram
EEMD	Ensemble Empirical Mode Decomposition
EMD	Empirical Mode Decomposition
EMG	ElectroMyoGram
EOG	ElectroOculoGram
EPSP	Excitatory PostSynaptic Potential
EU	EUclidean

F

fMRI	functional Magnetic Resonance Imaging

H

HEOG	Horizontal ElectroOculoGram
HOS	Higher-Order Statics

I

IC	Independent Component
ICA	Independent Component Analysis
IDWT	Inverse Discrete Wavelet Transform
IMF	Intrinsic Mode Function
InfoMax	Information Maximization
IS	Itakura-Saito

K

KL	Kullback-Leibler

L

LD	Log-Determinant
LFP	Local Field Potential
LMS	Least Mean Squares
LPS	Levator Palpebrae Superioris

M

MEG	MagnetoEncephaloGram
MF	Matrix Factorization
mMSE	modified Multiscale Sample Entropy
MP	MonoPolar recording
MSE	Mean Square Error
MU	Multiplicative Update
MUA	Multi-Unit Activity

N

NIRS	Near Infra-Red Spectroscopy
NMF	Non-negative Matrix Factorization

O

OO	Orbicularis Oculi

P

PCA	Principal Component Analysis
PET	Positron Emission Tomography
PSD	Positive Semi-Definite
PSDTF	Positive Semi-Definite Tensor Factorization

R

REOG	Radial ElectroOculoGram
RLS	Recursive Least Squares

	ROC	Receiver Operating Characteristic
S		
	SCA	Sparse Component Analysis
	SNR	Signal-to-Noise Ratio
	SOBI	Second Order Blind Interference
	SOS	Second-Order Statics
	SPECT	Single-Photon Emission Computed Tomography
	STFT	Short-Time Fourier Transform
	SUA	Single-Unit Activity
T		
	TNR	True Negative Rate
	TPR	True Positive Rate
V		
	VEOG	Vertical ElectroOculoGram
W		
	WICA	Wavelet-Independent Component Analysis

ACKNOWLEDGEMENTS

I have been a graduate student for seven and half years now and will end this stage with the submission of this thesis. Looking back now, I realize that enforced growth for accomplishing the mission with a short period might provide disequilibrating your mental and physical health. If possible, would you please spend enough time for stepping up to a new level.

First, and most importantly, I would like to show my greatest appreciation to my supervisor, Assoc. prof. Mitsukura who offered continuing support and constant encouragement for four years. I cannot thank you enough for molding me into an ebullient researcher and granting me the many, many chances to learn outside of your lab.

I also owe a very important debt to Prof. Murakami, Prof. Okada, and Assoc. prof. Aoki who provided technical help and sincere encouragement in writing this thesis. I sincerely appreciate the invaluable knowledge and advice given to me by Emer. prof. Hamada.

Over the course of my time at Keio University, I had a great time with everyone in and out the lab past and present. I would like to thank all of them. I particularly thank Dr. Fuji, Dr. Nakanishi, and Dr. Takahashi, who are the persons I respect the most because I have been seeing your progress stretched out for miles and miles, for their time in ensuring that my research is professional. Without your guidance, this thesis would not have been completed, and I stepped it up a notch to be a researcher like you.

My parents have been an uninterrupted source of support for me in every way, so I would also like to express my gratitude to my parents for their moral support and warm encouragements.

Finally, I would like to thank my little brother who gives a big dream to me. I will keep supporting you through my life.

March 28, 2016
Suguru Kanoga

Chapter 1

INTRODUCTION

1.1 Electroencephalogram and Systems

1.1.1 Neuroimaging Techniques

Tremendous patterns and trends of the brain function and dysfunction have yet to be defined today. Functional neuroimaging has established itself as a major visible tool to define indeterminate patterns and understand the brain functions [1]. In neuroscience studies and clinical applications, processing information through a neuroimaging technique provides researchers a visualizing way to assist handling intuitive understanding.

Neuroimaging techniques have vigorous and weak points in recording and visualizing brain activities, can be broadly separated into two classes (Figure 1.1): intracranial (invasive) and extracranial (noninvasive). Invasive techniques such as Single-Unit Activity (SUA), Multi-Unit Activity (MUA), Local Field Potential (LFP), and ElectroCorticoGram (ECoG) indicate electrical indices of neuronal activities or nerve firings using epidural, subdural, or intracortical electrodes [2, 3]. Nevertheless, they have excellent spatiotemporal resolution and specificity; the coverage is limited, and the imaging usage is restricted to animal models or specific patient population because of its necessity for surgical operation and perspective on bioethics.

Noninvasive techniques have been used to define brain patterns and adjust the wide applicability to a larger population including healthy and diseased users. The techniques can also be separated into two classes: hemodynamic and electrodynamic. Hemodynamic imaging techniques (e.g. functional Magnetic Resonance Imaging (fMRI), Near Infra-Red Spectroscopy (NIRS), Positron Emission Tomography (PET), and Single-Photon Emission Computed Tomography (SPECT)) indicate hemal indices in cephalic regions, noninvasively. While the techniques would have high spatial resolution, they

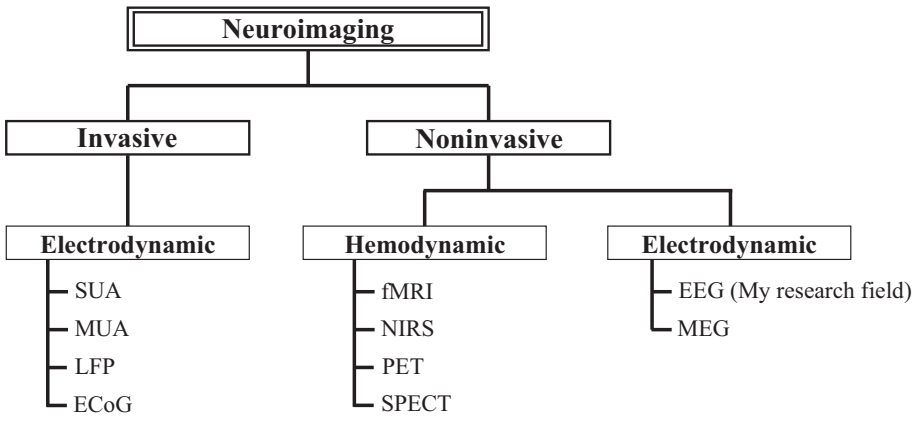

Figure 1.1 Tree diagram of neuroimaging techniques.

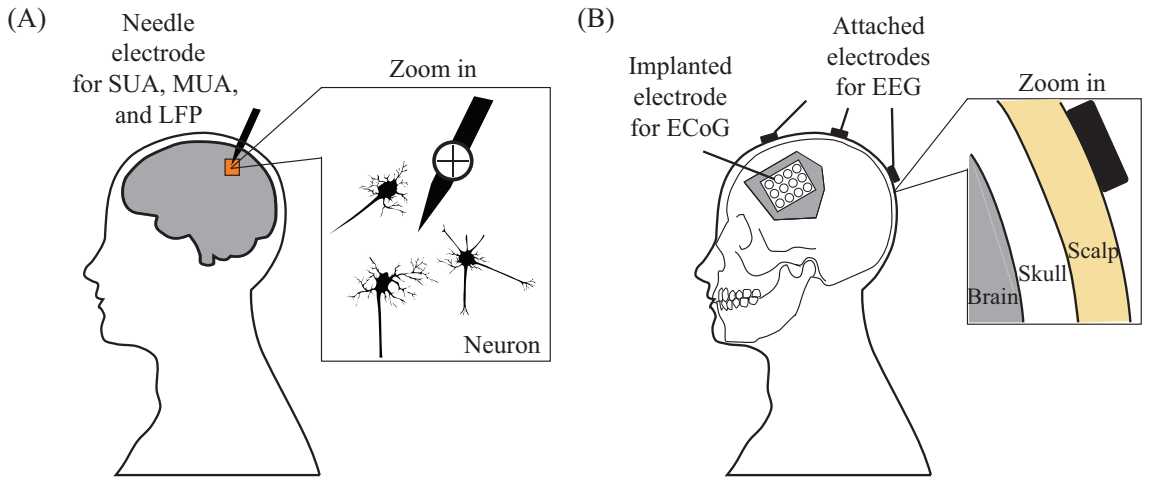

Figure 1.2 Illustration of electrodynamic imaging measurements modified from the reference [4]. (A) Single-unit activity, multi-unit activity, and local field potential. (B) Electrocorticogram and electroencephalogram.

compromise low temporal resolution because of the hemodynamic response property [5–8]. On the other hand, noninvasive electrodynamic imaging techniques such as ElectroEncephaloGram (EEG) and MagnetoEncephaloGram (MEG) indicate electrical indices of neural activities using electrodes attached to the scalp [9, 10]. They have high temporal resolution, flexibility, and portability, however, their spatial resolution and specificity are compromised because of the volume conduction effect [11]. An image of electrodynamic imaging measurements is shown in Figure 1.2. Up to now, integrated techniques (e.g. EEG and fMRI) called multi-modal neuroimaging techniques have shown their quality assurance of the spatiotemporal resolution. They would provide us with a perspective on an in-depth investigation of brain functions using enhanced resolution mapping [12, 13].

The analytical sensitivity depends crucially on the resolution in space-time domains

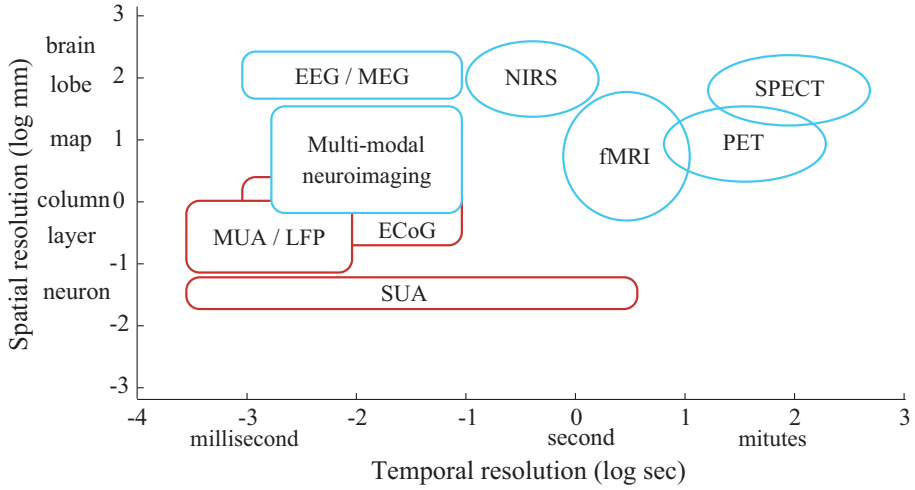

Figure 1.3 Schematic illustration of the ranges of spatiotemporal resolution in noninvasive (blue frame) and invasive (red frame) imaging techniques adapted from the reference [14].

when the spatially distributed and temporary dynamic neuronal activities are visualized as neuroimaging to discern a brain function or dysfunction based on cellular connections [14]. Researchers should retain the following points that are different from techniques, in the back of their head before planning measurements: (i) measurement target (hemodynamic activity or electrodynamic (neuronal) activity); (ii) spatiotemporal resolution; and (iii) physical property of the measurement device. In other words, choosing an imaging technique matching the purpose of the researcher is the primary factor in neurobiology, psychology, engineering, mathematics, computer science, and clinical neuroscience. Schematic illustration of the ranges of spatiotemporal resolution on neuroimaging techniques are shown in Figure 1.3.

1.1.2 Electroencephalographic Systems

Key benefits of the EEG modality holds over other neuroimaging techniques, are the high temporal resolution on the order of milliseconds, the small installation space for operating the system, and its usability for signal measurement. The high temporal resolution providing striking visualization in the noninvasive functional imaging techniques has contributed our capability to study kaleidoscopic functional states of the cerebral cortex: “where”, “when”, “how” and under “what” our brain functions come into being [15–17]. Therefore, neuroscience research using EEG regardless of whether the technique is integrated or not has been a major challenge to image the connected brain networks and define the neuronal patterns for useful user applications reflecting the functional states of the cerebral cortex.

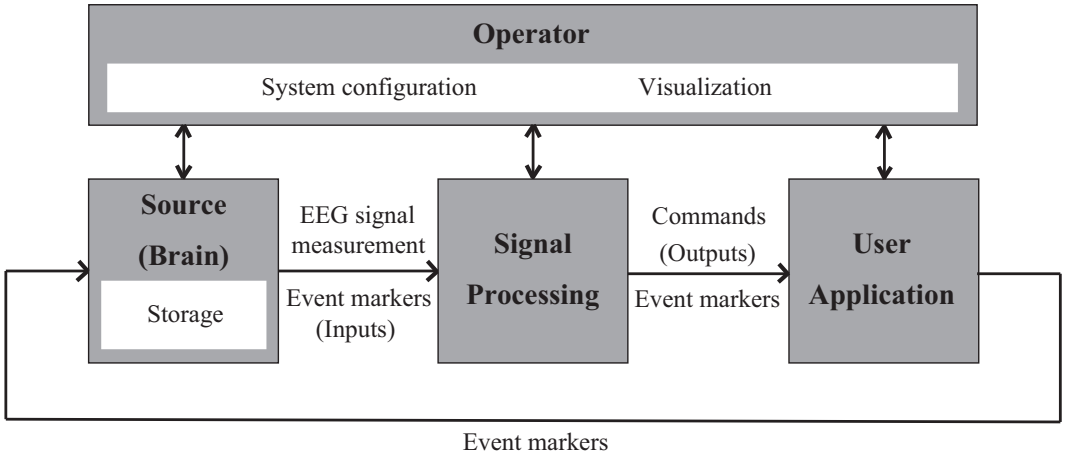

Figure 1.4 Basic design of an EEG system [18].

Over the past several decades, a collective understanding of the brain function has evolved from the identification and characterization of EEG signal. Understanding brain function, particularly in neural coupling responses to a specific endogenous or exogenous stimulus, contributes to developing the EEG system that outputs a visualized neural information or provides an interface between human and machine [19]. In most cases, an EEG system consists of four modules shown in Figure 1.4 including the following procedure: (i) operator; (ii) source (data acquisition and storage); (iii) signal processing; and (iv) user application. An operator module has a responsible role in system configuration management and online visualization to the investigator. Besides, the module defines onset, offset, and information transfer rate of the operation [20]. The electronic information transmitting signal, parameter, or event marker is communicated from source to signal processing, to user application, and back to source module. Interchangeability and independence are surely needed in each module of the system, to secure safety operation, and maximize durability as well as convenience. In other words, the system has the following properties: (i) different implementations can be used without changes elsewhere in the system, and (ii) modules can be combined in any fashion [18]. For the properties as mentioned earlier, each module has progressively been developed, separately.

EEG systems are vital for biological diagnoses and rehabilitation because disruption of the functional brain networks have been reported in a host of neurodegenerative diseases (e.g. Parkinson's disease [21], Huntington's disease [22], epilepsy [23], and autism [24]) and other psychiatric disorders. Existing systems can judge whether the user has any neurocognitive disorders or not and can find the region by using a dataset including EEG features of disordered patients and healthy persons. Outputs from the systems have already been used for aiding presurgical planning in patients [3]. Shortly, these systems would lead to improving the clinical diagnosis performance even before

user's manifestation becomes apparent. Such diagnostic techniques would allow us to propose an earlier rehabilitation, a treatment solution, and an enhanced measurement protocol.

Alternatively, the neuroscience research develops other kinds of EEG system, named Brain-Computer Interface (BCI). BCI provides communication channels to people with severe motor disabilities [18, 25–27]. This system mainly chooses, at least, one from the following EEG features; (i) visual-evoked response [28]; (ii) event-related potential [27]; (iii) sensorimotor rhythm [29]; and (iv) slow cortical potential [30]. Cortically induced EEG feature from an endogenous or exogenous stimulus that does not depend on the output pathway of peripheral nerves and muscles, attempts to select one of two alternatives (e.g. "Yes" or "No") or several choices (e.g. Roman alphabet). Some studies have suggested not only discrete control signals but also continuous control signals for spelling or numeral string output [31, 32], cursor movement, letter or icon selection [33], and electric wheelchair handling [34].

1.1.3 Electroencephalographic Measurement Devices

It goes without saying that basics of EEG measurement in human, which have been the same since 1929 [35], are imperative to operate EEG systems. An EEG measurement device is consisted of five elements: (i) electrodes with conductive media; (ii) a cap for fixing electrodes; (iii) an amplifier with filters; (iv) an analog-to-digital converter; and (v) a recording device (personal computer or another relevant device). Each of commercially available EEG measurement devices (Figure 1.5) is assembled by combining aforementioned first four elements and instantaneously measures an oscillating neuronal discharge induced by fibrous and synaptic activity.

Electrodes are the initial element for converting oscillating neuronal discharges in the extracellular fluid and other conductive paths reaching the skin-surface (tissue) into electrical signals. EEG electrodes are made of silver chloride (AgCl) in many cases because the inorganic compound quickly saturates and comes to equilibrium due to chemical property of Ag [36, 37]. Even if an electrode is made of AgCl, it would be polarized and then behaves as a significant capacitance as well as a low-frequency filter (low-pass filter) when there is no electrolyte including chloride ion. Avoiding polarization is necessary for the frequency dependency of the electrode-skin contact. Space (interface layer) between an electrode and the skin must be filled with an electrolyte such as gel or paste. Impregnation of the interface layer (e.g. skin preparation, fat mass, and hair) also leads to ensure low contact impedance (less than 40 kΩ). The layer not only is resistive but also consists of capacitive elements (see Figure 1.6 (A)). Biopotential source and tissue resistance are described as a voltage source and R_t.

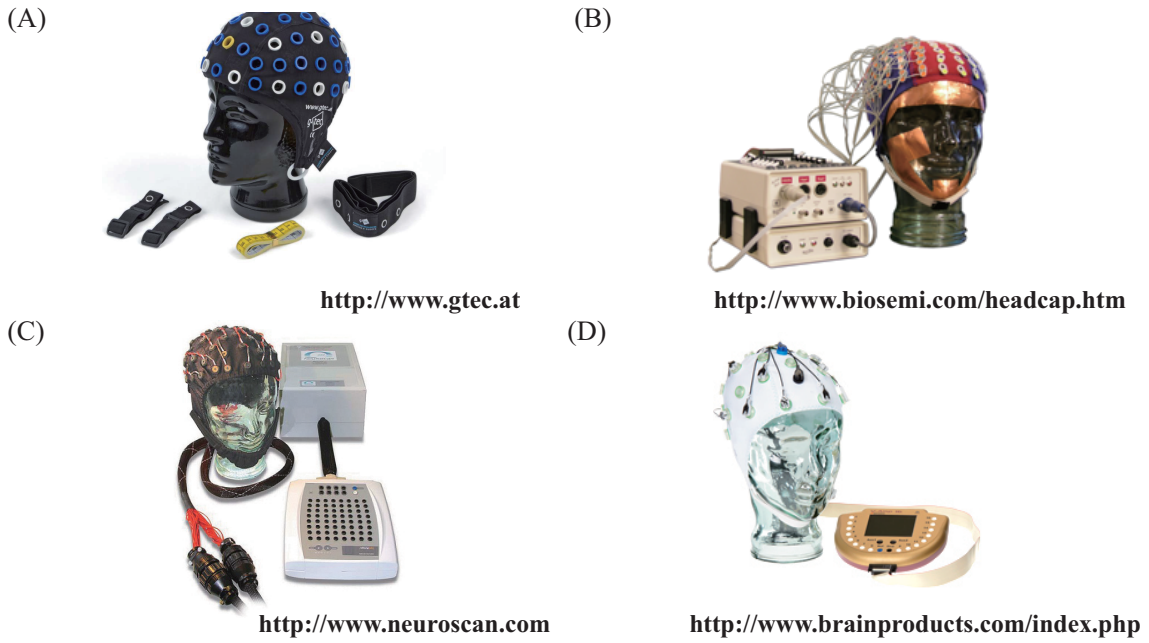

Figure 1.5 Commercially available multi-channel type EEG measurement devices. (A) g.tec. (B) ActiveOne. (C) Synamps 2/RT. (D) V-Amp.

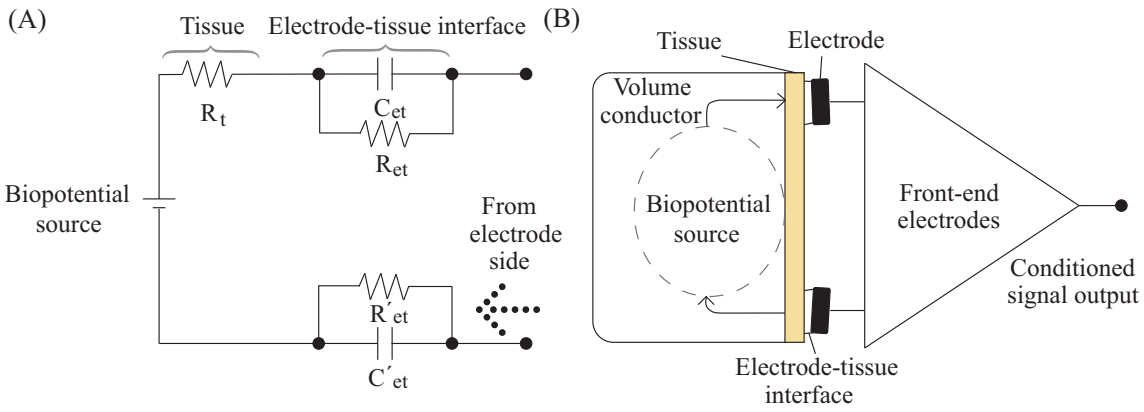

Figure 1.6 (A) Simplified equivalent circuit of biopotential source and electrode-tissue interface from electrode. (B) Biopotential measurement through electrodes modified from the reference [38].

Electrode-tissue equivalent elements C_{et} (C'_{et}) and R_{et} (R'_{et}) may change for each electrode contact. Therefore, less than 10 kΩ contact impedance allows us to obtain a clean signal, but greater than 40 kΩ contact impedance creates distorted the signal [39]. On the other hand, the weight loses due to evaporated electrolyte over time can easily debase the measurement performance. Circular shape has efficacy against enough volume to contain an electrolyte on contact point and minimum volume to retain long-term measurement; thus, EEG electrodes are usually molded into the shape. Considering these pitfalls in the session conditions of EEG measurement has obvious repercussions on keeping the high recording performance [38].

Spatial changes, as well as temporal changes in the electrical potential, are recorded as the potential difference over time between an active electrode and passive (reference) electrode called MonoPolar recording (MP) to eliminate common mode signals (see Figure 1.6 (B)). When common mode signals have the same interest rate on each electrode, attenuation of the signals will be complete. Researchers can flexibly change other potential difference deriving methods such as BiPolar recording (BP) and AVerage reference recording (AV) according to their purpose. A ground electrode is needed for recording differential voltage by subtracting the same voltages obtained from electrodes. Minimal EEG measurement has consisted of one (two) active electrode(s), one (zero) reference electrode, and one ground electrode with other elements. However, biological artifacts caused by extracerebral sources like muscle and eye will not be cancelled out by a differential amplifier because the degree of interest depends on the electrode position. Furthermore, the contamination owing to good conductivity of scalp is accepted as an unavoidable phenomenon on EEG recording. Such components have to be removed from observed EEG signals on the signal processing module in an EEG system.

After choosing session conditions, the researcher continuously has to select Alternating-Current (AC) or Direct-Current (DC) coupling amplifier. More than 10 bits digital resolution may be enough in AC amplification. EEG measurement device usually uses 12 to 16 bits of resolution. That means an EEG measurement device would have about 30 to 240 μV if the converter were designed to record voltages in the range from -1.0 to $+1.0$ V. On the other hand, more than 20 bits are necessary for the analog-digital converter in DC amplification because the number of valid bits is decreased. However, there is no amplifier saturation risk causing an analog signal loss in DC amplification. Also, selecting filtering (hardware or software) is essential for digitalizing and storing data. It is better to set a filter bandwidth between 0.5 and 70 Hz even though the recording device has enough data storage.

Many EEG studies using traditional multi-channel type EEG measurement devices have been improved user population (application quality) and reduced processing time in the structured environment (simulation or semi-simulation). Recently, specialized (headband-type or headset-type) EEG devices including electrodes like shown in Figure 1.7 have been developed as for compact, portable, and feasible EEG systems to use themselves in the real environment [40–44]. These devices can diminish user's burden by reducing the number of electrodes (the single-electrode case would be an extreme case) and eliminate the need for conductive gel or paste by improved electrodes. Although the aspect of entertainment or amusement associated with the usage of the application is emphasized as yet, the specialized EEG measurement devices have already been implemented in some EEG systems for noninvasive biological diagnoses to reduce the clinician's workload [9]. Potential changes are accurately recorded through them [45]; also, wireless sensor network technology contributes to improving degree of freedom

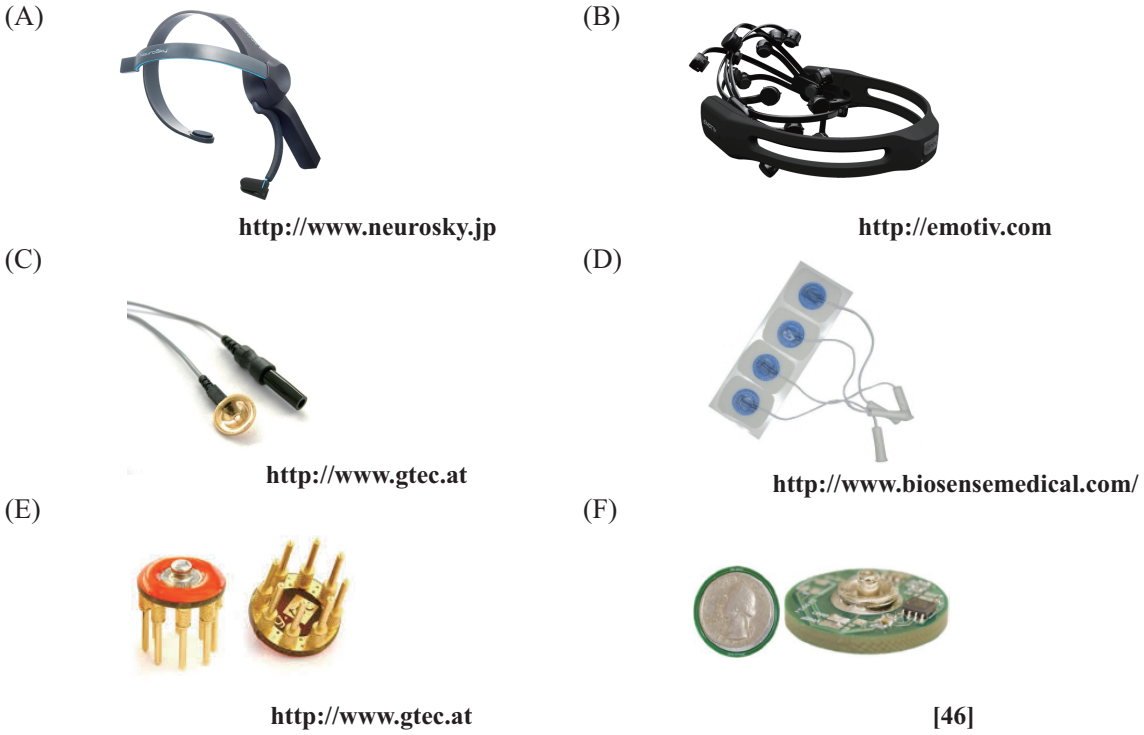

Figure 1.7 Specialized EEG measurement devices and improved electrodes. (A) and (B) Portable and wireless measurement devices. (C) Reusable disc electrode (gold, platinum, stainless steel, or tin). (D) Disposable electrodes (pre-gelled type) (E) Dry electrode. (F) Noncontact electrode [46].

of a moving amount of body movements which is equipping the measurement devices without wires plugged into an amplifier. Therefore, devices, as mentioned above, would become more important in the future. However, there is a trade-off between the quality of signal and the number of electrodes in any EEG system. Thus, a system will reduce its performance according to the session conditions get simpler. Furthermore, a fly in the ointment like electromagnetic interferences may be of grave consequence, is still lurking in an EEG measurement. Closely integrated measurement design and setting become essential regardless of whether the type of device is traditional or specialized. Simultaneously performing next two points: (i) good recording performance and (ii) a small number of electrodes, are considered as crucial tasks in the field of neuroscience.

1.1.4 Signal Processing in Electroencephalographic Systems

The signal processing module of an EEG system has an invaluable role to accommodate human (input) to the user application (output). Because of the bridge-building module, an application can understand the meaning of input data based on hypotheses and knowledge of implementation's maker, and can fulfill its unique potential. In

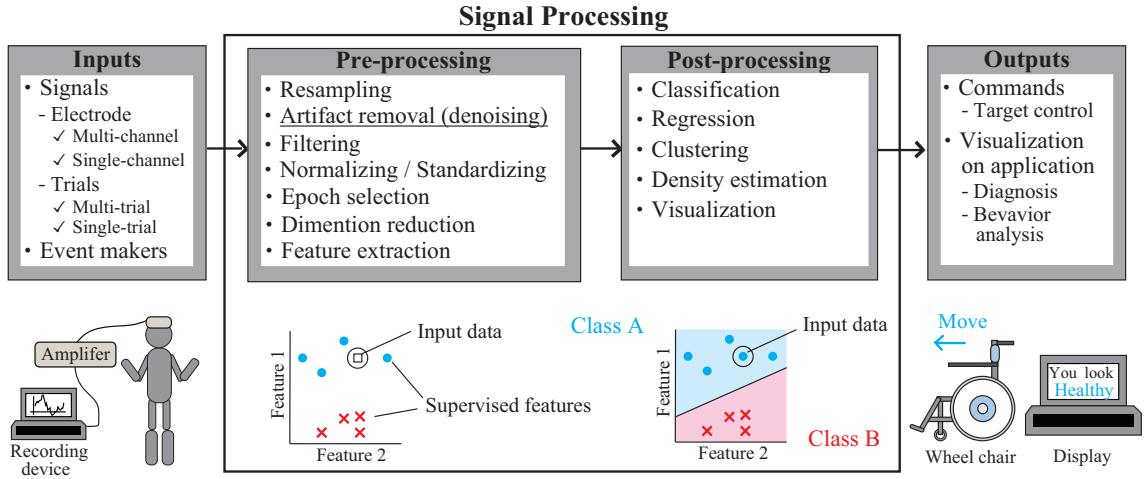

Figure 1.8 Basic process through EEG signal processing.

other words, this module should recognize latent information (pattern) in the input data and then, must convey comprehensible outputs to user applications. A signal processing module is implemented as a cascade of various schemes and has two steps: pre-processing and post-processing.

On a pre-processing step, input dataset would be projected some subspaces (feature spaces) that express each distribution of refined input dataset the most. When input data has intricately linked to each spatial/temporal data while having biased toward somewhere within the region, this step is highly active in promoting hyper-plane design to space. A careful pre-processing cascade strategy will provide a supportive learning subspace for post-processing step to convey comprehensible outputs to an applications [47–49]. A lot of pre-processing schemes are needed to project input data into some suitable feature spaces (Figure 1.8). This step is passable if the input data releases its information overtly for post-processing strategy even though no refinement scheme is applied, whereas I would never have encountered such a situation.

In the next place, training data would be used for learning a model to recognize the latent pattern in a post-processing step. The data is usually extracted from input dataset or already been arranged in the subspace as supervised features. Once a model has been learned, test set which is the rest of input dataset or all of the datasets would be categorized. In other words, the model conveys comprehensible outputs to user application. Pattern recognition and machine learning schemes such as supervised, unsupervised, and reinforcement learning have been developed for endowing superior generalization capability of the models [50].

It is important to recognize EEG patterns accurately for associating the estimated category/equally spaced value with the output command. The goal of EEG research is commonly implementation the outcome into systems and practical use of the system in a real environment with no restriction. Packaging the results of EEG research into

systems became easy because many factors like a collective understanding of the brain activity and developments in the EEG devices could reduce a discrepancy between a laboratory (controlled) environment and a real environment. However, noises (artifacts) described in the next section appear only under the actual environment, and unfailingly interfere popularization of the EEG systems because simply applying filtering is unlikely to be effective by overlapping the frequency band [51]. The external invaders disguise themselves as EEG components in observed EEG signals and cause a new discrepancy between research motivation and system realization. An artifact removal methods in pre-processing step can attenuate the discrepancy and refine intrinsic EEG data from observed data by using their exemplary algorithm based on the scientific way of viewing. Therefore, artifact removal schemes must be applied in EEG signal processing module and have been attracted attention over the past four decades [52–55].

1.2 Electroencephalogram and Artifacts

Technical/Biological artifacts, such as active power line interference, eyeblink, and muscle activity are often mixed with EEG signals due to recording setting mistake, good conductivity of the scalp, and so on (Figure 1.9). Such artifacts disguise themselves as EEG components and make EEG signal processing difficult in all respects because the oscillating discharge (energy) is larger than the neuronal discharge [56]. The presence causes perturbation in an EEG system which attempts to recognize a pattern of the input data with a time-domain-based strategy. Therefore, removing artifacts from observed EEG signals should be treated as the most important process in all EEG studies regardless of the type of measurement device.

1.2.1 Technical Artifacts

An EEG signal is observed as a potential difference over time using two electrodes. A reference or common electrode is usually placed on the scalp without soft tissue abrasion that breaks the surface epidermal layer containing high impedance than the underlying tissue. Active electrodes improve the signal quality of non-zero bioelectric sources received by the potential difference between the recording and common electrode, as well as between the recording and reference electrodes.

Technical artifacts such as power line interference, impedance fluctuation, and wire movement, superimpose their energy on observed EEG signals owing to careless recording setting [57, 58]. Each technical artifact has a distinctive trait described below. On using an electronic device, power line interference carries 50 or 60 Hz noise that de-

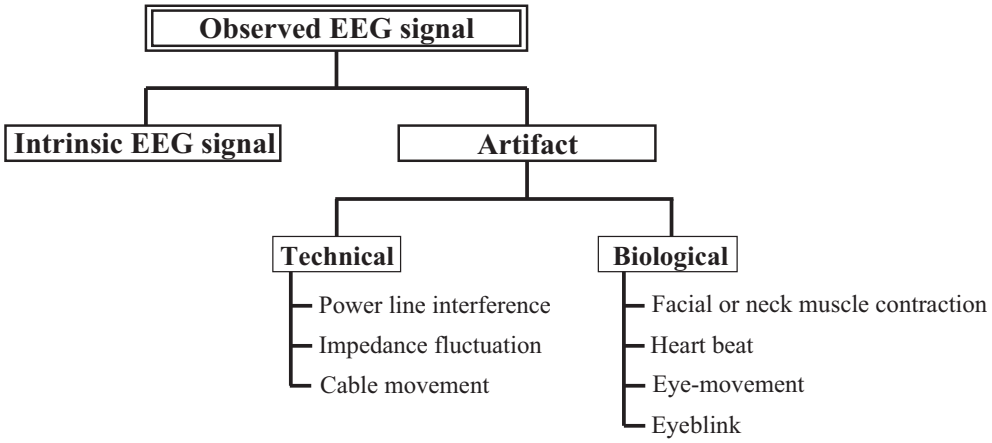

Figure 1.9 Tree diagram of observed EEG signal.

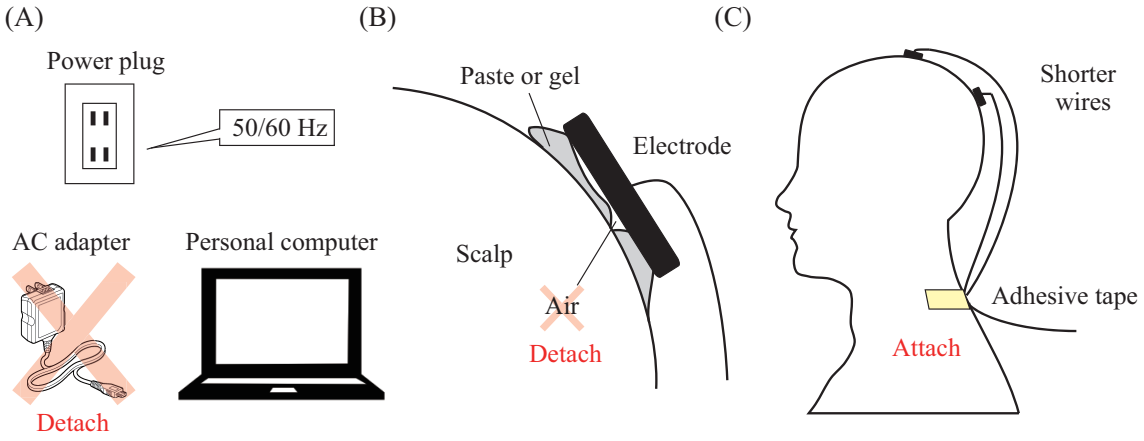

Figure 1.10 Ways of precluding technical artifacts. (A) Power line interference. (B) Impedance fluctuation. (C) Wire movement.

pends on your current place, into EEG signals because electric and magnetic fields are induced on electrode wires and user's body, and the effect contaminates linearly to the signals [59]. Impedance fluctuation caused by poor resistive contact between each electrode and scalp results in a high voltage drop and attenuation of signal-to-noise ratio, and allows contamination of broadband noise in EEG signals. When the user shakes the head or body, wires will be swung, and the motion carries broadband noise to EEG signals. The noise is called wire movement artifact.

All technological artifacts have immense energy than neuronal discharge. Therefore, experimenters must check epochs which contain one or more symptoms of artifacts before the system operation [39]. However, researchers can avoid contamination of the artifacts with comparative ease by detaching a charging AC adapter from the recording device, carefully attaching electrodes to the scalp, and by using appropriated electrode wires or adhesive tapes to stabilize wires or digital filtering algorithms (Figure 1.10).

The cross mark means detaching the source of technical artifact from the circumstance.

1.2.2 Biological Artifacts

Biological artifacts generated from extracerebral sources contaminate observed EEG signals owing to good conductivity of the scalp. On the surface of the scalp, discharged potential of electrophysiological factors diffuses its energy over the head and then disappears. An EEG measurement device captures comprehensive electrical potential which reaches an electrode even if the potential contains components of biological origin except EEG component. Since all kinds of electrical potential might be equally treated regardless of the researcher's purpose, recording a signal including only an EEG component obtained by attaching electrodes placed on the scalp, is hardly realized. Furthermore, frequency components of biological artifacts and EEG signal could be overlapped. That means shunning contact with biological artifacts would be outstandingly difficult compared with technical artifacts.

Biological artifacts can be broadly separated into four categories: (i) muscular; (ii) cardiac; (iii) eye-movement; and (iv) eyeblink (Figure 1.11). Muscular artifact derived from ElectroMyoGram (EMG) caused by muscle activities often appears in the observed EEG signal when facial or neck muscle contracted for swallowing or jaw clenching. The artifact has a broadband frequency distribution from 0 to 200 Hz with several more or less distinct spectral components [60–62] plus two peaks corresponding to the EMG beta rhythm and the Piper rhythm (a 35-60 Hz component) [63–65]. Cardiac artifact derived from an ElectroCardioGram (ECG) is caused by electrical activities of heart beats. The artifact also has a broadband frequency distribution from 0 to 75 Hz [66–68], however, the influence is relatively small among biological artifacts because of the large distance between an observation point and the source (the heart). Muscular and cardiac artifacts are generated by muscle contraction (the heart is a compact muscular organ). Alternatively, eye-movement and eyeblink artifacts derived from ElectroOculoGram (EOG) which have a narrow frequency distribution from delta to alpha band [69–71], appear in observed EEG signal when eyeball or eyelid moves for changing eye direction and eyeblinking. Sometimes, these activities are called ocular artifact in a lump because they have a mutually dependent relationship (e.g. spontaneous or induced eyeblink causes the eyeball to act as an electric dipole, with corneal positivity and retinal negativity [72], slightly moving up/down and inward [73,74]). However, these biological origin activities also have some different characteristics [75]. Characteristics of EEG signal and the biological artifacts are tabulated in Table 1.1.

The influence of the biological artifact is attenuated with increasing distance from the source. However, the frequency dependence of contamination varies with their

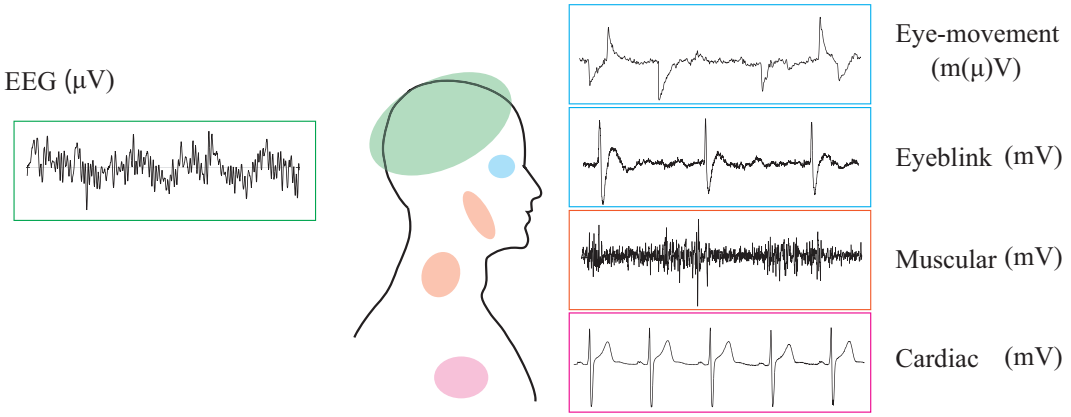

Figure 1.11 Illustration of EEG signal and main biological artifact.

Table 1.1 Characteristics of EEG signal and biological artifacts over the head.

Source	Spectral distribution	Main region	Trigger action
Volume conductor	0.5 - 70 (Hz)	All	Being alive
Eye-Movement	0 - 13 (Hz)	Frontal	Eyeball movement
Eyeblink	0 - 13 (Hz)	Frontal	Eyelid movement
Muscular	0 - 200 (Hz)	Temporal	Swallowing, Jaw clenching
Cardiac	0 - 75 (Hz)	Temporal	Being alive

active nervous (muscular) tissues or electrical field of the cornea-retinal dipole. In addition, the frequency of artifactual oscillations often overlaps with the frequency of neuronal oscillations (see Table 1.1). If contaminated epochs are found in visual or in quantitative EEG analysis, the system has to ignore them before deciding control command. Otherwise, the operator will make a fatal mistake in its system because artifacts can obscure almost any kind of EEG patterns [76, 77].

It is possible to extract EEG components from observed signals by a signal processing (artifact removal) scheme, although evading the attainment of biological artifacts on electrodes seems to be tough. Through this process, the EEG system would obtain intrinsic EEG signals and fulfill its unique and beneficial interface. Many studies for detection, classification, and removal of artifacts into observed EEG signals have been reported even today [77–86].

1.2.3 Presence of Eyeblink Artifact in Electroencephalogram

Dry spots on the precorneal tear layer emerge 15 to 30 s after an eyeblink [87]; therefore, humans need a recurring cycle of eyeblinks to maintain the ocular moisture

[the normal adult eyeblink rate is roughly 20 eyeblinks/min [88]]. The artifacts caused by eyeblinks have particularly profound effects on observed EEG signals as the eyes are close to the brain. In addition, humans are physiologically unable to maintain a gaze without eyeblinks. That means eyeblink artifacts have an adamant presence in observed EEG signals or are surely in the observed EEG signals recorded when a user wears an EEG measurement device with his/her eyes open.

The effects of eyeblinks on observed EEG signals depend on the orientation of the eyeball, the trajectory of the eyelid, the location of the electrode on the scalp, and the propagation path of the electric field across the head [89, 90]. Although researchers can avoid the issue by giving an instruction that asks users to keep their eyes closed during the EEG measurement, any constructed system based on the research would be impractical in the real environment because of the necessity of having users close their eyes while the system operates. In addition, the inhibition of eye movements or eyeblinks significantly distorts the neuronal activity [91]. Therefore, EEG signals should be recorded with the eyes open and without any constraints to allow an investigation into intrinsic endogenous brain activities, even if the eyeblink artifactual contamination of the EEG signal cannot be avoided because of the structure of human body. Removing eyeblink artifacts from observed EEG signals is most important and requisite process before analysis process in the practical use of the EEG systems.

1.2.4 Current Status and Issues of Numerical Approach to Eyeblink Artifact Removal

It is well-known that resolving signals created by various sources on a realistic head model for EEG boils down to the EEG inverse problem as Blind Source Separation (BSS) [92]. The BSS problem is typically ill-posed, however, imposing special considerations or prior information of the statistical nature (temporal sparseness, uncorrelation, and independence) lead to restoring the well-posedness of the problem. Eyeblink artifacts observed in EEG signals have the following properties: (i) the influence of the artifact is attenuated with increasing distance from the eyes [93]; and (ii) the activity of the artifacts appears to propagate along the anterior-posterior axis in a symmetrical fashion [56, 69]. By these properties, theoretically multivariate statistical analysis approaches such as Sparse Component Analysis (SCA), Principal Component Analysis (PCA), and Independent Component Analysis (ICA), which separate EEG signals into spatially and temporally distinguishable components, are useful for extracting EEG components from the scalp recordings (Table 1.2). In particular, ICA is a powerful tool for separating the observed EEG signals into maximally independent activity patterns derived from cerebral or non-cerebral (artifactual) sources [94–97]. ICA-based

Table 1.2 Comparison of typical eyeblink artifact removal schemes (for multi-channel signals).

Schemes	Accuracy	Automatic identification	Computational cost
Sparse component analysis [98]	Unknown	Unknown	Unknown
Principal component analysis [72]	Depends	✓	✓
Multivariate singular spectrum analysis [99]	Depends	✓	✓
Multiple-source eye correction [100]	Depends	Unknown	✓
Independent component analysis [101]	✓	✓	✓

approaches have shown an extraordinary ability to solve BSS problems on EEG signals using the assumption of independence among signal sources in each subject's data (see Figure 1.12). In addition, they accurately eliminate eyeblink artifacts from observed EEG signals with less loss of cerebral information [102]. Therefore, these approaches have been used in a wide range of EEG signal processing procedures for the removal of eyeblink artifact components from observed EEG signals [103, 104] and the extraction of signals of interest to improve the overall performance [105, 106], regardless of the distribution of blink amplitude and duration.

A smaller number of electrodes (i.e. the single-electrode case would be an extreme case) should result in better practical applications in daily life. ICA has a drawback that it can only deal with overdetermined mixtures; this method entails using at least as many electrodes as the number of artifact sources plus one to obtain meaningful information. Therefore, ICA is unsuitable for analyzing EEG signals recorded by a specialized EEG device. Single-channel ICA, which is an adaptation of ICA to single-channel signals, has been proposed [107]; however, the scheme does not always satisfy its assumptions in real-world applications.

Regression-based approaches include the well-known ocular artifact removal method for investigating plausible neuronal activities with the eyes open [85, 108]. In this approach, propagation factors are calculated using linear least-square regression to estimate the relationship between the observed EOG signals and the observed EEG signals. By subtracting the eyeblink artifact coordinated by the propagation factors, regression procedures remove eyeblink artifacts at a low computational cost. However, eyeblinks vary their amplitudes and durations according to the movement of the eyelid [109] and

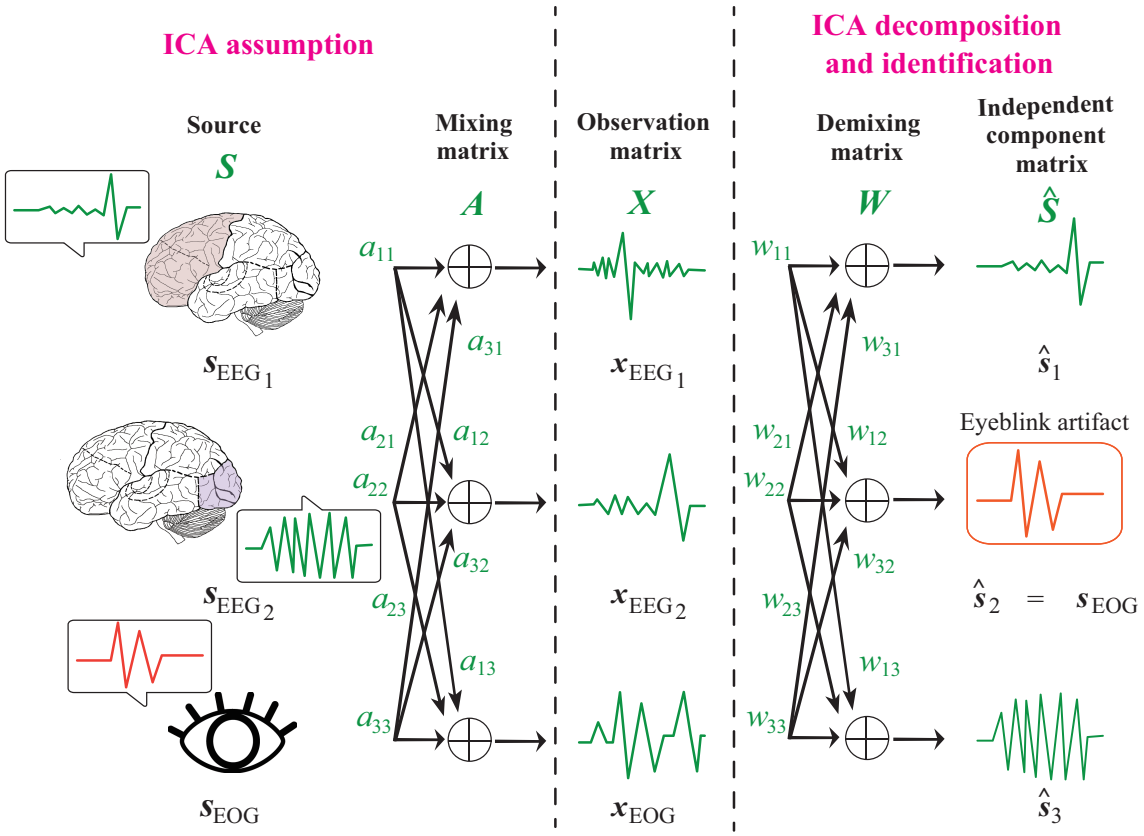

Figure 1.12 Assumption, decomposition, and identification of observed signals in ICA processing for three observed signals.

whether the blink occurs under voluntary or involuntary control [56,110–112]. For this property, the approximation performance of linear regression depends on the distribution of eyeblink amplitude and duration in the data set [113]. Furthermore, bidirectional contamination between EEG and EOG signals has been revealed; therefore, relevant cerebral information interfered with the EOG signal would also be cancelled in the EEG signal corrected using a regression-based approach [114].

Proposing an eyeblink artifact removal scheme for a single-channel EEG signal is now a major challenge within EEG signal processing [115–117]. Unfortunately, each proposed scheme for single-channel EEG signal has a full agenda for real-life data (Table 1.3). A scheme which discards polluted epochs from observed data is still used in a wide range of EEG signal processing procedures when researchers selected specialized EEG device for EEG measurement. The major scheme mangles an advantage on the easy measurement of specialized EEG devices because twice as many trials as traditional multi-channel type EEG measurement is needed in current single-channel EEG analysis. This problem did not arise until seven or eight years ago since most EEG systems were based on a multi-channel EEG measurement device [118]. However, a specialized EEG measurement device is convenient owing to its usability for measurement

Table 1.3 Comparison of typical eyeblink artifact removal schemes (for single-channel signals).

Schemes	Accuracy	Automatic identification	Epoch detection	Computational cost
Single-channel ICA [107]	×	×	-	✓
Linear regression [119]	×	-	-	✓
Adaptive filter [115]	Depends	-	-	✓
ICA-based source decomposition [116]	Depends	Depends	-	Depends
Non-negative matrix factorization [117]	✓	✓	×	Depends
Proposed	✓	✓	✓	Depends

and portability in real environments. Furthermore, single-channel EEG signal processing is now expected to be incorporated into mobile systems such as smartphones and tablet computers. Therefore, more practical eyeblink artifact removal scheme should be proposed.

1.3 Motivation of This Study and Thesis Outline

This research aims to propose an accurate section-based eyeblink artifact removal scheme in time-domain for single-channel EEG signals by using supervised tensor factorization. In EEG signal processing, as the levels:

Level 0 Automatic epoch detection (is not needed except for epoch-based scheme),
Level 1 High signal separation accuracy,
Level 2 Automatic separated component identification and signal reconstruction,
Level 3 Small number of arbitrary parameters in the scheme,
Level 4 Low computational cost (real-time processing),

gets higher the scheme is more likely to prevail as an effective tool for artifact removal. The objective of this thesis is to accomplish Level 3.

This thesis subsumes the knowledge from the great predecessors in this field, my research results, and future works under seven chapters including this chapter (Figure

1.13). Chapter 2 describes the fundamental awareness of the brain, eyeball, and eyelid which are sources of EEG and EOG signals. Moreover, the relationship between EEG signal and eyeblink artifact can be pursued in more detail using recording methods of EEG and EOG signals and their known characteristics.

Approaches for artifact removal change its working stance to the number of observed (multichannel or single-channel) signals. Algorithms of multichannel eyeblink artifact removal schemes are described in the first half of Chapter 3. Then, algorithms of single-channel eyeblink artifact removal schemes are presented in the last half of the chapter. To avoid inconsistency in separating components of a signal-channel EEG signal that has overlapping frequency components, reference data or separated multi-components data helps experimental data to converge to the values of estimated sources in the similar schemes. This chapter ends with the drawback of current single-channel artifact removal schemes and how this research responds to them.

Eyeblink artifact estimation using ICA allows us to investigate the plausible effects of eyeblinks on observed EEG signals. Research has analyzed the pattern of eyeblink artifacts only for voluntary control, using an ICA approach to developing subsequent eyeblink artifact removal approaches for multi-channel signals [104, 120–122]. Assessing eyeblink artifacts under voluntary and involuntary control leads to the (somewhat heuristically) development of more robust and more common references or training datasets based on the ideal attributes for a small number of channels in EEG analysis. Therefore, the objective of Chapter 4 is to characterize the effects of voluntary and involuntary eyeblinks on Independent Components (ICs) contributing to EEG signals to create templates for eyeblink artifact removal from an observed EEG signal with a single-electrode.

The eyeblink distribution represented in previous chapter will be used for eyeblink artifact removal from single-channel EEG signals in Chapter 5. This chapter describes its property of signal separation, component identification, and signal reconstruction. Moreover, arbitrary parameters are optimized for the real environmental data. The proposed scheme with the optimized parameters completes with other single-channel artifact removal schemes represented in Chapter 3 in artifact removal performance.

My proposed scheme will be applied to single-channel EEG analysis in Chapter 6. The analytical accuracy is compared with the accuracy without eyeblink artifact removal scheme. According to the above results, an accurate and practicable eyeblink artifact removal scheme for single-channel EEG that accomplishes Level 3 would be proposed.

The conclusion, summary of this thesis and future works in this field of neuroscience research are presented in Chapter 7.

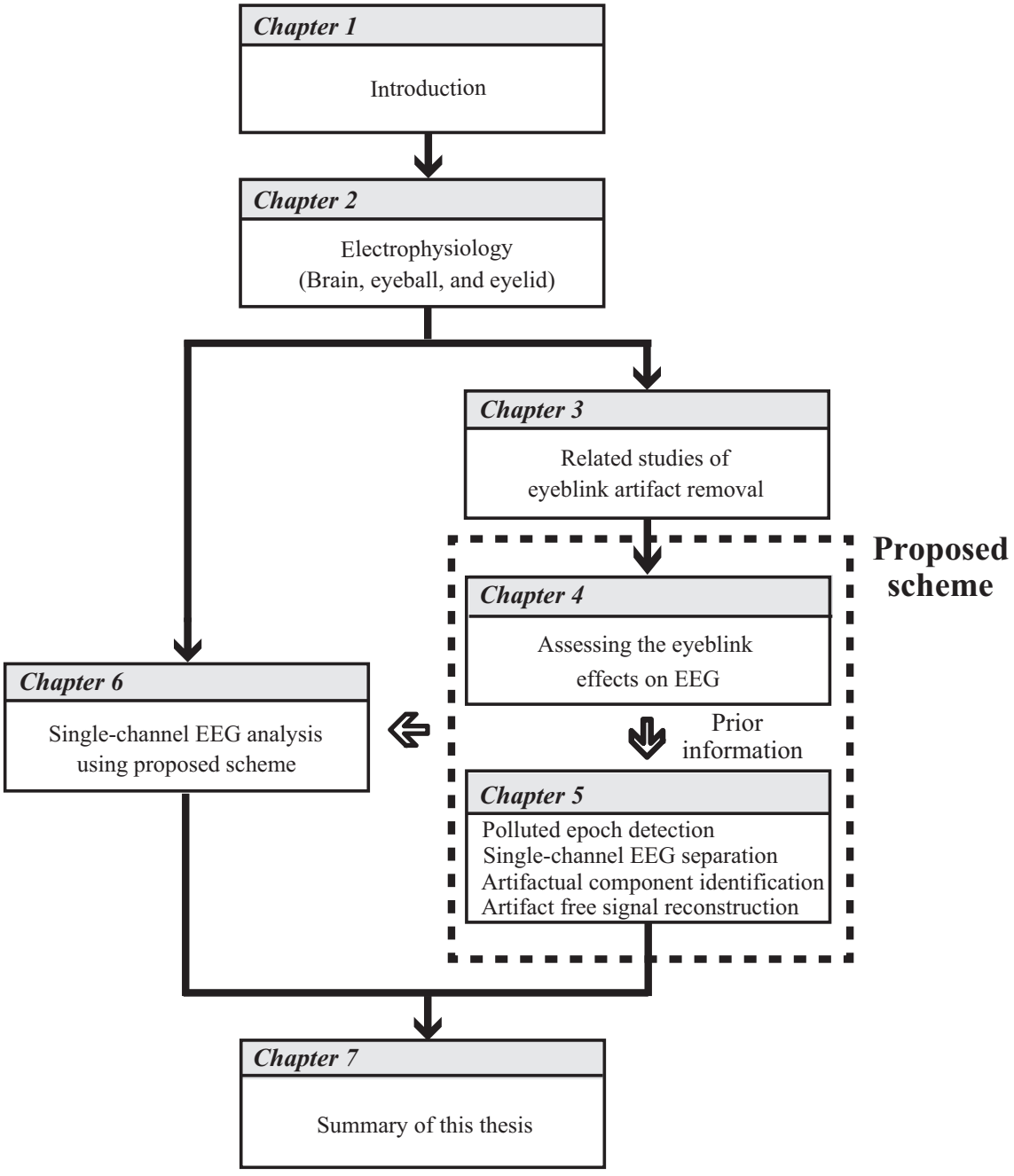

Figure 1.13 Thesis outline.

Chapter 2

FUNDAMENTAL AWARENESS OF BRAIN AND EYE, AND THEIR RECORDING METHODS

2.1 Human Brain

2.1.1 Brain Structures and Functions

The central nervous system has seven main parts: (i) spinal cord; (ii) medulla oblongata; (iii) pons; (iv) cerebellum; (v) midbrain; (vi) diencephalon; and (vii) cerebral hemispheres (Figure 2.1). The spinal cord conveys information from the skin, joints, and muscles to the brain through the brainstem that consists of the medulla oblongata, pons, and midbrain to provide required activities of the body from moment to moment.

The brain is part of the central nervous system and can be divided into three broader regions: (i) hindbrain (the medulla oblongata, pons, and cerebellum); (ii) midbrain; and (iii) forebrain (the diencephalon and cerebral hemispheres). The hindbrain modulates the force of movements and is involved in motor skills learning. The midbrain controls eye movement and the coordination of visual and auditory reflexes. The forebrain processes most of the information reaching the cerebral cortex, the heavily wrinkled outer layer which consists of nerve cells (neurons) and glial cells. In addition, functions involved in memory, learning, emotion, desire, thinking and so on, are realized in the brain. These complex process mainly take place in one or both hemispheres. The hemispheres are essentially symmetrical structures and can be divided into four anatomically distinct lobes: (i) frontal; (ii) parietal; (iii) temporal; and (iv) occipital (Figure 2.2). These lobes have specialized pathway called functional localization (stereotaxic atlas) to process information, thus other functions are expeditiously processed and simultaneously controlled in the associated specific regions [123].

However, the functional localization in the human is only a reference because the mechanisms of processing and controlling functions emerge from close mutual inter-

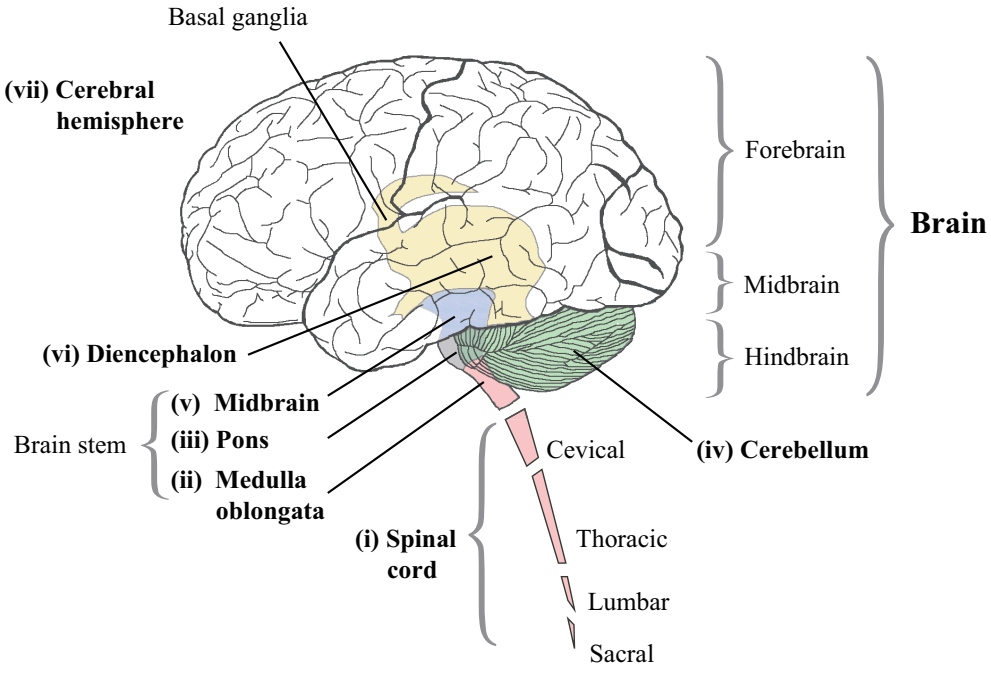

Figure 2.1 The central nervous system adapted from the reference [124].

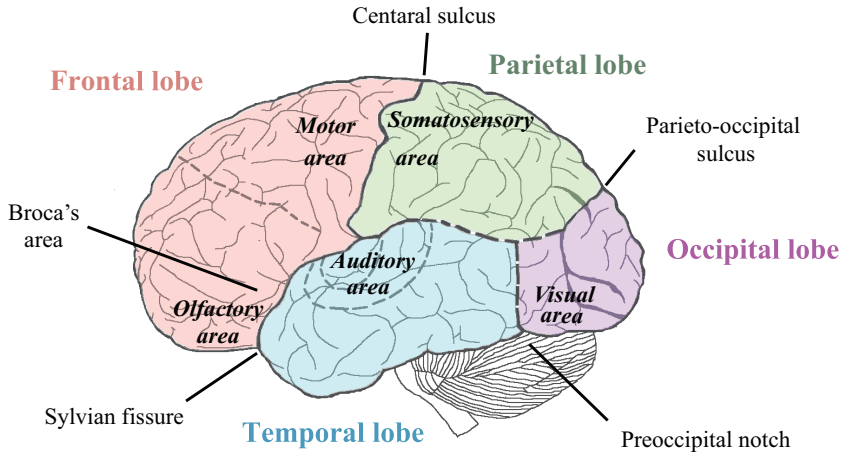

Figure 2.2 The left hemisphere divided into four lobes with functional localization [125].

actions, and because of the vast variability in the brain anatomy between individuals. Despite these mutual interactions have been piecemeal revealed by excellent pathfinders in neuroimaging, consistently specifying where in the brain an activation for processing a function has occurred is conceptually and technically more difficult than has been assumed [126]. Therefore, addressing kaleidoscopic functional states of the brain affected by neuronal activities (nerve firings) is still attracting attention.

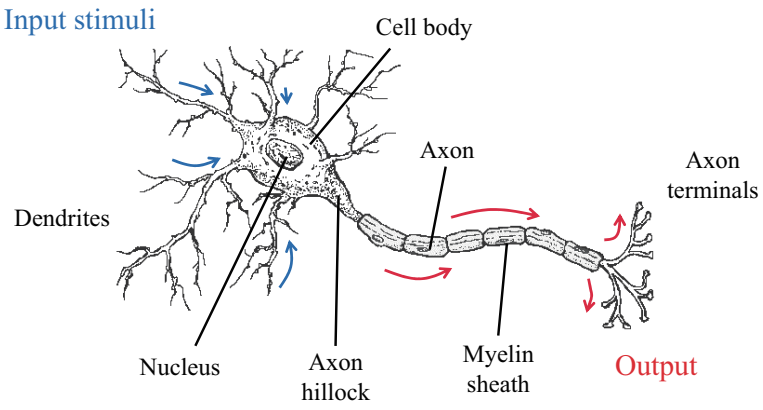

Figure 2.3 A microscopic view of a neuron modified from the reference [127].

2.1.2 Communication among Neurons for Achieving Functions

The cerebral cortex completes the vast majority of functions described in the preceding section with the cooperation of 16.34 ± 2.17 billion neurons in the case of a male adult male (86.06 ± 8.12 billion neurons in the whole-brain [128]). The neurons are specialized cells designed to communicate their information to another cell using chemical and electrical signals. Each neuron is composed of dendrites, a cell body, and an axonal process (Figure 2.3). Dendrites are the main part of input terminals of a neuron. They propagate the electronic information received from adjacent neurons to a cell body or soma that contains many biomolecules including protein and carbohydrates [129]. Propagated information is encoded in the nucleus by ionic activities [130]. Through an axon covered with myelin sheath that assists extracellular excitation of myelinated axon [131], the information travels to fusiform axon terminals and is sent out to adjacent neurons [132]. The functions are realized by cooperating neurons whereas a single neuron neither communicates with other neurons nor rests at all times.

Cerebrospinal fluid in the ventricles and surrounding the brain, not to mention cerebral cortex is essentially a saline solution. Cell membrane made from lipids mantles each neuron to control a number of ions within the cell and in the extracellular fluid [133]. The membrane has some types of permeable ion channels that pass inorganic ions, particularly sodium (Na^+), potassium (K^+), calcium (Ca^{2+}), and chloride (Cl^-). These ions customarily keep or move their position in or out of the cell based on concentration gradients (differences in concentration of the ion per distance unit in the local environment) and electrostatic gradients (differences in electrical charge per distance in the local environment). The charge of a neuron membrane at resting potential is approximately -70 mV. Moving the ions between the intracellular and extracellular sides (this action is called "pump") makes the electrical potential in the membrane change (Figure 2.4). During passive diffusion, a sodium-potassium pump continually pumps ions.

To receive a signal on the dendrites of the second neuron, the receptors have to catch

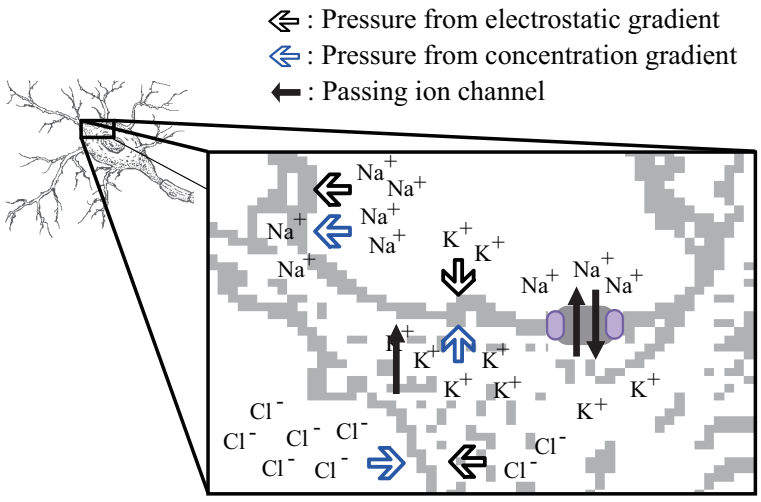

Figure 2.4 The ionic basis of the resting potential on passive diffusion based on the reference [127].

neurotransmitters or molecules translating from axon terminals of the first neuron on their portals for allowing more ions to flow through the membrane. A synapse is a point of connection between first neuron's axon terminal and second neuron's dendrite. It consists of the following three elements: (i) presynaptic terminal; (ii) synaptic cleft; and (iii) postsynaptic terminal. Furthermore, there are two main modalities of synaptic transmission: (i) chemical and (ii) electrical (Figure 2.5). At chemical synapses, a neurotransmitter such as acetylcholine and glutamic acid is firstly released from the synaptic vesicle of the first neuron in a probabilistic manner when an action potential (which is described in next paragraph) reaches the presynaptic terminal [134]. Moreover, afterwards, each of neurotransmitters or molecules reaches an ionotropic (ligand-gated ion channels) receptor or a metabotropic (G protein-coupled) receptor placed on second neuron's dendrite. A metabotropic receptor has an ability to conduct indirectly through a secondary messenger. These receptors can detect and translate messages into postsynaptic events by changing resting potential to gene expression [135]. On the other hand, the synaptic cleft is not required to communicate with adjacent cells because bridges between the presynaptic and postsynaptic terminal have already been built by clusters of intercellular channels called gap junction at electrical synapses [136]. The bridges based on two connections realize the bidirectional passage of electrical currents triggered by an action potential and carried by ions and small molecules like calcium [137]. Moreover, electrical synapses are highly effective at mediating lateral excitation and promoting the spread of chemically mediated synaptic inputs [138]. Although chemical and electrical synapses are now known to coexist in brain structure, details of the individual and interactive properties of these two modalities of transmission are still emerging [139].

Passing ions between the intracellular and the extracellular sides causes local voltage

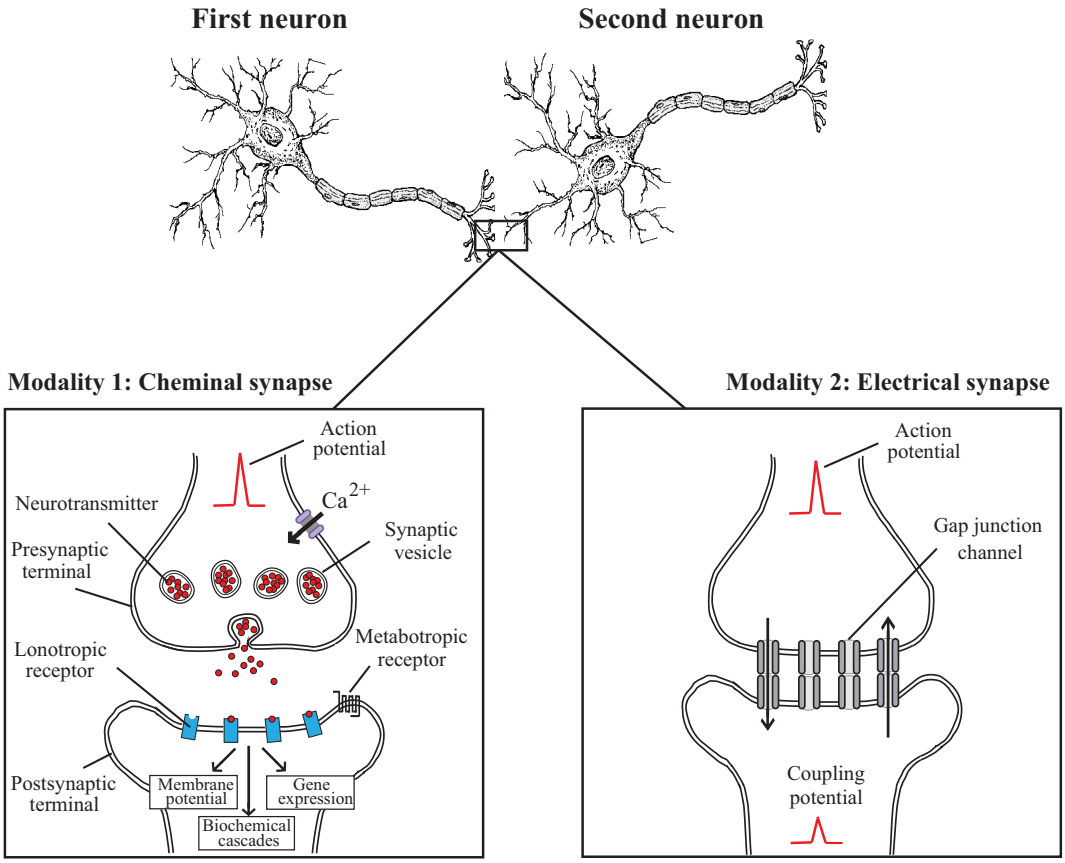

Figure 2.5 The two main modalities of synaptic transmission based on the reference [139].

changes in a neuron. The change is called graded potential, and its magnitude depends on the strength of the stimuli. If the potential membrane charges positively, the effect and graded potential are called depolarization and Excitatory PostSynaptic Potential (EPSP). Alternatively, if the potential membrane charges negatively, the effect and graded potential are called hyperpolarization and inhibitory postsynaptic potential. In the postsynaptic area, local voltage changes regardless of the types of graded potential combining to form an overall signal. When the potential membrane exceeds a threshold (about -55 mV), an action potential (that is an all-or-nothing electric scheme) and a transient depolarization of the neuron's membrane, will occur. It makes sodium and potassium channels open and close their channels to pass the propagated information.

In summary, each neuron has a membrane potential, and it changes its potential by chemical and electrical factors to communicate with another neuron or inhibit the communication. Propagated information from the first neuron is encoded in the nucleus as an action potential, and this information is sent out from second neuron's axon to the third neuron through synaptic transmission. The neural network has an elastic connection and exerts its powerful and flexible ability to control functions.

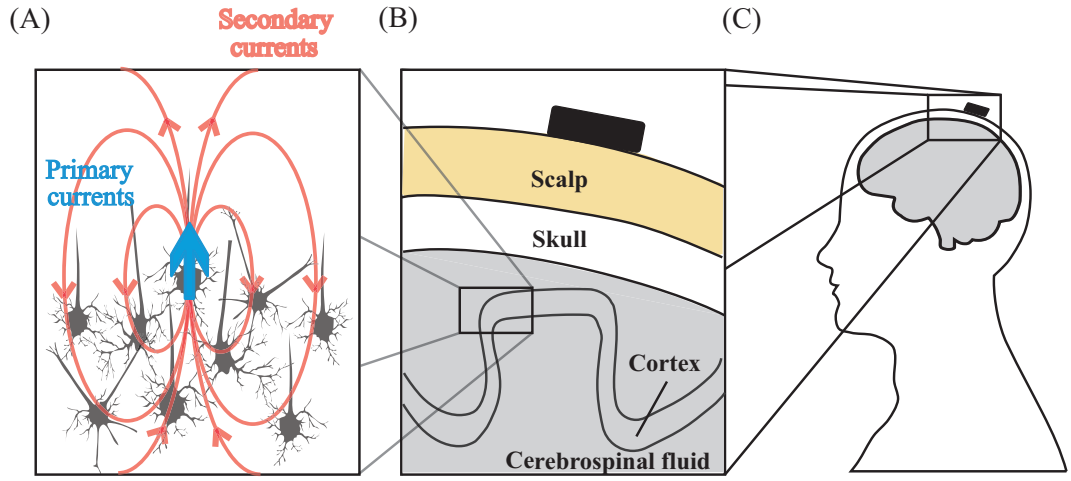

Figure 2.6 Networks of cortical neural cell assemblies modified from the reference [140]. (A) Pyramidal cell assembly, initiative current (primary current), and next currents (secondary currents). (B) Large cortical pyramidal nerve cells. (C) Translucent human head.

2.1.3 Discovery of Electroencephalogram

An English physician, Richard Caton discovered EEG from the exposed brains of rabbits and monkeys in 1875 [141], and a German neurologist, Hans Berger first observed the brain electrical activity on the human scalp in 1924 [35].

Differences of electrical potentials are caused by the apical dendrites and cell body in the pyramidal neurons (which are oriented perpendicular to the cell surface and create electrical dipole [142]) when synaptic transmissions of the apical dendrites are activated by the generation of the EPSP. This difference triggers the generation of a measurable current that flows through the volume conductor from the non-excited membrane of the cell body and basal dendrites to the apical dendritic tree sustaining the EPSPs (Figure 2.6). The conservation of electric charges makes the closed current loop with extracellular current flowing even through the most distant part of the volume conductor (second current), but shortest route between the source and the sink firstly makes more fast and robust current (primary current). An EEG signal comprises a mixture of the electrical currents. A voxel (volume element of several mm^3) contains on average 5.5 million neurons, 10^{10} synapses, 22 km of dendrites, and 220 km of axons [1]. Electrical indices recorded by electrodes attached to the scalp reflects the summation of excitatory or inhibitory postsynaptic potentials in the most superficial layers of the cortex. In other words, broad regions of cortex in the order of a few square centimeters, have to be fired synchronously to generate he observable potential for changes to be detected at electrodes attached on the scalp [23].

EEG oscillations have been categorized into the following five different frequency bands: (i) delta (0.5 - 4.0 Hz); (ii) theta (4.0 - 8.0 Hz); (iii) alpha (8.0 - 13.0 Hz); (iv) beta (13.0 - 30.0 Hz); and (v) gamma ($>$ 30.0, but typically $<$ 100 Hz). Alpha activity

observed in the posterior and occipital regions with a typical amplitude about 50.0 μV is well-known and most extensively studied activity [57]. The majority of people show a complete change of brain wave pattern to the alpha rhythm when closing eyes.

2.1.4 Electroencephalographic Recording Methods

The electrical currents can be easily measured and displayed as the differential signals between the two input terminals/electrodes of the differential amplifier without any surgical operation, defibrillator, and hazard of electric shock, although the signals have a weak oscillating range (0.5 to 100.0 μV in amplitude). Properly speaking, they have comparatively low spatial resolution and specificity to estimate sources in neuroimaging because the electrical currents must pass the skull having low electroconductivity. However, volume conductor models neglect holes in the skull, lesions, the ventricles, and anisotropic conductivity of the skull [143].

There are three main types of electrophysiologic recording techniques defined by where the recording electrode is placed.

✓ Extracellular (*in vitro*): the electrode is placed just outside the neuron of interest,
✓ Intracellular (*in vivo*) : the electrode is intercalated inside the neuron of interest,
✓ Patch clamp : the electrode is juxtaposed to the neuronal membrane.

These different recording types are used to investigate the electrical patterns of neurons. The EEG measurement is classed as an extracellular recording technique.

In 1958, a Canadian psychologist Herbert Henri Jasper proposed an essential placement and designations of the EEG electrodes called International 10-20 electrode system [144]. Using the system has been recommended by International Federation in Electroencephalography and Clinical Neurophysiology and known as the most popular system for EEG measurements. Each of electrode dispositions has proportional distance in percent between ears and nose, thus the distance depends on the individual (Figure 2.7). According to adjacent brain areas, electrode dispositions are separately labelled: Fp (prefrontal), F (frontal), C (central), T (temporal), P (posterior), and O (occipital). An odd suffix to each label indicates that the electrode is attached to the left hemisphere, and vice versa. A “z” suffix to each label means the electrodes place on the anterior-posterior axis of the head. There are several techniques for choosing reference and ground electrode placements. In this thesis, reference and ground electrodes are selected as linked-ears(mastoids) and forehead (Fpz) which are predominant for measurement in the EEG signal processing.

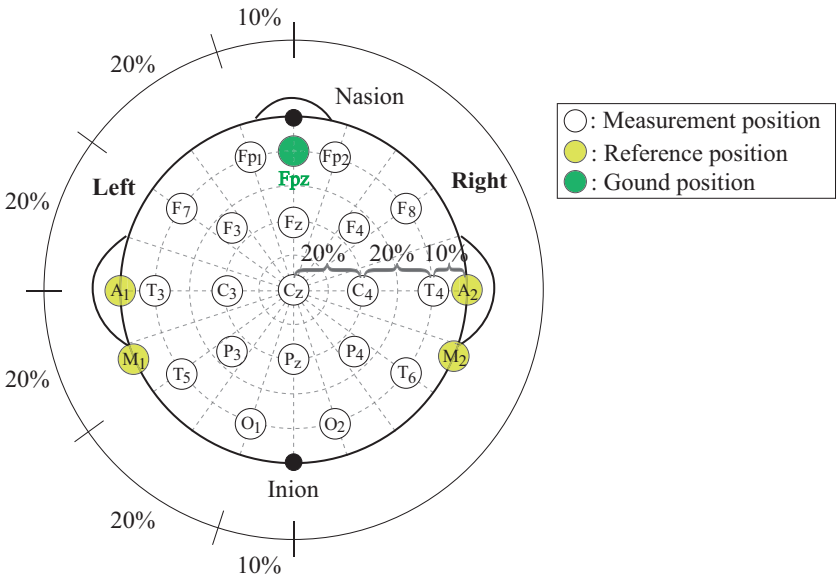

Figure 2.7 International 10-20 electrode system based on the reference [144].

2.2 Eyeball and Eyelid

2.2.1 Eyeball Structures and Functions

The eyeballs are essentially symmetrical conformations as well as the brain hemispheres. In addition, they have an almost spheroidal shape to avoid their deformation or curvature (Figure 2.8 (A)). A solid fibrotic membrane named sclera which is filled with a jelly-like substance (vitreous body), covers the eyeball. The sclera and intraocular pressure maintain eyeball shape; however, it might sometimes be asymmetrical by alteration of vitreous/anterior chamber shape induced by visual and neural mechanisms in ametropic eyeballs (e.g. myopia and astigmatism) [145–147].

Looking at the eyeball from the front, white and another color (that depends on the person) can be seen onto the eyeball. The white of the eyeball named conjunctiva protects the eyeball and makes eyelid movement easier by generating the ophthalmic lubricant [148]. Nevertheless, the other color of the eye depends on the iridial pigmentation [149], every eyeball necessarily has a pupil in the center of the iris. Furthermore, diaphanous tissue named cornea is situated on the contour of the sclera. Photic stimulation via the cornea is modified by contraction of the iris and passed the optic lens to assemble in a small concave (fovea centralis) [150, 151]. Afterward, the information of photic stimulation which made it of retinal photoreceptor cells will be translated into synaptic activities (Figure 2.8 (B)) [152, 153].

Summarizing the above sentence in this clause, the eyeball has following three functions: (i) image projection onto the retina; (ii) translation from photic stimulation to synaptic activities; and (iii) communication in the brain through the optic nerves.

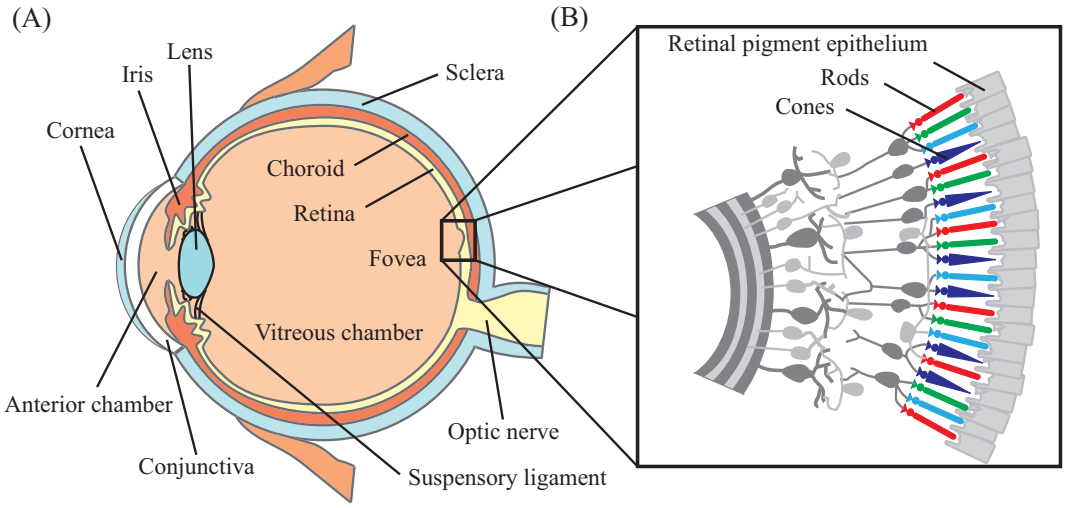

Figure 2.8 (A) Sagittal section of eyeball. (B) Close-up of the retina modified from the reference [154].

2.2.2 Eyelid Structures and Functions

The following six main layers structure the eyelid: (i) skin; (ii) subcutaneous tissue; (iii) striated muscle fibres of the orbicularis oculi; (iv) orbital septum; (v) tarsal plates; and (vi) conjunctiva (Figure 2.9 (A)). The eyelid's skin, in particular, upper eyelid's skin is the thinnest in the body, has sweat glands and eyelashes to intercept dust headed for the eyeball [155]. The subcutaneous tissue is almost devoid of fat and cooperates with other tissues to readily accept the accumulation of fluid and blood. The orbicularis oculi whose detail will be described in the next section has a significant role in an eyeblink. The orbital septum is a fibrous partition disposed along the orbital cavity. Owing to holding the orbital fat, it acts as a barrier to prevent superficial infection from spreading deeper to affect the orbit and brain [156]. The tarsal plate gives the eyelids firmness and shape. Furthermore, it contains numerous Meibomian glands that secrete oil onto the eyelid margins and, in turn, cap the tear film [157]. The conjunctiva described in the previous section lines the inner aspect of the eyelids. The margin of the eyelid and the non-keratinized epithelium of the conjunctiva represents a sandwich of tissues. It becomes keratinized at the mucocutaneous junction of the posterior border of the tarsus [158].

Healthy cornea requires moisture on the anterior surface of its epithelial layer that protects the eyeball from environmental factors. Water addition and loss of the lacrimal duct and precorneal tear film, whose physiological level of osmolarity is approximately 310 mOsm/l [159], are balanced by the homeostatic mechanism to control and maintain the anterior surface integrity [160]. However, the precorneal tear film would naturally lose its moisture and be ruptured (broke-up) by air pollution if it comes into contact with air for long hours [161]. Such chronic alteration of the precorneal tear film may cause eye complaints [162]. Therefore, isolating the eyeball from the air in an appropriate

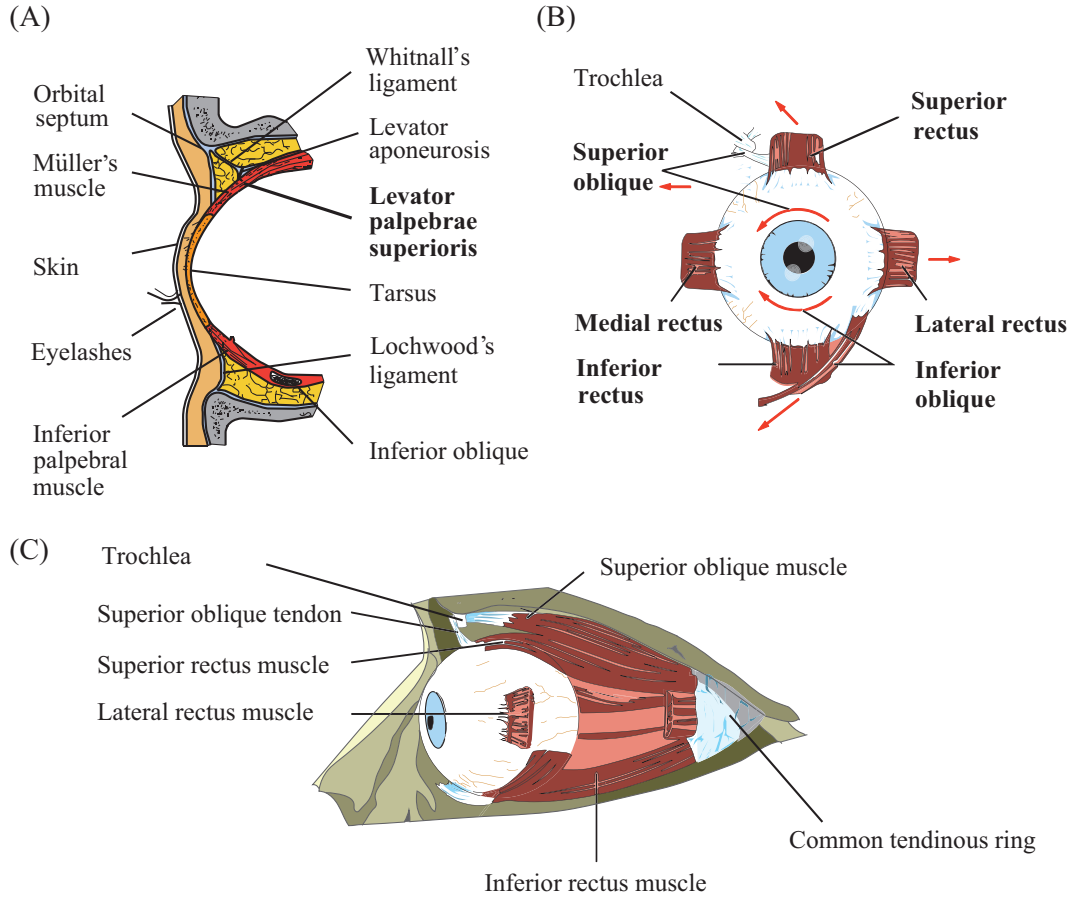

Figure 2.9 (A) Sagittal section of eyelid adapted from the reference [158]. (B) Sagittal view of the left orbit, and surrounding structure. (C) Anterior view of the left eye adapted from the reference [163].

manner is needed for maintenance of a normal condition. The two eyelids protect the precorneal tear film against potentially damaging external factors. Besides, each eyelid has many oil glands that overlay the aqueous layer of tears on the surface of the eyeball and lessen its evaporation. That means eyelids contribute to avoiding alteration of the precorneal tear film by helping to spread the tear film over the surface.

2.2.3 Extraocular Muscles

When the head or object of interest moves to any position from the locked position, eyeballs should be rotated to maintain the same image. Alternatively, eyeballs must keep their rotation for a stationary object. Moreover, the upper eyelid has to do tonic elevation and control its vertical position for segregation of eyeballs from the external environment to protect them. Extraocular muscles whose maximum discharge rates are less than 600 /s on single fiber recordings from ocular motor nerves [164] provide these

Table 2.1 Abilities of eyeball given by extraocular muscles modified from the reference [165].

Ability	**Main function**
Fixation	Holds images on the fovea
Conjugation	Retains the angular relationship between eyeballs
Optokinetic	Stabilizes images during sustained head motions
Saccade	Jumps from one eyeball position to another quickly
Smooth pursuit	Moves the eyeballs smoothly instead of in jumps
Vestibular	Holds images on the retina during brief linear head motions
Vergence	Changes the eyeballs in opposite directions

Table 2.2 Main functions and innervations of the seven extrapcular muscles modified from the reference [124].

Muscle	**Main function**	**Innervation**
Lateral rectus	Abduction	Abducens nerve
Superior oblique	Depression / Intorsion	Trochlear nerve
Medial rectus	Adduction	Oculomotor nerve
Superior rectus	Elevation / Intorsion	Oculomotor nerve
Inferior rectus	Depression / Extorsion	Oculomotor nerve
Inferior oblique	Elevation / Extorsion	Oculomotor nerve
Levator palpebrae superioris	Elevation	Oculomotor nerve

abilities to the eyeball and eyelid [166,167]. Generally, there are seven extraocular muscles surrounding an eyeball: (i) superior rectus; (ii) inferior rectus; (iii) lateral rectus; (iv) medial rectus; (v) superior oblique; (vi) inferior oblique; and (vii) levator palpebrae superioris (Figure 2.9). The first six muscles and the last one control eyeball movement and upper eyelid elevation, respectively [168]. Given abilities regarding eyeball and their primary duties are tabulated in Table 2.1.

The extraocular muscles without levator palpebrae superioris can be divided into three functional pairs based on the agonist-antagonist activity. Furthermore, three cranial nerves: (i) abducens nerve; (ii) trochlear nerve; and (iii) oculomotor nerve, innervate all extraocular muscles. The main functions and the innervations of the seven extraocular muscles are tabulated in Table 2.2. These cranial nerves mediate the brain stem and eye movements or eyeblinks [163]. Thus, eye movements and eyeblinks are controlled by extraocular muscle actions based on the ocular motor system in the brain.

2.2.4 Types of Eyeblink

In the first place, I have to clarify the definition of "Eyeblink". The word "Eyeblink" is typically used synonymously in the literatures for eyelid movement [169,170]. According to these literatures, I use the word of "Eyeblink" with the same definition in this study.

An eyeblink comprises movement of the eyeball/eyelid including contraction of the extraocular muscles and causes the eyeball to act like an electric dipole slightly moving up/down and inward [73, 74]. The upper eyelid starts to move to the lower eyelid with a high acceleration and reaches a peak velocity of up to 280 mm/s within 70 ms [171]. The movement is completed (zero velocity) from 100 to 150 ms; the reverse operation is accomplished more leisurely; it lasts roughly 300 ms. Healthy persons over 60 years of age have augmented mean lid-closing duration, diminished excitability, and longer latency of the electrically induced blink compared with younger individuals [172].

On the other hand, these muscular contractions can be divided into three types: (i) voluntary (commanded); (ii) involuntary (spontaneous); and (iii) reflex (elicited) [173]. The person initiates voluntary eyeblink in response to an external or internal command [174]. Involuntary eyeblink depends on the dopaminergic activity. It is spontaneously and unconsciously caused by drying of the cornea and conjunctiva [88]. Reflex eyeblink is also caused unconsciously but elicited by a sudden appearance of intense stimulation as auditory, visual, electrical, and air puff [175]. It has been known that how to elicit a reflex reaction is linearly or nonlinearly proportional to the intense stimuli [176–178]. Reflex eyeblink reaction has many labels (at least 16 labels) such as "defense blinking reflex" [179] and "cochleopalpebral reflex" [180], so it is too difficult to specify a unique set of reflex eyeblinks.

An EEG system user usually has to hold his head up for the presented stimuli according to the instructions on the system operation. Reflex responses would be induced in the first few times of training because the user is not used to the operation of the system. However, after training, electrical and cutaneous stimuli expect for an air flow directed into eye very rarely induce a reflex reaction during the system operation [181, 182]. Therefore, eyeblink artifacts generated by the first two types of eyeblink (voluntary and involuntary) must be rejected from observed EEG signals in the EEG processing procedure, whatever stimulus might be selected.

2.2.5 Eyeblink Mechanisms

All eyeblinks show a reciprocal innervation between the Levator Palpebrae Superioris (LPS) and the Orbicularis Oculi (OO) muscles mediated through the electrical stimulation of a region made up of the periaqueductal grey matter close to the superior

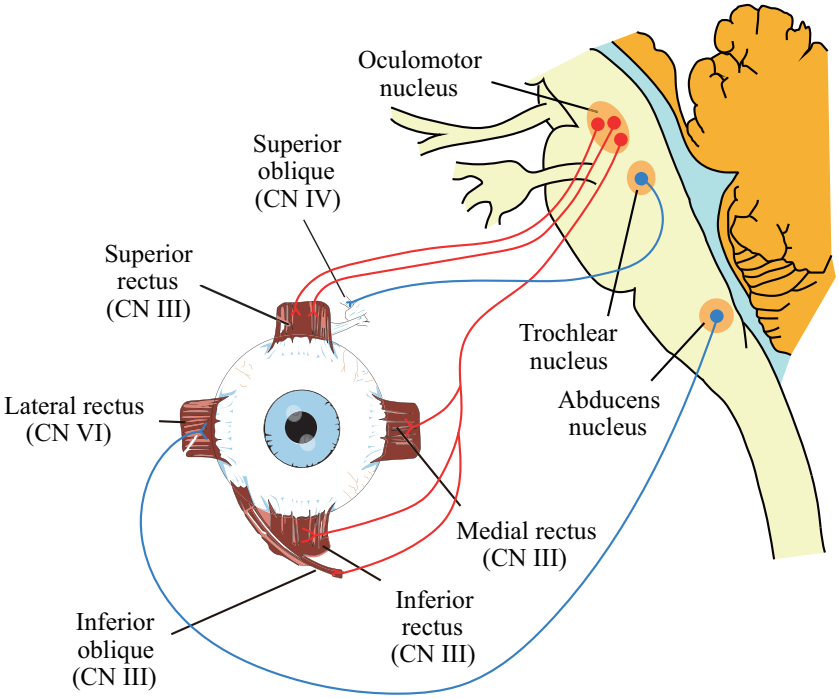

Figure 2.10 Extraocular muscles of eyeball and their relationship with CN III, IV, and VI [183].

colliculus and the posterior commissure [184–186]. In addition, two smooth muscles; the superior tarsal and inferior tarsal (Müller's) muscles are involved [187–189]. Stereotyped eyeball movements controlled by Cranial Nerves (CN) III, IV, and VI normally making its position more nasally downward accompany eyelid movements whose rotation depends on the initial eyeball position [190]. Origin and distribution of CN III, IV, and VI, which innervate extraocular muscles, are described in Figure 2.10. All types of eyeblink have much in common (e.g. precise conjugated movements between both eyes [191]). Meanwhile, each eyeblink type is distinguishably caused through different neural pathways linking the brain and OO muscle. To open new (known) frontiers and push back horizons of the neural pathway linking the brain and OO muscle, the corneal eyeblink reflex neural circuit is shown in Figure 2.11 as an example.

In a voluntary eyeblink, voluntarily sustained closure of eyeballs is achieved either by inhibition of the steady tonic activity of LPS without OO activation (for soft eyelid closure) or the inhibition and sustained OO contraction (for forceful eyelid closing) [192, 193]. The basal ganglia comprising a distributed set of the brain structures in the telencephalon, diencephalon, and mesencephalon, plays a significant role in controlling the coordination required during voluntary eyeblink between the phasic activation of the OO muscle and modulation of the tonic activity of the LPS [194, 195].

In an involuntary and reflex eyeblink, a short high-frequency burst of activity in the OO motoneurons leads to inhibit the LPS motoneuron firing just before a blink [197]. Consequently, passive forces are going to release the upper eyelid to downward.

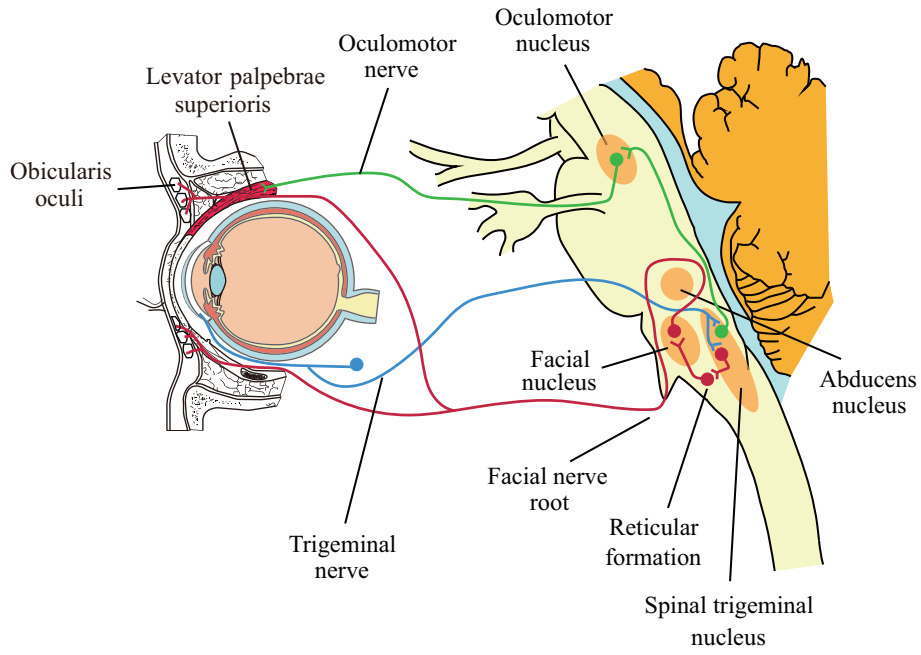

Figure 2.11 The corneal eyeblink reflex neural circuit [196].

When the OO muscle activity has stopped, and the LPS muscle has regained its tonic activity, the drooped upper eyelid opens again. Involuntary eyeblink is strictly related to dopamine activities in the central nervous system [88,198] whose generator might be composed of different premotor neural structures in the brainstem [199]. Emotional or state variables (e.g. speaking, memorizing, and reading) affect the rate of an involuntary eyeblink [200, 201]. Moreover, evidence suggests that dopamine D_1 [202] and D_2 [203] receptor systems play a role in the control of this action. However, subtle details of the mechanism in involuntary eyeblink are still unexplained [204].

Reflex eyeblink can be initiated by an electrical stimulation of supraorbital nerve; an air puff, a light flash (visual stimulus), or a sound (acoustic stimulus) [205]. Their afferent pathways are mainly trigeminal, and the premotor areas involve the pontine and medullary tegmental levels of the brainstem [206]. It is known that the reflex reaction consists of an early ipsilateral response (R_1) and a late bilateral response (R_2) [185]. During R_1 and R_2, the LPS muscle remains continuously inhibited.

2.2.6 Eyeblink Recording Methods

A potential difference across the retina, mainly derived from the pigment epithelium leads to maintain corneo-retinal standing potential, i.e. the eyeballs are electrically charged; positive at the cornea and negative at the retina (see Figure 2.12 (A)) [207–209]. Although the potential distribution of eyeball is permanent (not fixed but has been

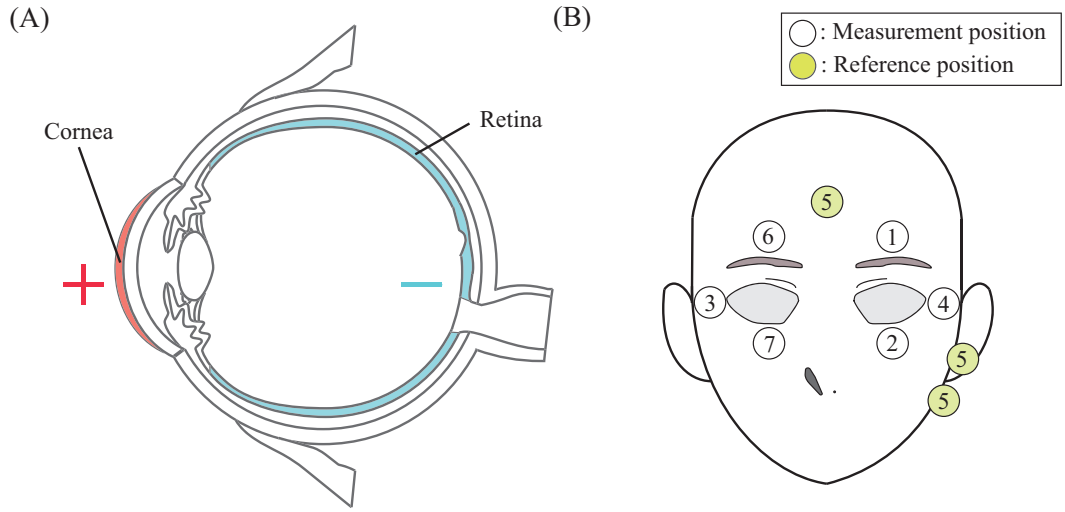

Figure 2.12 (A) Sagittal section of eyeball visualized with electrical field in the tissues surrounding the eyeball. (B) Electrode placement for EOG signal measurement.

found to vary diurnally), an electric potential field around the eyeball would be suddenly changed when the eyeballs and/or the eyelids move. This electrical change is multiply composed of the eyeball rotation (dipole movement) and the eyelid sliding down over the positively charged cornea acting as a sliding electrode [56,109]. It can be easily measured as EOG by electrodes placed on the periphery of eyeballs [72, 210]. Here, the good conductivity of the scalp leads to contaminating recorded EOG signals with potentials generated from contraction of the extraocular muscles as well as the electrical activity of neurons. Consequently, EOG signal has information of the eyeblink potentials that depends not only on eyeball movements but also on eyelid sliding including contraction of the extraocular muscles.

EOG signal measurement comprises six electrodes (Figure 2.12 (B)): four measurement electrodes (① to ④); one reference electrode placed on ear lobe, mastoid, or medial frontal region (⑤); and one ground electrode [211, 212]. There is no fixed-rule in electrode placement, but an EOG signal called Vertical EOG (VEOG) signal or Horizontal EOG (HEOG) signal, is recorded from two surface electrodes placed at the superior and inferior (① − ②) or right and left orbital rim of the eye (③ − ④) with minimal interference and background noise [213]. In rare cases, Radial EOG (REOG) signal is recorded from four surface electrodes surrounding both eyes ((① + ② + ⑥ + ⑦)/4) [89, 214]. VEOG, HEOG, and REOG signals capture blink potentials with vertical eyeball movement (e.g. Bell's phenomenon), horizontal eyeball movements, and vertical/horizontal eye movements.

In this thesis, I measure VEOG signals to obtain blink potentials. Moreover, reference and ground electrodes are commonly placed on left mastoid and Fpz in EEG and VEOG signal measurement.

Chapter 3

REVIEW OF EXISTING SCHEMES ON EYEBLINK ARTIFACT REMOVAL

3.1 In Multi-channel Recordings

3.1.1 Standard Assumption Concerning the Cerebral Sources

A typical approach to eyeblink artifact removal from an observed EEG signal is to adjust the standard assumption that the observed cerebral signal $x(n)$ is the sum of the cerebral source (local-field) activity $s(n)$ and the noise $d(n)$. Neuronal cells have only limited connections because a simple constraint on cortical signal dependence very highly weighted toward short (< 500 μm) connections [215]. Besides, synchrony in local-field activities should likely diffuse through a contiguous cortical area (closely-spaced cortical electrodes), rather than jump between distant and weakly connected cortical areas [104, 216, 217].

Therefore, an assumption that EEG signals generated from multiple cerebral sources and non-cerebral sources (artifacts) are linear mixtures, allows the formulation of the underlying biophysics of the generation and propagation of EEG potential [218]. The following equation can model it:

$$\boldsymbol{x}(n) = \boldsymbol{A}\boldsymbol{s}(n) + \boldsymbol{d}(n), \tag{3.1}$$

where: $\boldsymbol{x}(n) = [x_1(n), x_2(n), \ldots, x_P(n)]^T$ (superscript T means the transpose of a vector or matrix) is the P observed EEG data at the n-th sampling point ($1 \leq p \leq P$, $1 \leq n \leq N$), in which each row is an EEG channel; $\boldsymbol{s}(n) = [s_1(n), s_2(n), \ldots, s_Q(n)]^T$ is the Q unknown source data ($1 \leq q \leq Q$), in which each row means cerebral or non-cerebral source; $\boldsymbol{A}$ is the $P \times Q$ full-column rank unknown mixing matrix; and $\boldsymbol{d}(n) = [d_1(n), d_2(n), \ldots, d_P(n)]^T$ is the P additive zero-mean noise data. In real scenarios, there are likely to be more sources than observations ($Q > P$), however, treating

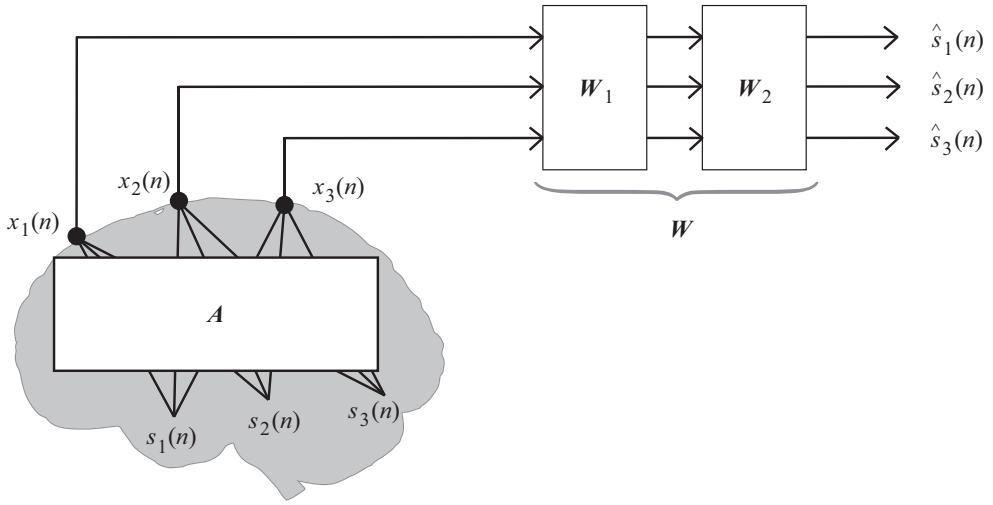

Figure 3.1 Linear mixture concept of blind EEG source separation modified from the reference [251].

the number of sources as same value of observations ($Q = P$) is not normally an issue because the dipole is modelling the neuronal activity of an elongated sheet of the cortex or several synchronously active sources. Most algorithms can extract a linear combination of sources belonging to the same subspace, blindly [45, 219]. By contrast, all schemes have a common drawback that they can only handle overdetermined (determined) mixture because the inverse process while having no priori information on the characteristics of the sources is evidently intractable. Thus, additional three assumptions are reluctantly accepted: (i) the noise is spatially uncorrelated with the observed data ($\mathbb{E}[\boldsymbol{A}\boldsymbol{s}(n)\boldsymbol{d}(n)^T] = \mathbf{0}$, where $\mathbb{E}[\cdot]$ is the expectation operator), and temporally uncorrelated ($\mathbb{E}[\boldsymbol{d}(n)\boldsymbol{d}(n+\tau)^T] = \mathbf{0}$, where τ is lag time and $\forall\tau{>}0$); (ii) the number of sources is equal to or lower than the number of observation signals ($P \geq Q$); and (iii) it is stationary, that is $\boldsymbol{A}$ does not change over time [220, 221].

To estimate the sources including non-cerebral activities $\hat{\boldsymbol{S}} = [\hat{\boldsymbol{s}}(1), \ldots, \hat{\boldsymbol{s}}(N)]$ from the observed EEG data (to solve BSS problem), unsupervised learning schemes such as PCA and ICA jointly estimate demixing matrix $\boldsymbol{W}(= \boldsymbol{A}^{-1})$ using multi-channel information $\boldsymbol{X} = [\boldsymbol{x}(1), \ldots, \boldsymbol{x}(N)]$ under the linear mixture concept.

$$\hat{\boldsymbol{s}}(n) = \boldsymbol{W}\boldsymbol{x}(n). \tag{3.2}$$

Each unsupervised learning scheme has an algorithm that is subject to various indices: uncorrelatedness, independence, non-Gaussianity, instantaneous propagation, linearity, and so on, has already been confirmed their effectiveness of eyeblink artifact removal [222]. In Figure 3.1, the concept accounts for demixing matrix $\boldsymbol{W}(= \boldsymbol{W}_1\boldsymbol{W}_2)$ because some algorithms first decorrelate the signals by $\boldsymbol{W}_1$ and then unmix the signals by $\boldsymbol{W}_2$. Given a mixing matrix $\boldsymbol{A}$ is composed of the three blind cerebral sources $\boldsymbol{s}(n)$ and provides the same number of observations $\boldsymbol{x}(n)$ in this figure.

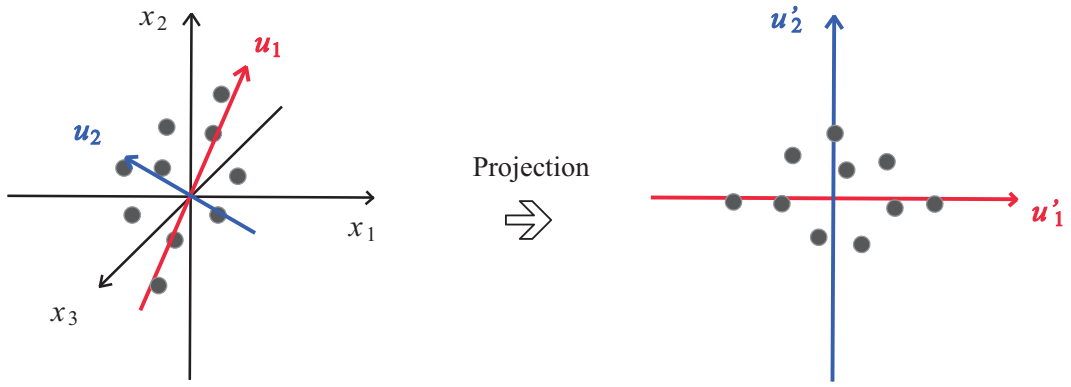

Figure 3.2 3-dimensional scatter diagram in input space and 2-dimensional scatter diagram in principal component space.

3.1.2 Unsupervised Learning Source Separation Schemes

Principal Component Analysis

PCA converts the observed EEG signals of possibly correlated variables into values of linearly uncorrelated variables named Principal Components (PCs) with the first-order and second-order statics [72, 223]. This algorithm included eigenvalue decomposition [224] to get the directions $\boldsymbol{u}$ of greater variance in the input space of the EEG data $\boldsymbol{X}$ based on an assumption that $\boldsymbol{X}$ is jointly normally distribution, and the sources are uncorrelated (see Figure 3.2). Input data $\boldsymbol{X}^{\text{old}}$ should be standardized to decorrelate samples of the same dimension ($\mathbb{E}[\boldsymbol{x}(n)\boldsymbol{x}(n+\tau)^T] = \boldsymbol{0}$) and to uniform unit ($\mathbb{V}[\boldsymbol{X}_p] = 1$). Standardized elements $x_{p,n}$ can be described by following equation.

$$x_{p,n} = \frac{x_{p,n}^{\text{old}} - \bar{x}_p}{\sigma_p} \quad , \tag{3.3}$$

where

$$\bar{x}_p = \frac{1}{N}\sum_{n=1}^{N} x_{p,n}^{\text{old}} \quad , \tag{3.4}$$

$$\sigma_p^2 = \frac{1}{N-1}\sum_{n=1}^{N} (x_{p,n}^{\text{old}} - \bar{x}_p)^2 \quad . \tag{3.5}$$

In PCA algorithm, the first PC, which has the largest variance in standardized input space, is a linear combination of $\boldsymbol{X}$ defined by weights $\boldsymbol{u}_1 = [u_1, \ldots, u_P]^T$:

$$\text{PC}_1 = \boldsymbol{X}^T\boldsymbol{u}_1 \quad , \tag{3.6}$$

$$\mathbb{V}[\text{PC}_1] = \mathbb{V}[\boldsymbol{X}^T\boldsymbol{u}_1] = \boldsymbol{u}_1^T\boldsymbol{\Sigma}\boldsymbol{u}_1 \quad , \tag{3.7}$$

where $\boldsymbol{\Sigma}$ ($= \boldsymbol{X}\boldsymbol{X}^T/(N-1)$) is covariance matrix of $\boldsymbol{X}$. To maximize $\boldsymbol{u}_1^T\boldsymbol{\Sigma}\boldsymbol{u}_1$ while constraining $\boldsymbol{u}_1$ to have unit length:

$$\begin{aligned} \max \quad & \boldsymbol{u}_1^T\boldsymbol{\Sigma}\boldsymbol{u}_1 \ , \\ \text{subject to} \quad & \boldsymbol{u}_1^T\boldsymbol{u}_1 = 1 \ , \end{aligned}$$

Lagrange multiplier method is introduced for solving the optimization problem [225].

$$L(\boldsymbol{u}_1, \lambda_1) = \boldsymbol{u}_1^T\boldsymbol{\Sigma}\boldsymbol{u}_1 + \lambda_1(1 - \boldsymbol{u}_1^T\boldsymbol{u}_1) \ , \tag{3.8}$$

$$\frac{\partial L(\boldsymbol{u}_1, \lambda_1)}{\partial \boldsymbol{u}_1} = 2\boldsymbol{\Sigma}\boldsymbol{u}_1 - 2\lambda_1\boldsymbol{u}_1 = 0 \ , \tag{3.9}$$

$$\boldsymbol{u}_1^T\boldsymbol{\Sigma}\boldsymbol{u}_1 = \lambda_1\boldsymbol{u}_1^T\boldsymbol{u}_1 = \lambda_1 \ . \tag{3.10}$$

In consequence, the covariance matrix $\boldsymbol{\Sigma}$ is sequentially decomposed into eigenvectors $\boldsymbol{u}_p$ and eigenvalue λ_p by an assumption that the PCs are orthogonal. The eigenvectors $\boldsymbol{u}_p$ is similar to the column of the inverse demixing matrix $\boldsymbol{W}^{-1}$.

Many extended PCA algorithms (e.g. kernel PCA [48], robust PCA [226], dual PCA [227], probabilistic PCA [228], and Gaussian process latent variable model [229]) have been proposed. As is common with all the PCA algorithms is that they consider the potential sources of observed EEG signals (neural activities and eyeblink artifacts) are algebraically orthogonal. These algorithms decompose the covariance matrix $\boldsymbol{\Sigma}$ or Gram matrix $\boldsymbol{G}(= \boldsymbol{X}^T\boldsymbol{X}/(N-1))$ to calculate eigenvalue λ that is equivalent to singular value decomposition of $\boldsymbol{X}$ or Karhunen-Loéve transform. PCA-based schemes have a competitive advantage over the input data which contain components regarding a fixed time course. However, they also have a weakness if the input data includes temporal jitter [230]. The assumption is hard to be satisfied because the orientation of individual ocular generators may even be nearly aligned with the direction of some EEG generators [114, 231]. Therefore, PCA-based schemes cannot completely remove eyeblink artifact, especially when EEG signal and eyeblink artifact have similar amplitudes [232, 233]. On the other hand, PCA algorithm is often incorporated into a first decorrelation or whitening step of some ICA algorithms which are based on higher-order statics since it is useful to reduce computational cost [234].

Independent Component Analysis

ICA is the most famous unsupervised learning algorithm to decompose multi-channel observed EEG signals $\boldsymbol{X}$ into independent sources $\boldsymbol{S}$ with higher-order (spacial) moments, beyond the second-order statics (e.g. power spectrum, or its time domain analog, autocorrelation) used in PCA, whereas some algorithms use the statics as well as

PCA [9,235]. Independence is a stronger assumption than decorrelation because it can unilaterally establish the definition of decorrelation [236]. An enormous number of ICA algorithms (e.g. adaptive mixture of ICA [237], algorithm for multiple unknown signals extraction [96], canonical decomposition of hermitian positive semi-definite arrays based on procrustes problem [238], fastICA [239, 240], fourth-order blind identification of underdetermined mixtures of sources [241], fourth-order only blind identification [242], ICA using redundancies in the quadricovariance [243], (extended) Information Maximization (InfoMax) [94, 244], joint approximate diagonalization of eigenmatrices [245,246], pearson-ICA [247], Second Order Blind Interference (SOBI) [248], and temporal decorrelation source separation [249]), which can be broadly separated into two types: Higher-Order Statics (HOS) based or Second-Order Statics (SOS) based, has been extended so far to effectively separate observed signals into sources. In the first step of most HOS-based ICA algorithms which find a linear demixing matrix $\boldsymbol{W}$ for the estimated sources $\hat{\boldsymbol{S}}$ to be as independent as possible, the covariance matrix of the input data is decorrelated by using PCA. They minimize the Mutual Information (MI) by using the normalized version of the differential entropy called negentropy which is connected to the MI, to directly measure independence of outputs. On the other hand, SOS-based ICA algorithms make the data diagonalize their unique matrices such as time-lagged correlation matrices.

As is common with all the ICA algorithms is that they consider artifacts as odd data in the EEG signal and find them using statistical criteria [250]. A state-of-the-art topical review published on 2015 reported that SOBI and InfoMax are the most commonly used algorithm for EEG signal processing; nevertheless each algorithm has an excellent strategy [251]. The strategy of SOBI remains correlated components to isolate highly temporally correlated sources by simultaneously diagonalizing the covariance matrices calculated at different time lags, sometimes works particularly well in source separation because the relationships across time (relationships between component values at different time lags) are usually not counted toward most ICA algorithms [231, 252]. Meanwhile, InfoMax algorithm can separate sources with maximum accuracy when there is a powerful electrical artifact like eyeblink in the data [254, 255]. In this thesis, InfoMax algorithm is applied to research, so let me describe the algorithm.

The fundamental problem tackled by InfoMax ICA is how to minimize the MI of the output vector $\hat{\boldsymbol{s}}$.

$$\mathrm{MI}(\hat{\boldsymbol{s}}) = \sum_{p=1}^{P} H(\hat{s}_p) - H(\hat{\boldsymbol{s}}). \tag{3.11}$$

Probability Density Functions (PDF) of observed signal $p(\boldsymbol{x})$ and estimated signal $p(\hat{\boldsymbol{s}})$

have following relationship:

$$p(\hat{\boldsymbol{s}})d\hat{\boldsymbol{s}} = p(\boldsymbol{x})d\boldsymbol{x}, \tag{3.12}$$

$$d\hat{\boldsymbol{s}} = \boldsymbol{J}(x)d\boldsymbol{x} = |\boldsymbol{W}|d\boldsymbol{x}, \tag{3.13}$$

$$p(\hat{\boldsymbol{s}}) = p(\boldsymbol{x})d\boldsymbol{x} = p(\boldsymbol{W}^{-1}\hat{\boldsymbol{s}})|\boldsymbol{W}|^{-1}, \tag{3.14}$$

where $\boldsymbol{J}(x)$ is Jacobian matrix. The estimating entropy $H(\hat{\boldsymbol{s}})$ is given by:

$$\begin{aligned} H(\hat{\boldsymbol{s}}) &= -\int p(\hat{\boldsymbol{s}}) \log p(\hat{\boldsymbol{s}}) d\hat{\boldsymbol{s}} \\ &= -\int (\log p(\boldsymbol{W}^{-1}\hat{\boldsymbol{s}}) - \log |\boldsymbol{W}|)\, p(\boldsymbol{W}^{-1}\hat{\boldsymbol{s}})\, |\boldsymbol{W}|^{-1}\, d\hat{\boldsymbol{s}} \\ &= -\int (\log p(\boldsymbol{x}) - \log |\boldsymbol{W}|)\, p(\boldsymbol{x}) d\boldsymbol{x} \\ &= -\int p(\boldsymbol{x}) \log p(\boldsymbol{x}) d\boldsymbol{x} + \log |\boldsymbol{W}| \\ &= H(\boldsymbol{x}) + \log |\boldsymbol{W}|. \end{aligned} \tag{3.15}$$

Therefore, the MI (Eq. (3.11)) can be rewritten as following:

$$\mathrm{MI}(\hat{\boldsymbol{s}}) = \sum_{p=1}^{P} H(\hat{s}_p) - H(\boldsymbol{x}) - \log |\boldsymbol{W}|. \tag{3.16}$$

By partially differentiating this index on parameters $\boldsymbol{W}$, optimized solution for source separation will be obtained.

$$\begin{aligned} \frac{\partial \mathrm{MI}(\hat{\boldsymbol{s}})}{\partial \boldsymbol{W}} &= \sum_{p=1}^{P} \frac{\partial H(\hat{s}_p)}{\partial \boldsymbol{W}} - \frac{\partial H(\boldsymbol{x})}{\partial \boldsymbol{W}} - \frac{\partial \log|\boldsymbol{W}|}{\partial \boldsymbol{W}} \\ &= \sum_{p=1}^{P} \frac{\partial(-\int p(\hat{\boldsymbol{s}}) \log p(\hat{s}_p) d\hat{\boldsymbol{s}})}{\partial \boldsymbol{W}} - 0 - \frac{\tilde{\boldsymbol{W}}^T}{|\boldsymbol{W}|} \\ &= -\mathbb{E}[\boldsymbol{\varphi}(\hat{\boldsymbol{s}})\boldsymbol{x}^T] - (\boldsymbol{W}^T)^{-1}, \end{aligned} \tag{3.17}$$

where

$$\varphi(\hat{s}_p) = \frac{d \log p(\hat{s}_p)}{d\hat{s}_p} \quad . \tag{3.18}$$

As analytical computation of equation as mentioned above is difficult, this algorithm uses a gradient update rule based on the natural gradient $\frac{\partial \mathrm{MI}(\hat{\boldsymbol{s}})}{\partial \boldsymbol{W}} \boldsymbol{W}^T \boldsymbol{W}$ [253] and learning rate η that is a positive constant:

$$\boldsymbol{W} \leftarrow \boldsymbol{W} + \eta \Delta \boldsymbol{W}, \tag{3.19}$$

$$\begin{aligned}\Delta \boldsymbol{W} &= (\mathbb{E}[\boldsymbol{\varphi}(\hat{\boldsymbol{s}})\boldsymbol{x}^T] + (\boldsymbol{W}^T)^{-1})\boldsymbol{W}^T\boldsymbol{W} \\ &= (\mathbb{E}[\boldsymbol{\varphi}(\hat{\boldsymbol{s}})\hat{\boldsymbol{s}}^T] + \boldsymbol{I})\boldsymbol{W}. \end{aligned} \tag{3.20}$$

On every iteration, distribution of estimated signal $\varphi(\hat{s}_p)$ is appropriately changed to super-Gaussian or sub-Gaussian according to positive and negative of the fourth cumulant $c[\hat{s}_p^4] = \mathbb{E}[\hat{s}_p^4] - 3\mathbb{E}[\hat{s}_p^2]^2$ for each estimated signal, that is called extended InfoMax algorithm [254].

$$\varphi(\hat{\boldsymbol{s}}) = -\begin{pmatrix} \hat{s}_1 + \mathrm{sgn}(c[\hat{s}_1^4])\tanh(\hat{s}_1) \\ \vdots \\ \hat{s}_P + \mathrm{sgn}(c[\hat{s}_P^4])\tanh(\hat{s}_P) \end{pmatrix}. \tag{3.21}$$

Other Component Based Schemes

There are some component based schemes other than above-mentioned blind source separation schemes (e.g. multiple-source eye correction [100, 256], multivariate singular spectrum analysis [99], and singular spectrum analysis [257]) for eyeblink artifact removal. In this thesis, I do not, however, deal with these algorithms in detail because an assumption of each algorithm is rarely fulfilled in the context of EEG signal and consistency EEG signal processing is difficult in the presence of such complex signal.

3.1.3 Precautions in Using Source Separation Schemes

Component Identification after Source Separation

After source separation, the estimated sources $\hat{\boldsymbol{S}}$ have to be identified as artifactual or neuronal sources to reconstruct artifact-free EEG matrix $\hat{\boldsymbol{X}}$. Visual inspection (empirical judgement) of scalp topography was most confided in the identification of separated components [102, 114] since the distribution of eyeblink artifact on the head is well-known (see Table 1.1). The overused technique is still examined in an expedient manner for accuracy checking of identification results, but the user's workload increases. Therefore, hard/soft threshold, probability approach, and machine learning algorithm with features (e.g. correlation, mean power, standard deviation, maximum amplitude, kurtosis, skewness, auto mutual information, and so on) of the prepared material (e.g. resting state background rhythms or observed reference EOG signal) have been used for automatically identifying the ocular artifacts in estimated sources to reduce the workload and to get more repeatable label [232, 258–264]. However, eyeblink artifacts

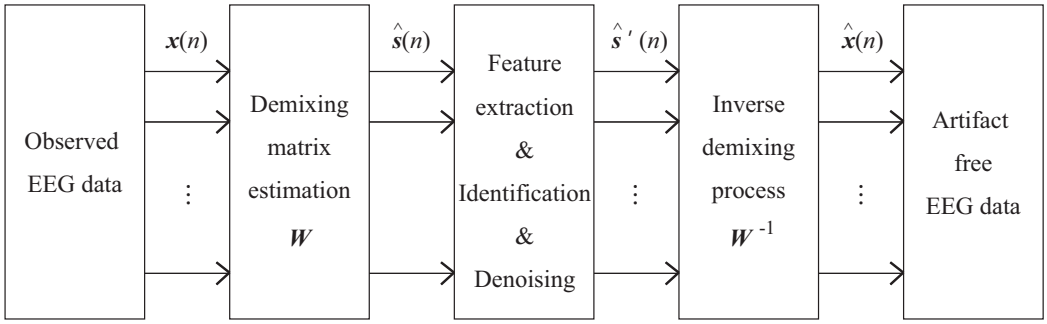

Figure 3.3 Block diagram of the blind source separation scheme adapted from the reference [259].

are allocated to one or more estimated sources, meaning that the identification steps are sometimes not able to accurately select the correct components. Also, the main drawback of these algorithms is that it is restricted to having the reference EOG channels (training data) which might not be usable if one would like to process previously obtained data.

Proposing automatic and unsupervised source identification algorithm that provides information concerning labelling more flexibly and accurately has been still an active research area [265–268]. Once the estimated source vectors $\hat{\boldsymbol{s}}(n)$ are identified, they advance to next step called denoising step, and then an underlying (non-artifact) EEG matrix $\hat{\boldsymbol{X}}$ would be obtained using inverse linear demixing process (see Figure 3.3).

Procedure for Denoising the Artifactual Components

In general, observed EOG signal is in turn contaminated by the EEG signal [90, 269]. Since the bidirectional relationship, spectral distortion is unavoidable in source separation process even if a researcher applied the ICA-based algorithm [258]. Researchers should give careful handling of the highlighted components and tease out the artifacts from the data on the denoising step. Currently, Discrete Wavelet Transform (DWT)-based denoising procedure composed of three stages, (see Figure 3.4) makes it increasingly being major [270, 271]. In the procedure, estimated signals $\hat{\boldsymbol{s}}$ are respectively decomposed into wavelet coefficients until level l. Furthermore, a wavelet coefficient which has a higher value than the threshold T will be set to 0. In consequence, artifact-free ICs $\hat{\boldsymbol{s}}'$ are reconstructed from the thresholded wavelet coefficients $W'(l,k)$ via inverse DWT.

If all values of the wavelet coefficients at l-th level dip below the threshold on the second step, the operator should choose an alternative approach: non-processing or polishing. These approaches are assigned to hard and soft thresholding operators.

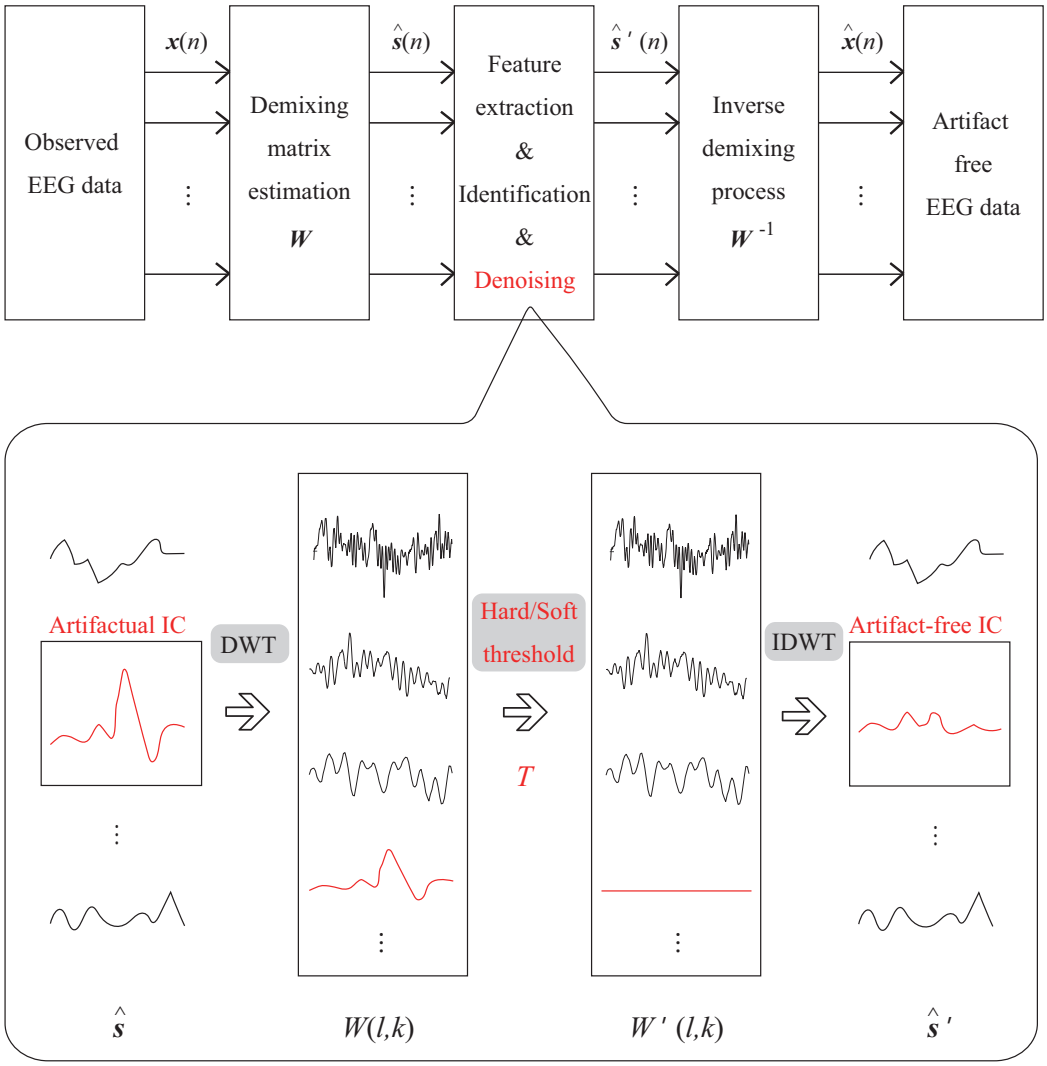

Figure 3.4 Discrete wavelet transform based denoising procedure.

They are respectively defined by:

$$W'(l,k) = \begin{cases} 0\,, & (|W(l,k)| > T) \\ W(l,k), & (|W(l,k)| \leq T) \end{cases} \tag{3.22}$$

and

$$W'(l,k) = \begin{cases} 0\,, & (|W(l,k)| > T) \\ \mathrm{sgn}(W(l,k))(|W(l,k)| - T), & (|W(l,k)| \leq T) \end{cases} \tag{3.23}$$

where $W(l,k)$ and l denote wavelet representation of p-th estimated signal $\hat{s}_p(n)$ and temporal localization at the level. Soft thresholding operator decreases signal quality as its indefiniteness [272]; therefore, I apply a hard threshold for denoising procedure.

3.2 In Single-channel Recordings

3.2.1 Separation Scheme Using Regression

Regression algorithm was most frequently used to remove eyeblink artifact up to the mid 1990s. In this algorithm, an observed signal $x(n)$ can be expressed as

$$x(n) = x_{\mathrm{EEG}}(n) + x_{\mathrm{EA}}(n) + d(n), \tag{3.24}$$

where, $x_{\mathrm{EEG}}(n)$, $x_{\mathrm{EA}}(n)$, and $d(n)$ are intrinsic (unknown) EEG data, eyeblink artifact, and noise, respectively. It is assumed that the expected value of $d(n)$ is 0, and $x_{\mathrm{EA}}(n)$ is a constant scaled value of the observed VEOG signal ($x_{\mathrm{EA}}(n) = C(x_{\mathrm{VEOG}}(n))$).

The artifact would be corrected by calculating propagation factors and subtracting the regressed portion between one or more reference VEOG channels and observed EEG signal [113, 119]. The rationale of the procedure is follows:

1) Separately average over observed EEG and VEOG signals of T trials to estimate the eyeblink related variation for the EEG and VEOG-channels:

$$\bar{x}(n) = \frac{1}{T}\sum_{t=1}^{T} x_t(n), \tag{3.25}$$

2) Subtract the averages from every single trial data to obtain deviations:

$$\boldsymbol{x}'(n) = \boldsymbol{x}(n) - \bar{\boldsymbol{x}}(n), \tag{3.26}$$

where $\bar{\boldsymbol{x}}(n)$ is duplicated $T \times 1$ matrix of the observed EEG average,

3) Calculate the propagation factor C by linear least-square regression, whereby the observed EEG data are considered as a dependent variable and the VEOG data are considered as the independent variable:

$$\boldsymbol{X} = C(\boldsymbol{X}_{\mathrm{VEOG}}), \tag{3.27}$$

where

$$\boldsymbol{X} = [\boldsymbol{x}'(1), \ldots, \boldsymbol{x}'(t), \ldots, \boldsymbol{x}'(T)]^T, \tag{3.28}$$

$$\boldsymbol{x}'(t) = [x'(1 + N(t-1)), \ldots, x'(tN)], \tag{3.29}$$

4) Correct the observed EEG data by subtracting the EOG data scaled by the propagation factor C:

$$\hat{\boldsymbol{x}}(n) = \boldsymbol{x}(n) - C(\boldsymbol{x}_{\mathrm{VEOG}}(n)). \tag{3.30}$$

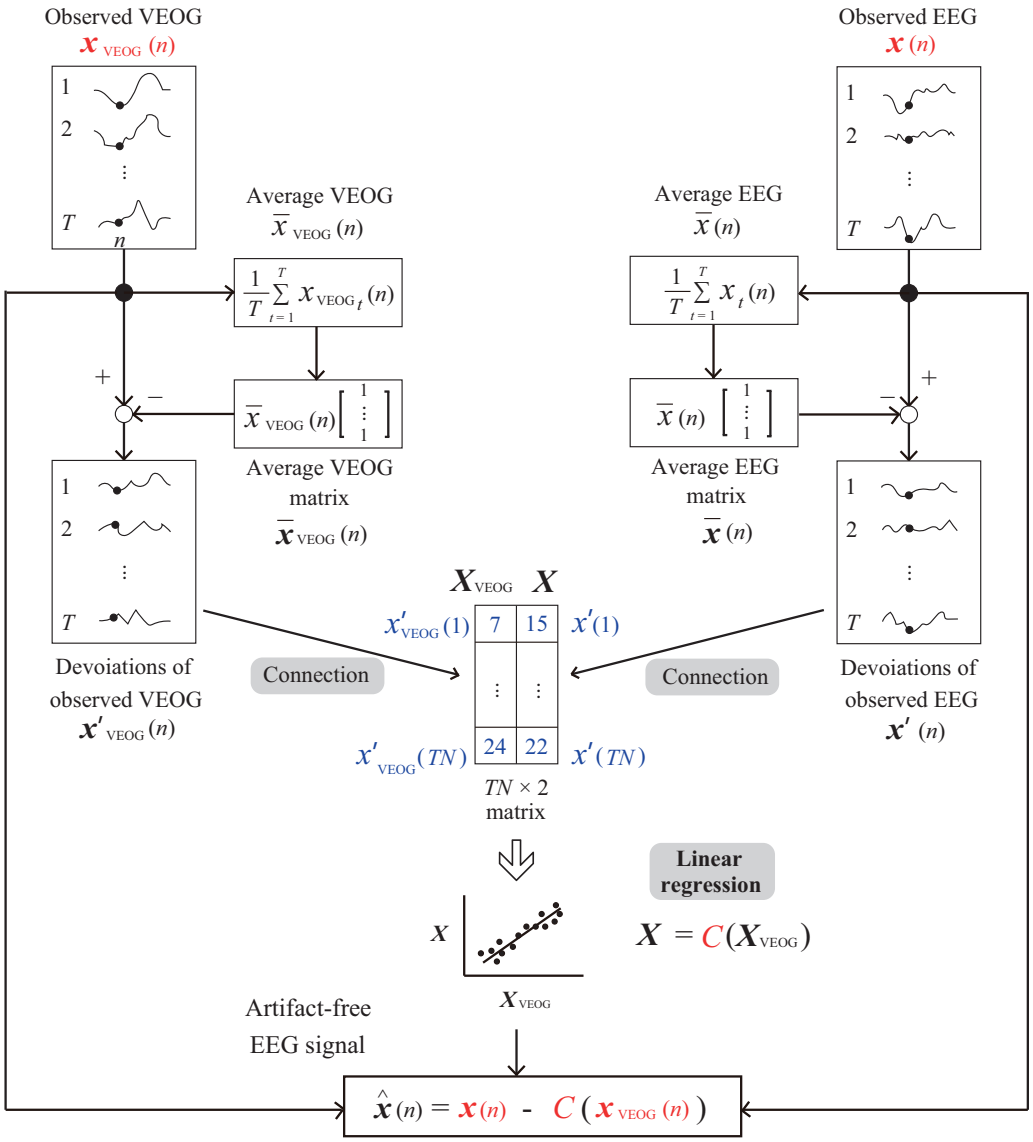

Figure 3.5 Schematic representation of the regression procedure.

This scheme, separately calculates a scaling value for each subject, requires an observed reference EOG channel and is only powerful when the operating system treats event-related brain potentials because averaging operator emphasizes a time-locked activity in observed signals. Although expanded algorithms of regression had been provided [273, 274], cerebral activities are usually not time-locked. Thus, important nontime-locked components might be lost by the averaging operation. Moreover, this scheme does not take bidirectional contamination, which refers to neuronal activities being invaded in the observed EOG signal, into account and cancels the cerebral information from the each observed EEG signal upon linear subtraction [214].

Despite its drawbacks described above, regression is still used as the 'gold-standard' scheme to which the performance of any artifact removal algorithms may be compared.

The schematic representation of the regression procedure in the time domain is described in Figure 3.5.

3.2.2 Separation Scheme Using Filtering

Band-pass or High-pass Filtering

Band-pass or high-pass filtering represents one of the classical separation attempts to remove artifacts from an observed EEG signal. This scheme is effective when the spectral distributions of the EEG signal and artifact do not overlap, and there are small band artifacts like power line noise (50 or 60 Hz interference) into observed EEG signal [275]. However, the overlapping frequency spectra between EEG and eyeblink artifact have been reported [69,71], so fixed filtering is not effective for eyeblink artifact removal as it will attenuate EEG component in theta and delta band and change both amplitude and phase of each frequency signals if the filtering keeps doing that [276]. Some alternative algorithms such as adaptive filtering try to adapt the filter parameters $\boldsymbol{w}$ to minimize the error between the artifact-free EEG signal $\hat{\boldsymbol{x}}(n)$ and the desired original signal $\boldsymbol{x}(n)$ to suppress the limitations of this scheme. They are sometimes employed in the removal of eyeblink artifacts from single-channel EEG signals.

Adaptive Filtering

Adaptive filtering assumes that the intrinsic EEG signal and artifact are uncorrelated; therefore, the artifact is considered to be an additive noise within the observed EEG signal.

$$x_t(n) = s_t(n) + n_{0_t}(n), \tag{3.31}$$

where $x_t(n)$ is the corrupted EEG signal of t-th trial, $n_0(n)$ is the additive noise to offset and is uncorrelated with intrinsic EEG signal $s_t(n)$. To achieve optimal filtering, the filter parameters $\boldsymbol{w}(n)$ are iteratively adjusted by a feedback process designed to make the output $\hat{\boldsymbol{x}}(n)$ as close as possible to some desired response with an additive noise interference (a reference) [277, 278]. Figure 3.6 shows the noise canceller system using adaptive filtering. In the system, the primary input $x_t(n)$ and the reference input $x_{\mathrm{VEOG}_t}(n)$ are the observed EEG and VEOG signals. A reference input $x_{\mathrm{VEOG}_t}(n) = n_{1_t}(n)$ which is a noise correlated with $n_{0_t}(n)$ and uncorrelated with intrinsic EEG signal $s_t(n)$.

Least Mean Squares (LMS) or Recursive Least Squares (RLS) method [279] is usually selected as an adaptive algorithm to minimize the error $e_t(n)$ between the response

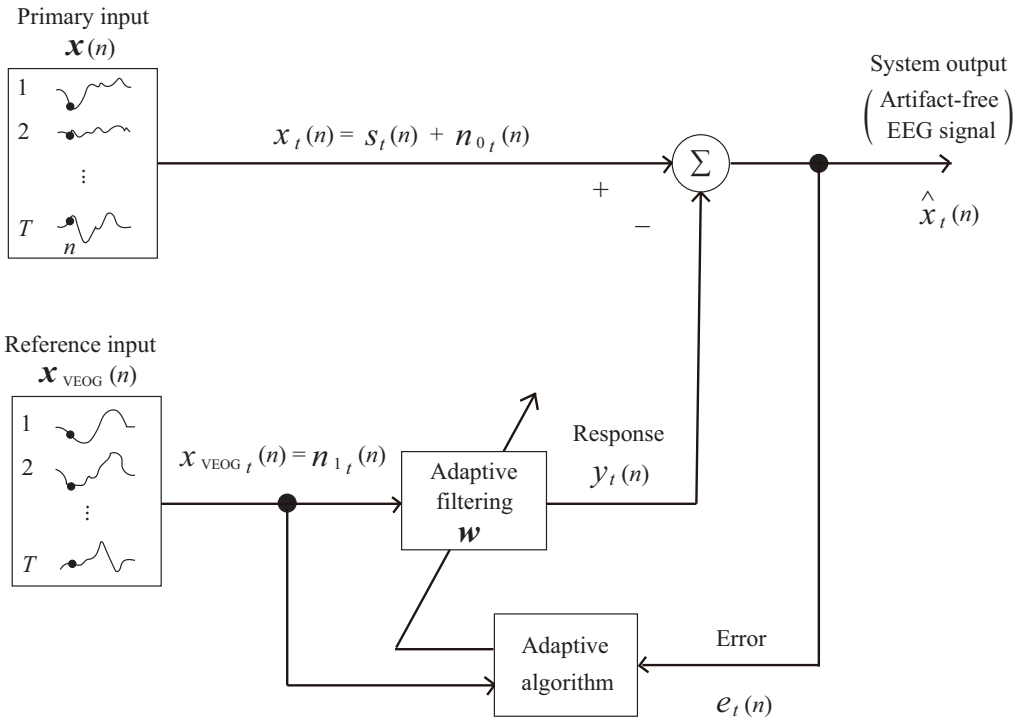

Figure 3.6 Noise canceller system using adaptive filtering modified from the reference [280].

$y_t(n)$ and the desired response. In many cases, RLS-based adaptive filtering presents a superior performance at removing eyeblink artifacts from observed EEG signals [115, 280]. The algorithm can be implemented using the following equations:

$$\boldsymbol{g}(n) = \frac{\boldsymbol{R}(n-1)\boldsymbol{x}_{\mathrm{VEOG}}(n)}{\lambda + \boldsymbol{x}_{\mathrm{VEOG}}{}^{T}(n)\boldsymbol{R}(n-1)\boldsymbol{x}_{\mathrm{VEOG}}(n)} , \tag{3.32}$$

$$\boldsymbol{e}(n) = \boldsymbol{x}(n) - \boldsymbol{y}(n), \tag{3.33}$$

$$\boldsymbol{y}(n) = \boldsymbol{w}(n)\boldsymbol{x}_{\mathrm{VEOG}}(n), \tag{3.34}$$

$$\boldsymbol{R}(n) = \frac{\boldsymbol{R}(n-1) - \boldsymbol{g}(n)\boldsymbol{x}_{\mathrm{VEOG}}{}^{T}(n)\boldsymbol{R}(n-1)}{\lambda} , \tag{3.35}$$

$$\boldsymbol{w}(n) = \boldsymbol{w}(n-1) + \boldsymbol{g}(n)\boldsymbol{e}(n), \tag{3.36}$$

where $\boldsymbol{g}(n)$ and $\boldsymbol{w}(n)$ are the gain vector and the filtering parameters. The initial value of cross-correlation $\boldsymbol{R}(0)$ is $\delta\boldsymbol{I}$, where δ and $\boldsymbol{I}$ are some sufficiently large positive value and identity matrix. In this thesis, the value of δ is set to 10^4. The updated filter parameters $\boldsymbol{w}(n)$ lead to output artifact-free EEG signal $\hat{\boldsymbol{x}}(n)$. The order of adaptive

finite impulse response filter M and forgetting factor λ have profound effect on the filter's performance [281]. This algorithm with M and λ will be set as 1 and 0.43 to 0.995, respectively.

Consequently, adaptive filtering scheme has a potential to recover 'pure' EEG signal more fastly and accurately than linear regression [282]. However, these algorithms have limited success because separation of overlapping frequency components is getting nowhere. Furthermore, the performance depends on the choice of the reference input which is perfectly synchronized with desired response. That means this alternative filtering scheme needs reference input channel simultaneously during EEG recording.

3.2.3 Separation Scheme Using Multi-components

When the number of independent sources is equal to or lower than observation signals, ICA will achieve an eyeblink artifact removal with a remarkable performance. Unfortunately, this scheme is only applicable to multi-channel signals; however, some of the research extended the idea to single-channel signal to unmix a set of observed signal-channel EEG signals into intrinsic sources [116, 283, 284]. These schemes decompose a single-channel signal into multiple components by dividing into a sequence of blocks or different spectral modes (see Figure 3.7).

Single-channel Independent Component Analysis

Single-channel ICA is the oldest scheme according to the idea of multi-components in a single-channel signal [107]. Before applying ICA algorithm, an observed signal $x(n)$ is broken up into K short segments $\boldsymbol{X}$, a sequence of contiguous blocks of length L, which is to be treated as a set of observations $\boldsymbol{x}(n)$.

$$\boldsymbol{X} = [\boldsymbol{x}(1), \ldots, \boldsymbol{x}(k), \ldots, \boldsymbol{x}(K)]^T, \tag{3.37}$$

$$\boldsymbol{x}(k) = [x(L(k-1)+1), \ldots, x(kL)]^T, \tag{3.38}$$

where k is the block index. A standard ICA algorithm then performs to the matrix $\boldsymbol{X}$ to derive the demixing matrix $\boldsymbol{W}$.

It is worth to note that the performance of this scheme significantly depends on heretofore described parameters. Removing interference spectrum of eyeblink artifact by this scheme is all but impossible because this scheme assumes stationary sources are being disjoint in the frequency domain whereas the artifact components overlap

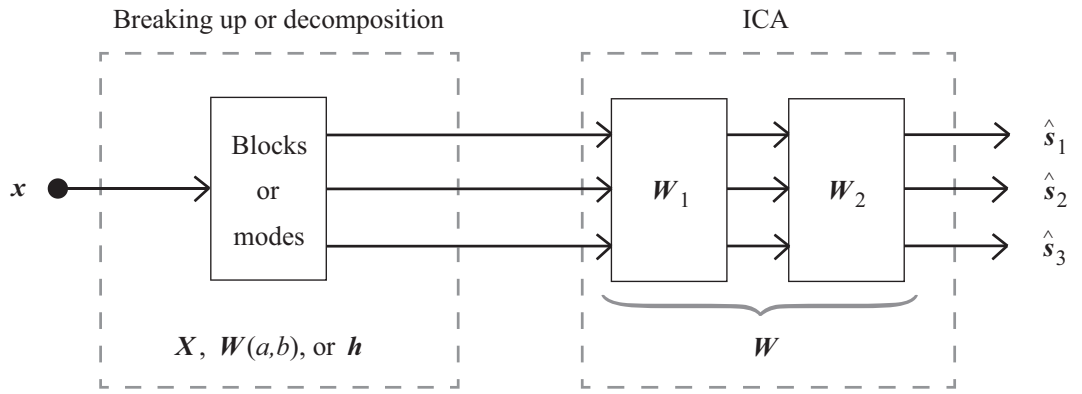

Figure 3.7 Concept of separation scheme using multi-components.

with EEG components largely, and EEG signal has non-periodic components [116]. Many schemes: Wavelet-ICA (WICA), Empirical Mode Decomposition (EMD)-ICA, and Ensemble EMD (EEMD)-ICA, and Complete EEMD (CEEMD)-ICA have already been reported successful in removing artifacts for solving the similar problem than this scheme [66, 275]. Therefore, I am not going to handle this scheme as a rival plan.

Wavelet Transform-Based Independent Component Analysis

In WICA algorithm, a single-channel EEG signal $x(n)$ is transformed into components of disjoint spectra (a matrix) instead of signal (a vector) via DWT [285, 286].

$$W(a,b) = \frac{1}{\sqrt{a}} \int x(n)\psi_{a,b}(n)dn, \tag{3.39}$$

$$\psi_{a,b} = \psi(\frac{n-b}{a}), \tag{3.40}$$

where $W(a,b)$ and $\psi_{a,b}$ denote the wavelet representation of $x(n)$ and the mother wavelet, respectively, with a and b defining the time-scale and location.

Before applying ICA algorithm, mother wavelet and order of the wavelet transform have to be selected. For this thesis, the mother wavelet and order of decompositions were set to Daubechies 7 and 5, implemented using $db7$ in the $liftwave$ function of Matlab. The decision of parameters is hard if the user does not have a priori knowledge of the signal of interest. Each IC is respectively characterized as either neuronal or artifactual by manually. The artifactual ICs are replaced its values with an array of zeros and then reconstructed to wavelet components. Finally, single-channel artifact-free signals are acquired by Inverse DWT (IDWT).

Empirical Mode Decomposition-Based Independent Component Analysis

The EMD-based scheme is data-driven and adaptive to non-linear and non-stationary signal decomposition, so the scheme can remove artifacts without a prior knowledge regarding characteristics of the signal embedded in the data before EEG analysis [287, 288]. In EMD-ICA algorithm, a single-channel EEG signal $x(n)$ is decomposed into a number of K Intrinsic Mode Functions (IMFs) $h_k(n)$,

$$x(n) = \sum_{k=1}^{K} h_k(n) + d(n) \;\; (1 \leq k \leq K), \tag{3.41}$$

where $d(n)$ is a residue of the original signal and a nonzero-mean slowly varying function with only a few or no extreme [287]. Each IMF has monocomponent of the original signal and is estimated by an iterative process called "shifting process" in accordance with the following steps:

1. Find the local maxima and minima in $x_k(n)$,
2. Connect all of the local maxima and minima by cubic splines to form an upper and a lower envelope separately,
3. Calculate the mean of the two envelopes, respectively,
4. Obtain improved IMF $h_{k+1}(n)$ by subtracting the mean of the two envelopes from the current IMF $h_k(n)$,
5. Go to step 1 until the residue is below a stopping criterion.

This process must be done under three conditions: (i) the number of extreme and the number of zero-crossing must be equal or up to plus/minus one; (ii) zero mean; and (iii) all the maxima and all the minima of IMF will be positive and negative everywhere. A stopping criterion proposed in original EMD is used.

Artifactual ICs are manually characterized after applying ICA algorithm; then the ICs have replaced its values with an array of zeros. Reconstructed IMFs are summed simply together to obtain single-channel artifact-free signals.

However, the performance of EMD-based scheme depends on the relation between the first derivation of envelope described by local extremum points on one side and the multiplication of envelope by the instantaneous frequency on the other side [289]. A presence of similar oscillations in different modes or a presence of disparate amplitude oscillations in the same mode, named "mode mixing" makes the performance of artifact rejection worse [290]. EEMD is an extended algorithm of EMD to obtain more robust features without mode mixing [291]. The algorithm defines the "true" IMFs $\bar{h}_k(n)$ as the mean of the corresponding IMFs obtained from original EMD over an ensemble of trials, and adds the original signal to independent, identically distributed white Gaussian noise. Noisy components are expected to be cancelled out by properties of

the white noise. EEMD algorithm can be described by the following steps:

1. Make added noise signals $x^i(n) = x(n) + \epsilon w^i(n)$, where $w^i(n)$ $(i = 1, \ldots, I)$ are different realizations of white Gaussian noise calculated from finite variance to the original signal $x(n)$,
2. Decompose each $x^i(n)$ into their modes ${h_k}^i(n)$,
3. Average over the ensemble to obtain a set of averaged IMFs ("true" IMFs):

$$\bar{h}_k(n) = \frac{1}{I}\sum_{i=1}^{I} {h_k}^i(n). \tag{3.42}$$

The noise scaling factor and the ensemble size were set as 0.2 and 500 by referring to the reference [292]. The subsequent processing is same to EMD-ICA.

CEEMD-ICA is newest scheme in EMD-based schemes [293]. This scheme can successfully decompose original signal into modes with less than half of the shifting iteration that EEMD does by the following steps:

1. Make signals $x^i(n) = x(n) + \epsilon_0 w^i(n)$,
2. Decompose each noise added signal $x^i(n)$ into their first modes ${h_1}^i(n)$,
3. Average over the ensemble to obtain first averaged IMF:

$$\tilde{h}_1(n) = \frac{1}{I}\sum_{i=1}^{I} {h_1}^i(n) = \bar{h}_1(n), \tag{3.43}$$

4. Calculate the first residue:

$$d_1(n) = x(n) - \tilde{h}_1(n), \tag{3.44}$$

5. Decompose realizations $d_1(n) + \epsilon_1 \mathbb{E}_1[w^i(n)]$, where $\mathbb{E}_k[\cdot]$ indicates realizations of white Gaussian noise calculated from finite variance to the k-th mode by EMD until their first mode, and define the mode:

$$\tilde{h}_2(n) = \frac{1}{I}\sum_{i=1}^{I} \mathbb{E}_1[d_1(n) + \epsilon_1 \mathbb{E}_1[w^i(n)]], \tag{3.45}$$

6. Calculate the k-th residue:

$$d_k(n) = x(n) - \tilde{h}_k(n), \tag{3.46}$$

7. Decompose realizations $d_k(n) + \epsilon_k \mathbb{E}_k[w^i(n)]$ until their first mode, and define the mode:

$$\tilde{h}_{k+1}(n) = \frac{1}{I}\sum_{i=1}^{I} \mathbb{E}_1[d_k(n) + \epsilon_k \mathbb{E}_k[w^i(n)]], \tag{3.47}$$

8. Go to step 6 until residue is below a stopping criterion.

The final residue satisfies:

$$D(n) = x(n) - \sum_{k=1}^{K} \tilde{h}_k(n), \tag{3.48}$$

where K is the total number of modes. Finally, the single-channel EEG signal is decomposed into K modes.

$$x(n) = \sum_{k=1}^{K} \tilde{h}_k(n) + D(n). \tag{3.49}$$

The noise scaling factor on the first mode ϵ_0 and the ensemble size I were also set as 0.2 and 500 which are same condition of EEMD. In CEEMD, the value of noise scaling factor since second mode depends on residue at each stage.

3.2.4 Inconsistent Relationship between Assumption in Above Mentioned Algorithms and Real Data

The suspicion, an algorithm erroneously decomposes a single-channel signal into multi-components in the first place is concerned about signal distortion. Avoiding excessive interference (neuronal information should be retained, and no distortion should be caused) from an artifact removal algorithm is desirable to keep as much of the observed signal as possible [294]. Above mentioned separation algorithms, linear regression, and filtering do not explicitly solve the problem because there is no constraint on an observed signal that has overlapped property in its component. That implies that parameters $\boldsymbol{W}$ cannot converge to a solution for perfectly demixing the mixtures without partially restricting the active space when single-channel signals are the target. However, it is not possible to capture the morphological properties of the brain activities regarding amplitude and duration. Thus, a stochastic process is needed for treating EEG data, even if some properties of the data have been already known [295].

3.2.5 Separation Scheme Using Matrix Factorization

Matrix Factorization (MF) techniques have recently attracted attention as effective algorithms to remove artifacts from single-channel signals because they can find the latent features underlying the interactions between EEG components and artifacts. Non-negative Matrix Factorization (NMF) is one of the MF techniques as it can additively

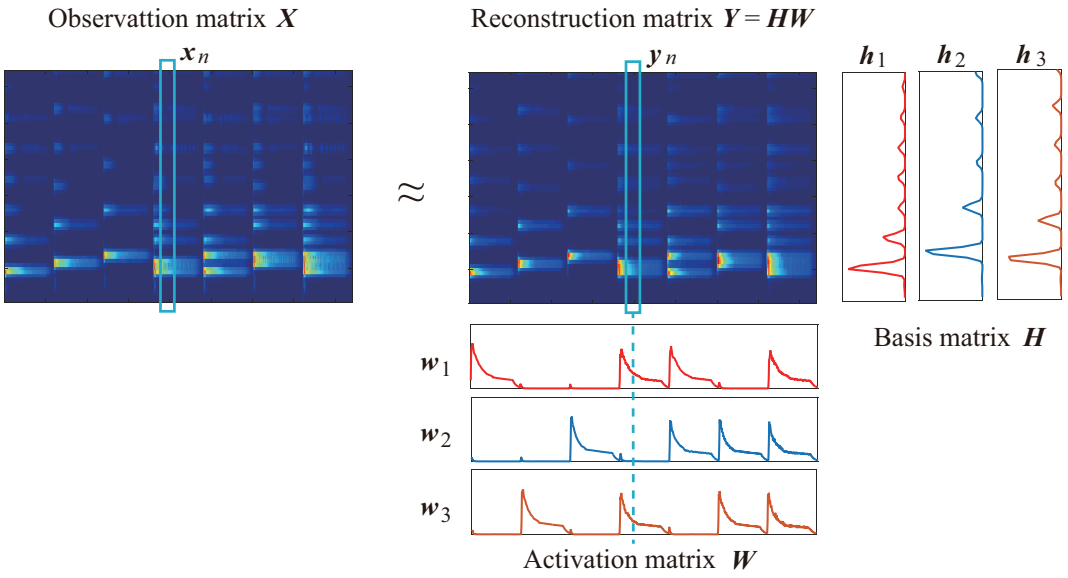

Figure 3.8 Observation matrix $\boldsymbol{X}$ and reconstruction matrix $\boldsymbol{Y}$. The matrix $\boldsymbol{X}$ was approximately factorized into three basis vectors $\boldsymbol{h}$ and three activation vectors $\boldsymbol{w}$ by NMF.

factorize non-negative matrix (e.g. power spectrum) $\boldsymbol{X}$ based on Short-Time Fourier Transform (STFT) to two non-negative matrices, basis $\boldsymbol{H}$ and activation $\boldsymbol{W}$ [296–298]. The NMF has been used in many situations, for example, the automatic transcription [299], the sound emphasis or separation [300], and the band spreading [301]. This method also has been used for EEG feature extraction for classification [302]. An M-dimensional non-negative data vector $\boldsymbol{x}_n$ is placed in the columns of $M \times N$ matrix $\boldsymbol{X}$ where N is number of data vectors in the dataset. $\boldsymbol{x}_n$ is called an observation vector. The matrix $\boldsymbol{X}$ is approximately factorized into an $M \times K$ non-negative matrix $\boldsymbol{H}$ and a $K \times N$ non-negative matrix $\boldsymbol{W}$ where K is the number of "basis" which is optimized for linear approximation of the observation vectors (Figure 3.8). It can be given by following equation:

$$\boldsymbol{x}_n \approx \boldsymbol{y}_n = \sum_{k=1}^{K} \boldsymbol{h}_k w_{k,n}, \quad (n = 1, \cdots, N) \tag{3.50}$$

where an $\boldsymbol{h}_k$ and a $w_{k,n}$ denote an entry of $\boldsymbol{H}$ and $\boldsymbol{W}$, respectively. In other words, respective non-negative EEG feature vector $\boldsymbol{x}_n$ is approximated by linear combination of the basis vector $\boldsymbol{h}_k$ weighted by the component of $w_{k,n}$. Therefore, it can be rewritten by following equation:

$$\boldsymbol{X} \approx \boldsymbol{H}\boldsymbol{W}. \tag{3.51}$$

For finding an approximate factorization, iterative algorithms that quantify the quality of approximation will be designed. The iterative algorithms can be given by some measures of approximations between two non-negative matrices. This measure is not

called "distance" if it is asymmetric. Such measure is referred to as the "divergence" [297]. There are various kinds of distance and divergence used in the NMF, for example, the EUclidean (EU) distance, the Kullback-Leibler (KL) divergence, and the Itakura-Saito (IS) divergence. In the case of NMF, these measures can be written as

$$D.(\boldsymbol{X}, \boldsymbol{HW}) = \sum_{m,n} D.(x_{m,n}|h_{m,k}w_{k,n}), \tag{3.52}$$

where $D.$ denotes the kinds of algorithms, EU, KL, and IS divergences. In this thesis, I select the IS divergence for the measure of an approximation since this divergence is designed for the factorization of the power spectrum [303]. The iterative algorithm of the IS divergence repeats the following multiplicative update rules.

$$h_{m,k} \leftarrow h_{m,k} \left(\frac{\sum_n x_{m,n} w_{k,n} / y_{m,n}^2}{\sum_n w_{k,n} / y_{m,n}} \right)^{1/2}, \tag{3.53}$$

$$w_{k,n} \leftarrow w_{k,n} \left(\frac{\sum_m x_{m,n} h_{m,k} / y_{m,n}^2}{\sum_m h_{m,k} / y_{m,n}} \right)^{1/2}, \tag{3.54}$$

where

$$y_{m,n} = \sum_k h_{m,k} w_{k,n}. \tag{3.55}$$

If the basis matrix $\boldsymbol{H}$ finds the structure that is latent in the data, the dimension of $\boldsymbol{H}$ will be smaller than the dimensions of $\boldsymbol{X}$. Finding the structure can be said that proper factorization is achieved. Therefore, the basis number K should be determined less than the half of M when an NMF algorithm is used for getting the valid basis.

Damon et al. proposed an eyeblink artifact reduction method based on NMF [304]. They reported that the NMF could effectively decompose the recorded EEG signals into the brain activity components and the artifacts. However, NMF is one of unsupervised learning scheme and is based on some degree of arbitrariness while making bases. Besides, automatic identification of bases is impossible by standard NMF algorithm.

Subsequently, an eyeblink artifact removal scheme based on supervised NMF named 2-step NMF was proposed [117]. For supervised learning, template matrix $\boldsymbol{X}_{\mathrm{EA}}$ comprised of eyeblink artifact estimated by ICA with multi-channel signals has previously been factorized into two nonnegative matrices $\boldsymbol{H}_{\mathrm{EA}}$ and $\boldsymbol{W}_1$. In the second step, the matrix of the observed single-channel EEG signals $\boldsymbol{X}_r$ is factorized into two nonnegative matrices $\boldsymbol{H}_{\mathrm{all}}$ and $\boldsymbol{W}_2$ where $\boldsymbol{H}_{\mathrm{all}}$ contains $\boldsymbol{H}_{\mathrm{EA}}$ and $\boldsymbol{H}_{\mathrm{EEG}}$. The elements of matrix $\boldsymbol{H}_{\mathrm{EA}}$ usually have no relation to the elements of matrix $\boldsymbol{H}_{\mathrm{all}}$ because the initial values are set randomly and updated by multiplicative update rules. In this algorithm, the matrix $\boldsymbol{H}_{\mathrm{EA}}$ is used as a fixed value. By contrast, activation components $\boldsymbol{W}_1$ are a variable value. For this constraint, the matrix $\boldsymbol{H}_{\mathrm{all}}$ can attempt to express EEG

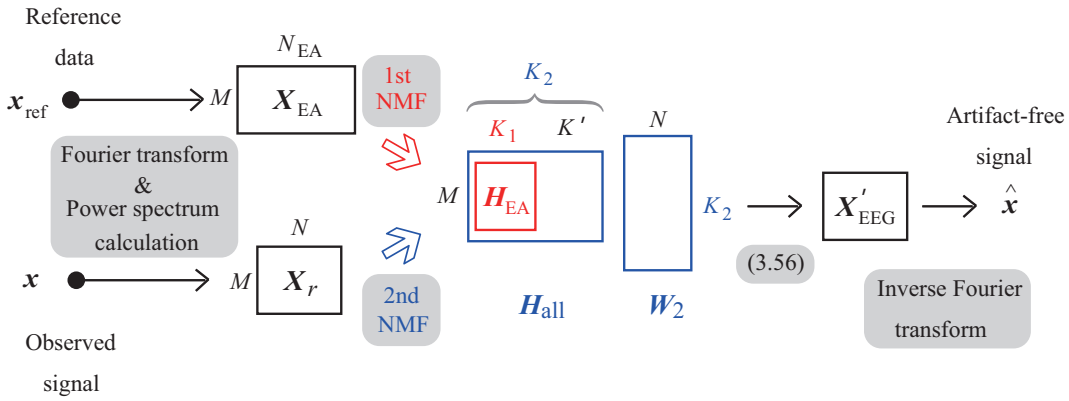

Figure 3.9 2-step NMF algorithm for eye-blink artifact removal using single-channel EEG signals.

components in the matrix $\boldsymbol{X}_r$ using the remaining bases K' ($K' = K_2 - K_1$). EEG components are stored in the bases (Figure 3.9).

After these processing, power spectrum data of artifact-free EEG and estimated eye-blink artifact are reconstructed from the following equations:

$$\boldsymbol{X}'_{EEG} = \boldsymbol{X}_r * \sum_{k=K_1+1}^{K_2} \sum_{n=1}^{N} \frac{\boldsymbol{H}_{\text{all}k} W_{2k,n}}{\boldsymbol{H}_{\text{all}} \boldsymbol{W}_2} \quad , \tag{3.56}$$

$$\boldsymbol{X}'_{EA} = \boldsymbol{X}_r * \sum_{k=1}^{K_1} \sum_{n=1}^{N} \frac{\boldsymbol{H}_{\text{all}k} W_{2k,n}}{\boldsymbol{H}_{\text{all}} \boldsymbol{W}_2} \quad . \tag{3.57}$$

Eq. (3.56) and inverse Fourier transform make it possible to reconstruct the artifact-free signal with recorded signal.

3.2.6 Precautions in Using Matrix Factorization Algorithms

Regression, filtering, and separation algorithms intend to separate entire data thoroughly. MF algorithm can ignore time segments where an artifact is not present because this technique is epoch-based. Supervised MF algorithm is still in its infancy, showed the best performance in the eyeblink artifact removal schemes. However, epoch detection step that is not part of normal procedures in the eyeblink artifact removal should be embedded in the epoch-based scheme. That leads to increasing the computational cost inevitably. Existing some low cost (real-time) artifact detection algorithm for single-channel EEG [305, 306], is a silver lining in a dark cloud.

NMF has an excellent performance and is a major scheme for matrix factorization problem to find an approximate factorization of input data $\boldsymbol{X}$. On the other hand, this algorithm has a constraint that all elements of $\boldsymbol{A}$ and $\boldsymbol{B}$ where $\boldsymbol{A} \in \mathbb{R}^{M \times K}$ and $\boldsymbol{B} \in$

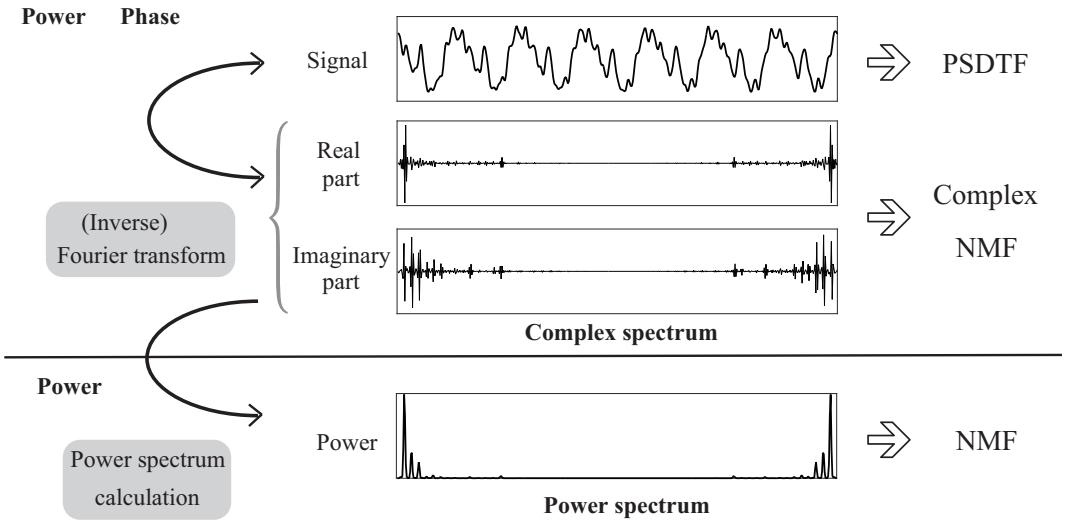

Figure 3.10 Information amount of the data in each MF technique.

$\mathbb{R}^{K\times N}$ ($K \ll \min\{M, N\}$) must be no less zero. This restriction reflects some physical quantities whose value can not be negative such as signal energy, pixel brightness, and power spectrogram, however, the algorithm entails spectrogram for MF of the single-channel mixture. In other words, observed signals have to be transformed to the frequency domain for creating M frequency bins and N frames of a dataset. All goes well if the system continues its process in the frequency domain; however, consistent signal reconstruction from factorized matrices is hard when researchers apply NMF (Figure 3.10). Proposing a scheme which can extract recurrent patterns of time-series input data in the complex spectrum domain or in the time domain is an essential issue to reduce computational cost and provide a new means elucidating the mechanism of brain activities. It is ongoingly essential issue to sparsely represent co-occurring components by fewer bases because the appropriate basis number is unknown in the case of EEG analysis. On both now and in the future, an algorithm that automatically finds optimal basis number or avoids relying on the number while the MF techniques perform, has been required regardless of the research field.

In the last two decades, NMF has steadily germinated and begun to improve or extend its model because of its straightforward and robust model [307–315]. Various NMF techniques that directly decompose input data in the complex spectrum domain such as complex NMF [316] as a typical example had already been proposed. Based on the NMF algorithm, Positive Semi-Definite Tensor Factorization (PSDTF) has been devised during recent years. This algorithm is a variant of tensor factorization (canonical polyadic decomposition) using Bregman matrix divergence and factorizes autocovariance matrix $\boldsymbol{X} \in \mathbb{R}^{M\times M\times N}$ which is Positive Semi-Definite (PSD) matrix. PSDTF decomposes N PSD matrices (a tensor)as a conic sums of K PSD matrices in time domain [317]. The image of NMF and PSDTF is shown in Figure 3.11. The detail of

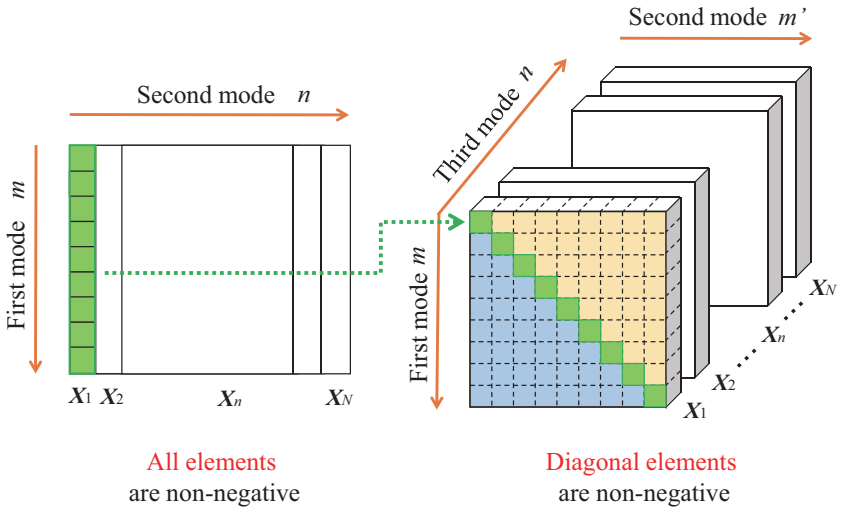

Figure 3.11 Datasets for employing NMF (left) and PSDTF (right) modified from the reference [318].

PSDTF will be described in Chapter 5.

Whenever you extract a signal from mixtures, an input of supervised space helps to converge to the solution. If the supervised space is close to a true value of the desired signal, you will obtain the signal you want from the mixtures. Let us now turn the attention to the three eyeblink types: (i) voluntary, (ii) involuntary, and (iii) reflex. Whereas each generation process is different, voluntary and reflex eyeblink show a correlation of over 0.9 [190]. However, the most supervised (reference or template-based) scheme considers only voluntary eyeblink as the target. On the real environment, one dilemma by all researcher and user, when trying to remove eyeblink artifact from the observed signal, is a lack of diffuseness for eyeblink types because what type of eyeblink will be occurred by the user is unknown. No matter how an algorithm shows excellent performance, it is not practicable when a priori hypothesis is wrong. I have to say this wrong hypothesis shows existing supervised schemes are slacking off their efforts as an eyeblink artifact removal scheme.

Meanwhile, proposed algorithms are presently evaluated using simulated data in many cases, and therefore, the quality of the conclusions depends on the contingent on the fidelity of the dataset that contains artifact epoch of one or two seconds. My intuition based on my knowledge and experience appeals a suspicion that the length of artifact is not one or two seconds but longer. Without knowledge of eyeblink artifact, it is not possible to accurately determine the efficacy of a proposed artifact removal scheme. Under such background, I will assess the effects of voluntary and involuntary eyeblinks in EEG for robust template making.

Chapter 4

ASSESSING THE EFFECTS OF VOLUNTARY AND INVOLUNTARY EYEBLINK IN INDEPENDENT COMPONENTS OF ELECTROENCEPHALOGRAM

4.1 Introduction and Objectives

A single-channel EEG device is supposed to result in better practical EEG applications in daily life. The beneficialness of eyeblink artifact removal for EEG applications has already been described in Chapter 1. To avoid inconsistency in separating components of a single-channel EEG signal that has overlapping frequency components, the reference data helps experimental data to converge to the values of estimated sources in the supervised learning schemes. However, most supervised learning schemes consider only voluntary eyeblink. The presence of involuntary eyeblink artifacts in the target signal leads to a distorted signal after applying the supervised scheme, because the reference is usually based only on voluntary eyeblink data. Although several kinds of literature have analyzed the pattern of eyeblink artifacts to develop eyeblink artifact removal schemes for multichannel EEG signals, the effect of involuntary eyeblinks on scalp EEG signals is still missing [104, 120–122].

In this chapter, I investigate the plausible effects of voluntary and involuntary eyeblinks on scalp EEG signals using multi-channel ICA. Investigation of eyeblink artifacts under voluntary and involuntary control lead to development of more robust and more common references or training datasets based on the representative attributes for a single-channel EEG analysis. Since recent studies have suggested wavelet-enhanced ICA algorithm is suitable for separating EEG signals into cerebral and non-cerebral sources [319], I employ this method.

The objective of this chapter is to characterize the effects of voluntary and involuntary eyeblinks on ICs contributing to EEG signals by wavelet-enhanced ICA to create templates for eyeblink artifact removal from an observed EEG signal with a single-electrode.

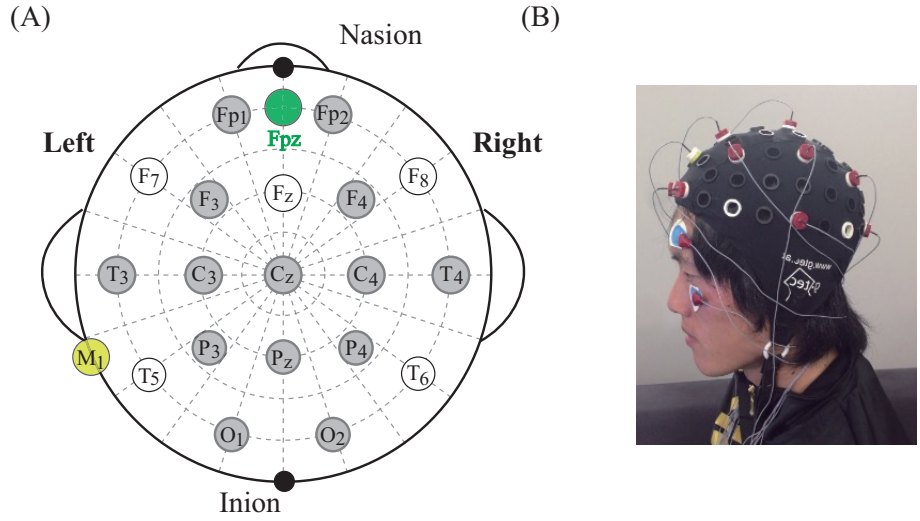

Figure 4.1 (A) Measurement (gray circle), reference (yellow circle), and ground (green circle) positions for EEG signals in this study. (B) A subject who equips g.tec according to placement order of (A) additionally attached two electrodes around left eye for VEOG signal.

4.2 Materials and Methods

4.2.1 Data Recordings

In this study, EEG signals were recorded at 14 positions (Fp1, Fp2, F3, F4, T3, C3, Cz, C4, T4, P3, Pz, P4, O1, and O2) according to the International 10-20 electrode system [144]. Active electrodes for EEG data were made of sintered Ag/Ag-Cl material (g.tec Medical Engineering GmbH, Austria) and their metallic tips were attached to the scalp. A VEOG signal was recorded from two surface Ag/Ag-Cl electrodes (Blue Sensor P, Ambu Corp., Denmark) placed at the superior and inferior orbital rims of the left eye (Figure 4.1). Reference and ground electrodes were placed on the left mastoid and Fpz, respectively. The EEG and EOG data were band-pass filtered from 0.5 Hz and 60 Hz with a Butterworth filter with order seven and digitized at a sampling rate of 256 Hz using g.USBamp. The first 5 s of recorded data is discarded. All electrodes were pasted with an electrolyte, g.GAMMAgel, to reduce skin resistance.

Twenty subjects (14 males and 6 females, mean age: 22.75 $\pm$ 1.45 years, 14 right and 6 left eye dominants) participated in the experiments. All neuroimaging studies and ensuring inferences aim to establish the observed effect as the typical or average characteristics of a population. If the researcher could assemble infinite sample for the study, the observed data would be the true distribution. However, it is unreasonable to make researchers do the duty and there is no method for comparing the empirical distribution function with the true distribution. In the field of neuroscience, it is considered that the actual critical number of subjects required in a conjunction analysis with a less sensitive test, under the null hypothesis, is exceedingly small (Figure 4.2). The

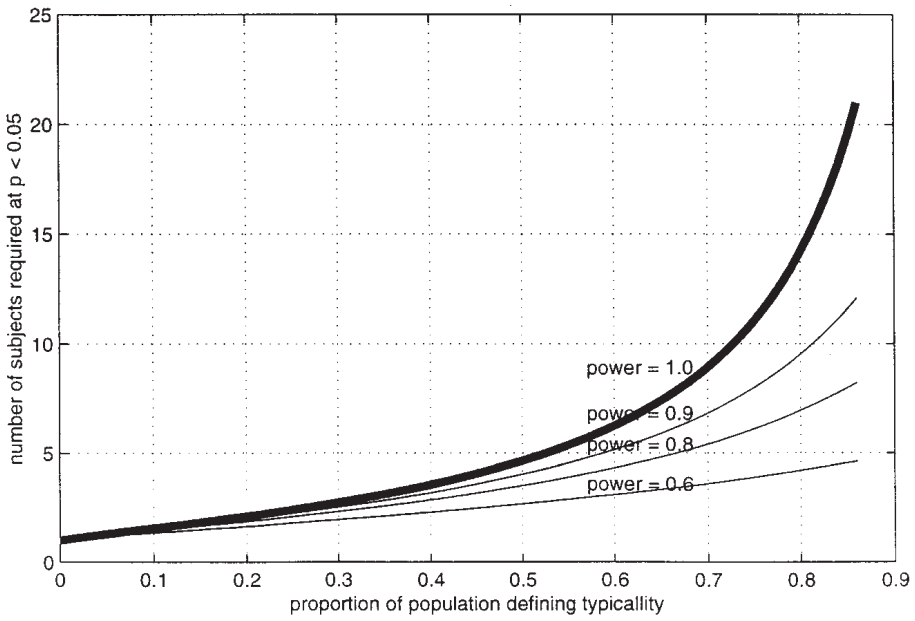

Figure 4.2 Plot of the critical number of subjects required in a conjunction analysis using a fixed-effect model for a test with 5% specificity and a range of sensitivities (1.0, 0.9, 0.8, and 0.6) [320].

expected width of the 95% confident interval plays an important role in many of the statistical indexes to show the plausible characteristics of a population [321]. Therefore, I assembled twenty subjects for this study. No subjects had a history of sensorimotor, ophthalmologic, or auditory abnormalities. All subjects were asked to read and sign an informed consent approved by the Research Ethics Committee of Keio University before participating the study. None of the subjects were permitted to wear eyeglasses and all used canal-type earphones during the experiments.

4.2.2 Stimuli and Procedure

Each subject was seated in a dim room (mean illuminance: 188.95 ± 24.50 lx) in front of a laptop PC. The distance between subject and display was roughly 60 cm, and the third highest lightness-contrast was selected while displaying a cross-fixation on the screen. During the experiments, the subject's face was video recorded using a tablet PC fixed to the frame of the monitor. The experimental procedure was written in Matlab using the Psychophysics Toolbox extensions [322–324], as follows.

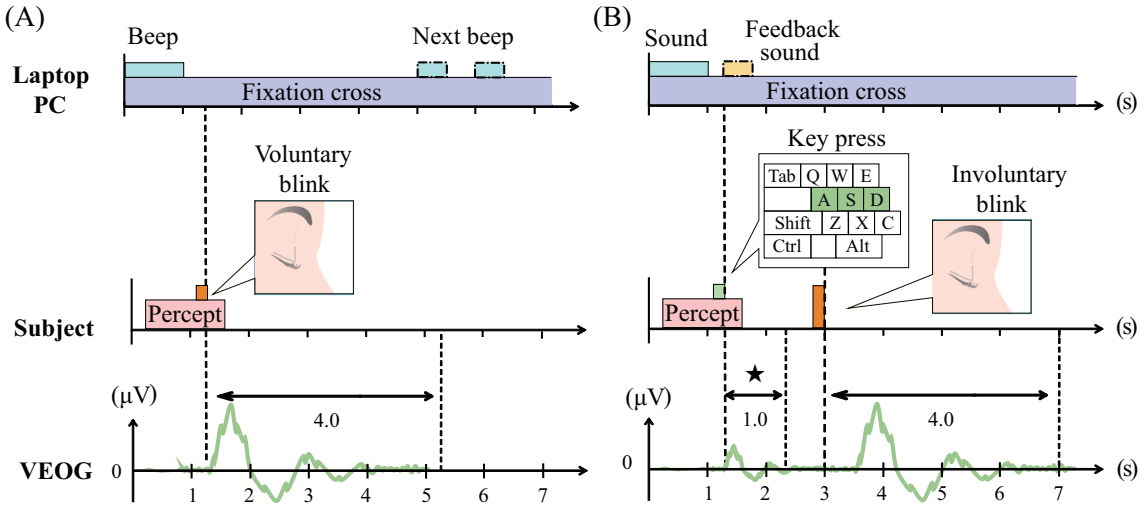

Figure 4.3 (A) Diagram of a trial for a voluntary eyeblink. The 4-s epoch was used for analysis. However, the entire period was used for calculating ICA spatial filtering. (B) Diagram of a trial for involuntary eyeblink. The 4-s epoch, excluding the period indicated by the black star, was used for analysis. However, the entire time period was also used for calculating ICA spatial filtering.

Exp. 1 (for voluntary eyeblink)

An audio file (Windows Background.wav, 55.0 dB), which is used as an alert sound (a beep) in the Windows 8.1 operating system was used to obtain voluntary eyeblink data. The task is simply to focus on a black cross-fixation in the center of the display and to blink with both eyes within 1 s after the sound stimulus (see Figure 4.3 (A)). The simple auditory stimulus was repeated for this experiment to avoid interference with other eye-related potentials: (i) the occipital positive potential (the lambda wave) that is an evoked potential based on the changed visual stimulus, which typically occurs roughly 300 ms after the onset of a blink [325, 326]; (ii) the cerebral potential caused by the efference copy, which represents a process for the anticipation of the change in the visual stimulus from the eye-movement [327]. In each of the experiments, the subject was instructed to blink naturally, in addition to the prescribed blinks, and not to blink stiffly or strongly, but instead, to simply react quickly. The datasets for each subject consist of 3 sessions. Each session includes 20 trials; the next session is started after a 60-s resting period to maintain ocular moisture. Whereas normal adults blink every 3.0 s, a sound was presented every 5.0 or 6.0 s in a randomized order. In short, subjects had to blink in a slightly unusual way. However, the presentation interval was deliberately decided (as mentioned above) because I experimentally found that the effects of eyeblink on EEG signals have continued their influence for 3.0-4.0 s.

Exp. 2 (for involuntary eyeblink)

Three sounds called "A" (440.0 Hz, 55.0 dB), "S" (554.0 Hz, 55.0 dB), and "D" (659.0 Hz, 55.0 dB) were prepared to obtain involuntary eyeblink data. One of the three sounds (in a randomized order) is presented for 1 s after 10-14 s. During the experiments, subjects put their left fingertips (the ring finger, the middle finger, and the index finger) on the "A", "S", and "D" keys of the keyboard (see Figure 4.3 (B)). The subject presses the key corresponding to the associated sound after the sound stimulus. Then, a feedback sound is presented to the subject in accordance with the answer. After 20 trials, the rate of correct answers is shown on the display. In each of the experiments, the subject was instructed to attempt to answer 90% of the full trials correctly and to fix their eyes at the central black cross-fixation. There were no other restrictions, meaning the subject could blink naturally (involuntarily). The datasets of each subject consist of 3 sessions.

4.3 Eyeblink Feature Extraction Scheme

The InfoMax ICA algorithm [94] is employed as the signal separation scheme to obtain ICs and relative projection strengths. Furthermore, double thresholds based on indexes of modified Multiscale Sample Entropy (mMSE) and kurtosis are employed to classify the ICs automatically as either neuronal or artifactual. Then, the identified artifactual ICs are carefully purified using biorthogonal wavelets to extract eyeblink features from the observed signals. Finally, the extracted features are used to assess the effects of voluntary and involuntary eyeblink on ICs contributing to EEG signals.

4.3.1 ICA-based Signal Separation

The ICA algorithm already described in Chapter 3 jointly estimates the demixing matrix $\boldsymbol{W}$ that defines the weights with which each estimated source is present in the observed EEG data. The unknown demixing matrix $\boldsymbol{W}$ is a square $P \times P$ matrix. In this study, the number of electrodes for EEG recording is 14; therefore, $P = 14$. The matrix gives the relative projection strengths of the respective ICs to each of the scalp electrodes [114]. There are several kinds of ICA algorithm for accuracy improvement for source separation. I applied the logistic InfoMax ICA algorithm that has been implemented using the *runica* function in the EEGLAB Matlab toolbox [19] with its default settings. This scheme separates the observed signals into the same number of ICs ($P = Q = 14$).

After ICA-based signal separation, each IC is suspended as an artifactual component and identified as an artifactual or neuronal IC using concrete steps (visual inspection, thresholding, and so on). Then, intrinsic (non-artifact) EEG signals and artifacts are spuriously separated using the inverse ICA linear demixing process.

4.3.2 Eyeblink Artifactual Component Identification

ICA gives researchers the ability to investigate the plausible effects of eyeblink on observed EEG signals based on the assumptions described in Chapter 3 and an assumption that propagation delays through the mixing medium (i.e. brain, scalp, and body) are negligible. Visual inspection of scalp topographies and correlation analysis of the IC that has the highest correlation with the observed VEOG signal have been conducted for identifying the ocular artifacts in ICs from observed EEG signals [232, 258, 265]. However, eyeblink artifacts are allocated to one or more ICs, meaning that the identification steps are sometimes not able to accurately select the correct components. The issue has been solved by combining ICA with a wavelet transform [268]. The new scheme automatically identifies artifactual components using double thresholds based on the indexes of mMSE and kurtosis.

The index of mMSE is based on the concept of sample entropy [328,329], which is an index quantifying the regularity and complexity of data. Given the p-th estimated IC $\{\hat{s}_p(n) : 1 \leq n \leq N_s\}$ by logistic InfoMax ICA that has N_s data points, the following vector sequence is formed:

$$\hat{S}_i^m = \{\hat{s}_p(i), \hat{s}_p(i+1), \ldots, \hat{s}_p(i+m-1)\} - \hat{s}_p 0(i)$$

$$(i = 1, \ldots, N_s - m + 1), \tag{4.1}$$

$$\hat{s}_p 0(i) = \frac{1}{m} \sum_{j=0}^{m-1} s_p(i+j), \tag{4.2}$$

where $\hat{s}_p 0(i)$ and m are a baseline for generalization of the vector sequence and the maximum length of epochs for matching templates, respectively. The minimum length is set to 2 (i.e. $m = 2$). Despite the fact that the actual number of data points is N (25,600 to 31,920 in the Exp.1 and 51,200 to 71,680 in the Exp.2), the first 10 s of data (i.e. $N_s = 2,560$) is used in this step.

Then, the distance between two vectors is defined as

$$\begin{aligned} d_{ij}^m &= d[\hat{S}_i^m, \hat{S}_j^m] \\ &= \max_{h\in(0,m-1)} |\hat{s}_p(i+h) - \hat{s}_p 0(i) - (\hat{s}_p(j+h) - \hat{s}_p 0(j))| \\ &\qquad (i,j = 1,\ldots,N_s - m,\ \ j \neq i), \end{aligned} \tag{4.3}$$

and the degree of similarity between vectors is defined using Eq. (4.1).

$$D_{ij}^m = f(d_{ij}^m,\ r) = \frac{1}{1+\exp[(d_{ij}^m - 0.5)/r]}, \tag{4.4}$$

where r is the tolerance or the slope of the Sigmoid function. I set the value at 0.2 $\sigma_{\hat{s}_p}$ ($r = 0.2 \times \sigma_{\hat{s}_p}$). The input pattern assesses its belongingness to a given class using the continuous boundary, instead of the Heaviside function [330]. Furthermore, functions B and A, which are used to count m and $(m+1)$ template matches within the tolerance, are defined as

$$B_r^m(i) = \frac{1}{N_s - m - 1} \sum_{j=1,\ j\neq i}^{N_s-m} D_{ij}^m, \tag{4.5}$$

$$B_r^m = \frac{1}{N_s - m} \sum_{i=1}^{N_s-m} B_r^m(i), \tag{4.6}$$

$$A_r^m(i) = \frac{1}{N_s - m - 1} \sum_{j=1,\ j\neq i}^{N_s-m} D_{ij}^{m+1}, \tag{4.7}$$

$$A_r^m = \frac{1}{N_s - m} \sum_{i=1}^{N_s-m} A_r^m(i). \tag{4.8}$$

Finally, index of mMSE is defined by using negative natural logarithm of deviation of B_r^m from A_r^m,

$$\mathrm{mMSE}(m,r) = \lim_{N_s\to\infty} (\ln B_r^m - \ln A_r^m), \tag{4.9}$$

$$\mathrm{mMSE}(m,r,N_s) = -\ln(A_r^m / B_r^m). \tag{4.10}$$

The index of mMSE with a 95% Confidence Interval (CI) of the mean in the Student's t-distribution is used for the threshold for detecting eyeblink artifactual ICs using the following equation:

$$\mathrm{Threshold}_1 = m_{\mathrm{mMSE}} - \frac{\sigma_{\mathrm{mMSE}}}{\sqrt{N_s}} \times t_{N_f}, \tag{4.11}$$

where m_{mMSE}, σ_{mMSE}, and t_{N_f} are the mean of mMSE, the standard deviation of mMSE, and the index in the t-distribution with 13 degrees of freedom ($N_f = p - 1$). An

artifactual IC is expected to have a value of mMSE that is less than that of a neuronal IC.

One index of kurtosis is the fourth-order cumulant, which is used to characterize the location and variability of data and is a measure of whether the variables are peaked or flat relative to a Gaussian distribution.

$$\text{kurtosis}_p = m_{p_4} - 3m_{p_2}^2, \tag{4.12}$$

$$m_{p_c} = \mathbb{E}\{(\hat{s}_p - m_{p_1})^c\}, \tag{4.13}$$

where m_{p_c} and m_{p_1} are the c-th order central moment of the variable and its mean of the p-th IC. I calculated the kurtosis using the *kurtosis* function of Matlab for each IC. Eyeblink activities can be effectively detected by combining this index with mMSE because kurtosis is positive for peaked spasmodic activities [331]. Therefore, the index of kurtosis with a 95% CI for the mean is used for the threshold to detect eyeblink artifactual ICs based on the following equation:

$$\text{Threshold}_2 = m_{\text{kurtosis}} - \frac{\sigma_{\text{kurtosis}}}{\sqrt{N_s}} \times t_{N_f}, \tag{4.14}$$

where m_{kurtosis} and σ_{kurtosis} are the mean and the standard deviation of kurtosis.

All of the ICs with mMSE and kurtosis values that are outside the double thresholds are identified as eyeblink artifactual ICs.

4.3.3 Wavelet-enhanced ICA

There may be cases in which a contradiction occurs between the ICA assumption and the neural patterns of activation because neural networks are often overlapping (not independent). ICs presenting artifactual activities obtained from the stimulus-presenting analysis, especially in the event-related potential analysis, might have distinctive interfering neuronal activities in the components. Discarding all components will lead to losing of neuronal data in the ICA procedure. The wavelet-enhanced ICA algorithm uses wavelet thresholding of ICs as an intermediate step. This step allows recovery of substantial parts of the neural signal with artifacts and extraction of eyeblink artifactual components from identified artifactual ICs, all of which is done automatically [272,319]. All identified artifactual ICs are passed to the following thresholding procedure.

1. The identified artifactual ICs $\hat{\boldsymbol{s}}_p$ are transformed into components of disjointed

spectra (a matrix) instead of signals (vectors) via DWT.

$$W(a,b) = \frac{1}{\sqrt{a}} \int \hat{s}_p(n)\psi_{a,b}(n)dn, \tag{4.15}$$

$$\psi_{a,b} = \psi(\frac{n-b}{a}). \tag{4.16}$$

where $W(a,b)$ denotes the wavelet representation of $\hat{s}_p(n)$ with a and b defining the time-scale and location. Usually, the time-scale a and location b are defined as $a = 2^l$ and $b = k2^l$ where l and k denote the level of decompositions and temporal localization at the level, respectively. DWT must be applied to select the mother wavelet and level of the decompositions. The mother wavelet and level of decompositions were set to Daubechies-4 and five, respectively, implemented using $db4$ in the $liftwave$ function of Matlab.

2. If the wavelet coefficient $W(a,b)$ of each level l is lower than the wavelet threshold, the coefficient will be set to $W'(l,k) = 0$. The threshold value is defined as

$$\text{Threshold}_3 = \sigma\sqrt{2\ln N}, \tag{4.17}$$

where

$$\sigma^2 = \frac{\text{median}(|W(l,k)|)}{0.6745}, \tag{4.18}$$

estimates the magnitude of the neuronal wideband signal with a constant value of 0.6745, related to Gaussian noise [319], and N is the length of the data.

3. Enhanced eyeblink artifactual ICs $\hat{\boldsymbol{s}}_p$ are reconstructed from the thresholded wavelet coefficients $W'(l,k)$ via inverse DWT.
4. Fourteen-channel eyeblink artifacts in recorded EEG signals are reconstructed using the inverse ICA linear demixing process.

4.3.4 Extracted Eyeblink Features

Figures 4.4 (A) and 4.5 (A) show an 8-s EEG signals that includes voluntary and involuntary eyeblinks from subject data measured at 14 scalp positions. Two or three eyeblink artifacts appear on all channels; frontal positions (e.g. Fp1, Fp2, F3, and F4) show large eyeblink effects in the data. The ICA algorithm separated the contributions of neuronal and artifactual components into 14 ICs [Figures 4.4 (B) and 4.5 (B)]. Each IC was classified as either artifactual or neuronal on the basis of double thresholds and indices of mMSE and kurtosis [Figures 4.4 (C) and 4.5 (C)] and blink-origin components were extracted from the identified artifactual ICs via a wavelet threshold. The extracted eyeblink features [Figures 4.4 (D) and 4.5 (D)] are used to assess the effects of voluntary

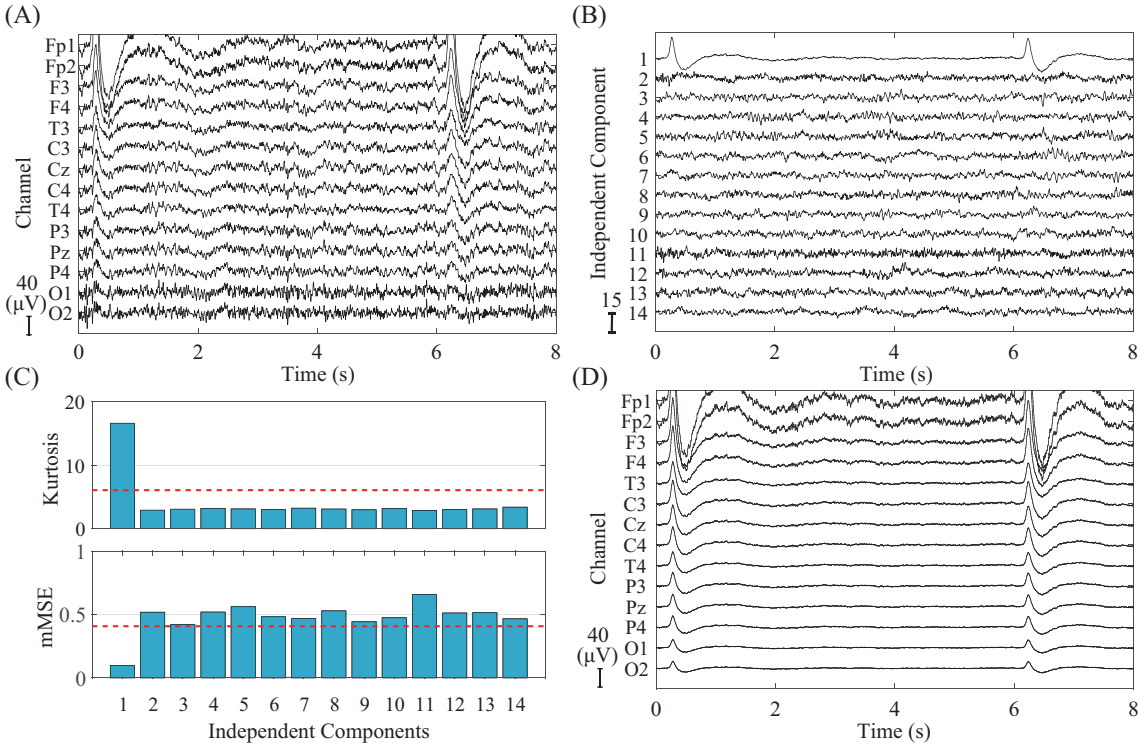

Figure 4.4 Separation of EEG data including voluntary eyeblinks by wavelet-enhanced ICA. (A) An 8-s EEG signals. (B) ICs of the 14-channel signals. (C) Calculated kurtosis, mMSE (blue bars), and thresholds (red dashed lines) with 95% CI for the mean for both markers in regard to 14 ICs. The first IC was classified as an artifactual component using the markers. (D) Extracted voluntary eyeblink features of 14-channel signals.

and involuntary eyeblink on ICs contributing to EEG signals.

4.4 Analysis of Epochs

As shown in the previous section, I obtained consecutive 14-channel eyeblink features for 20 subjects.

Here, I also have consecutive VEOG signals. All channel features are separated into 4-s epochs to obtain time-locked data. The scheme for separating the epoch is determined from the VEOG signal. First, each observed EOG signal passes through a Butterworth low-pass filter whose cutoff frequency is 8.0 Hz with order eleven, so as to reduce the cerebral activities in the EOG signal [93, 332]. Second, the first positive peaks of blinks in the filtered EOG signal are detected using a hard threshold. The threshold value was set to 50 μV (common to all EOG signals). A value exceeding the threshold is compared to the adjacent 50 sampling points (roughly $\pm$ 0.20 s). In this study, if the detected value is the highest in the range, the value is further classified

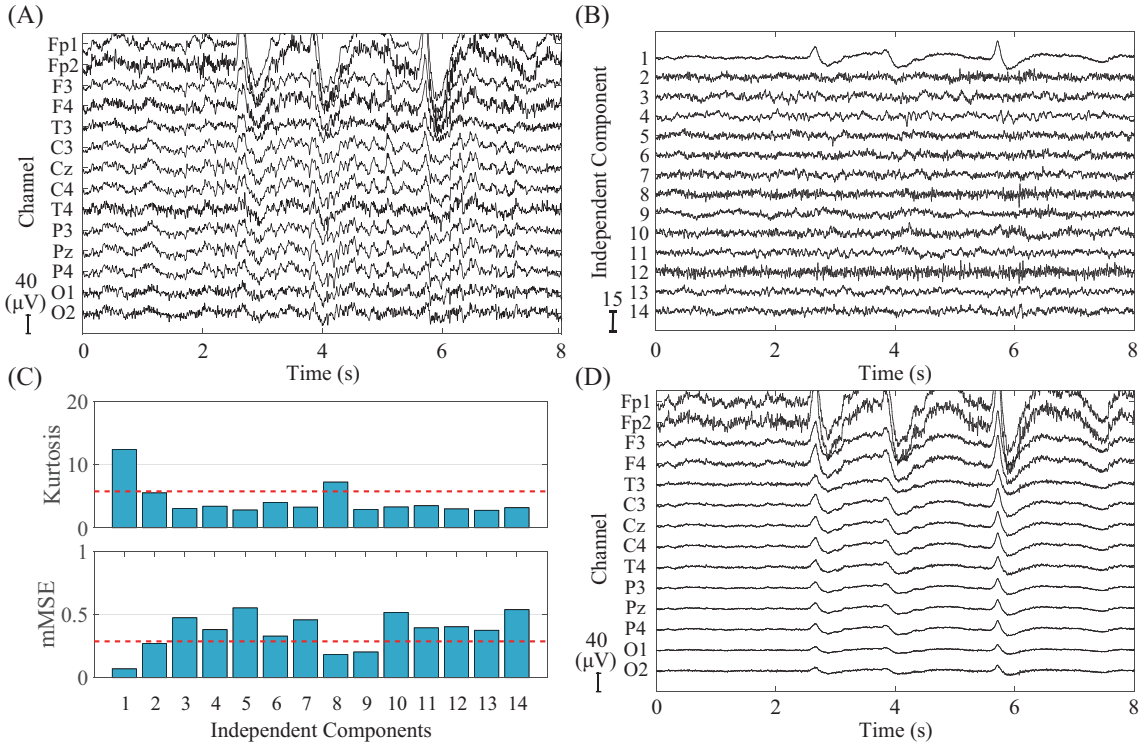

Figure 4.5 Separation of EEG data including involuntary eyeblinks by wavelet-enhanced ICA. (A) An 8-s EEG signals. (B) ICs of the 14-channel signals. (C) Calculated kurtosis, mMSE (blue bars), and thresholds (red dashed lines) with 95% CI for the mean for both markers for the 14 ICs. The first and eighth ICs were classified as artifactual components based on the markers. (D) Extracted involuntary eyeblink features of 14-channel signals.

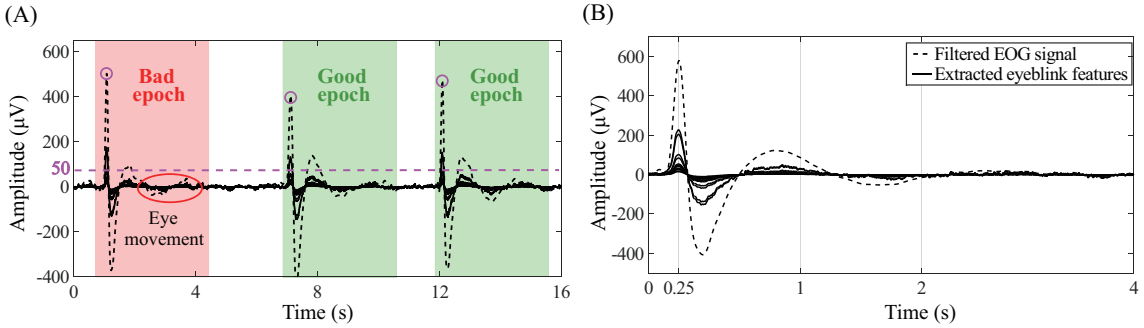

Figure 4.6 (A) Peak detection using a hard threshold (pink dashed line) and epoch selection by visual inspection. Right two epochs are selected as exemplary signals that have only blinked effects in the epochs. (B) A filtered VEOG signal (black dashed line) and extracted eyeblink features in EEG signals (solid black lines) that first positive peaks of amplitude are aligned at time 0.25 s (64th sampling point).

as to whether it is an actual peak or not by visual inspection; then, it is identified as the first positive peak of the blink. Third, 14-channel eyeblink features and a VEOG signal are separated into 4-s epochs based on the point of maximum amplitude in the EOG data. The point is located at the 64th sampling point (i.e. 0.25 s). An epoch as defined above, is shown in Figure 4.6.

Table 4.1 The number of epochs for voluntary and involuntary eyeblinks selected from each subject by visual inspection for the following analysis.

	Voluntary	Involuntary		Voluntary	Involuntary		Voluntary	Involuntary
Sub. 01	40	22	Sub. 08	11	8	Sub. 15	35	33
Sub. 02	24	20	Sub. 09	32	15	Sub. 16	30	29
Sub. 03	35	40	Sub. 10	25	18	Sub. 17	24	15
Sub. 04	13	6	Sub. 11	13	11	Sub. 18	11	11
Sub. 05	25	18	Sub. 12	13	13	Sub. 19	18	11
Sub. 06	37	40	Sub. 13	26	23	Sub. 20	17	28
Sub. 07	17	13	Sub. 14	21	20	Total	467	394

In the Exp. 2, there is no restriction on the times and duration of blinks. Selecting an exemplary signal that has only a blink effect in its own epoch is needed to compare the voluntary eyeblink characteristics. It is hard to control conscious eyelid motion, although each subject was instructed to blink only after cue presentation in the Exp. 1. Subject's eyelids sometimes quivered convulsively during motion execution; there were also instances in which two (or more) blinks were reflexively induced. Therefore, the identified epochs were carefully selected as a dataset to avoid contaminating other motions, e.g. eye movement and body motion based on video recordings and visual inspections [see Figure 4.6 (A)]. The number of voluntary and involuntary eyeblink epochs obtained from each subject and the total number of the epochs are presented in Table 4.1. The amounts of data are uneven, however, the numerical range of differences between voluntary and involuntary for each subject lies within ± 10, except for three subjects (Sub. 01, Sub. 09, and Sub. 20).

The eyeblink artifacts contributing to EEG signals are characterized with their respective epochs in the frequency-domain, time-frequency-domain, and time-domain. In this study, I assessed the following three phenomena: (i) propagation effects across the head (in a symmetrical fashion); (ii) power distributions; and (iii) overlapping durations.

In the frequency-domain analysis, Welch's overlapped segment averaging estimator [333], implemented using the *pwelch* function in Matlab with a Hamming window, is performed to estimate the one-sided power spectral density. The window size, overlapping samples between adjoining sections, and number of Discrete Fourier Transform (DFT) points were set to 512, 256, and 512 (frequency resolution: 0.50 Hz). The values of estimated power spectral density are averaged over the delta (0.5-4.0 Hz), theta (4.0-8.0 Hz), alpha (8.0-13.0 Hz), and beta (13.0-30.0 Hz) bands. Moreover, the relative power in each frequency band for 14-channel voluntary eyeblink features for 20 subjects is separately compared with the relative power of involuntary eyeblink features.

In time-frequency-domain analysis, grand means of eyeblink features are used to compute spectrograms, implemented using the *spectrogram* function in Matlab with

Hamming window. The window size, overlapping samples, and number of DFT points were set at 32, 16, and 256. The log-transformed power distribution and overlapping duration are investigated from the spectrogram.

Finally, the duration of eyeblink effect in the ICs (overlapping length of eyeblink artifacts in EEG signal), and peak amplitude value of 14-channel eyeblink features are separately computed to assess the effects of voluntary and involuntary eyeblinks on ICs contributing to EEG signals in the time-domain analysis. The electrical potential caused by eyeblink will reduce its impact on EEG signals by the reiteration of the positive-negative inversion although the overall amount of discharge with eyeblink depends on the subject and the manner of eyelid/eyeball movement [109,334–336]. I experimentally found that the effects continue their influence for 3.0-4.0 s. In other words, each electric potential caused by an eyeblink crosses the zero points several times after passing the first positive peak; then, the potential ceases to exist. Therefore, several zero-crossing points and potential peaks are analyzed for the characterization of eyeblinks. The number will be determined in the time-frequency-domain analysis.

4.5 Results and Discussion

In the Exp. 2, all but two subjects accomplished the criterion (90% of correct answers). The instruction got each subject to tackle the experiments wholeheartedly; therefore, all data were used in the analysis.

4.5.1 Frequency-domain Analysis

Figure 4.7 depicts the grand means of the estimated power spectral densities for 14-channel eyeblink features in EEG signals and the observed VEOG signals, used to evaluate the differences among eyeblink features occurring under voluntary or involuntary control. The statistically significant results in the Student's t-test for two blink types are depicted together with the grand means in Figure 4.7 (the bolded asterisk and N.S. indicate a significant difference and no significant difference, respectively, between voluntary and involuntary eyeblink features in the frequency band). The significance level was decided to be 1%; the results were computed for each frequency band and each EEG channel.

For eyeblinks, all of the EEG channels have a power whose frequency range and peak are less than 8.0 Hz and less than 4.0 Hz, respectively, for all eyeblink types. The power decreased with increasing distance from the eyes, and the propagation of activity proceeded along the anterior-posterior axis in a symmetrical fashion. These

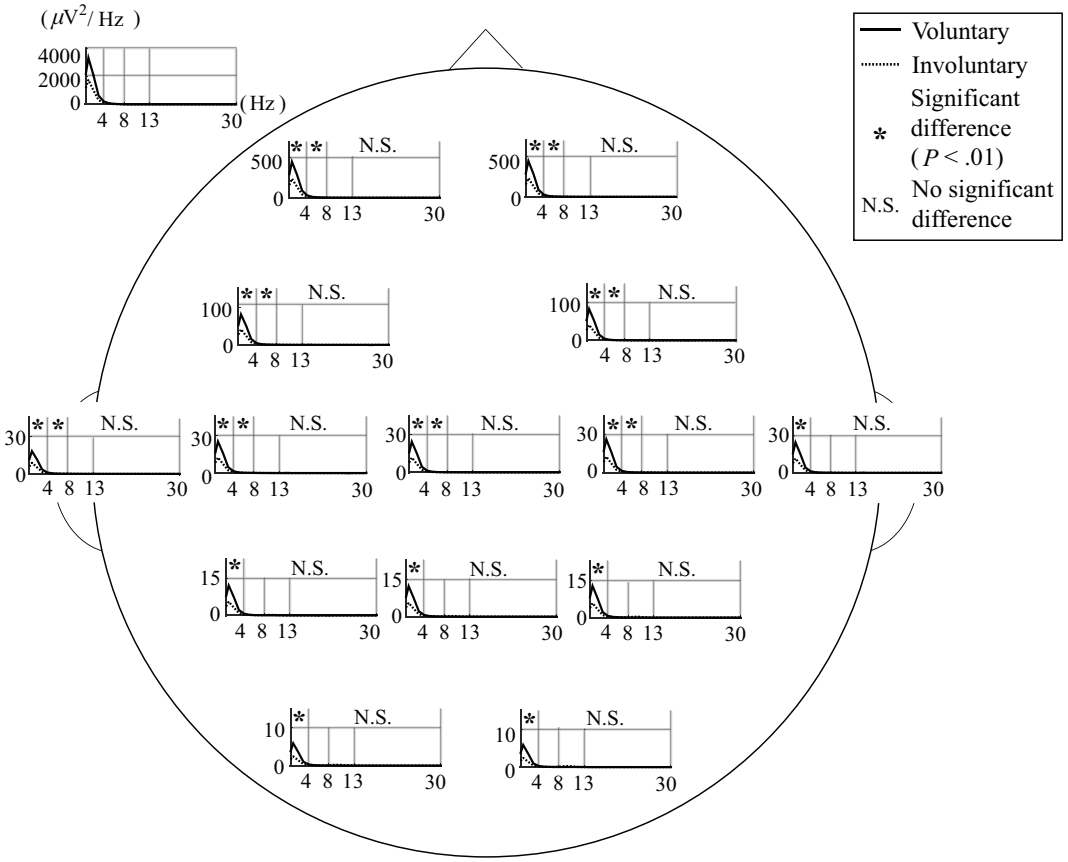

Figure 4.7 Grand means of estimated power spectral densities at a VEOG and 14 EEG channels evaluated for voluntary (solid black line) and involuntary (black dashed line) eyeblink features; significant results at the 1% significance level are presented for the two blink types in each frequency band.

results support the existing literature: (i) the distorting effects of eyeblink artifacts on the EEG are within the delta and theta bands [69, 70, 90, 103, 337]; (ii) the electric potentials (dipole projections) caused by eyeblinks decrease with increasing distance between measurement points and eyes [89, 93, 338]; and (iii) the propagation effects across the scalp present in a bilaterally symmetrical fashion [71, 339].

In the delta band, eyeblink features extracted from all channels presented significant differences between voluntary and involuntary data. In the theta band, the eyeblink features extracted from all channels, excluding the right anterior temporal and occipital regions (T4, P3, Pz, P4, O1, and O2), presented significant differences. In contrast to these bands, there was no significant difference in the alpha and beta bands in any channels. In the real-world environment, whether an eyeblink is voluntary or involuntary is unknown. These results indicate that if an eyeblink artifact removal system had been constructed from a training dataset that contained only voluntary or involuntary eyeblink data, intrinsic EEG data might not be extricable from the observed EEG data contaminated by eyeblink artifacts when applying the system, because there is a sig-

Table 4.2 Averaged relative power of EEG signals measured from 14 scalp positions during voluntary and involuntary eyeblinking across 20 subjects.

	Delta (0.5-4.0 Hz)		Theta (4.0-8.0 Hz)		Alpha (8.0-13.0 Hz)		Beta (13.0-30.0 Hz)	
	Voluntary	Involuntary	Voluntary	Involuntary	Voluntary	Involuntary	Voluntary	Involuntary
Fp1	0.94±0.057	0.93±0.053	0.03±0.026	0.03±0.022	0.01±0.013	0.01±0.018	0.02±0.023	0.02±0.023
Fp2	0.94±0.057	0.93±0.054	0.03±0.026	0.03±0.022	0.01±0.013	0.01±0.018	0.02±0.023	0.02±0.024
F3	0.94±0.057	0.93±0.053	0.03±0.026	0.03±0.022	0.01±0.013	0.02±0.017	0.02±0.023	0.02±0.023
F4	0.94±0.057	0.93±0.061	0.03±0.026	0.03±0.023	0.01±0.014	0.02±0.024	0.02±0.023	0.02±0.028
T3	0.94±0.058	0.93±0.066	0.03±0.026	0.03±0.024	0.01±0.015	0.02±0.032	0.02±0.024	0.02±0.025
C3	0.94±0.061	0.93±0.067	0.03±0.032	0.03±0.022	0.01±0.015	0.02±0.039	0.02±0.023	0.02±0.023
Cz	0.94±0.058	0.92±0.073	0.03±0.026	0.03±0.024	0.01±0.016	0.02±0.042	0.02±0.023	0.02±0.028
C4	0.94±0.060	0.92±0.090	0.03±0.026	0.04±0.026	0.01±0.020	0.02±0.055	0.02±0.024	0.02±0.034
T4	0.94±0.060	0.91±0.097	0.03±0.026	0.04±0.032	0.01±0.019	0.02±0.047	0.02±0.024	0.03±0.044
P3	0.94±0.062	0.92±0.101	0.03±0.028	0.03±0.024	0.01±0.020	0.03±0.074	0.02±0.024	0.02±0.026
Pz	0.93±0.063	0.91±0.101	0.03±0.027	0.04±0.027	0.01±0.022	0.03±0.079	0.02±0.025	0.02±0.032
P4	0.93±0.067	0.91±0.118	0.03±0.026	0.04±0.028	0.01±0.028	0.03±0.083	0.02±0.025	0.03±0.037
O1	0.93±0.069	0.90±0.137	0.03±0.027	0.04±0.028	0.02±0.026	0.03±0.092	0.02±0.027	0.03±0.046
O2	0.93±0.063	0.91±0.128	0.03±0.026	0.04±0.032	0.01±0.020	0.03±0.086	0.02±0.025	0.03±0.045

nificant difference between voluntary and involuntary eyeblink information in the delta and theta bands.

Relative power in each frequency band and at each scalp position for voluntary and involuntary eyeblink features for 20 subjects is listed in Table 4.2. Eyeblink features were largely composed of frequency components in the delta band (over 0.90). In both types, the eyeblink artifact propagated along the spherical layer of the head, from anterior to posterior, with almost the same frequency composition. When I consider the electrodynamic models for the ocular dipole field on the scalp in spherical coordinates, the potentials generated by both eyes can be described as the scalar product of the dipole moment, where the vector depends on that placement of electrodes [72,89,340].

According to the model, decaying power should occur for an electrode located in the occipital region, because the dipole projection at the moment is lower than that of an electrode placed near the eyes. However, no channel avoids the effects of eyeblink as long as the scalp has some conductivity (zero conductivity is hard to realize), even if the target signal derived from a source located in the occipital region. Therefore, removing the ocular potentials from all recorded EEG channels is necessary, irrespective of the installation site. Inter alia, research on the method of visual stimulus in the EEG signal (such as steady-state visual evoked potential-based research) often selects only the occipital region for EEG measurement positions [341, 342]. Prudent consideration is needed to avoid eyeblink artifact contamination when the stimulus frequency used in the research is low.

4.5.2 Time-frequency-domain Analysis

Figure. 4.8 shows the grand means of spectrograms of the a VEOG and 14 EEG channels to investigate the overlapping duration and frequency component of eyeblink artifacts. Both eyeblink effects spread over all channels and exert a strong influence on the frontal scalp positions from Fp1 to F4. Although a similar trend of inversion is apparent in both eyeblink types, the high discharged electrical quantity of voluntary eyeblink made the eyeblink effect in EEG signals have a longer duration than that of an involuntary eyeblink. As shown in the previous section, I could observe the effects only in the delta and theta bands; however, in actuality, the eyeblink effect distorts the EEG signals up to the alpha band immediately after a blink. The literature suggests that the ocular activity might not be restricted to the lower frequency region [71, 343]; the results of this study confirm this.

Both eyeblink effects decay rapidly after a blink and pass the zero-amplitude point. Then, the power rises again to a maximum value. By repeating this inversion several times, the power of the entire frequency band ceases to derive from EEG signals. For Figure 4.8, two or three repetitions represented in the occipital region and other regions represent four peaks in the spectrogram. In particular, the frontal region was polluted for periods longer than other regions. The duration of the eyeblink effect in all channels is from 2 to 4 s; it was proven that my intuitive assumption is, in essence, correct. Moreover, the low-frequency power remained until the end of the effect, which means that the power of the low-frequency band is colossal compared to the power of the eyeblink effect as a whole (see Table 4.2).

In many studies proposing eyeblink artifact denoising techniques, 1-s epochs of EOG data including the eyeblink section are mixed with recorded EEG data to create simulated datasets for performance verification [84, 266], or raw EEG data, which shows the effects of intentionally short and constant eyeblink intervals, is prepared for testing data [261]. Preparing simulated datasets is needed for performance verification because utilizing raw EEG data contaminated with eyeblink artifacts has the drawback that the true EEG signal is unknown [344]. However, each eyeblink artifact maintains its effect for 2 s in the EEG signals. Therefore, if researchers use epochs of EOG data including the eyeblink section for making simulated datasets or raw EEG data, which shows the effects of constant eyeblink intervals, they should use epochs of EOG data or sets with the eyeblink intervals that are 4 s or longer (if the target position is the occipital region, the lengths should be over 2 s). Otherwise, researchers will produce datasets that are similar, but not realistic.

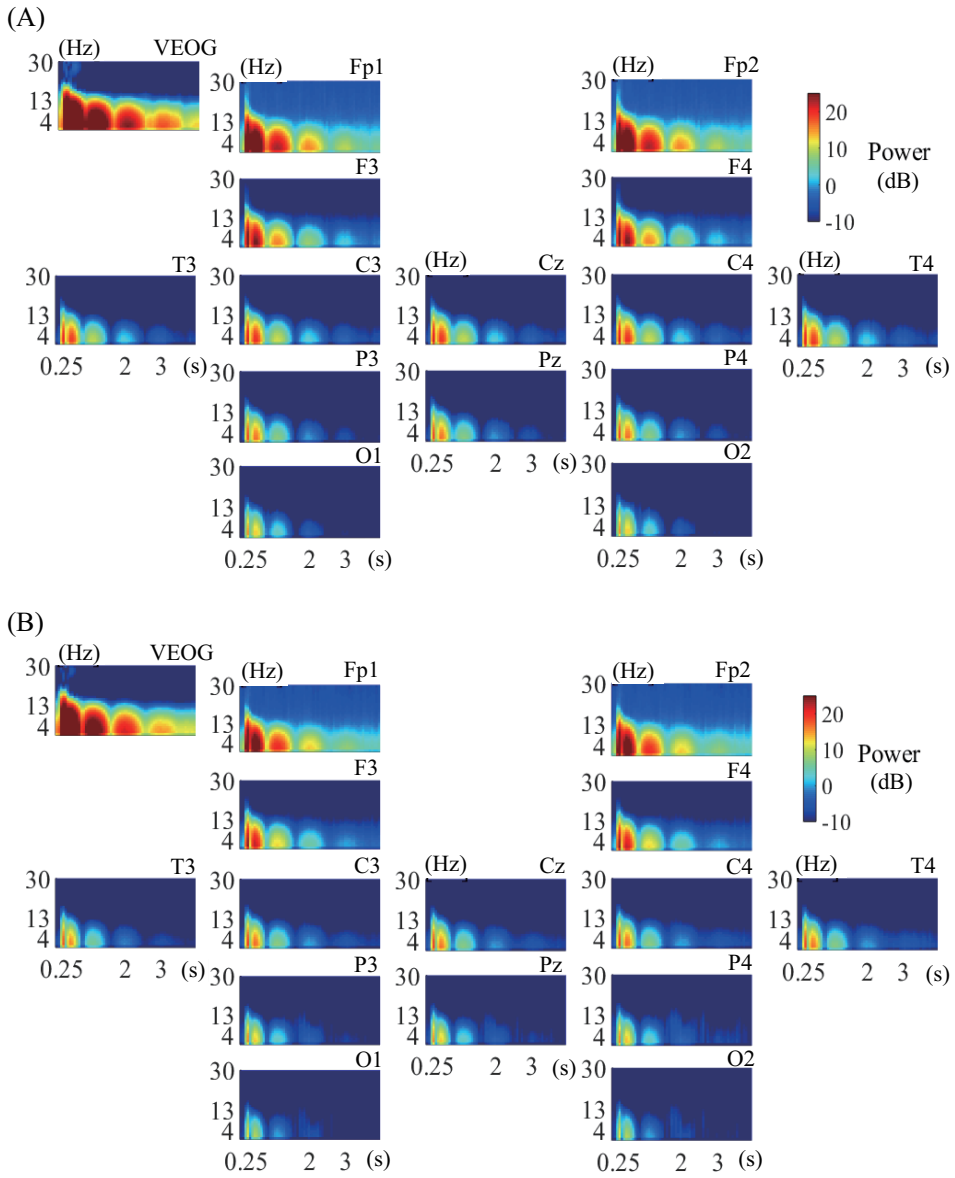

Figure 4.8 (A) Grand means of spectrograms for VEOG and EEG channels for voluntary eyeblink features. (B) Grand means of spectrograms for VEOG and EEG channels for involuntary eyeblink features.

4.5.3 Time-domain Analysis

Figure 4.9 shows the grand means and standard deviations of eyeblink features separated into 8 sampling bins, the grand means of eyeblink features and markers indicating potential peaks and zero-crossing points, plots of zero-crossing points, and a red line indicating the first positive peak of an eyeblink feature. For visualization, I used epochs at the Fp1 electrode that is placed in the prefrontal region and is sensitive to eyeblink effects. Voluntary eyeblinks had higher potentials and larger descriptions than involuntary eyeblinks [Figure 4.9 (A)]; therefore, the datasets of voluntary eyeblink features

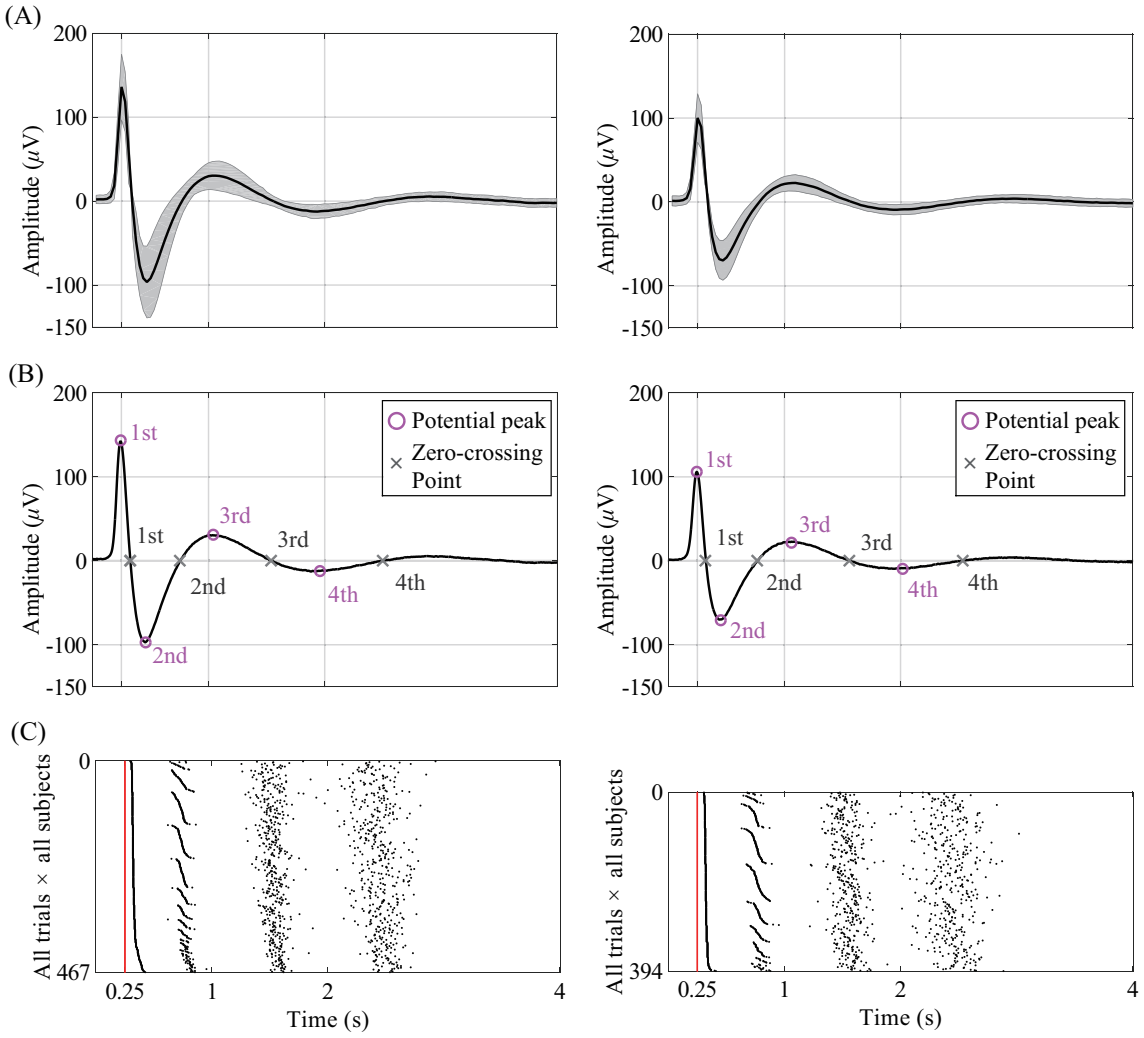

Figure 4.9 Comparison between voluntary (left column) and involuntary (right column) eyeblink features in the time domain. Eyeblink features obtained at the Fp1 position were selected for visualization because the prefrontal area is nearest to the eyes and is most affected by eyeblink. (A) Grand means and SDs of eyeblink features separated into 8 sampling bins. (B) Grand means of eyeblink features and markers indicating potential peaks (pink circles) and zero-crossing points (gray x-marks). The markers of each feature are presented in Tables 4.3 and 4.4 to allow statistical comparison of the two eyeblink types. (C) Plots of zero-crossing points and a red line indicating the first positive peak of an eyeblink feature. The data is sorted based on the first zero-crossing points.

included large differences among individuals. On the other hand, the difference of zero-crossing time between voluntary and involuntary was not significantly different [Figure 4.9 (B)]. However, by sorting the plots based on the first zero-crossing point, the plots revealed an interesting eyeblink characteristic: the orchestrated crossing time is extended over a period of 500 ms after passing the third zero-amplitude point [Figure 4.9 (C)].

Because the differences in zero-crossing time could not be distinguished, the potential peak and zero-crossing point in each channel were compared and tabulated in Tables

Table 4.3 Averaged absolute value of amplitude (μV) and latency (s) of voluntary eyeblink data at the first four potential peaks and zero-crossing points from the stimulus onset, respectively.

	First		Second		Third		Fourth	
	Peak (μV)	Crossing (s)	Peak (μV)	Crossing (s)	Peak (μV)	Crossing (s)	Peak (μV)	Crossing (s)
Fp1	146.45±40.2	0.33±0.021	109.34±49.6	0.75±0.042	39.89±19.2	1.53±0.083	23.34±9.4	2.44±0.144
Fp2	145.89±40.0	0.33±0.021	109.11±48.7	0.75±0.043	39.73±18.6	1.53±0.086	23.30±9.3	2.42±0.160
F3	61.94±17.0	0.33±0.021	46.39±21.2	0.75±0.043	16.97±8.4	1.53±0.087	9.95±4.2	2.42±0.165
F4	61.12±17.9	0.33±0.022	45.77±21.4	0.75±0.043	16.72±8.6	1.52±0.090	9.86±4.4	2.41±0.164
T3	29.91±9.1	0.33±0.021	22.61±11.9	0.75±0.043	8.33±4.7	1.52±0.094	4.94±2.4	2.41±0.161
C3	34.08±10.1	0.33±0.021	25.37±11.7	0.75±0.045	9.36±4.8	1.52±0.092	5.50±2.4	2.40±0.170
Cz	32.58±10.7	0.33±0.021	24.20±11.6	0.75±0.043	8.92±4.9	1.52±0.089	5.28±2.5	2.41±0.165
C4	33.43±11.0	0.33±0.022	24.95±12.4	0.75±0.043	9.19±5.2	1.52±0.090	5.44±2.7	2.41±0.169
T4	31.04±11.6	0.33±0.022	23.23±13.0	0.75±0.043	8.55±5.4	1.52±0.096	5.09±2.9	2.40±0.170
P3	23.02±7.7	0.33±0.021	17.09±8.3	0.75±0.043	6.31±3.5	1.52±0.087	–	–
Pz	22.73±8.3	0.33±0.021	16.83±8.5	0.75±0.044	6.24±3.6	1.52±0.101	–	–
P4	22.81±8.5	0.33±0.021	16.95±9.0	0.75±0.043	6.27±3.8	1.52±0.099	–	–
O1	15.11±6.6	0.33±0.021	11.24±6.7	0.75±0.043	4.19±2.8	1.52±0.105	–	–
O2	14.61±7.2	0.33±0.021	10.88±7.2	0.75±0.043	4.02±3.1	1.52±0.095	–	–

Table 4.4 Averaged absolute value of amplitude (μV) and latency (s) of involuntary eyeblink data at the first four potential peaks and zero-crossing points from the stimulus onset, respectively.

	First		Second		Third		Fourth	
	Peak (μV)	Crossing (s)	Peak (μV)	Crossing (s)	Peak (μV)	Crossing (s)	Peak (μV)	Crossing (s)
Fp1	109.04±30.1	0.33±0.011	77.13±24.9	0.77±0.047	31.88±9.7	1.54±0.096	20.18±6.3	2.44±0.166
Fp2	109.04±28.4	0.33±0.011	77.35±24.0	0.77±0.047	32.08±9.4	1.54±0.101	20.30±6.3	2.42±0.176
F3	45.69±12.1	0.33±0.011	32.48±10.8	0.77±0.047	13.47±4.3	1.55±0.099	8.58±2.9	2.42±0.179
F4	45.46±11.6	0.33±0.011	32.43±10.6	0.77±0.048	13.60±4.3	1.54±0.101	8.74±3.0	2.42±0.184
T3	21.34±5.9	0.33±0.011	15.20±5.3	0.77±0.047	6.31±2.1	1.54±0.103	4.09±1.6	2.41±0.191
C3	24.85±6.8	0.33±0.011	17.67±6.0	0.77±0.047	7.37±2.5	1.54±0.100	4.79±1.9	2.41±0.187
Cz	23.98±6.6	0.33±0.011	17.13±5.8	0.77±0.048	7.24±2.5	1.54±0.106	4.76±2.0	2.42±0.186
C4	24.90±6.7	0.33±0.011	17.86±6.1	0.77±0.051	7.61±2.6	1.54±0.101	5.06±2.4	2.41±0.190
T4	23.51±6.6	0.33±0.012	16.94±6.0	0.77±0.052	7.32±2.7	1.54±0.108	4.89±2.5	2.41±0.193
P3	16.48±4.9	0.33±0.013	11.81±4.3	0.77±0.049	5.04±2.2	1.54±0.106	–	–
Pz	16.33±5.0	0.33±0.011	11.71±4.4	0.77±0.050	5.06±2.4	1.53±0.119	–	–
P4	16.69±5.1	0.33±0.011	12.05±4.6	0.76±0.053	5.28±2.7	1.52±0.129	–	–
O1	10.48±4.0	0.33±0.013	7.61±3.5	0.77±0.053	3.46±2.4	1.52±0.124	–	–
O2	10.48±4.0	0.33±0.012	7.61±3.5	0.76±0.054	3.39±2.1	1.52±0.133	–	–

4.3 and 4.4. Four potential peaks and crossing points were analyzed in each channel; however, only three peaks and points were analyzed in the occipital region, since the effects in the regions had already ceased after passing the fourth zero-amplitude point. All potential peaks and first and second zero-crossing points in all channels were significant at the 1% significance level when compared between voluntary and involuntary. All peaks and points were at least 3 μV for both eyeblink types. Moreover, voluntary eyeblink features had zero-crossing times rapidly, despite their high potentials.

Dry spots on the precorneal tear layer emerge 15 to 30 s after an eyeblink [87]; therefore, humans need a recurring cycle of eyeblinks to maintain the ocular moisture [the

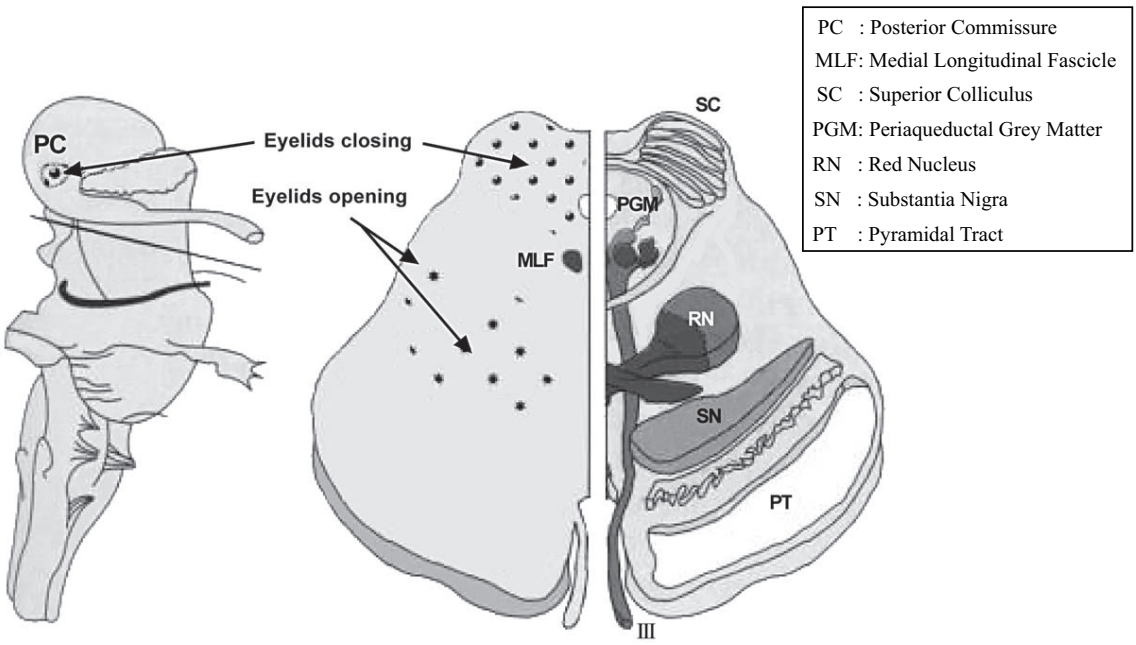

Figure 4.10 Schematic depiction of brainstem loci regarding movements of the eyelids based on data described in the reference [184, 345–347]. This figure is refereed to the reference [193].

standard adult eyeblink rate is roughly twenty eyeblinks/min [88]]. The upper/lower eyelid starts to move to the lower/upper eyelid with a high acceleration and reaches a peak velocity of up to 280 mm/s within 70 ms [171]. The eyelid movement is completed (zero velocity) from 100 to 150 ms; the reverse operation is accomplished more leisurely; it lasts roughly 300 ms. The human eyelid closure is provoked by an electric nerve stimulation of a region made up of the periaqueductal grey matter close to the superior colliculus and the posterior commissure (Figure 4.10) [184, 193]. During each eyeblink, the LPS muscle contracts, with a minor contribution from Müller's muscle and the orbicularis oculi muscle [187–189]. Nuclei of the posterior commissure control the inhibitory modulation of LPS motor-neuronal activity except when the lid-eye coordination disorders such as lid retraction caused by the dorsal midbrain syndrome, parkinsonism, or progressive supranuclear palsy appear [195]. Spontaneous or induced eyeblink causes the eyeball to act as an electric dipole, with corneal positivity and retinal negativity [72], slightly moving up/down and inward regardless of whether the eyes are natural or artificial [73,74,109]. Using search coils, embedded in self-adhering scleral annuli, in a magnetic field has revealed that restraining of the one eyelid in the open or closed position dose not significantly alter the eye movements during eyeblinks [171]; thus, eye movement and eyelid movement are independent during an eyeblink. Furthermore, muscular movements persist even after removal of the eyeball [348]. Therefore, the factors mentioned above produce electrical potentials after an eyeblink, and these potentials are mixed with the respective potentials on the scalp in the EOG signal,

which can be observed using two electrodes placed on the superior and inferior orbital rims of the eyes. However, a person who has a brain diseases like blepharospasm that cause strong eyeblinking to clonic spasm to tonic spasm of the eyelids, or a blend of all them would generate an electrical signal alien from the one generated from healthy person [349, 350].

I described how eyelid and eyeball movements influence the electrical potential in complex ways in preceding paragraph. The first positive potential is caused by combining up/down and inward eyeball movements (dipole rotation changing) and the sliding eyelid on a positively charged cornea [89, 109] with extraocular muscle co-contraction. In contrast to the stated blink motions, the first negative potential is caused by combining the down/up and outward eyeball movements and inverse eyelid movement. The third and fourth potential peaks (second positive and negative potentials) were caused not only by the eyeblink potential occurring at right and left eyes respectively but also each simultaneous potential and three-dimensional diffusion, similar to circular wave patterns in the brain. In my opinion, the diffused potentials would pile up at a specific point within the cranium, and the magnified potential would reach each electrode. However, it is known that EEG signals generated from mammal brains have high spatiotemporal complexity and that the cortical connectivity is very highly weighted toward short ($< 500\ \mu$V) connections, which means that neuronal activities spread through a contiguous cortical region with a high attenuation penalty, based on the distance from sources [215–217]. The ICA algorithm accomplishes source separation of EEG signals because of these dynamics [104]. The attenuation penalty with increasing distance may affect the genuineness of our supposition; nevertheless, the propagation path of the EOG potential does not determine whether the EOG penalty coefficient is identical to that of the EEG. Therefore, this is simply my opinion.

4.6 Summary of Chapter 4

In this chapter, the effect of voluntary and involuntary eyeblinks on ICs contributing to EEG signals was characterized for creating templates of eyeblink artifact rejection from observed EEG signals with single-channel electrode. Fourteen EEG signals and one VEOG signal have been registered for twenty healthy subjects during two different experiments, which prompted subjects to blink voluntarily and involuntarily. Wavelet-enhanced ICA with two markers (mMSE and kurtosis) was employed as a source-separation and feature extraction scheme. The extracted eyeblink features were separated into epochs and analyzed in the frequency, time-frequency, and time domains.

The extracted eyeblink features confirmed three characteristics reported in the literature: (i) the distorting effects of eyeblink artifacts on the EEG are within the delta and

theta bands; (ii) electric potentials (dipole projections) caused by eyeblinks decrease with increasing distance between measurement points and eyes; and (iii) the propagation effects across the scalp present in a bilaterally symmetrical fashion. Furthermore, additional characteristics were found: (i) eyeblink features obtained from all channels presented significant differences between voluntary and involuntary; (ii) eyeblink effects continue to have an influence on EEG signals for 3.0 to 4.0 s (in the occipital region, 2.0 s); and (iii) these effects cease to exist after the zero-crossing point four (in the occipital region: two) times, for both eyeblink types.

Eyeblink artifactual contamination, which inevitably occurs with EEG applications, should be rejected from recorded EEG signals to allow precise diagnosis and system construction. The differences among the effects of voluntary and involuntary eyeblink in EEG signals were shown in this study. These results and dataset are helpful for making templates of eyeblink artifact rejection from observed EEG signals with a single-channel electrode as prior information because the dataset is enough to trust in a distribution of eyebkink effects on EEG signal. In Chapter 5, the eyeblink distribution will be used as a priori information for eyeblink artifact removal from single-channel EEG signals.

Chapter 5

AN EYEBLINK ARTIFACT REMOVAL SCHEME FOR SINGLE-CHANNEL ELECTROENCEPHALOGRAPHIC SIGNALS USING PRIOR INFORMATION OF EYEBLINK DISTRIBUTION

5.1 Introduction and Objectives

Although a certain amount of researchers tends to select wavelet or EMD-based ICA (my empirical knowledge) over recent periods, there is no 'gold-standard' scheme for single-channel EEG device (linear regression is used for a multi-channel device because the scheme needs reference channel). All of the existing schemes for single-channel EEG signals without the band(high)-pass filtering have still required additional information or technique: (i) reference channel (e.g. EOG channel); (ii) automatic component identification; and (iii) automatic epoch detection (see Chapter 3 Section 2). These drawbacks complicate the design of EEG measurement and increase the burden of manual operation. Also, comprehensively comparing all schemes over the same datasets had never been achieved because the artifact removal scheme for single-channel EEG signals has been attracted attention in nearly five years and a benchmark dataset for the development of removal schemes has not existed long enough in the field of biological signal processing. Therefore, the efficiency depends on the original and highly confidential dataset of respective literature. Such background leads to confusion or taking researchers' time and makes the selection of scheme difficult.

To clearly articulate the overall picture of artifact removal and overcome the drawbacks, in this chapter, I propose a section-based eyeblink artifact removal scheme by using supervised tensor factorization which has four beneficial properties: (i) automatic epoch detection; (ii) high signal separation accuracy; (iii) automatic separated component identification and signal reconstruction; and (iv) small number of arbitrary parameters.

The objective of this chapter is to explain the proposed scheme, to compare its efficiency for eyeblink artifact removal with eight schemes (linear regression, band-pass

filtering, adaptive filtering, WICA, EMD-ICA, EEMD-ICA, CEEMD-ICA, and 2-step NMF) with a common dataset, and to verify its efficiency for real-life data.

5.2 Materials

5.2.1 Data Recordings

The conditions of recordings are the same as Chapter 4 Section 2 Subsection 1 except for one measurement position. In this study, I selected Fz instead of Cz. Fifteen males and five females (mean age: 22.85 $\pm$ 1.42 years) demonstrated the experiments. Five persons (Sub. 03, Sub. 05, Sub. 07, Sub. 08, and Sub. 19) are the same in Chapter 4, but this experiment was conducted on more than one-year ago. The relation between aging and pronounced changes in the dopamine system is well known [351]. From early to later adulthood, both D_1 and D_2 receptor densities have decreased themselves with the rate of decline being just below 10% per decade [352, 353]. In addition, age-related decline in the dopamine transporter which is a commonly used presynaptic marker has been observed by postmortem studies [354, 355] and the losses means that reuptake of dopamine from the synapse to the presynaptic neuron will not be controlled little by little [356]. Therefore, I handled these data as completely different things. No subjects had a history of sensorimotor, ophthalmologic, or auditory abnormality. All subjects were asked to read and sign an informed consent approved by the Research Ethics Committee of Keio University before participating the research. There is no restriction on equipment for an eyeglasses including contact lenses.

5.2.2 Stimuli and Procedure

Each subject who had already equipped the EEG device on the head was asked to seat on a chair and stay in the position for several seconds. A few seconds later, a metronome begins to sound every 5 s. The subject blinks ten times by both eyes to the sound of the metronome. In each of the experiment, the subject was instructed to watch a laptop PC that display shows a cross-fixation. The datasets for each subject consist of 1 session of 55 s (10 trials plus 5 s margin). The first 5 s of recorded data is discarded; therefore, the length of each data is 50 s (10,240 data points). Through the experiments, 14-channel EEG and VEOG signals of twenty subjects were observed. The dataset has 200 eyeblinks in total. Observed signals regarding Fp1 position were extracted as a target because an electrode of this post is placed in the left prefrontal area where is nearest to the left eye. In other words, the observed signals from Fp1

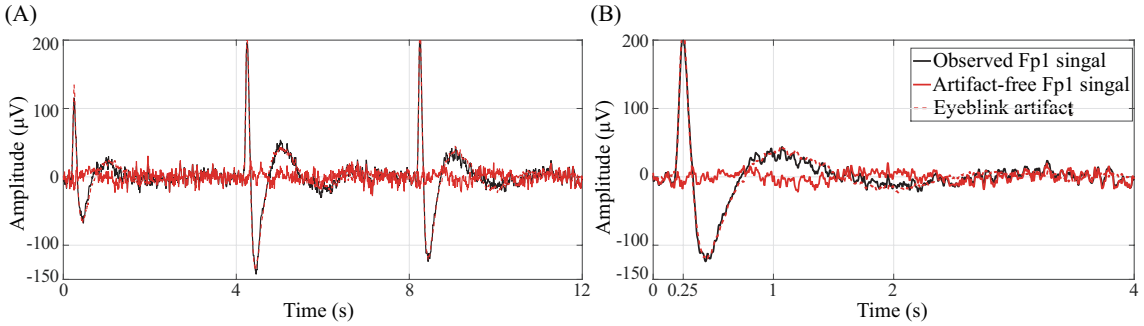

Figure 5.1 (A) A continuous observed Fp1 signal, artifact-free Fp1 signal, and artifact estimated by logistic InfoMax ICA. (B) A 4-s epoch.

position are essentially fragile to eyeblink artifacts. Moreover, the position has been chosen as a key measurement point for single-channel EEG device [118, 357]; therefore, I chose Fp1 signals as a target. A continuous observed Fp1 signal, artifact-free Fp1 signal, and artifact estimated by logistic InfoMax ICA with 14-channel data are shown in Figure 5.1. Extracted 4-s epochs of artifact-free Fp1 signals and artifacts will be treated as correct data for comparison of eyeblink artifact removal schemes.

5.3 Positive Semi-definite Tensor Factorization

In my proposed scheme, PSDTF is employed to factorize input data $\boldsymbol{X}$. PSDTF decomposes N PSD matrices (tensors) as a conic sums of K PSD matrices in time domain [317]. How to decompose elements on PSDTF is presented as follow.

Let's suppose given a three-mode tensor $\boldsymbol{X} = [\boldsymbol{X}_1, \boldsymbol{X}_2, \cdot, \boldsymbol{X}_N] \in \mathbb{R}^{M \times M \times N}$, where M and N are the width of matrix and number of matrix in the dataset. Each slice $\boldsymbol{X}_n \in \mathbb{R}^{M \times M}$ is a real symmetric PSD matrix. This algorithm approximates each PSD matrix $\boldsymbol{X}_n$ by a convex combination of PSD matrices $\{\boldsymbol{V}_k\}_{k=1}^{K}$ (K basis matrices).

$$\boldsymbol{X}_n \approx \sum_{k=1}^{K} \boldsymbol{V}_k w_{k,n} \stackrel{\text{def}}{=} \boldsymbol{Y}_n, \tag{5.1}$$

where $w_{k,n} \geq 0$ is a weight at the n-th slice. It can be rewritten as

$$\boldsymbol{X} \approx \sum_{k=1}^{K} \boldsymbol{V}_k \otimes \boldsymbol{w}_k \stackrel{\text{def}}{=} \boldsymbol{Y}, \tag{5.2}$$

where $\otimes$ denotes the Kronecker product.

In order to find good approximate factorization (low reconstruction error), the Log-Determinant (LD) divergence [358] which is a kind of the Bregman matrix divergence

[359] given by

$$\mathcal{D}_{LD}(\boldsymbol{X}_n \mid \boldsymbol{Y}_n) = -\log|\boldsymbol{X}_n {\boldsymbol{Y}_n}^{-1}| + \mathrm{tr}(\boldsymbol{X}_n {\boldsymbol{Y}_n}^{-1}) - M, \tag{5.3}$$

is selected for the algorithm of PSDTF. The LD divergence is always non-negative and is zero if and only if $\boldsymbol{X}_n = \boldsymbol{Y}_n$. This algorithm employs Multiplicative Update (MU) rules [312] to minimize the divergence as cost function $\mathcal{C}(\boldsymbol{X}|\boldsymbol{Y}) = \Sigma_n \mathcal{D}_{LD}(\boldsymbol{X}_n|\boldsymbol{Y}_n)$ and to estimate unknown variables $\boldsymbol{W} = [\boldsymbol{w}_1, ..., \boldsymbol{w}_K] \in \mathbb{R}^{K\times N}$ and $\boldsymbol{V} = [\boldsymbol{V}_1, ..., \boldsymbol{V}_K] \in \mathbb{R}^{M\times M\times K}$. The variables $\boldsymbol{W}$ and $\boldsymbol{V}$ are imposed on non-negativity and positive semidefiniteness constraint, respectively.

Minimizing the cost function $\mathcal{C}(\boldsymbol{X}|\boldsymbol{Y})$ is not analytically tractable problem. Hence, an auxiliary function approach [312] in terms of $\boldsymbol{Y}$ indirectly derives the MU rules for minimizing the cost function. The following update rule relevant to activation coefficients $w_{k,n}$ monotonically decreases the total auxiliary function.

$$w_{k,n} \leftarrow w_{k,n} \sqrt{\frac{\mathrm{tr}({\boldsymbol{Y}_n}^{-1} \boldsymbol{V}_k {\boldsymbol{Y}_n}^{-1} \boldsymbol{X}_n)}{\mathrm{tr}({\boldsymbol{Y}_n}^{-1} \boldsymbol{V}_k)}} \quad , \tag{5.4}$$

where the non-negativity of $\boldsymbol{W}$ is ensured because of that the number used to multiply $w_{k,n}$ is non-negative.

On the other hand, an equation relevant to basis matrix $\boldsymbol{V}_k$ is obtained as follows:

$$\boldsymbol{V}_k \boldsymbol{P}_k \boldsymbol{V}_k = {\boldsymbol{V}_k}^{\mathrm{old}} \boldsymbol{Q}_k {\boldsymbol{V}_k}^{\mathrm{old}}, \tag{5.5}$$

where ${\boldsymbol{V}_k}^{\mathrm{old}}$ indicates before updating the (current) values of $\boldsymbol{V}_k$. PSD matrices $\boldsymbol{P}_k$ and $\boldsymbol{Q}_k$ are given by

$$\boldsymbol{P}_k = \sum_{n=1}^{N} w_{k,n} {\boldsymbol{Y}_n}^{-1}, \tag{5.6}$$

$$\boldsymbol{Q}_k = \sum_{n=1}^{N} w_{k,n} {\boldsymbol{Y}_n}^{-1} \boldsymbol{X}_n {\boldsymbol{Y}_n}^{-1}. \tag{5.7}$$

An update rule with regard to $\boldsymbol{V}_k$ is derived from Eq. (5.5) under the Cholesky decomposition $\boldsymbol{Q}_k = \boldsymbol{L}_k {\boldsymbol{L}_k}^T$ where $\boldsymbol{L}_k$ is a lower triangular matrix.

$$\boldsymbol{V}_k \leftarrow \boldsymbol{V}_k \boldsymbol{L}_k ({\boldsymbol{L}_k}^T \boldsymbol{V}_k \boldsymbol{P}_k \boldsymbol{V}_k \boldsymbol{L}_k)^{-\frac{1}{2}} {\boldsymbol{L}_k}^T \boldsymbol{V}_k, \tag{5.8}$$

where the positive semidefiniteness of $\boldsymbol{V}_k$ is ensured because of that a real matrix $\boldsymbol{A}$ is said to be positive semidefinite if and only if $\boldsymbol{A} = \boldsymbol{Z}\boldsymbol{Z}^T$ is ensured for some real matrix $\boldsymbol{Z}$.

5.4 Proposed Scheme

The explain of my proposed scheme is wordiness; thus, it is summarized in Figure 5.2. This scheme can be separated into four sections; (i) contaminated epoch detection and extraction, (ii) tensor calculation, (iii) tensor factorization (supervised PSDTF), and (iv) signal reconstruction and replacement.

5.4.1 Contaminated Epoch Extraction

Before applying PSDTF, an epoch which has been contaminated by eyeblink artifact must be detected for tensor calculation. Three step algorithm employed statistical rules for automatic epoch detection and extraction. Firstly, Eyeblink Master Library [306] which can detect eyeblink artifacts contaminated zone from single prefrontal channel EEG signal with variable size moving the window and the summation of the first-order derivatives within the sliding window, was used. The local minimum and maximum within the range should be the same, and if a range fully included in another range, the included range will be discarded. In this thesis, the minimum, maximum window lengths, and predetermined threshold are set to 24 data points (about 94 ms), 56 data points (about 220 ms), and 75 μV.

However, there is no universal threshold for all subjects because each person has different size of eyeball and amount of exercise-induced muscular. It has been evidence to suggest that the electrical potential has a different distribution from that due to vertical ocular ration [334–336] and the movements of eye lid [109]. Therefore, the second positive peak caused by an eyeblink is occasionally incorrectly equated to first positive peak of the eyeblink. Here, I focused on the speed of amplitude convergence caused by an eyeblink. For Chapter 4, I have known a characteristic of eyeblink artifact that the first zero-crossing point after an eyeblink is within 0.10 s (25 data points), and the duration has been found no significant difference between voluntary and involuntary. For this reason, peak amplitude in the zone was sifted by using a fixed threshold on the second step. I set the value of the threshold θ, that is equivalent to $\tan^{-1}\frac{b}{a}$, where a and b indicate amplitude and data points, at 18.43 degree to judge whether the peak amplitude is first positive peak caused by an eyeblink or not. If the value is highest in the range and the angle is within 18.43 degree, the value is identified as the actual peak amplitude (see Figure 5.3).

Finally, an observed signal $\boldsymbol{x}_{\mathrm{Raw}}$ is separated into ten 4-s epochs $\boldsymbol{x}_{\mathrm{Epoch}}$ according to the point of peak amplitude. The point locates on 64th data point (0.25 s).

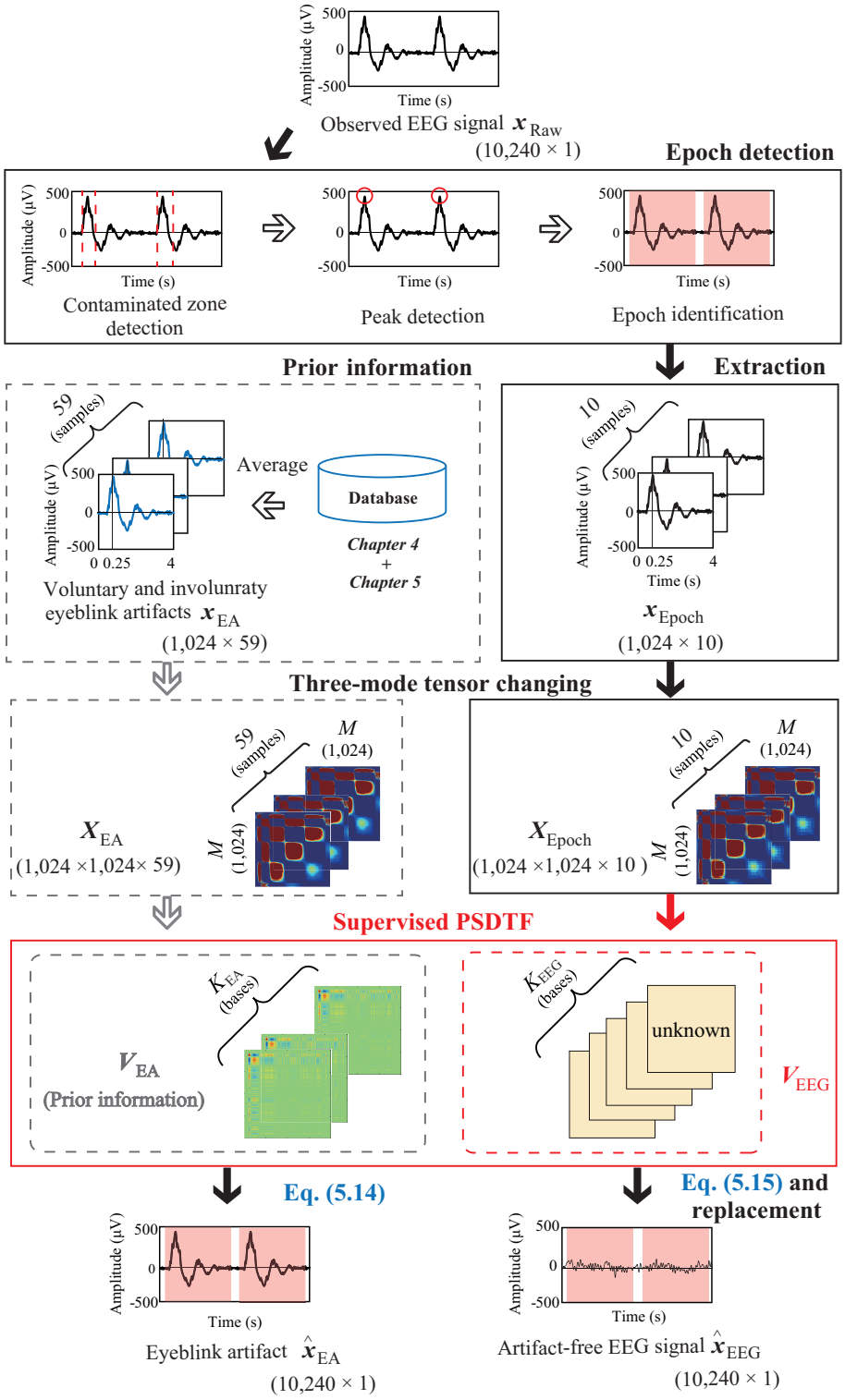

Figure 5.2 Proposed overall eyeblink artifact removal scheme for a subject.

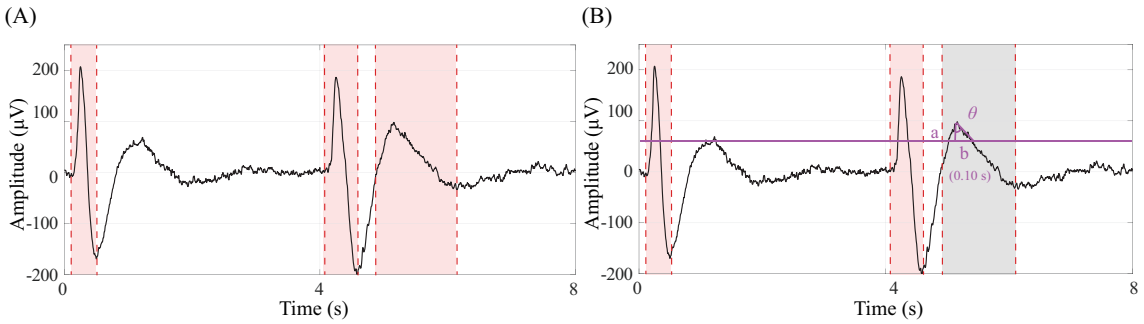

Figure 5.3 (A) Detected contaminated zones. (B) Actual peak amplitudes marked with red boxes judged by a fixed threshold in the second step of contaminated epoch extraction.

5.4.2 Tensor Calculation

The extracted epochs of one subject $\boldsymbol{x}_{\mathrm{Epoch}}$ will be changed to three-mode tensor:

$$\boldsymbol{X}_{\mathrm{Epoch}} = [\boldsymbol{x}_{\mathrm{Epoch1}}\boldsymbol{x}_{\mathrm{Epoch1}}{}^{T}, \ldots, \boldsymbol{x}_{\mathrm{Epoch}N}\boldsymbol{x}_{\mathrm{Epoch}N}{}^{T}] \in \mathbb{R}^{M\times M\times N}. \tag{5.9}$$

Their diagonal components are equivalent to square value of the epochs (Figure 5.4). Thus, each slice $\boldsymbol{X}_{\mathrm{Epoch}\,n} \in \mathbb{R}^{M\times M}$ is an auto-covariance matrix and a real symmetric PSD matrix. In this research, the width of matrix and number of matrix in the dataset for one subject are 1,024 (256 Hz multiplied by 4 s) and ; therefore, $M = 1,024$ and $N = 10$.

5.4.3 Prior Information Conveying in Basis and Factorization

My goal is to factorize a given mixture PSD matrix ($\boldsymbol{X}_{\mathrm{Epoch}}$) into the sum of K source PSD matrices and to lead EEG PSD matrices ($\boldsymbol{X}_{\mathrm{EEG}}$) from the mixture PSD matrix. If specific bases $\boldsymbol{V}_k$ have been characterized as eyeblink artifacts, other matrices are able to express EEG components. This idea is the same as 2-step NMF.

In processing the input data $\boldsymbol{X}_{\mathrm{Epoch}}$, 40 voluntary and involuntary eyeblink data averaged over trials that number depends on each subject described in Chapter 4 and 19 eyeblink data averaged over 10 trials of each subject with the exception of 1 subject described in Chapter 5, are used as a prior information in this scheme. The three-mode tensor data which contains 59 samples had been already factorized into $\boldsymbol{V}_{\mathrm{EA}}$ and $\boldsymbol{W}_{\mathrm{EA}}$ on the supervised PSDTF algorithm. Obtained bases $\boldsymbol{V}_{\mathrm{EA}}$ express voluntary and involuntary eyeblinks. In this thesis, the number of bases K_{EA} and iteration of MU algorithm are set as 5 and 200, experimentally.

Generally, the default values of basis matrix and activation value ($\boldsymbol{V}_k^{(0)}$ and $w_{k,n}^{(0)}$) are based on specifying prior distributions (in PSDTF algorithm, PSD matrix $\boldsymbol{V}_k$ and

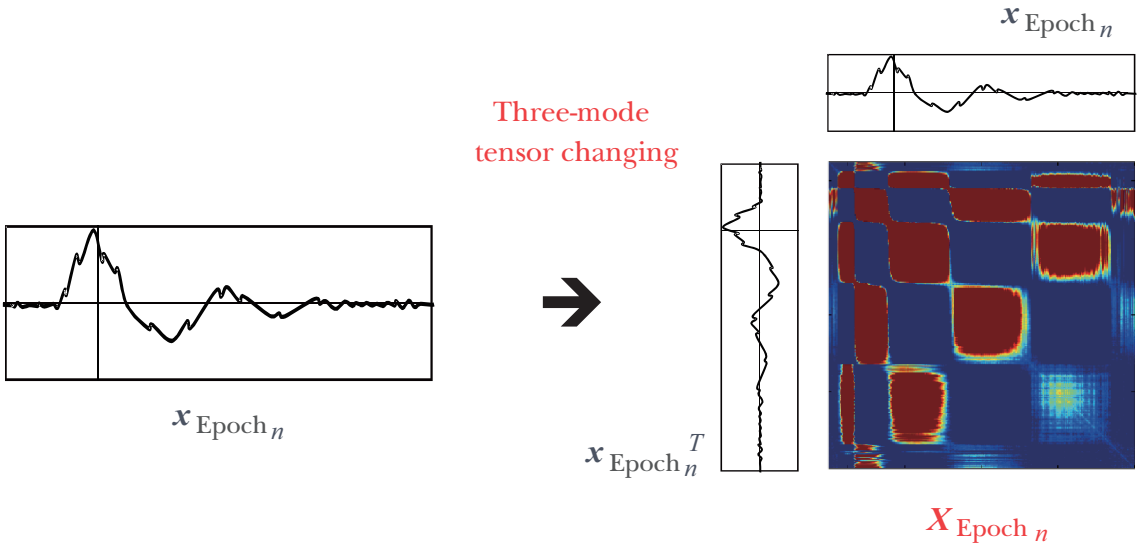

Figure 5.4 Visualization of tensor calculation from an extracted epoch.

nonnegative value $w_{k,n}$ are initialized by placing Wishart and gamma priors [318]).

$$\boldsymbol{V}_k \sim \mathcal{W}(\nu_0, \boldsymbol{V}_0), \tag{5.10}$$

$$w_{k,n} \sim \mathcal{G}(a_0, b_0), \tag{5.11}$$

where: ν_0 and $\boldsymbol{V}_0$ are the Degree Of Freedom (DOF) and scale of matrix of the Wishart distribution, a_0 and b_0 are the shape and rate parameters of the gamma distribution.

There is the assumption that the given PSD matrix (input data) $\{\boldsymbol{X}_{\text{Epoch } n}\}_{n=1}^{N}$ is independently Wishart distributed:

$$\nu \boldsymbol{X}_{\text{Epoch } n} | \boldsymbol{V}, \boldsymbol{W} \sim \mathcal{W}\big(\nu, \sum_{k=1}^{K} \boldsymbol{V}_k w_{k,n}\big), \tag{5.12}$$

where ν is also a DOF of the Wishart distribution. It is important to bear in mind that $\mathbb{E}[\boldsymbol{X}_{\text{Epoch } n}] = \boldsymbol{Y}_n$ and $\mathbb{M}[\boldsymbol{X}_{\text{Epoch } n}] = \frac{\nu - M - 1}{\nu} \boldsymbol{Y}_n$, where $\mathbb{M}[\cdot]$ is the mode operator. If the DOF is overwhelmingly larger than the width ($\nu \gg M$), the mode operator regarding the input data will be approximated as a reconstruction matrix ($\mathbb{M}[\boldsymbol{X}_{\text{Epoch } n}] \approx \boldsymbol{Y}_n$). Meanwhile, the DOF is smaller than the width ($\nu < M$); the input data will be rank-deficient. Still, the distribution boils down to an exponential distribution when the DOF and width are tantamount to 1 ($\nu = M = 1$). The log-likelihood of the input data can be expressed as:

$$\begin{aligned} \log p(\boldsymbol{X}_{\text{Epoch } n} | \boldsymbol{Y}_n) = \; & C(\nu) + \frac{\nu - M - 1}{2} \log |\boldsymbol{X}_{\text{Epoch } n}| \\ & - \frac{\nu}{2} \log |\boldsymbol{Y}_n| - \frac{\nu}{2} \operatorname{tr}(\boldsymbol{X}_{\text{Epoch } n} \boldsymbol{Y}_n^{-1}) \, , \end{aligned} \tag{5.13}$$

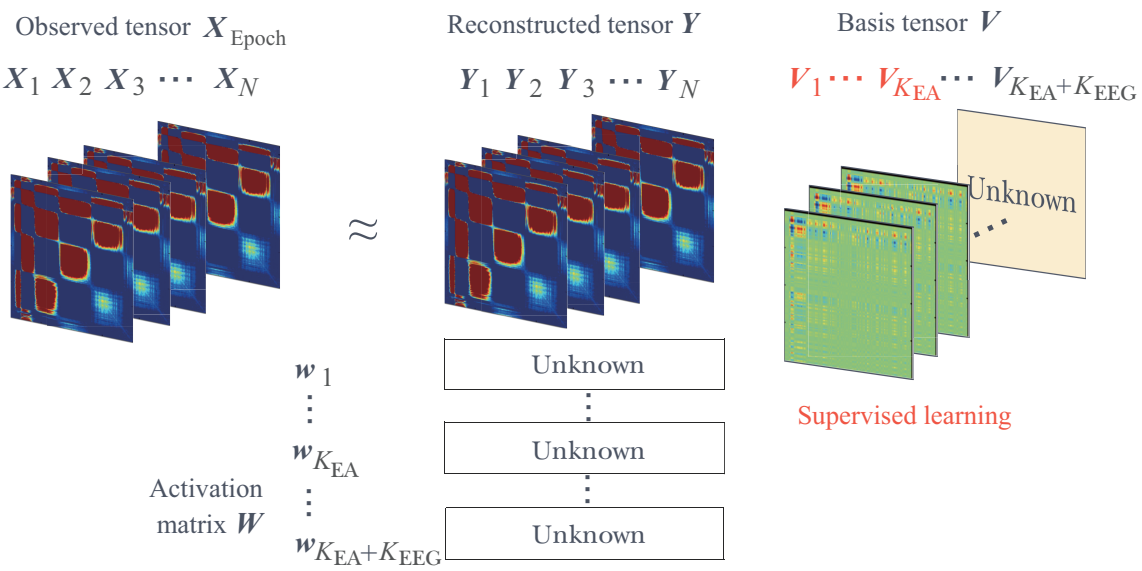

Figure 5.5 Observation tensor $\boldsymbol{X}_{\text{Epoch}}$ and reconstruction tensor $\boldsymbol{Y}$. The tensor $\boldsymbol{X}_{\text{Epoch}}$ was approximately factorized into basis tensors $\boldsymbol{V}$ and activation vectors $\boldsymbol{w}$ by supervised PSDTF.

where the first and second terms are constant; therefore, the maximization of the likelihood $p(\boldsymbol{X}_{\text{Epoch}\,n}|\boldsymbol{Y}_n) = \Pi_n(\boldsymbol{X}_{\text{Epoch}\,n}|\boldsymbol{Y}_n)$ regarding $\boldsymbol{Y}$ is equivalent to the minimize the cost function $\mathcal{C}(\boldsymbol{X}|\boldsymbol{Y}) = \Sigma_n \mathcal{D}_{LD}(\boldsymbol{X}_n|\boldsymbol{Y}_n)$. In brief, this technique is based on probabilistic model and MU algorithm, and can be functionally extended from finite model to nonparametric Bayesian model (I handle finite model in this thesis). The default values are randomly generated according to Wishart or gamma distribution, and then updated by the MU rules in a regular PSDTF algorithm. When an input tensor $\boldsymbol{X}_{\text{Epoch}\,n}$ is factorized into $\boldsymbol{V}$ and $\boldsymbol{W}$, the elements of $\boldsymbol{V}$ does not routinely have relation to elements of $\boldsymbol{V}_{\text{EA}}$. In the supervised PSDTF processing, the elements of $\boldsymbol{V}_{\text{EA}}$ is used as default and fixed values that means these values split off from the MU algorithm. For this constraint, the matrix $\boldsymbol{V}_{\text{EEG}}$ can express only EEG components using its K_{EEG} PSD matrices, I assumed that (Figure 5.5). Alternatively, activation elements $\boldsymbol{W}_{\text{EA}}$ are variable value on the processing. The number of bases K_{EEG} and iteration of MU algorithm are set as 5 and 30 according to the reference [360].

5.4.4 Eyeblink Artifact Removal and Signal Reconstruction

After passing through the processes, EEG signal and artifacts estimated by the proposed scheme are reconstructed from the following equations:

$$\hat{\boldsymbol{x}}_{\mathrm{EA}\,n} = \left(\sum_{k=1}^{K_{\mathrm{EA}}} \boldsymbol{V}_k w_{k,n}\right)\left(\sum_{k=1}^{K_{\mathrm{EA}}+K_{\mathrm{EEG}}} \boldsymbol{V}_k w_{k,n}\right)^{-1} \boldsymbol{x}_{\mathrm{Epoch}\,n}\ , \tag{5.14}$$

$$\hat{\boldsymbol{x}}_{\mathrm{EEG}\,n} = \left(\sum_{k=K_{\mathrm{EA}}+1}^{K_{\mathrm{EA}}+K_{\mathrm{EEG}}} \boldsymbol{V}_k w_{k,n}\right)\left(\sum_{k=1}^{K_{\mathrm{EA}}+K_{\mathrm{EEG}}} \boldsymbol{V}_k w_{k,n}\right)^{-1} \boldsymbol{x}_{\mathrm{Epoch}\,n}\ . \tag{5.15}$$

Above Eqs. make it possible to reconstruct signals in time-domain only with observed single-channel epochs $\boldsymbol{x}_{\mathrm{Epoch}}$. The estimated artifact-free EEG signal would supplant the observed signals based on a marker obtained by the step of epoch identification. This section has no necessary to detect or identify factorized component because I have already known each base has artifactual or neuronal component. That means this section achieved automatic artifact removal and signal reconstruction.

5.5 Efficiency Metrics

To measure how much eyeblink artifact has been estimated and how much reconstructed artifact-free EEG signal has been similar to the reference signal (estimated by logistic InfoMax ICA), I use Signal-to-Noise Ratio (SNR) and Mean Square Error (MSE) as following equations:

$$\mathrm{SNR} = 10\log_{10}\frac{\sigma^2_{\hat{x}_{\mathrm{EEG\ or\ EA}}}}{\sigma_e^2}, \tag{5.16}$$

$$\mathrm{MSE} = \frac{1}{N_{\mathrm{Point}}}\sum_{n=1}^{N_{\mathrm{Point}}} e(n)^2, \tag{5.17}$$

where

$$e(n) = \hat{x}_{\mathrm{EEG\ or\ EA}}(n) - \hat{x}_{\mathrm{EEG\ or\ EA\ by\ ICA}}(n). \tag{5.18}$$

In this experiments, the number of data points N_{Point} is calculated by 10,240.

5.6 Results and Discussion

5.6.1 Eyeblink Features in Bases

Basis matrices ($\boldsymbol{V}_1 \sim \boldsymbol{V}_{10}$) factorized by my proposed scheme are shown in Figure 5.6 (A). First five bases ($\boldsymbol{V}_1 \sim \boldsymbol{V}_5$) were the results of the prior information in the supervised PSDTF algorithm. Other five bases ($\boldsymbol{V}_6 \sim \boldsymbol{V}_{10}$) were additional results of my scheme.

The first five bases has high value on bottom left in all of their components. The electrical potentials seen with eyeblink are thought to involve a mix of factors (e.g. changes in the orientation of the corneoretinal potential difference [361], the movement of the eyelid [109, 334–336]). Therefore, the energy (waveform) is not always fixed. In addition, the amount of electricity also depends on the strength of the levator palpebrae superioris muscle. In other words, each electric potential of eyeblink is difference. Nevertheless, I have already investigated the pattern of the electric potential and the distribution in Chapter 4, components that are within 1.5 s after an eyeblink have significant presence in the first five bases. The distorting effects of eyeblink artifact on the EEG cease to exist after the zero-crossing point four times. If an epoch including the effect of an eyeblink will be changed to three-more tensor based on calculation of auto-covariance matrix, the observed EEG epoch likely to be seriously abused by electrical potential generated from an eyeblink. The orchestrated crossing time is extended over a period of 500 ms after passing the third zero-amplitude point (see Figure 4.9). These features imply that the eyeblink artifact among subjects regardless of eyeblink type (voluntary or involuntary) can be comprehended by initiative three zero-crossing in potential to express eyeblink artifact in the database.

On the other hand, K_{EEG} basis matrices in $\boldsymbol{V}_{\mathrm{EEG}}(\boldsymbol{V}_6 \sim \boldsymbol{V}_{10})$ indicate no distinctive feature. The EEG signal depends on the lead fields which is a vector filed in a volume conductor; this field is the pattern of sensitivity of an EEG to sources at various locations and orientations in the volume conductor [340]. Furthermore, the signal reflects the summation of excitatory or inhibitory postsynaptic potentials in the most superficial layers of the cortex. In the other words, there is no specific waveform in the EEG because synaptic transmissions of the apical dendrites are not activated while the person was provided no stimulus. In this experiments, the subjects only blinked; therefore, supervised PSDTF extracted above-mentioned features for EEG components. The meaning of that there is no distinctive feature can replace that there is no artifact in the data. Here, I show factorized PSD matrices with regular PSDTF which applied its algorithm to factorize input data into ten bases, in Figure 5.6 (B). This figure visually revealed that regular PSDTF algorithm (simple factorization) can not extract EEG components, but distribute eyeblink artifact to all bases. The supervised PSDTF can extract EEG features from contaminated single-channel EEG signals because it is

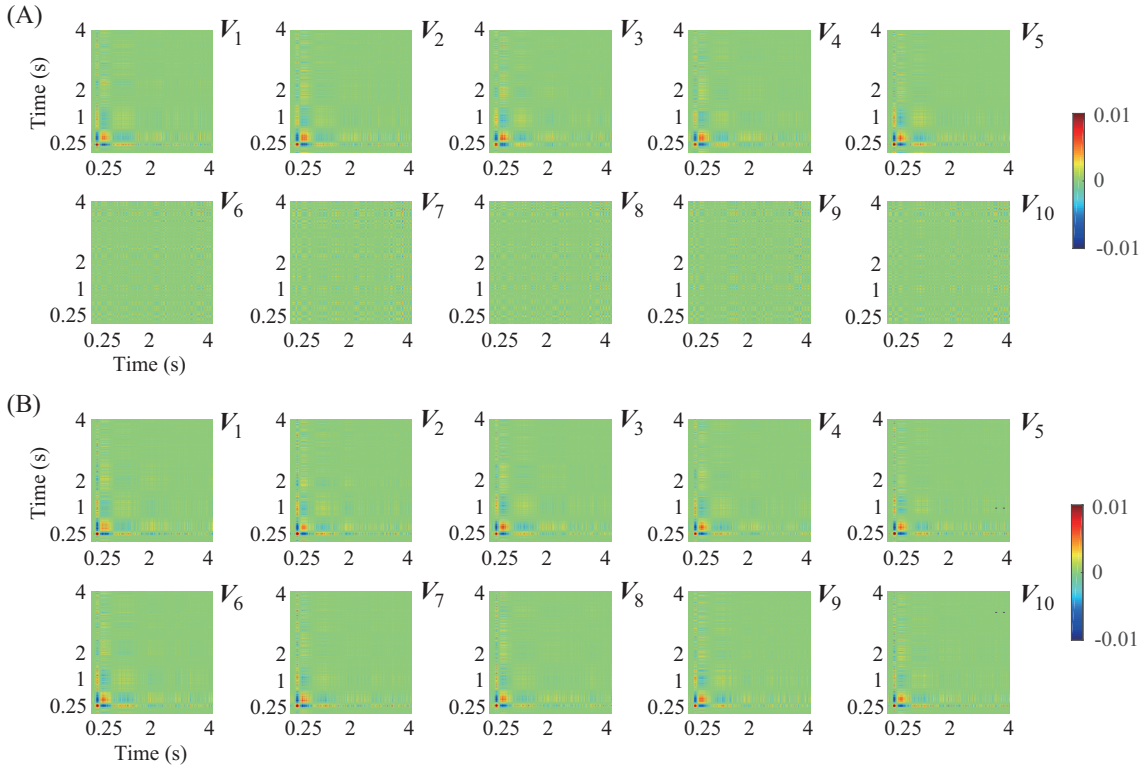

Figure 5.6 (A) Estimated artifact PSD matrices (upper row) and other PSD matrices (bottom row) by proposed scheme. (B) Factorized PSD matrices with no constraint.

natural that EEG signal included a feature only of eyeblink artifact.

5.6.2 Quantitative Evaluation

The results of efficiency metrics in regard to artifact-free EEG signals and estimated artifacts are shown in Figure 5.7 and Tables 5.1 - 5.4. In the figure, nine schemes including proposed scheme are separated into groups by four categories: (i) regression (black); (ii) filtering (blue); (iii) ICA-based (green); and (iv) section-based (red). Red lines lying in boxes, black lines, and red crosses are median values, maximum or minimum adjacent values, and outliner values based on the interquartile range.

Linear regression and adaptive filtering can automatically remove eyeblink artifact with astonishing performance and high-speed processing if the parameters have already been optimized. However, one or more reference channels that are synchronized with the target channel must be required to make the output as close as possible to some desired response. The limitation on the convergence factor and filter order of the filtering method is that it cannot remove eyeblink artifacts as much as eye movement when the reference channel has the distortion of phase [280].

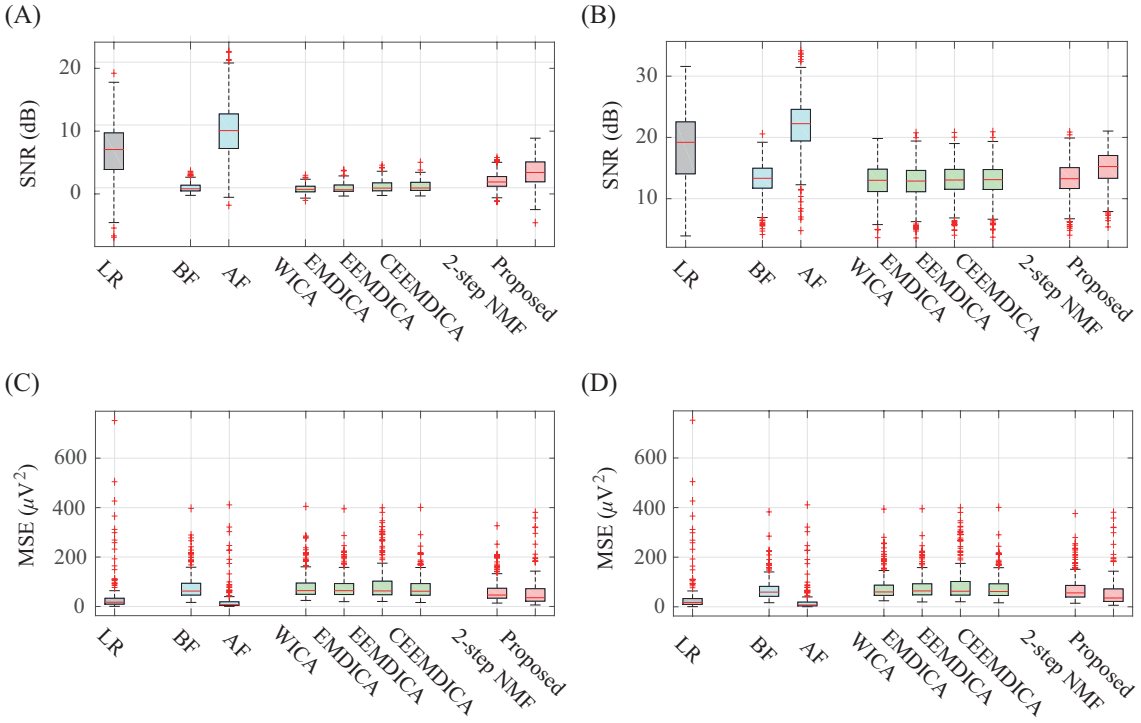

Figure 5.7 Quantitative performance evaluation of eyeblink artifact removal schemes (Linear Regression (LR), Band-pass Filtering (BF), Adaptive Filtering (AF), Wavelet-ICA (WICA), EMD-ICA, EEMD-ICA, CEEMD-ICA, 2-step NMF, and supervised PSDTF (Proposed)). (A) Estimated artifact-free EEG signal visualized by SNR. (B) Estimated eyeblink artifact visualized by SNR. (C) Estimated artifact-free EEG signal visualized by MSE. (D) Estimated eyeblink artifact visualized by MSE.

Table 5.1 Estimation performance of artifact-free EEG signal for nine schemes verified by SNR (dB). The results are reported for each subject separately and averaged over 10 trials.

	LR	BF	AF	WICA	EMD-ICA	EEMD-ICA	CEEMD-ICA	2-step NMF	Proposed
Sub. 01	7.25±2.44	1.07±0.43	10.13±2.77	1.05±0.38	0.58±0.21	1.29±0.30	1.12±0.29	2.48±0.71	4.14±1.82
Sub. 02	15.01±0.89	0.99±0.33	16.83±2.94	-0.02±0.67	0.57±0.20	0.72±0.29	1.06±0.34	1.29±0.51	5.65±0.89
Sub. 03	9.63±0.64	0.71±0.15	10.34±0.79	0.70±0.14	0.79±0.25	0.80±0.22	0.75±0.15	1.67±0.38	2.26±1.49
Sub. 04	10.43±0.66	0.76±0.12	10.39±1.52	0.77±0.14	0.78±0.19	0.87±0.21	0.74±0.12	2.15±0.45	3.03±1.72
Sub. 05	2.78±1.22	0.18±0.13	2.70±1.55	-0.01±0.29	0.09±0.06	0.11±0.09	0.15±0.10	0.27±0.90	-0.60±1.54
Sub. 06	6.24±1.46	1.49±0.37	11.76±2.44	1.39±0.33	1.77±0.37	1.73±0.38	2.09±0.42	4.65±0.83	5.67±1.97
Sub. 07	5.32±2.29	0.71±0.35	10.04±1.62	0.57±0.32	0.41±0.20	0.77±0.49	0.78±0.37	1.52±0.77	3.99±1.13
Sub. 08	6.33±1.68	2.59±0.64	18.28±4.65	1.36±0.39	2.62±0.69	3.11±0.83	3.07±0.93	3.77±1.70	6.28±2.29
Sub. 09	4.13±1.20	2.38±0.51	16.95±1.75	2.17±0.49	2.16±0.47	2.57±0.56	2.41±0.52	3.13±0.66	4.23±1.12
Sub. 10	16.79±1.51	0.77±0.21	17.47±2.32	0.65±0.18	0.46±0.13	0.82±0.25	0.83±0.23	1.54±0.44	3.44±0.83
Sub. 11	9.39±1.22	1.58±0.53	8.67±1.36	1.45±0.43	1.44±0.48	1.22±0.42	1.11±0.38	3.05±0.88	3.23±2.73
Sub. 12	0.44±1.00	0.57±0.13	8.99±2.31	0.40±0.47	0.65±0.22	0.85±0.24	0.67±0.16	1.56±0.59	3.14±0.63
Sub. 13	-2.45±3.36	-0.10±0.07	-0.28±0.13	-0.05±0.09	-0.11±0.13	-0.12±0.07	-0.16±0.10	0.32±0.74	-0.64±0.89
Sub. 14	4.73±2.05	0.29±0.17	10.77±1.84	0.28±0.27	0.35±0.24	0.21±0.13	0.33±0.19	0.96±0.62	2.02±0.95
Sub. 15	6.93±0.56	1.96±0.32	6.72±0.69	1.54±0.39	1.67±0.40	2.08±0.32	2.01±0.32	2.75±0.47	2.28±0.98
Sub. 16	3.19±2.32	0.75±0.17	4.74±2.74	0.71±0.19	1.46±0.13	2.61±0.77	2.39±0.49	1.70±0.23	2.57±1.48
Sub. 17	5.46±2.57	0.95±0.29	10.91±2.45	0.79±0.31	0.60±0.20	0.67±0.41	0.97±0.30	1.39±0.38	1.61±1.51
Sub. 18	8.44±0.93	1.40±0.28	11.81±3.21	1.37±0.27	1.50±0.39	1.98±0.42	2.08±0.42	3.88±0.25	5.48±1.71
Sub. 19	10.25±0.81	0.37±0.07	9.71±1.23	0.38±0.14	0.36±0.10	0.32±0.07	0.37±0.09	1.87±0.91	5.18±0.91
Sub. 20	9.76±0.95	0.58±0.29	7.94±2.28	0.57±0.25	0.83±0.33	1.00±0.32	0.94±0.43	2.16±0.58	3.59±1.46
All	7.00±4.70	1.00±0.76	10.24±5.12	0.80±0.66	0.95±0.77	1.18±0.95	1.19±0.92	2.10±1.32	3.33±2.34

ICA-based schemes has about the same performance of band-pass filtering (see Figure 5.7). Unfortunately, the assumption of ICA-based schemes is that each component such

Table 5.2 Estimation performance of eyeblink artifact for nine schemes verified by SNR (dB). The results are reported for each subject separately and averaged over 10 trials.

	LR	BF	AF	WICA	EMD-ICA	EEMD-ICA	CEEMD-ICA	2-step NMF	Proposed
Sub. 01	18.28±2.68	13.25±1.24	21.15±3.37	12.45±1.39	11.60±1.40	12.30±1.46	12.14±1.43	12.30±1.51	15.15±2.70
Sub. 02	28.67±1.36	14.10±0.93	30.49±2.91	13.71±1.26	14.23±1.01	14.37±1.02	14.71±1.02	14.29±1.00	19.30±1.43
Sub. 03	22.50±0.41	14.30±1.33	23.21±0.83	14.17±0.97	13.67±0.87	13.69±0.87	13.62±0.85	13.64±0.90	15.13±1.52
Sub. 04	23.41±0.57	14.40±1.23	23.37±1.32	14.32±0.95	13.76±0.87	13.86±0.87	13.72±0.85	14.34±0.91	16.00±1.93
Sub. 05	20.60±1.46	17.16±1.90	20.52±1.76	17.52±1.42	17.92±1.59	17.95±1.60	17.98±1.61	18.17±1.55	17.22±1.90
Sub. 06	14.22±1.18	11.04±1.75	19.74±3.21	9.96±1.81	9.75±1.92	9.72±1.79	10.07±1.65	10.94±1.84	13.63±1.29
Sub. 07	18.75±1.05	14.34±2.15	23.47±2.43	14.34±2.67	13.84±2.70	14.21±2.42	14.21±2.67	14.75±2.51	17.41±2.17
Sub. 08	13.58±0.18	10.43±2.28	25.52±4.09	9.38±1.87	9.86±2.12	10.35±2.24	10.31±2.18	12.11±2.09	13.51±2.51
Sub. 09	14.39±0.18	12.82±1.68	27.21±2.05	12.69±1.46	12.42±1.53	12.83±1.58	12.67±1.56	12.30±1.56	14.48±1.85
Sub. 10	29.25±1.57	12.91±1.71	29.93±2.75	13.25±1.68	12.91±1.67	13.28±1.73	13.28±1.72	13.28±1.75	15.88±1.49
Sub. 11	22.64±1.83	14.69±1.70	21.92±1.36	14.89±2.11	14.69±2.13	14.47±2.16	14.36±2.16	15.28±2.08	16.47±18.5
Sub. 12	12.19±0.21	12.85±1.13	20.74±2.02	12.41±1.13	12.41±1.04	12.61±1.05	12.42±1.03	12.96±1.07	14.89±0.74
Sub. 13	8.05±2.19	10.47±2.99	10.22±3.18	10.40±3.09	10.39±3.16	10.38±3.15	10.34±3.14	10.61±3.16	9.86±2.80
Sub. 14	19.25±0.86	14.53±2.40	25.30±2.80	14.76±2.60	14.87±2.78	14.74±2.61	14.85±2.76	15.29±3.00	16.54±2.08
Sub. 15	21.02±1.11	15.97±1.07	20.81±1.21	15.96±1.19	15.75±0.95	16.17±1.09	16.10±1.10	16.01±1.15	16.35±1.28
Sub. 16	14.15±1.72	13.71±1.68	15.71±2.37	12.12±1.74	12.42±1.62	13.58±1.81	13.36±1.54	11.76±1.68	13.47±1.11
Sub. 17	17.16±0.38	12.45±2.79	22.61±2.66	12.55±2.78	12.31±2.85	12.38±2.68	12.68±2.89	12.53±2.91	13.30±2.50
Sub. 18	12.56±0.64	6.18±1.08	15.93±2.98	5.87±1.10	5.62±1.08	6.09±1.10	6.20±1.17	6.22±1.20	9.60±2.05
Sub. 19	22.80±1.53	12.83±2.11	22.26±2.78	13.14±2.12	12.91±2.12	12.87±2.16	12.92±2.15	13.77± 2.21	17.74±2.69
Sub. 20	20.61±2.21	12.24±2.76	18.79±4.29	11.71±2.52	11.68±2.54	11.86±2.57	11.78±2.45	12.02±2.64	14.43±2.96
All	18.70±5.53	13.03±2.90	21.94±5.29	12.78±3.08	12.65±3.11	12.89±3.05	12.89±3.04	13.13±3.04	15.01±3.04

Table 5.3 Estimation performance of artifact-free EEG signal for nine schemes verified by MSE (μV^2). The results are reported for each subject separately and averaged over 10 trials.

	LR	BF	AF	WICA	EMD-ICA	EEMD-ICA	CEEMD-ICA	2-step NMF	Proposed
Sub. 01	13.40±11.60	46.89±9.52	7.44±7.48	47.17±9.79	57.45±11.10	44.88±10.00	46.49±10.23	34.10±7.67	24.31±8.60
Sub. 02	1.10±0.18	27.95±6.03	0.96±1.12	35.14±6.84	30.63±6.00	37.73±7.59	27.54±6.07	26.26±6.29	9.82±3.21
Sub. 03	12.53±3.17	97.26±24.18	10.82±3.65	97.31±23.91	96.27±24.42	100.96±22.97	96.37±23.97	78.37±20.54	75.36±47.27
Sub. 04	9.31±2.53	85.43±19.97	9.58±3.47	85.19±19.97	85.03±19.25	117.05±18.71	85.95±19.55	62.37±15.68	58.81±45.82
Sub. 05	28.16±6.18	54.27±24.03	28.71±6.43	56.04±22.09	55.15±23.55	55.35±24.05	54.61±23.79	53.73±25.20	79.02±86.43
Sub. 06	28.17±10.19	82.06±20.14	8.87±6.19	83.79±19.83	76.69±18.37	78.05±18.65	69.94±8.92	39.51±9.37	35.12±23.75
Sub. 07	20.27±8.24	54.01±9.18	6.90±4.00	55.76±9.45	57.72±9.13	55.92±9.28	53.11±9.02	45.24±10.42	25.79±6.19
Sub. 08	18.27±7.45	40.95±8.26	2.02±3.54	54.23±10.50	40.99±9.37	36.63±8.29	36.72±6.76	35.88±23.69	23.63±28.90
Sub. 09	42.72±10.01	63.45±11.99	2.33±1.08	66.59±12.15	66.75±12.04	62.53±10.71	63.97±12.22	53.57±10.37	42.59±13.88
Sub. 10	0.87±0.26	34.74±9.22	0.83±0.62	35.58±8.82	37.15±9.22	47.62±9.05	34.33±9.37	29.12±7.91	18.86±5.62
Sub. 11	9.86±1.25	60.56±13.11	11.86±2.94	62.36±13.42	63.14±15.63	69.50±16.07	73.81±17.09	43.12±9.45	47.48±27.90
Sub. 12	58.03±18.48	54.94±12.27	9.01±6.12	56.83±10.50	54.09±12.66	52.35±12.75	53.87±12.51	44.52±12.77	30.74±7.98
Sub. 13	339.80±185.14	196.76±98.63	205.44±102.65	195.50±100.64	197.18±98.20	198.58±98.91	199.04±98.74	172.29±74.12	221.01±104.60
Sub. 14	20.89±7.11	67.72±47.62	5.97±4.22	67.58±47.23	67.12±47.49	79.26±49.44	66.57±46.98	59.61±44.15	42.81±26.11
Sub. 15	33.29±4.09	105.79±21.89	35.01±4.86	117.15±26.44	113.98±22.52	313.50±30.83	134.66±21.50	89.13±22.71	100.11±27.46
Sub. 16	128.72±72.83	205.36±42.75	96.29±82.13	207.55±44.90	173.84±32.37	268.58±39.76	157.63±36.45	164.98±35.28	141.38±61.25
Sub. 17	25.39±14.02	75.74±55.65	7.40±5.38	78.13±55.83	81.48±57.90	86.73±54.26	76.47±55.34	69.87±53.64	59.17±23.22
Sub. 18	11.56±2.02	58.70±10.85	6.39±4.22	59.09±10.60	57.21±9.66	54.82±9.53	51.79±9.88	33.01±4.95	24.45±10.39
Sub. 19	5.64±0.71	55.62±10.74	6.79±2.92	55.61±11.04	55.74±10.67	56.51±10.91	55.63±10.71	39.27±6.51	18.70±5.35
Sub. 20	14.82±4.14	121.56±29.19	25.78±20.01	121.48±28.50	114.73±27.53	110.47±28.14	111.83±26.10	85.74±27.31	64.14±25.61
All	41.14±85.50	79.49±56.01	24.42±54.58	81.91±55.74	79.12±51.87	96.35±80.94	77.52±52.32	62.98±47.59	57.59±62.12

as disjoint spectrum or mode is independent (if the two signals which have the same frequency component were mixed, such feature identifies as same signal); therefore, I expected ICA-based and band-pass filtering cannot completely separate intrinsic EEG components and artifacts. As I speculated, the thorough rejection of each frequency band would lead to collapse of artifact-free EEG signal. No matter how much the artifact estimation has successfully been completed, artifact rejection belongs in the preprocessing in the EEG system; therefore, it's quite meaningless when the artifact-free EEG signal has been distorted by artifact removal scheme.

Table 5.4 Estimation performance of eyeblink artifact for nine schemes verified by MSE (μV^2). The results are reported for each subject separately and averaged over 10 trials.

	LR	BF	AF	WICA	EMD-ICA	EEMD-ICA	CEEMD-ICA	2-step NMF	Proposed
Sub. 01	13.40±11.60	36.01±8.05	7.44±7.48	43.14±8.39	57.45±11.10	44.96±9.99	46.49±10.23	44.81±9.36	24.37±8.61
Sub. 02	1.10±0.18	31.72±6.63	0.96±1.12	34.62±7.07	30.63±6.00	37.78±7.60	27.54±6.07	30.18±5.97	9.84±3.22
Sub. 03	12.53±3.17	82.72±21.60	10.82±3.65	84.63±19.27	96.27±24.42	100.71±23.07	96.37±23.97	95.85±23.06	75.46±47.33
Sub. 04	9.31±2.53	73.21±15.49	9.58±3.47	74.52±15.62	85.03±19.25	116.84±18.77	85.95±19.55	74.74±18.60	58.94±46.02
Sub. 05	28.16±6.18	63.37±17.61	28.71±6.43	59.20±21.23	55.15±23.55	55.10±23.93	54.61±23.79	52.36±23.54	79.09±86.31
Sub. 06	28.17±10.19	56.83±12.39	8.87±6.19	73.09±16.58	76.69±18.37	77.95±18.67	69.94±8.92	57.87±11.49	35.23±23.84
Sub. 07	20.27±8.24	52.09±11.76	6.90±4.00	51.67±9.16	57.72±9.13	55.84±9.27	53.11±9.02	47.22±10.27	25.82±6.18
Sub. 08	18.27±7.45	35.87±7.89	2.02±3.54	45.33±8.78	40.99±9.37	36.63±8.31	36.72±6.76	24.85±7.57	23.69±29.00
Sub. 09	42.72±10.01	61.09±13.18	2.33±1.08	62.41±9.89	66.75±12.04	62.48±10.79	63.97±12.22	68.60±13.29	42.67±13.86
Sub. 10	0.87±0.26	37.32±9.88	0.83±0.62	34.34±8.52	37.15±9.22	47.58±9.07	34.33±9.37	34.27±9.06	18.89±5.60
Sub. 11	9.86±1.25	62.20±12.09	11.86±2.94	59.36±11.55	63.14±15.63	69.48±16.08	73.81±17.09	54.96±13.26	47.58±27.96
Sub. 12	58.03±18.48	48.93±11.74	9.01±6.12	53.53±9.16	54.09±12.66	52.26±12.75	53.87±12.51	47.93±12.77	30.75±7.97
Sub. 13	339.80±185.14	191.44±93.29	205.44±102.65	195.72±96.15	197.18±98.20	198.39±98.80	199.03±98.74	187.68±94.03	220.96±104.59
Sub. 14	20.89±7.11	68.54±39.06	5.97±4.22	68.36±48.73	67.12±47.49	79.17±49.49	66.57±46.98	62.88±47.14	42.84±26.13
Sub. 15	33.29±4.09	109.02±29.94	35.01±4.86	108.68±24.75	113.98±22.52	313.24±30.82	134.66±21.50	107.12±23.47	100.41±27.54
Sub. 16	128.72±72.83	130.65±30.86	96.29±82.13	187.70±42.83	173.84±32.37	268.24±40.02	157.63±36.45	202.46±38.48	141.90±62.04
Sub. 17	25.39±14.02	77.68±52.54	7.40±5.38	76.85±54.51	81.48±57.90	86.58±54.17	76.47±55.34	78.31±57.49	59.29±23.28
Sub. 18	11.56±2.02	50.16±7.75	6.39±4.22	54.13±10.44	57.21±9.66	54.79±9.55	51.79±9.88	49.86±8.41	24.46±10.38
Sub. 19	5.64±0.71	56.82±11.48	6.79±2.92	52.80±9.75	55.74±10.67	56.43±10.92	55.63±10.71	45.99±9.78	18.66±5.34
Sub. 20	14.82±4.14	100.00±20.21	25.78±20.01	113.68±27.16	114.73±27.53	110.27±28.10	111.83±26.10	106.21±25.74	64.18±25.53
All	41.14±85.50	71.28±46.66	24.42±54.58	76.69±52.93	79.12±51.87	96.24±80.87	77.52±52.32	73.71± 55.16	57.68±62.20

In 2-step NMF already optimized the numbers of bases $K_1 = 15, K_2 = 15$ and used same database of prior information, it showed relatively high performance among nine schemes. By importing automatic epoch detection method as the proposed scheme, development of 2-step NMF would be promised. My proposed scheme outperformed all of existing schemes when there is only single-channel data. In both cases, the estimation of artifact-free EEG signal and eyeblink artifact, supervised PSDTF has significantly outperformed the accuracy of 2-step NMF ($P < .001$). Much less the outlier values (stable operation) than other schemes appeared in the proposed scheme.

Unsupervised learning algorithms with multi-channel data use statistical relationships between the signals to decompose artifacts by estimation of demixing matrix $\boldsymbol{W}$. The reconstructed signal would include other channel's information. On the estimation of artifact-free EEG signal, it was impossible to estimate the component only using the single-channel scheme. Therefore, the two types of signals ($\hat{\boldsymbol{x}}_{\text{EEG}}$ and $\hat{\boldsymbol{x}}_{\text{EEG by ICA}}$) will not ever be the same. However, my proposed scheme could factorize single-channel data with good approximation in the time domain (see Figure. 5.7). The supervised tensor (matrix) factorization stores the blind features embedded in epochs, into some bases and manages the activation. The extremely workable performance should come in useful scheme for single-channel EEG signal analysis.

Table 5.5 Processing time (s) for signal separation or all procedures.

	Separation	All		Separation	All
LR	0.008±0.003	0.008±0.003	EMD-ICA	4.676±3.361	–
BF	0.006±0.001	0.006±0.001	EEMD-ICA	1342.487±908.349	–
AF	0.116±0.004	0.116±0.004	CEEMD-ICA	968.788±566.404	–
wICA	0.628±0.759	–	2-step NMF	6.530±6.982	–
			Proposed	2620.863±64.921	2621.448±387.754

5.6.3 Computational Cost

The computational costs to complete signal separation process and all procedure are tabulated in Table 5.5. The results of all procedure regarding ICA-based schemes and 2-step NMF are in blank because they need a manual operation. The PC environment is follows: Windows 10 64 bit; CPU, Inter(R) Core(TM) i7-4510U CPU 2.00 GHz; RAM, 8.00 GB.

For this results, it noticed that EEMD-ICA, CEEMD-ICA, and proposed scheme need overwhelming cost. It cannot be avoidable because of their repetitive or complex algorithms. EEMD-ICA generates a lot of signals by adding different realizations of Gaussian white noise of finite variance to the original signal to perform the EMD over an ensemble of the input data for "true" IMF components. In this thesis, the ensemble size $I = 500$; therefore, this algorithm have to decompose signals 500 times. No wonder the computational cost of EEMD-ICA has 500-fold larger than EMD-ICA. Although CEEMD-ICA provides an improvement regarding computational cost of the sifting iterations of the EEMD-ICA, ICA-based schemes cannot be said for sure.

Linear regression, band-pass filtering, and adaptive filtering might operate eyeblink artifact rejection in real-time processing system. However, linear regression and adaptive filtering require reference channel; therefore, these schemes have no way of operation in the real-time processing system using single-channel EEG device.

Supervised PSDTF showed excellent performance for eyeblink artifact removal. On the other hand, it needs higher computational cost than matrix factorization because of its complex calculation for tensor factorization. The computational cost of PSDTF ($O(KNM^3)$) depends on the width of matrix M than NMF ($O(KNM)$) [317,362–364]. Downsampling to 64 Hz makes the cost one sixty-fourth; however, real-time processing is obviously difficult. While an fast-acting algorithm computing auto-covariance matrix has been developed, my proposed scheme would be powerful tool for eyeblink artifact removal in off-line processing.

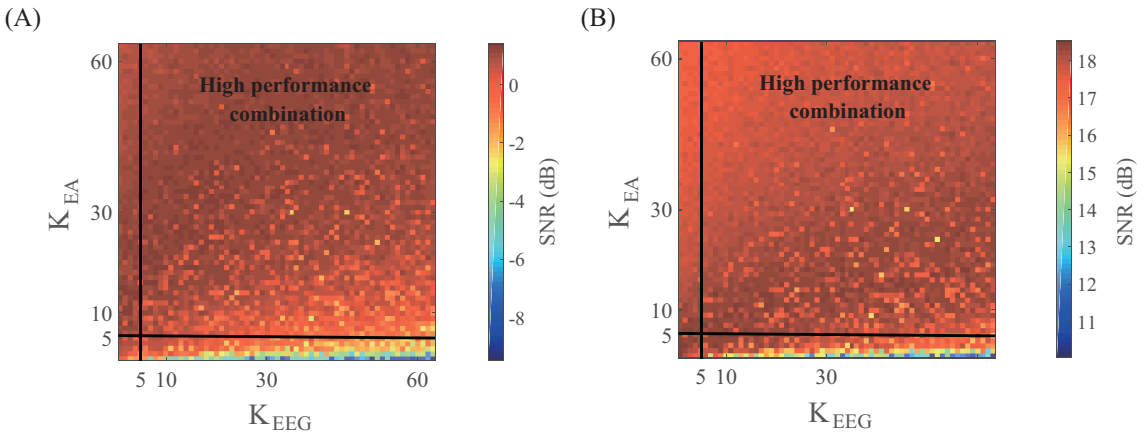

Figure 5.8 Results of average SNRs between the reference signals and estimated signals by 2-step NMF (A) artifact-free signal. (B) estimated artifact.

5.6.4 Optimal Number of Iterations and Basis

I have already validated how many number of iterations are optimal for tensor factorization in eyeblink artifact removal [360]. The cost function $\mathcal{C}(\boldsymbol{X}|\boldsymbol{Y})$ has been fully-converged single the number of iterations exceeded about 20 to 30. I recommend setting number of iterations as 30.

By contrast, the optimization of the number of basis is pretty difficult because the facile choosing the number leads directly to lost sparsity of tensor (matrix) factorization [365–367]. The performance of approximation increases approximately linearly with increasing the number of bases due to the space to express various patterns in the input data [368, 369]. In this study, I had already applied 2-step NMF before applying proposed scheme. Usually, the optimization of arbitrary parameters in tensor factorization will be specified by matrix factorization algorithm with brute-force search because tensor factorization takes a lot of time [318, 370, 371]. Figure 5.8 summarizes the results and compares them to brute-force search with the setting the values of K_{EA} and K_{EEG} as 2 to 64 and 2 to 64, respectively. For this results, I obtained experimental knowledge that the performance of approximation algorithm depends on the factorization of prior information. In my opinion, the continuous quality improvement process of approximation by NMF has converged if K_{EA} exceeds 5. Therefore, I set the number of basis K_{EA} as 5. The points which seems to be outliers mean the local solutions of reconstructed matrix. Multiplicative update rules are subject to the initial values and the performance is sometimes whimsical even if they are generated from appropriate probability distributions. Applying decomposition algorithms like PCA and singular value decomposition that maximize informational orthogonality between bases of observed matrix can effectively evade the initial-value problem [372, 373]. It's kind of late to bring this up now, the rank should be set to be equal to the number of classes of the dataset

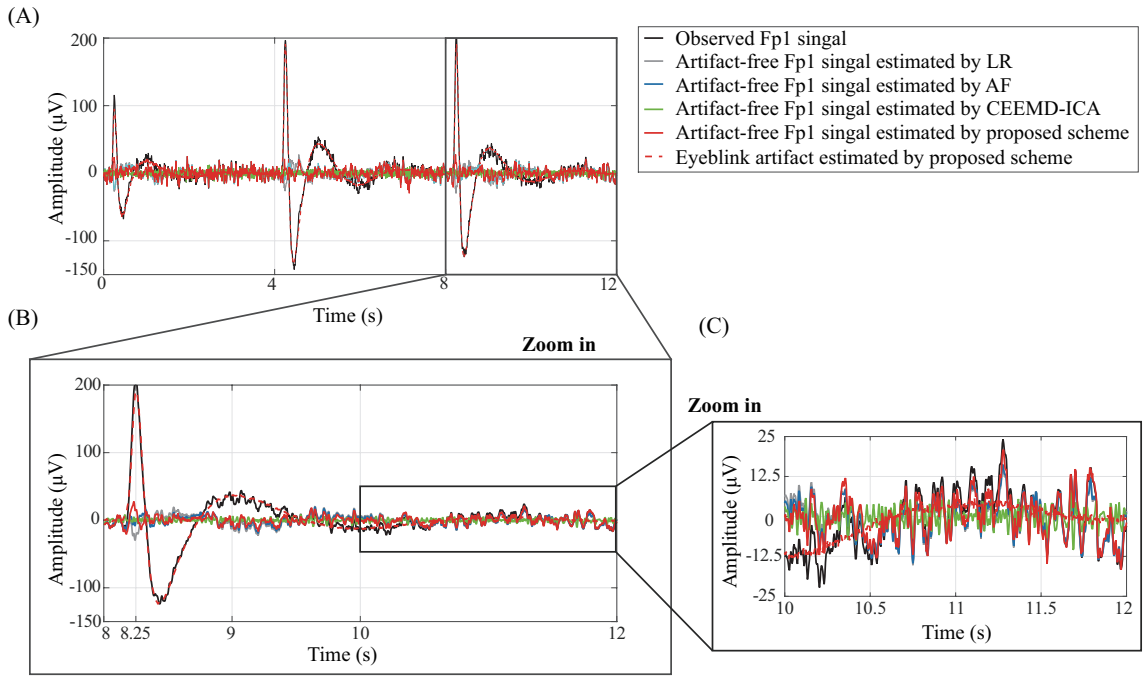

Figure 5.9 (A) A continuous observed Fp1 signal, artifact-free Fp1 signals estimated by four schemes, and artifact estimated by proposed scheme. (B) A 4-s epoch. (C) A 2-s epoch.

by clustering algorithm regardless of whether agglomerative or partitional [374–376]. However, my proposed scheme showed best accuracy among schemes using only single-channel data with 10 bases; therefore this scheme has reasonable efficacy to remove eyeblink artifact for single-channel EEG devices (see Figure 5.9).

As noted earlier in Chapter 5 Section 4 Subsection 3, Bayesian model handles its infinite extension ($K \to \infty$). By the model changing, this scheme would be extended to more high-accuracy and high-speed scheme in the future.

5.7 Summary of Chapter.5

In this chapter, a section-based eyeblink artifact removal scheme by using supervised tensor factorization was proposed for single-channel EEG (Fp1) signal. Fourteen EEG signals and one VEOG signal have been registered for twenty healthy subjects who blink every 5 s according to metronomic sounds. PSDTF with supervised learning algorithm was employed as an eyeblink artifact removal scheme using only single-channel data. The estimated artifact-free EEG signals into real-life data are compared with eight schemes to verify the efficiency of proposed scheme.

As a result, the highest SNR (dB) and lowest MSE (μV^2) were obtained by proposed scheme among nine schemes except for linear regression and adaptive filter which need

reference channel. Each basis could express prior information and extract EEG feature from contaminated single-channel EEG signal. This scheme has an ability of automatic processing; therefore, all you have to input single-channel data and the number of bases K to obtain artifact-free EEG signal. Making a summary of my proposed scheme above, this scheme has four beneficial properties: (i) automatic epoch detection; (ii) high signal separation accuracy; (iii) automatic separated component identification and signal reconstruction; and (iv) small number of arbitrary parameters (the number of bases K_{EA} is a sole arbitrary parameter). Therefore, a useful eyeblink artifact removal scheme for single-channel EEG signals was proposed. Reduction of computational cost is the main future work.

In this chapter, I described eyeblink artifact removal scheme thus far. If the research completed proposing a scheme, it will declare that my research has been accomplished. This kind of research will have second thoughts about new scheme and does not continue to investigate its efficiency for real-life data obtained from the real environment. It must be noted that artifact removal scheme is nothing more than one of the preprocessing algorithms of EEG system. The proposed scheme will not always be effective if it does not improve the performance of outputs. In Chapter 6, the proposed scheme will be applied to actual single-channel EEG analysis to valid its efficiency for single-channel EEG system, indirectly. The analytical accuracy would be compared with the efficiency without eyeblink artifact removal scheme.

Chapter 6

A STUDY OF PATTERN RECOGNITION IN CHILDREN USING SINGLE-CHANNEL ELECTROENCEPHALOGRAM

6.1 Introduction and Objectives

EEG has been used to define neural patterns and to adjust the wide applicability to a larger population of healthy and diseased users. Specialized EEG devices have recently developed as for compact and portable measurement system using them in a real environment. Owing to the development, researchers can avert behavioral constraint and pressure overload of regular EEG measurement device from subjects. The concern over a new target that was encountering difficulties of implementation has risen along with such background.

Meanwhile, dual-income households who leave their children in nursery schools have been increasing because the law related to child-rearing is nor similar to the United Stated in Japan [377]. Such parents are not able to grasp their children' behavior in daily life. Therefore, many parents take thought for their children. Since quite a while ago, child behavioral analysis has been researched in various research fields [378–381]. In particular, several types of research which analyze child behavior and discriminate the child conditions using image data taken from digital cameras has been proceeded to solve the parents' distress in Japan. Some nursery schools currently provide the child behavioral information taken from digital cameras in their parents. However, it is difficult to acquire the child behavioral information from the digital devices at anytime, anywhere. Furthermore, there is a problem of privacy since digital devices take a movie which mirrors not related to the target (Figure 6.1 (A)). Thereby, the parent needs another method which can take information from the specific target at anytime, anywhere.

There are many reports in the research literature of behavioral and psychophysiological correlates of the temperamental patterns in early childhood (before a child would be

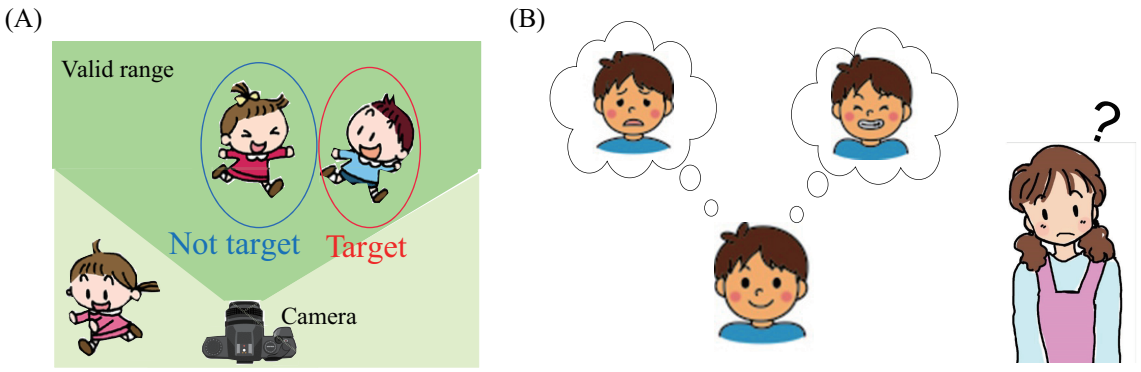

Figure 6.1 (A) Child behavioral information from a digital device. (B) The difficulty of gathering children' internal states from appearance.

primary school student) [382,383]. Early childhood education promoting the growth of mental condition is well-liked. In particular, knowledge gained through books has been considered to be as a factor behind the development of a child's sense of self [384,385]. Such factor and an aim to communicate with their children lead the parents to read picture books to their children. For eliciting a good response in the development of the sense and their communication, it is imperative to know what type of picture book is liked by the children. Understanding a child liking by listening to the child talking is difficult as an absence of vocabulary since he/she is less than six years old (Figure 6.1 (B)). Recently, research of EEG signals has been revealed that frontal lobes of the brain have relation to human emotions [386,387]. In the research, frontal EEG activity is described as a useful measure to explain and predict state and trait.

Under such background, single-channel EEG analysis for children with specialized EEG device has recently been attracted attention [388]. Changing the infant central rhythm (the emergence of 3 - 5 Hz) to the classical adult alpha rhythm (the 8 - 12 Hz frequency range) is accompanied by growth [389]. It can be observed in a weaker form at other locations on the scalp, although the classical adult alpha rhythm is most pronounced at occipital and parietal positions. Therefore, a system including a database that contains only adult data may not produce enough performance for children because the patterns of children' brain activities are different from adults' one.

Usually, an EEG analysis for children has a purpose: (i) anatomical abnormality identification [390], (ii) long-term follow-up care of medicative or operative treatment [391], or (iii) construction of diagnosis system [392]. In other words, it is obvious that the subject suffers from a disease, and multi-channel EEG device must be used for measurements. Nevertheless, the knowledge of EEG has become popular than before through the intermediary of TV and internet; an EEG measurement still has been had an impression of tumid from that keeps shunting healthy children away from the measurement. Over time, EEG measurement for healthy children has waxed coming closer to reality due to the specialized EEG devices. If there is an estimation system of multiple inter-

nal states (e.g. emotions) with EEG through a specialized EEG device, it would be a powerful tool for neuroscience studies, clinical applications, long-term watching system, and education for children. Here, I focus an internal state, concentration, as the target of this study because it is often thought of as a key factor in proceeding development of children [393–395]. By making the state quantify, providing an educational program corresponding to the child and supporting ability improvement of the child smoothly would be realized. Furthermore, the quantification is so good at using classification between stable and unstable state that the algorithm would be beneficial for unsupervised anomaly detection in the framework of child care system.

The objective of this chapter is to classify two classes (meditation and concentration) in children by using single-channel EEG signals and to indirectly verify the practical efficiency of the proposed eyeblink artifact removal scheme.

6.2 Materials

6.2.1 Single-channel Electroencephalographic Recordings

Specialized EEG device would often be mistaken for a toy (see Figure 1.7); therefore, there are some risk factors that breakage of the device and physical damage occurred through the spread of the parts of the device. By considering such factors, EEG signals were recorded using multi-channel device g.tec (Medical Engineering GmbH, Austria). The cap gives much discomfort to the children on the EEG measurement; therefore, a disposable electrode, Blue Sensor P (Ambu Corp., Denmark) attached to an Fp1 position according to the international 10-20 system was used for the recordings. Reference and ground electrodes were put at A1 and Fpz, respectively. For removing some noises such as wire movements and swallowing vibrations, Butterworth digital band-pass filters were set as 0.5 to 60 Hz with a sampling rate of 256 Hz.

The experiments were conducted in a nursery school where I have frequented there one or two days on every week for over three years. Hence, the experimenter fits in the school, and every child naturally participates in the experiment. No child teases the subject when he/she is equipping EEG device. If a child without the subject occurred a problem such as physical altercation and hot temper, the measurement was abandoned. After experiments, double-check safety inspections were conducted using movie and visualized observed EEG data in off-line processing to remove bad data contaminated a critical noise which obscures EEG components in the observed data. Consequently, data of four male and six female (mean age: 4.18 ± 1.17 years) has no problem with analysis although eight male and eight female nursery school children participated the experiments.

(A)

(B)

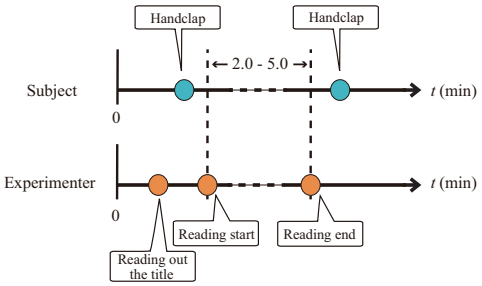

Figure 6.2 (A) Trial for recording EEG in watching picture-story show. (B) Diagram of a trial for recording EEG in watching picture-story show.

All parents of participators received informed consent with their children and permitted it before their participation. Regardless of whether the parents accept the participant or not, all children who are the classmate of the subject will be called to join a reading picture-story show in the hope of avoiding an awkward relationship that would be a cause of a quarrel.

6.2.2 Measurement Procedure

In this experiment, each subject was asked to sit on a mat and keep resting state or watch a picture-story show as the condition of meditation and concentration. I have to note that if the subject were the quite type, an experimenter would not need to take measures, however, it's not going to work that way. I have already known that most of the children will get several antsy seconds after starting the experiment. Therefore, the subject firstly sat on a mat in a room with the experimenter and a classmate and was recorded EEG signal with eyes open for five minutes as a class of meditation. In this measurement, the subject and the classmate were heading to the same direction and played a competition: who keeps silent longer, you or your friend? I put a tablet PC in the center of children and said to children, "Don't mess with your friend and make a fuss, if you do that, I will go back to my home without reading picture-story show, but... there may be no need to worry because you are mature for your age." After this measurement, I complimented children on the serious attitude, "Good on you!"

All classmates will come in the room to watch the picture-story show. As for the concentration in children, almost all the studies define the state of concentration as keeping watching a target such as pop-out toy [395–397]. In this study, I defined the state of concentration as keeping watching picture-story show. The subject sits in the front row and the center for the display (Figure 6.2 (A)). The procedure of experiments is indicated in Figure 6.2 (B). In each experiment, I presented different picture-story

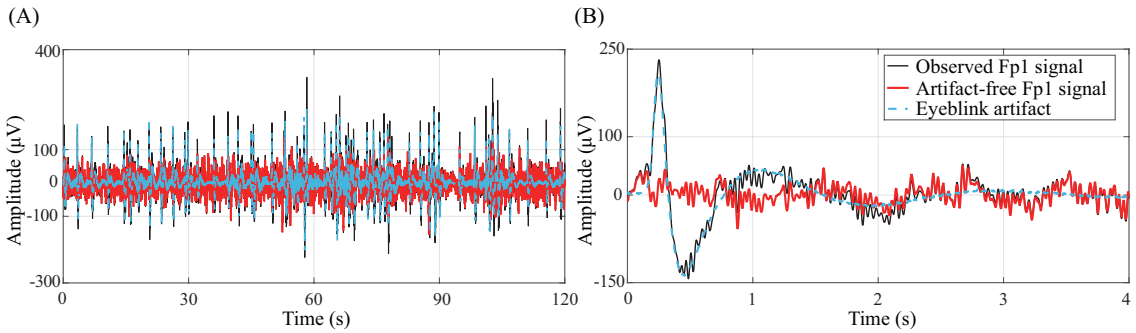

Figure 6.3 (A) A continuous 120-s observed Fp1 signal, artifact-free Fp1 signal, and artifact estimated by supervised PSDTF. (B) A 4-s epoch randomly extracted from a continuous signal.

show which takes two to five minutes, and every experiment was recorded though movie by tablet PC. By using the movie with visual inspection, I checked whether a subject could keep watching the picture-story show or not during the experiment.

6.3 Analytical Methods

6.3.1 EyeBlink Artifact Removal

On the pre-processing step, I used my proposed scheme described in Chapter 5 to remove eyeblink artifact from single-channel data. The number of bases K_{EA}, K_{EEG}, and iteration of MU algorithm are set as 5, 5, and 200. These parameters are the same of the setting in Chapter 5. In addition, other parameters such as windows lengths and predetermined threshold for contaminated epoch extraction are also the same of the setting in Chapter 5. Figure 6.3 indicates a continuous 120-s observed Fp1 signal, artifact-free Fp1 signal, and artifact estimated by supervised PSDTF with database that contains 36 subjects' data.

6.3.2 Feature Extraction

In this study, amplitude spectrum was calculated on each feature extraction method. I selected Fourier transform, wavelet transform, and EMD as the method. Initial two-minute-long EEG signals were extracted from obtained each data (meditation and concentration) because the shortest duration of a picture-story show is two minutes. In selecting a feature for the classification of the system, the time scale and shift amount are important factors. This study aims to construct real-time processing in the future; therefore, eight patterns described in Table 6.1 were selected as the scale and amount

Table 6.1 Window and shifting size combinations and total number of data for elastic net logistic regression.

Pattern	Window size	Shifting size	Overlap (s)	Total number of data
1	256	256	0	2,400
2	256	128	0.5	4,820
3	256	64	0.75	9,660
4	512	512	0	1,200
5	512	384	0.5	1,620
6	512	256	1	2,420
7	512	128	1.5	4,860
8	512	64	1.75	9,740

for classification. The detail of transform conditions whose features will be used as inputs in the elastic net logistic regression are described following sections.

Fourier Transform

Fourier transform is a most famous method to characterize a signal's frequency content in terms of a weighted superposition of the elementary oscillatory function [398]. This method can capture effective EEG features from the original signal when the signal has periodic features. The fast Fourier transform algorithm has become like a traditional method of the EEG signal analysis. The signal defined over a finite time interval of a window function would be converted into a complex exponential function or a sinusoidal function. I performed short-time Fourier transform for 1-s epochs or 0.5-s epochs (Hamming window, 0 to 87.5% overlap); the frequency resolution is 1 Hz or 0.5 Hz. The Fourier spectra ranged 1 to 30 Hz were extracted and transformed to amplitude spectra. Therefore, extracted features by Fourier transform has 30-dimensions (Patterns 1 to 3) or 60-dimensions (Patterns 4 to 8).

Wavelet Transform

Wavelet transform is a versatile signal processing tool to find non-stationary features. This method displays great ability to capture transient EEG features [399]. Wavelet coefficients were obtained by lifting-based DWT [400]. In wavelet transform processing, mother wavelet and level of the transform have to be selected. For this study, the function and the level were set to Daubechies-4 and five, respectively. Daubechies'

wavelet family [401] is designed with the maximum regularity or smoothness and has often been selected for EEG signal analysis with experimental knowledge [59, 402]. Thus, decomposed coefficients of wavelet transform correspond to the range of clinical and physiological interests: (i) D3 (16-32 Hz, beta band); (ii) D4 (8-16 Hz, alpha band); (iii) D5 (4-8 Hz, theta band); and A5 (0-4 Hz, delta band) [15].

The four local detail and one approximation coefficients were extracted and transformed into wavelet amplitude spectra. These spectra have frequency and time information; they were further converted into five indices (mean, variance, skewness, kurtosis, and integral values). Skewness is distribution's deviation from a perfectly symmetrical shape. Kurtosis is general peakedness of distribution. Therefore, all extracted features by wavelet transform have 20-dimensions (4 coefficients $\times$ 5 indices).

Empirical Mode Decomposition

EMD is a data-driven processing tool and adaptive to nonlinear and non-stationary signal by decomposing into some IMFs [287]. The detail has been described in Chapter 3 Section 2 Subsection 3.

The number of IMF is underspecified because each IMF has monocomponent of the original signal, and is sequentially estimated by an iterative process named shifting process. In this study, first to twelfth IMFs were extracted and transformed into Hilbert amplitude spectra. These spectra have frequency and time information as well as wavelet amplitude spectra; they were further transformed into the five indices. Therefore, extracted features by EMD has 60-dimensions (12 modes $\times$ 5 indices) in common.

6.3.3 Generating Classifier of Elastic Net Logistic Regression

Logistic regression is a probabilistic generative modelling method using the logistic sigmoid function for classification [403]. This method models the class-conditional densities $p(\boldsymbol{x}|\mathcal{C}_1)$, as well as the class priors $p(\mathcal{C}_k)$ assigned based on the two classes of meditation and concentration in this study. The posterior probability for class 1 (meditation), $p_{\boldsymbol{\beta}}(\mathcal{C}_1|\boldsymbol{x})$, of an $(M+1)$-dimensional explanatory vector $\boldsymbol{x}_n = [1, x_1, \ldots, x_M]$ including constant term, $n = 1, \ldots, N$, where N means the total number of data (see the rightmost term in Table 6.1), is computed through Bayes' theorem:

$$p_{\boldsymbol{\beta}}(\mathcal{C}_1|\boldsymbol{x}) = \frac{\exp(\boldsymbol{\beta}^T\boldsymbol{x})}{1+\exp(\boldsymbol{\beta}^T\boldsymbol{x})} \ , \tag{6.1}$$

$$\boldsymbol{\beta} = [\beta_0, \beta_1, \cdots, \beta_M] \ , \tag{6.2}$$

where $\boldsymbol{\beta}$ is the parameter vector including intercept term β_0 associated with the explanatory vector $\boldsymbol{x}_n$. Once the parametric functional form for the class-conditional densities has been specified, the values of the parameters is determined using maximum binomial log-likelihood $l(\boldsymbol{\beta})$ together with the prior class probabilities $p(\mathcal{C}_k)$.

$$\begin{aligned}\hat{\boldsymbol{\beta}} &= \underset{\boldsymbol{\beta}}{\operatorname{argmax}}\big\{l(\boldsymbol{\beta})\big\} \\ &= \underset{\boldsymbol{\beta}}{\operatorname{argmax}}\Big\{\sum_{n=1}^{N}\big(y_n\boldsymbol{\beta}^T\boldsymbol{x}_n - \log(1+\exp(\boldsymbol{\beta}^T\boldsymbol{x}_n))\big)\Big\} \ ,\end{aligned} \tag{6.3}$$

where y_n is a binary response variable ($y_n \in \{0, 1\}$).

The objective of this chapter is to classify two classes. However, multi-class classification will be needed for the system in the future. Logistic regression is easy to extend for multi-class data by using multinomial models. Furthermore, the logistic regression model can be easily extended for regularized learning framework by adding a regularization term to an error function in order to control over-fitting: there are some objective functions for the penalized logistic regression [404–406]. Therefore, I selected this method for classification.

In this analysis, the model was generated together with variable selection via sparse learning using L_1-norm because I have relatively large dimension data (60-dimension in maximum). To optimize the parameters with variable selection and group structure preservation, I selected a sparse learning algorithm that has different constraints (L_1 and L_2-norm). Concretely speaking, elastic net logistic regression was applied to input data [407]. The parameter vector estimated by elastic net regularization $\hat{\boldsymbol{\beta}}^{elastic}$ has been defined:

$$\hat{\boldsymbol{\beta}}^{elastic} = \underset{\beta}{\operatorname{argmax}}\big(\frac{1}{N}l(\boldsymbol{\beta}) - \lambda\big((1-\alpha)||\boldsymbol{\beta}||_2^2/2 + \alpha||\boldsymbol{\beta}||_1\big)\big) \ , \tag{6.4}$$

where λ and α are nonnegative value and scalar value from 0 to 1. The regularization parameter λ turns parameters. The weight α controls the balance of lasso (L_1-norm) and ridge (L_2-norm) optimization. The elastic net with $\alpha = 1 - \epsilon$ for some small $\epsilon > 0$ performs much like the lasso, but removes any degeneracies and wild behavior by extreme correlation [408]. These values can be determined by using Cross Validation (CV) or information criteria like Akaike's information criterion. In this study, λ and α were specified by using 10-fold CV and minimizing deviance D:

$$D = -\frac{2}{N}l(\boldsymbol{\beta}). \tag{6.5}$$

6.3.4 Performance Evaluation

To evaluate the accuracy of the elastic net logistic regression model, leave one-subject out CV was conducted. Owing to ten subjects who participated in the experiments, the classifier was generated ten times. Here, each model used normalized data based on the training data. Likelihoods of test data computed from the estimated parameter vector $\hat{\boldsymbol{\beta}}^{elastic}$ will be binarized into 0 and 1 by considering two classes of meditation and concentration. The estimated class was compared with correct label and stored in a two-by-two confusion matrix. To evaluate the accuracy of the classifier, sensitivity (True Positive Rate (TPR)), specificity (True Negative Rate (TNR)), and Balanced Error Rate (BER) are calculated from a confusion matrix.

$$\text{Sensitivity (TPR)} = \frac{\text{TP}}{\text{TP} + \text{FN}} , \tag{6.6}$$

$$\text{Specificity (TNR)} = \frac{\text{TN}}{\text{TN} + \text{FP}} , \tag{6.7}$$

$$\text{BER} = \frac{\text{FP} + \text{FN}}{2} . \tag{6.8}$$

The confusion matrix is managed by replacing concentration ($y = 1$) and meditation ($y = 0$) with positive and negative. Furthermore, the area under the curve of a Receiver Operating Characteristic (ROC) is calculated for evaluation. The ROC curve represents a plot of the TPR against the false positive rate ($= 1 - \text{TNR}$) for each possible cutoff value between 0 and 1. These indices are major for evaluation of classifier such as logistic regression. In particular, the area under an ROC curve is an important parameter used to quantify in a single numerical value the overall location of an ROC curve about the predictive model [409]. I will comprehensively assess each of extracted features for multiple state estimation system by focusing on the area under an ROC curve.

6.4 Results

6.4.1 Difference of Classifiers Generated with Eyeblink Artifact or not

The results of elastic net logistic regression models are shown in Table 6.2. Model performances of each feature extraction with eight patterns were compared by using four metrics (sensitivity, specificity, BER, and area under ROC curve), and best pattern in

Table 6.2 Results of predictive models using elastic net logistic regression and three feature extraction methods (Fourier Transform (FT), Wavelet Transform (WT), and Empirical Mode Decomposition (EMD)).

Transform type	Best pattern	Sensitivity	Specificity	Balanced error rate	Area under ROC curve
FT	5	0.618 ± 0.138	0.680 ± 0.178	35.1 ± 14.7	0.696 ± 0.187
	(6	0.591 ± 0.105	0.664 ± 0.152	37.2 ± 11.9	0.659 ± 0.148)
WT	**7**	**0.922 ± 0.086**	**0.946 ± 0.145**	**6.6 ± 7.2**	**0.988 ± 0.019**
	(5	0.616 ± 0.150	0.677 ± 0.173	35.3 ± 15.3	0.683 ± 0.178)
EMD	4	0.708 ± 0.128	0.755 ± 0.174	27.1 ± 14.0	0.791 ± 0.150
	(6	0.606 ± 0.260	0.675 ± 0.236	35.9 ± 22.7	0.682 ± 0.249)

the method was separately tabulated in the table. A pair of parentheses means the result was obtained without eyeblink artifact removal process. Wavelet transform with artifact removal significantly overcame the performance of wavelet transform without artifact removal ($P < .001$). The model did not depend on whether artifact removal scheme employed or not if Fourier transform or EMD was selected as feature extraction method. All methods presented that effective time scale and shift amount vary under the processing procedure.

6.4.2 Recognition Performance and Feature Extraction Schemes

Nevertheless, all methods do not have fixed optimal pattern of shift amount, 2-s (512 sampling data) window size showed the best performance in common. Extracted features by wavelet transform most committedly worked for classification (area under ROC curve showed $F(2, 18) = 17.46, P < .001$). The pattern 2 with wavelet transform showed worst accuracy in the method. EMD showed good performance next to wavelet transform, and Fourier transform showed worst performance for classification in the elastic net logistic regression models. The pattern 3 with EMD or Fourier transform provided worst accuracy. However, in the metric of area under ROC curve, EMD revealed that captures features of EEG data for generating models with the highest minimum limit of performance (0.764 ± 0.147) compared with Fourier transform (0.676 ± 0.181) and wavelet transform (0.707 ± 0.180). The performance showed significant difference in the methods using ANOVA ($F(2, 18) = 4.00, P < .05$).

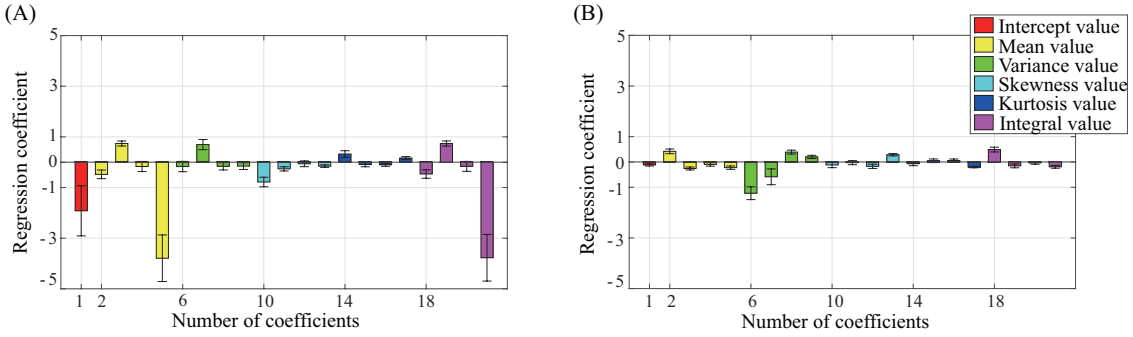

Figure 6.4 (A) Regression coefficients for extracted five kinds of features based on pattern 7 with supervised PSDTF and wavelet transform that showed best recognition performance among rival models. (B) Regression coefficients for extracted features based on pattern 5 with wavelet transform.

6.4.3 Parameter Comparison of Generated Classifiers

Regression coefficients for input data based on pattern 7 with supervised PSDTF and wavelet transform are shown in Figure 6.4 (A). This figure shows average value and standard deviation visualized by bars and error bars. Twenty-one bars starting at left red bar and finishing at right purple bar have been separated into six colors: (i) red (intercept term β_0); (ii) yellow (mean value); (iii) green (variance value); (iv) cyan (skewness value); (v) blue (kurtosis value); and (vi) purple (integral value). Moreover, four bars in the same color mean beta, alpha, theta, and delta band oscillations from left to right. For the figure, it is indicated that mean and integral values of wavelet amplitude spectra regarding all frequency bands worked as good features for classification between meditation and concentration. On comparing models with the frequency bands, each frequency band has different effective indices for classification: (i) mean, skewness, integral values in the beta band; (ii) mean, variance, and integral values in the alpha band; (iii) mean and integral values in the delta band. All indices in theta band were 0 in most every model by the shrinkage effect of elastic net regularization.

Meanwhile, regression coefficients for input data based on pattern 7 with wavelet transform are shown in Figure 6.4 (B). For Figure 6.4 (B), interpret value and five indices except for variance has been effected by elastic net regularization. Furthermore, only alpha and beta band frequency values were selected as good variables for the model. Therefore, the optimal parameters in elastic net logistic regression depend on preprocessing procedure even if the same feature extraction method employed.

6.5 Discussions

6.5.1 Important Features to Classify Concentration

The parameters obtained from supervised PSDTF, and wavelet transform revealed that mean and integral values are important to classify the discrete classes of meditation and concentration. It is easy to see that a larger parameter value means more important variable in the model for classification. In this case, the parameters correspond to wavelet amplitude spectra that are a nonnegative value; therefore, the negative/positive of parameters controls the shrinkage direction for likelihood (0 or 1). The mean and integral values of spectra in meditation had a larger value than in concentration. Also, the state of meditation is assigned to class 1 ($\mathcal{C}_1$). By considering the characteristics of spectra and Eq. (6.1), I can interpret the model outputs $\mathcal{C}_1$ when the explanatory variables selected by elastic net have large values and vice versa.

The indexes of variance, skewness, and kurtosis may be effective while a transient EEG event takes a strong presence in the distribution. However, you know the stimuli of meditation and concentration could not elicit a radical change in neuronal activities. Therefore, these features are not effective for classification in this case. On the other hand, the model represented a clear difference of brain activities between the meditation and concentration by using only single-channel EEG data because it showed 0.988 area under ROC curve on the best feature combination. Long focusing picture-story show decreases brain activities of delta band frequency components by taking into account the last paragraph. In other words, the brain activities may be synchronized and generate high-frequency oscillations (for Figure 6.4 (A), I guess alpha band oscillation increased) in the concentration to process much information for a short time. Here, wavelet amplitude spectra of delta band in pattern 7 is visually compared among classes. Figure 6.5 (A) visualizes an example of 2-s delta band oscillation coupling of wavelet amplitude spectra based on pattern 7. Moreover, Figure 6.5 (B) shows the probability density functions of four cases regarding mean value of delta band frequency oscillation. On pattern 6, two classes have a similar distribution. Conversely, the mean values of two classes have distributed apart from each other on pattern 7. The same tendency has been observed among integral values. Thus, mean and integral values of delta band frequency components based on pattern 7 with supervised PSDTF and wavelet transform would work to accurately classify two classes in the EEG system whose input data is obtained from single-channel EEG device.

6.5.2 Important Role in Eyeblink Artifact Removal

In this chapter, I represented results of whether an eyeblink artifact removal scheme was applied or not. The pre-processing improved the classification performance and extricated EEG components from the observed signal that was have already obscured by any factors such as technical noise and biological artifact. The distorting effects of eyeblink artifacts on the EEG in the frontal are are within the delta and alpha [71]. Furthermore, eyeblink artifact removal has to be applied all of EEG data because the effects propagate across the scalp presenting in a bilaterally symmetrical fashion if the subject recorded EEG with the eyes open.

The subjects kept states of meditation and concentration with eyes open. Therefore, each class will have the same feature (eyeblink component) in the data if the artifact was not removed. Consequently, the constructed model weighted indices of alpha and beta band frequency that has less effect of eyeblink for classification (Figure 6.4 (B)). The best accuracy in all extraction methods has low performance (under 0.70 area under ROC curve). Plus, I cannot help being suspicious of a model which only put alpha and beta band frequency components to good practical use for classification. Eyeblink artifact removal is one of an essential processing of the EEG system regardless of whether the input was obtained from a multi-channel device or single-channel device. At the same time, my proposed scheme could show its efficiency for single-channel EEG system, indirectly.

Incidentally, MF algorithm has recently been used as an EEG feature extraction method for classification in many EEG analysis [410–414]. PSDTF has the same property; therefore, the artifact-free signal have perhaps already been adjusted to a relatively intelligible signal.

6.5.3 Confirmation of Mediation in Children

I should take a retrospective look at measurement procedure. Could I actually obtain EEG signal during meditation? There is a big question as to the content of the meditation in children. In this study, the subject sat on a mat with a classmate for mental tranquility. However, keeping meditation may give children stress-intensity factors because they are three to six years old. There is a risk of misdirected effort to obtain a class of stress named meditation.

Based on three lines of evidence, it is considered that long-term memory for extinction depends on the medial prefrontal cortex, in particular the infralimbic subregion [415, 416]; therefore, the cortex appears to be essential for inhibition of negative responses after extinction [421]. Medial prefrontal cortex sends robust projections to the amygdala

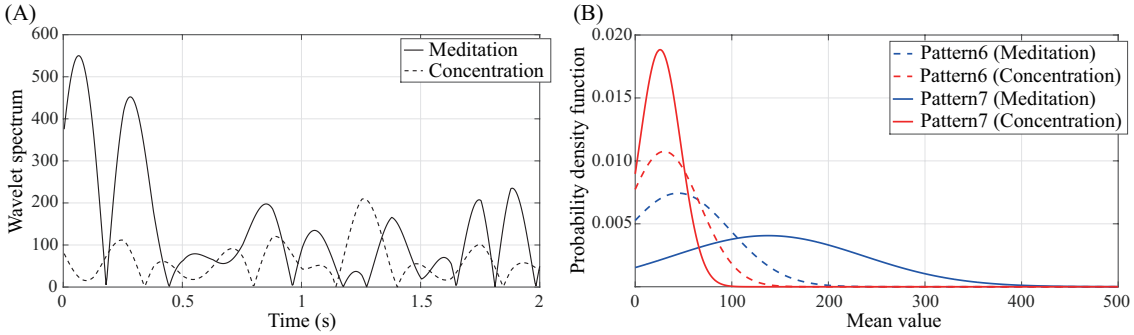

Figure 6.5 (A) A two-second delta band oscillation coupling of wavelet spectrum based on pattern 7. (B) Probability density functions of mean wavelet spectrum value.

for feedforward inhibition of the central nucleus [417], and directly projects to the hypothalamic and brainstem targets of the central nucleus [418–420] that leads to inhibition of emotional response independently of the amygdala [422]. The projection makes the strength of EEG oscillations in left prefrontal area strong [423]. The same projection occurs in the children' brain. Therefore, frontal asymmetry difference scores of EEG alpha power band have been employed as a physiological metric to index aspects of positive/negative emotion [386, 387] because of neuroanatomical structures. The observed EEG signal obtained from the Fp1 position where places on the left prefrontal area should have difference scores of alpha power if the signal contains oscillations of stress. The regression coefficients for mean, variance, and integral values of alpha band component certainly had large value in Figure 6.4 (A). However, the coefficients for mean and integral values of delta band component had more than three times as large as the alpha band had. For this results, I concluded that I could obtain EEG signal during meditation from children, and the model constructed using elastic net logistic regression has been optimized by three feature extraction methods and eight patterns of time scale and shift amount to classify meditation and concentration. Finally, multiple state estimation model including stress should be investigated in the future research.

6.6 Summary of Chapter.6

This chapter aimed to classify two classes (meditation and concentration) in children by using single-channel EEG signals and to indirectly verify the practical efficiency of the proposed eyeblink artifact removal scheme. Recordings were processed to remove eyeblink artifacts, and then extracted their periodic or non-periodic features by three methods (Fourier transform, wavelet transform, and empirical mode decomposition). Elastic net logistic regression constructed predictive models to classify two classes of the optimized extracted features.

A model showed 0.988 area under ROC curve when wavelet transform was selected as feature extraction method. Mean and integral values of delta band frequency components based on pattern 7 (512 and 128 sampling data (2-s and 0.5-s) for window size and shifting size) with supervised PSDTF and wavelet transform had worked to accurately classify two classes. The brain activities may be synchronized and generate high-frequency oscillations (for Figure 6.4 (A), I guess alpha band oscillation increased) in the concentration to process much information for a short time: therefore, long focusing picture-story show decreases brain activities of delta band frequency components. The next of this research is to construct a multiplex state estimation system. Finally, portable applications using a specialized EEG device that include the multiplex model and encourage children to develop the child's sense would be implemented in the real environments.

My proposed scheme described in Chapter 5 proved the following advantages: (i) no need to discard contaminated data; (ii) no signal distortion after denoising; and (iii) deliverance of low-frequency components. So far, artifact removal processing in the system of single-channel EEG device can discard the epoch or data on trials which have eyeblink artifacts or remove artifacts with many manual operations. Such background was the disturbing popularization of the single-channel EEG analysis. However, single-channel EEG device (headset) has been attracted attention: one day at a time (from the year 2012, the keywords of "single-channel EEG" were included in about 5,000 documents, but the number of the year 2015 is about 1,500). Automatic eyeblink artifact removal using only single-channel EEG data would be a powerful tool for easy measurement and careful analysis.

Chapter 7

CONCLUSIONS

7.1 Summary of This Thesis

This thesis aimed to propose an accurate removal scheme of eyeblink artifact from single-channel EEG signals by supervised tensor factorization.

Kaleidoscopic functional states of the cerebral cortex affected by neuronal activities (nerve firings) can be measured using an electrical non-invasive index, in the form of an EEG signal. This modality holds over other neuroimaging techniques, are the high temporal resolution on the order of milliseconds, the small installation space for operating the system and its usability for signal measurement. In addition, EEG signals have been widely used in BCI systems that provide communication channels to people with severe motor disabilities. Over the past three decades, the spatiotemporal event-related neural dynamics revealed from various experimentally manipulated events and interpretation of EEG signals have been developed to integrate dynamics with practical applications.

Technologies using EEG signals have been penetrated into public by the appearance of specialized EEG devices. Such devices can capture oscillating neuronal discharge with only an electrode. Although the aspect of entertainment or amusement associated with the usage of the system is emphasized, many applications based on EEG signal processing will be beneficial of its usability and portability for signal measurement. Therefore, single-channel EEG device has been attracted attention since nearly five years because of its facility and portability for measurement in real environment conditions.

During EEG system operation, EEG signals should be recorded with his/her eyes open for practical use in the real world. That allows eyeblink artifact contamination into observed EEG signals. The artifacts disguise themselves as EEG components and

make EEG signal processing difficult in all respects because the oscillating discharge (energy) is larger than the neuronal discharge. By the properties of eyeblink artifacts, theoretically multivariate statistical analysis approached such as PCA and ICA, which separate EEG signals into spatially and temporally distinguishable components, are useful for extracting EEG components from the scalp recordings. In particular, ICA is a powerful tool for separating the observed EEG signals into maximally independent activity patterns derived from cerebral or non-cerebral (artifactual) sources. However, ICA is unsuitable for analyzing EEG signals recorded by a specialized EEG device because of mismatching of its assumption in the real-world applications. Thus, proposing a removal scheme of eyeblink artifact from single-channel EEG signals is a major challenge in EEG signal processing for the widespread use of systems as a conventional technology.

In Chapter 4, the effect of voluntary and involuntary eyeblinks on ICs contributing to EEG signals was characterized for creating templates of eyeblink artifact removal from observed EEG signals with a single-channel electrode. Fourteen EEG signals and one VEOG signal were recorded for twenty healthy subjects during two different experiments, which prompted subjects to blink voluntarily and involuntarily. Wavelet-enhanced ICA with two markers (mMSE and kurtosis) was employed as a source separation and feature-extraction scheme. The extracted eyeblink features were separated into epochs and analyzed in the frequency, time-frequency, and time domain. The extracted eyeblink features confirmed three characteristics already reported in the literature: (i) the distorting effects of eyeblink artifacts on the EEG are within the delta and theta bands; (ii) electric potentials (dipole projections) caused by eyeblinks decrease with increasing distance between measurement points and eyes; (iii) the propagation effects across the scalp present in a bilaterally symmetrical fashion. Moreover, additional three characteristics were found: (i) eyeblink features obtained from all channels presented significant differences between voluntary and involuntary; (ii) eyeblink effects continue to have an influence on EEG signals for 3.0 to 4.0 s (in the occipital region, 2.0 s); and (iii) these effects cease to exist after the zero-crossing point four (in the occipital region: two) times, for both eyeblink types. The results which would have differences among the effects of voluntary and involuntary eyeblink in EEG signals, are collected in a dataset as prior information for supervised learning algorithm.

In Chapter 5, a section-based eyeblink artifact removal scheme by using supervised tensor factorization was proposed for single-channel signals. Fourteen EEG signals and one VEOG signal have been recorded for twenty healthy subjects who blink every 5 s according to metronomic sounds. Automatic contaminated epoch extraction based on simple fixed-thresholds and PSDTF with supervised learning algorithm have worked in my scheme. The estimated artifact-free EEG signals into real-life data were compared with eight schemes (linear regression, band (high)-pass filtering, adaptive

filtering, WICA, EMD-ICA, EEMD-ICA, CEEM-ICA, and 2-step NMF) to verify the efficiency of proposed scheme. As a result, the geometric and simple fixed-thresholds could markedly detect epochs contaminated by eyeblink artifacts automatically, and supervised PSDTF showed highest performance among nine schemes except for linear regression and adaptive filter which need reference channel. Good approximation with keeping constraint could be achieved, and each basis can express prior information and extract EEG features from contaminated single-channel EEG signal.

In Chapter 6, single-channel EEG data obtained from ten children which contains two classes (meditation and concentration) was classified. Recordings were processed to remove eyeblink artifacts, and then extracted their periodic or non-periodic features by three methods (Fourier transform, wavelet transform, and empirical mode decomposition). Elastic net logistic regression constructed an predictive models to classify two classes of the optimized extracted features. The model showed 0.988 area under ROC curve when wavelet transform was selected as feature extraction method. Mean and integral values of delta band frequency components based on pattern 7 (512 and 128 sampling data (2-s and 0.5-s) for window size and shifting size) with supervised PSDTF and wavelet transform had worked to accurately classify two classes. The brain activities may be synchronized and generate high-frequency oscillations in the concentration to process many information for a short time; therefore, long focusing picture-story show decreases brain activities of delta band frequency components.

Last of all, I accomplished the objective of this thesis; proposing an effective removal scheme of eyeblink artifact from single-channel EEG signals which has four properties: (i) automatic epoch detection; (ii) high signal separation accuracy; (iii) automatic separated component identification and signal reconstruction; and (iv) small number of arbitrary parameters. The scheme proved the following advantages: (i) no need to discard contaminated data; (ii) no signal distortion after denoising; and (iii) deliverance of low frequency components. Owing to this proposed scheme, I hope EEG systems with a single electrode would be less cumbersome than now.

7.2 Future Works

Neuronal activity in the human brain causes local changes in the cerebral cortex. In many cases, patterns and trends of the changes have yet to be defined today. Consequently, the sampling distribution is unknown. An approach assuming a distribution of real-life data and trying its theory is good research. However, an approach using simulation data which is based on known observed data is not good research because I consider the approach would be adapted to real-life data. On the other hand, artifact removal (denoising) belongs to a pre-processing part in the signal processing module.

The module is comprised of complex combinations of algorithms like recognition and feature extraction. Therefore, it is not until the proposed pre-processing scheme can be declared as an effective tool that all algorithms are activated in the system for real-life data.

Newcomers who are attracted by the strengths of specialized EEG devices, seem to make light of the artifact removal. In practice, some kinds of research output the result of EEG signal analysis without pre-processing, and they show the features including unique noise or artifact as if the features were only EEG components. The easy measurement means the quality of the observed signal is easy to fall. EEG signal processing without a pre-processing is out of the question. However, the rapid popularization of the system which has no pre-processing method is a fact as well. To countervail the case, researchers have to propose an effective and straightforward artifact removal scheme.

Conventional schemes have many manual operations or do not support specialized EEG devices as reference channel requirement. The research field of single-channel EEG analysis can not see the future as long as such schemes are major for artifact removal. Under such a situation, the restriction of open-source observed biological data makes EEG signals analysis blind and prevents development. I firstly decided to give researchers open-source data by considering competition policy in the equal access market of proposing artifact removal.

My proposed scheme focuses on eyeblink artifacts which have an adamant presence in observed EEG signals or are surely in the observed EEG signals recorded when a user wears a specialized EEG device with his/her eyes open. This study has contributed to the practical use of specialized EEG devices. I guess this scheme is useful not only for eyeblink artifacts but also for cardiac artifacts because I know both artifacts have similar characteristics. I expect the heuristic development of more robust EEG systems based on the representative attributes for single-channel EEG analysis and encourage the practical use of EEG applications in daily life.

Please keep in mind to muscular artifact that will be the biggest wall standing against single-channel EEG analysis because the artifact has a similar trend in the EEG signal. Unsupervised learning algorithms can not separate mixture signal of EEG and EMG components effectively. Muscular artifacts reflecting body actions are natural enemies of EEG systems. The inevitable encounter must be solved by artifact rejection. At this time, researchers should carefully analyze the characteristics of artifacts and integrate them in a supervised learning algorithm. This is how I believe supervised learning algorithms are useful in known characteristics.

Signal processing techniques are not magic. They can only have just so much limitation. Until finishing the development of removing muscular artifact scheme, you can not feel free to use EEG systems in the real environments. I am eagerly awaiting a real-time EEG system removing all artifacts without altering the underlying brain activity.

BIBLIOGRAPHY

[1] K. J. Friston, "Modalities, Modes, and Models in Functional Neuroimaging," *Science*, vol. 326, no. 5951, pp. 399–403, 2009.

[2] M. Zeitler, P. Fries, and S. Gielen, "Assessing Neuronal Coherence with Single-unit, Multi-unit, and Local Field Potentials," *Neural Computation*, vol. 18, no. 9, pp. 2256–2281, 2006.

[3] W. H. Pilcher, D. L. Silbergeld, M. S. Berger, and G. A. Ojemann, "Intraoperative Electrocorticography during Tumor Resection: Impact on Seizure Outcome in Patients with Gangliogliomas," *Journal of Neurosurgery*, vol. 78, no. 6, pp. 891–902, 1993.

[4] S. Gibson, J. W. Judy, and D. Markovic, "Spike Sorting," *IEEE Signal Processing Magazine*, vol. 29, no. 1, pp. 124–143, 2012.

[5] N. K. Logothetis, J. Pauls, M. Augath, T. Trinath, and A. Oeltermann, "Neurophysiological Investigation of the Basis of the fMRI Signal," *Nature*, vol. 412, no. 6843, pp. 150–157, 2001.

[6] A. Villringer, J. Planck, C. Hock, L. Schleinkofer, and U. Dirnagl, "Near Infrared Spectroscopy (NIRS): A New Tool to Study Hemodynamic Changes during Activation of Brain Function in Human Adults," *Neuroscience Letters*, vol. 154, no. 1, pp. 101–104, 1993.

[7] H. T. Chugani, M. E. Phelps, and J. C. Mazziotta, "Positron Emission Tomography Study of Human Brain Functional Development," *Annals of Neurology*, vol. 22, no. 4, pp. 487–497, 1987.

[8] N. Rajagopalan, T. D. Miller, D. O. Hodge, R. L. Frye, and R. J. Gibbons, "Identifying High-risk Asymptomatic Diabetic Patients who are Candidates for Screening Stress Single-photon Emission Computed Tomography Imaging," *Journal of the American College of Cardiology*, vol. 45, no. 1, pp. 43–49, 2005.

[9] I. J. Rampil, "A Primer for EEG Signal Processing in Anesthesia," *The Journal of the American Society of Anesthesiologists*, vol. 89, no. 4, pp. 980–1002, 1998.

[10] M. Hämäläinen, R. Hari, R. J. Ilmoniemi, J. Knuutila, and O. V. Lounasmaa, "Magnetoencephalography – Theory, Instrumentation, and Applications to Noninvasive Studies of the Working Human Brain," *Reviews of Modern Physics*, vol. 65, no. 2, pp. 413–505, 1993.

[11] M. F. Bear, B. W. Connors, and M. A. Paradiso, "Brain Rhythms and Sleep," *Lippincott Williams and Wilkins*, pp. 585–616, 1996.

[12] R. I. Goldman, J. M. Stern, J. Engel Jr, and M. S. Cohen, "Simultaneous EEG and fMRI of the Alpha Rhythm," *Neuroreport*, vol. 13, no. 18, pp. 2487–2492, 2002.

[13] A. M. Dale, A. K. Liu, B. R. Fischl, R. L. Buckner, J. W. Belliveau, J. D. Lewine, and E. Halgren, "Dynamic Statistical Parametric Mapping: Combining fMRI and MEG for High-resolution Imaging of Cortical Activity," *Neuron*, vol. 26, no. 1, pp. 55–67, 2000.

[14] B. He, L. Yang, C. Wilke, and H. Yuan, "Electrophysiological Imaging of Brain Activity and Connectivity – Challenges and Opportunities," *IEEE Transactions on Biomedical Engineering*, vol. 58, no. 7, pp. 1918–1931, 2011.

[15] H. Adeli, Z. Zhou, and N. Dadmehr, "Analysis of EEG Records in an Epileptic Patient Using Wavelet Transform," *Journal of Neuroscience Methods*, vol. 123, no. 1, pp. 69–87, 2003.

[16] K. K. Ang, C. Guan, K. S. Phua, C. Wang, I. Teh, C. W. Chen, and E. Chew, "Transcranial Direct Current Stimulation and EEG-based Motor Imagery BCI for Upper Limb Stroke Rehabilitation," *2012 Annual International Conference in Engineering in Medicine and Biology Society*, pp. 4128–4131, 2012.

[17] G. Pfurtscheller, B. Z. Allison, C. Brunner, G. Bauernfeind, T. Solis-Escalante, R. Scherer, T. O. Zander, G. Mueller-Putz, C. Neuper, and N. Birbaumer, "The Hybrid BCI," *Frontiers in Neuroscience*, vol. 4, no. 30, 2010.

[18] G. Schalk, D. J. McFarland, T. Hinterberger, N. Birbaumer, and J. R. Wolpaw, "BCI2000: A General-purpose Brain-computer Interface (BCI) System," *IEEE Transactions on Biomedical Engineering*, vol. 51, no. 6, pp. 1034–1043, 2004.

[19] A. Delorme and S. Makeig, "EEGLAB: An Open Source Toolbox for Analysis of Single-trial EEG Dynamics Including Independent Component Analysis," *Journal of Neuroscience Methods*, vol. 134, no. 1, pp. 9-21, 2004.

[20] M. Cheng, X. Gao, S. Gao, and D. Xu, "Design and Implementation of a Brain-computer Interface with High Transfer Rates," *IEEE Transactions on Biomedical Engineering*, vol. 49, no. 10, pp. 1181–1186, 2002.

[21] R. Soikkeli, J. Partanen, H. Soininen, A. Pääkkönen, and P. Riekkinen, "Slowing of EEG in Parkinson's Disease," *Electroencephalography and Clinical Neurophysiology*, vol. 79, no. 3, pp. 159–165, 1991.

[22] F. W. Bylsma, C. E. Peyser, S. E. Folstein, C. Ross, and J. Brandt, "EEG Power Spectra in Huntington's Disease: Clinical and Neuropsychological Correlates," *Neuropsychologia*, vol. 32, no. 2, pp. 137–150, 1994.

[23] S. J. M. Smith, "EEG in the Diagnosis, Classification, and Management of Patients with Epilepsy," *Journal of Neurology, Neurosurgery and Psychiatry*, vol. 76, no. 2, ii2–ii7, 2005.

[24] R. Bernier, G. Dawson, S. Webb, and M. Murias, "EEG Mu Rhythm and Imitation Impairments in Individuals with Autism Spectrum Disorder," *Brain and Cognition*, vol. 64, no. 3, pp. 228–237, 2007.

[25] M. Nakanishi, Y. Wang, Y. T. Wang, Y. Mitsukura, and T. P. Jung, "Generating Visual Flickers for Eliciting Robust Steady-state Visual Evoked Potentials at Flexible Frequencies Using Monitor Refresh Rate," *PloS One*, vol. 9, no. 6, e99235, 2014.

[26] J. R. Wolpaw, N. Birbaumer, D. J. McFarland, G. Pfurtscheller, and T. M. Vaughan, "Brain-computer Interfaces for Communication and Control," *Clinical Neurophysiology*, vol. 113, no. 6, pp. 767–791, 2002.

[27] L. A. Farwell and E. Donchin, "Talking off the Top of Your Head: Toward a Mental Prosthesis Utilizing Event-related Brain Potentials," *Electroencephalography and Clinical Neurophysiology*, vol. 70, no. 6, pp. 510–523, 1988.

[28] J. J. Vidal, "Real-time Detection of Brain Events in EEG," *Proceedings of the IEEE*, vol. 65, no. 5, pp. 633–641, 1977.

[29] B. Blankertz, G. Dornhege, M. Krauledat, K. R. Müller, and G. Curio, "The Non-invasive Berlin Brain-computer Interface: Fast Acquisition of Effective Performance in Untrained Subjects," *NeuroImage*, vol. 37, no. 2, pp. 539–550, 2007.

[30] W. Lutzenberger, T. Elbert, B. Rockstroh, and N. Birbaumer, "The Effects of Self-regulation of Slow Cortical Potentials on Performance in a Signal Detection Task," *International Journal of Neuroscience*, vol. 9, no. 3, pp. 175–183, 1979.

[31] E. Donchin, "Surprise!... Surprise?," *Psychophysiology*, vol. 18, no. 5, pp. 493–513, 1981.

[32] C. Jia, H. Xu, B. Hong, X. Gao, Z. Zhang, and S. Gao, "A Human Computer Interface Using SSVEP-based BCI Technology," *Foundations of Augmented Cognition. Springer Berlin Heidelberg*, vol. 4565, pp. 113–119, 2007.

[33] J. R. Wolpaw, D. J. McFarland, G. W. Neat, and C. A. Forneris, "An EEG-based Brain-computer Interface for Cursor Control," *Electroencephalography and Clinical Neurophysiology*, vol. 78, no. 3, pp. 252–259, 1991.

[34] K. Tanaka, K. Matsunaga, and H. O. Wang, "Electroencephalogram-based Control of an Electric Wheelchair," *IEEE Transactions on Robotics*, vol. 21, no. 4, pp. 762–766, 2005.

[35] H. Berger, "Über das Elektrenkephalogramm des Menschen," *European Archives of Psychiatry and Clinical Neuroscience*, vol. 87, no. 1, pp. 527–570, 1929.

[36] C. M. Sinclair, M. C. Gasper, and A. S. Blum, "Basic Electronics in Clinical Neurophysiology," *In the Clinical Neurophysiology Primer. Humana Press*, pp. 3–18, 2007.

[37] D. Prutchi and M. Norris, "Design and Development of Medical Electronic Instrumentation: A Practical Perspective of the Design, Construction, and Test of Medical Devices," *John Wiley and Sons, Hoboken*, 2005.

[38] A. B. Usakli, "Improvement of EEG Signal Acquisition: An Electrical Aspect for State of the Art of Front End," *Computational Intelligence and Neuroscience*, vol. 2010, no. 12, 2010.

[39] T. C. Ferree, P. Luu, G. S. Russell, and D. M. Tucker, "Scalp Electrode Impedance, Infection Risk, and EEG Data Quality," *Clinical Neurophysiology*, vol. 112, no. 3, pp. 536–544, 2001.

[40] L. D. Liao, C. Y. Chen, I. J. Wang, S. F. Chen, S. Y. Li, B. W. Chen, J. Y. Chang, and C. T. Lin, "Gaming Control Using a Wearable and Wireless EEG-based Brain-computer Interface Device with Novel Dry Foam-based Sensors," *Journal of Neuroengineering and Rehabilitation*, vol. 9, no. 5, 2012.

[41] M. Engin, T. Dalbastı, M. Güldüren, E. Davaslı, and E. Z. Engin, "A Prototype Portable System for EEG Measurements," *Measurement*, vol. 40, no. 9, pp. 936–942, 2007.

[42] Y. M. Chi, T. P. Jung, and G. Cauwenberghs, "Dry-contact and Noncontact Biopotential Electrodes: Methodological Review," *IEEE Reviews in Biomedical Engineering*, vol. 3, pp. 106–119, 2010.

[43] Y. M. Chi, Y. T. Wang, Y. Wang, C. Maier, T. P. Jung, and G. Cauwenberghs, "Dry and Noncontact EEG Sensors for Mobile Brain-computer Interfaces," *IEEE Transactions on Neural Systems and Rehabilitation Engineering*, vol. 20, no. 2, pp. 228–235, 2012.

[44] T. J. Sullivan, S. R. Deiss, and G. Cauwenberghs, "A Low-noise, Non-contact EEG/ECG Sensor," *IEEE Conference on Biomedical Circuits and Systems*, pp. 154–157. 2007.

[45] T. W. Picton, S. Bentin, P. Berg, E. Donchin, S. A. Hillyard, R. Johnson, G. A. Miller, W. Ritter, D. S. Ruchkin, M. D. Rugg, and M. J. Taylor, "Guidelines for Using Human Event-related Potentials to Study Cognition: Recording Standards and Publication Criteria," *Psychophysiology*, vol. 37, no. 2, pp. 127–152, 2000.

[46] Y. M. Chi, P. Ng, and G. Cauwenberghs, "Wireless Noncontact ECG and EEG Biopotential Sensors," *ACM Transactions on Embedded Computing Systems*, vol. 12, no. 4, 2013.

[47] D. Flotzinger, G. Pfurtscheller, C. Neuper, J. Berger, and W. Mohl, "Classification of Non-averaged EEG Data by Learning Vector Quantisation and the Influence of Signal Preprocessing," *Medical and Biological Engineering and Computing*, vol. 32, no. 5, pp. 571–576, 1994.

[48] B. Schölkopf, S. Mika, C. J. Burges, P. Knirsch, K. R. Müller, G. Rätsch, and A. J. Smola, "Input Space Versus Feature Space in Kernel-based Methods," *IEEE Transactions on Neural Networks*, vol. 10, no. 5, pp. 1000–1017, 1999.

[49] E. Martnez-Montes, P. A. Valdás-Sosa, F. Miwakeichi, R. I. Goldman, and M. S. Cohen, "Concurrent EEG/fMRI Analysis by Multiway Partial Least Squares," *NeuroImage*, vol. 22, no. 3, pp. 1023–1034, 2004.

[50] C. M. Bishop, "Pattern Recognition and Machine Learning," *Springer*, 2006.

[51] J. Felblinger, J. Slotboom, R. Kreis, B. Jung, and C. Boesch, "Restoration of Electrophysiological Signals Distorted by Inductive Effects of Magnetic Field Gradients during MR Sequences," *Magnetic Resonance in Medicine*, vol. 41, no. 4, pp. 715–721, 1999.

[52] J. L. Whitton, F. Lue, and H. Moldofsky, "A Spectral Method for Removing Eye Movement Artifacts from the EEG," *Electroencephalography and Clinical Neurophysiology*, vol. 44, no. 6, pp. 735–741, 1978.

[53] P. J. Allen, O. Josephs, and R. Turner, "A Method for Removing Imaging Artifact from Continuous EEG Recorded during Functional MRI," *Neuroimage*, vol. 12, no. 2, pp. 230–239, 2000.

[54] M. A. Kabir and C. Shahnaz, "Denoising of ECG Signals Based on Noise Reduction Algorithms in EMD and Wavelet Domains," *Biomedical Signal Processing and Control*, vol. 7, no. 5, pp. 481–489, 2012.

[55] H. C. Kim, S. S. Yoo, and J. H. Lee, "Recursive Approach of EEG-segment-based Principal Component Analysis Substantially Reduces Cryogenic Pump Artifacts in Simultaneous EEG-fMRI Data," *NeuroImage*, vol. 104, pp. 437–451, 2015.

[56] O. G. Lins, T. W. Picton, P. Berg, and M. Scherg, "Ocular Artifacts in EEG and Event-related Potentials I: Scalp Topography," *Brain Topography*, vol. 6, no. 1, pp. 51–63, 1993.

[57] M. Teplan, "Fundamentals of EEG Measurement," *Measurement Science Review*, vol. 2, no. 2, pp. 1–11, 2002.

[58] J. C. Huhta and J. G. Webster, "60-Hz Interference in Electrocardiography," *IEEE Transactions on Biomedical Engineering*, vol. 20, no. 2, pp. 91–101, 1973.

[59] M. E. Saab and J. Gotman, "A System to Detect the Onset of Epileptic Seizures in Scalp EEG," *Clinical Neurophysiology*, vol. 116, no. 2, pp. 427–442, 2005.

[60] S. F. Farmer, F. D. Bremner, D. M. Halliday, J. R. Rosenberg, and J. A. Stephens, "The Frequency Content of Common Synaptic Inputs to Motoneurones Studied during Voluntary Isometric Contraction in Man," *The Journal of Physiology*, vol. 470, no. 1, pp. 127–155, 1993.

[61] D. M. Halliday, B. A. Conway, S. F. Farmer, and J. R. Rosenberg, "Using Electroencephalography to Study Functional Coupling between Cortical Activity and Electromyograms during Voluntary Contractions in Humans," *Neuroscience Letters*, vol. 241, no. 1, pp. 5–8, 1998.

[62] J. H. McAuley, J. C. Rothwell, and C. D. Marsden, "Frequency Peaks of Tremor, Muscle Vibration and Electromyographic Activity at 10 Hz, 20 Hz and 40 Hz during Human Finger Muscle Contraction may Reflect Rhythmicities of Central Neural Firing," *Experimental Brain Research*, vol. 114, no. 3, pp. 525–541, 1997.

[63] P. Brown, "Cortical Drives to Human Muscle: The Piper and Related Rhythms," *Progress in Neurobiology*, vol. 60, no. 1, pp. 97–108, 2000.

[64] A. Van Boxtel, "Optimal Signal Bandwidth for the Recording of Surface EMG Activity of Facial, Jaw, Oral, and Neck Muscles," *Psychophysiology*, vol. 38, no. 1, pp. 22–34, 2001.

[65] A. Van Boxtel, P. Goudswaard, G. M. Van der Molen, and W. E. Van Den Bosch, "Changes in Electromyogram Power Spectra of Facial and Jaw-elevator Muscles during Fatigue," *Journal of Applied Physiology*, vol. 54, no. 1, pp. 51–58, 1983.

[66] J. Taelman, B. Mijovic, S. Van Huffel, S. Devuyst, and T. Dutoit, "ECG Artifact Removal from Surface EMG Signals by Combining Empirical Mode Decomposition and Independent Component Analysis," *4th International Conference on Bio-Inspired Systems and Signal Processing*, pp. 421–424, 2011.

[67] K. J. Lee and B. Lee, "Removing ECG Artifacts from the EMG: A Comparison between Combining Empirical-mode Decomposition and Independent Component Analysis and Other Filtering Methods," *2013 13th International Conference on Control, Automation and Systems*, pp. 181–184, 2013.

[68] T. Jing-tian, Z. Qing, T. Yan, L. Bin, and Z. Xiao-kai, "Hilbert-huang Transform for ECG De-noising," *The 1st International Conference on Bioinformatics and Biomedical Engineering*, pp. 664–667, 2007.

[69] T. Gasser, L. Sroka, and J. Möcks, "The Transfer of EOG Activity into the EEG for Eyes Open and Closed," *Electroencephalography and Clinical Neurophysiology*, vol. 61, no. 2, pp. 181–193, 1985.

[70] T. Gasser, L. Sroka, and J. Möcks, "The Correction of EOG Artifacts by Frequency Dependent and Frequency Independent Methods," *Psychophysiology*, vol. 23, no. 6, pp. 704–712, 1986.

[71] D. Hagemann and E. Naumann, "The Effects of Ocular Artifacts on (Lateralized) Broadband Power in the EEG," *Clinical Neurophysiology*, vol. 112, no. 2, pp. 215–231, 2001.

[72] P. Berg and M. Scherg, "Dipole Models of Eye Movements and Blinks," *Electroencephalography and Clinical Neurophysiology*, vol. 79, no. 1, pp. 36–44, 1991.

[73] C. Bell, "On the Motions of the Eye, in Illustration of the Uses of the Muscles and Nerves of the Orbit," *Philosophical Transactions of the Royal Society of London*, vol. 113, pp. 166–186, 1823.

[74] M. Iwasaki, C. Kellinghaus, A. V. Alexopoulos, R. C. Burgess, A. N. Kumar, Y. H. Han, H. O. Lüders, and R. J. Leigh, "Effects of Eyelid Closure, Blinks, and Eye

Movements on the Electroencephalogram," *Clinical Neurophysiology*, vol. 116, no. 4, pp. 878–885, 2005.

[75] S. Yuval-Greenberg, O. Tomer, A. S. Keren, I. Nelken, and L. Y. Deouell, "Transient Induced Gamma-band Response in EEG as a Manifestation of Miniature Saccades," *Neuron*, vol. 58, no. 3, pp. 429–441, 2008.

[76] M. Fatourechi, A. Bashashati, R. K. Ward, and G. E. Birch, "EMG and EOG Artifacts in Brain Computer Interface Systems: A Survey," *Clinical Neurophysiology*, vol. 118, no. 3, pp. 480–494, 2007.

[77] I. I. Goncharova, D. J. McFarland, T. M. Vaughan, and J. R. Wolpaw, "EMG Contamination of EEG: Spectral and Topographical Characteristics," *Clinical Neurophysiology*, vol. 114, no. 9, pp. 1580–1593, 2003.

[78] P. Anderer, S. Roberts, A. Schlögl, G. Gruber, G. Klösch, W. Herrmann, P. Rappelsberger, O. Filz, M. J. Barbanoj, G. Dorffner, and B. Saletu, "Artifact Processing in Computerized Analysis of Sleep EEG – A Review," *Neuropsychobiology*, vol. 40, no. 3, pp. 150–157, 1999.

[79] T. Olund, J. Duun-Henriksen, T. W. Kjaer, and H. B. D. Sorensen, "Automatic Detection and Classification of Artifacts in Single-channel EEG," *36th Annual International Conference of the IEEE Engineering in Medicine and Biology Society*, pp. 922–925, 2014.

[80] D. P. Brunner, R. C. Vasko, C. S. Detka, J. P. Monahan, C. F. Reynolds III, and D. J. Kupfer, "Muscle Artifacts in the Sleep EEG: Automated Detection and Effect on All-night EEG Power Spectra," *Journal of Sleep Research*, vol. 5, no. 3, pp. 155–164, 1996.

[81] J. Sijbers, J. Van Audekerke, M. Verhoye, A. Van der Linden, and D. Van Dyck, "Reduction of ECG and Gradient Related Artifacts in Simultaneously Recorded Human EEG/MRI Data," *Magnetic Resonance Imaging*, vol. 18, no. 7, pp. 881–886, 2000.

[82] J. A. Jiang, C. F. Chao, M. J. Chiu, R. G. Lee, C. L. Tseng, and R. Lin, "An Automatic Analysis Method for Detecting and Eliminating ECG Artifacts in EEG," *Computers in Biology and Medicine*, vol. 37, no. 11, pp. 1660–1671, 2007.

[83] N. Mourad and R. K. Niazy, "Automatic Correction of Eye Blink Artifact in Single Channel EEG Recording Using EMD and OMP," *The 2013 European Signal Processing Conference*, pp. 1–5, 2013.

[84] M. L. Shoker, S. Sanei, W. Wang, and J. A. Chambers, "Removal of Eye Blinking Artifact from the Electro-encephalogram, Incorporating a New Constrained Blind Source Separation Algorithm," *Medical and Biological Engineering and Computing*, vol. 43, no. 2, pp. 290–295, 2005.

[85] J. C. Woestenburg, M. N. Verbaten, and J. L. Slangen, "The Removal of the Eye-movement Artifact from the EEG by Regression Analysis in the Frequency Domain," *Biological Psychology*, vol. 16, no. 1, pp. 127–147, 1983.

[86] J. Hu, C. S. Wang, M. Wu, Y. X. Du, Y. He, and J. She, "Removal of EOG and EMG Artifacts from EEG Using Combination of Functional Link Neural Network and Adaptive Neural Fuzzy Inference System," *Neurocomputing*, vol. 151, no. 1, pp. 278–287, 2015.

[87] M. G. Doane, "Interaction of Eyelids and Tears in Corneal Wetting and the Dynamics of the Normal Human Eyeblink," *American Journal of Ophthalmology*, vol. 89, no. 4, pp. 507–516, 1980.

[88] C. N. Karson, "Spontaneous Eye-blink Rates and Dopaminergic Systems," *Brain*, vol. 106, no. 3, pp. 643–653, 1983.

[89] T. Elbert, W. Lutzenberger, B. Rockstroh, and N. Birbaumer, "Removal of Ocular Artifacts from the EEG – A Biophysical Approach to the EOG," *Electroencephalography and Clinical Neurophysiology*, vol. 60, no. 5, pp. 455–463, 1985.

[90] G. Gratton, "Dealing with Artifacts: The EOG Contamination of the Event-related Brain Potential," *Behavior Research Methods, Instruments, and Computers*, vol. 30, no. 1, pp. 44–53, 1998.

[91] R. Verleger, "The Instruction to Refrain from Blinking Affects Auditory P3 and N1 Amplitudes," *Electroencephalography and Clinical Neurophysiology*, vol. 78, no. 3, pp. 240–251, 1991.

[92] P. Xu and D. Yao, "A Novel Method Based on Realistic Head Model for EEG Denoising," *Computer Methods and Programs in Biomedicine*, vol. 83, no. 2, pp. 104–110, 2006.

[93] T. Gasser, P. Ziegler, and W. F. Gattaz, "The Deleterious Effect of Ocular Artefacts on the Quantitative EEG, and a Remedy," *European Archives of Psychiatry and Clinical Neuroscience*, vol. 241, no. 6, pp. 352–356, 1992.

[94] A. J. Bell and T. J. Sejnowski, "An Information-maximization Approach to Blind Separation and Blind Deconvolution," *Neural Computation*, vol. 7, no. 6, pp. 1129–1159, 1995.

[95] S. Makeig, A. J. Bell, T. P. Jung, and T. J. Sejnowski, "Independent Component Analysis of Electroencephalographic Data," *Advances in Neural Information Processing Systems*, vol. 8, pp. 145–151, 1996.

[96] L. Tong, V. C. Soon, Y. F. Huang, and R. Liu, "AMUSE: A New Blind Identification Algorithm," *IEEE International Symposium on Circuits and Systems*, vol. 3, pp. 1784–1787, 1990.

[97] T. P. Jung, C. Humphries, T. W. Lee, S. Makeig, M. J. McKeown, V. Iragui, and T. J. Sejnowski, "Extended ICA Removes Artifacts from Electroencephalographic Recordings," *Advances in Neural Information Processing Systems*, vol. 10, pp. 894–900, 1998.

[98] P. Georgiev, F. Theis, A. Cichocki, and H. Bakardjian, "Sparse Component Analysis: A New Tool for Data Mining," *Springer Optimization and Its Applications*, vol. 7, pp. 91–116, 2007.

[99] I. Daly, N. Nicolaou, S. J. Nasuto, and K. Warwick, "Automated Artifact Removal from the Electroencephalogram: A Comparative Study," *Clinical EEG and Neuroscience*, vol. 44, no. 4, pp. 291–306, 2013.

[100] P. Berg and M. Scherg, "A Multiple Source Approach to the Correction of Eye Artifacts," *Electroencephalography and Clinical Neurophysiology*, vol. 90, no. 3, pp. 229–241, 1994.

[101] P. Comon, "Independent Component Analysis, a New Concept," *Signal Processing*, vol. 36, no. 3, pp. 287–314, 1994.

[102] S. Romero, M. A. Mañanas, and M. J. Barbanoj, "A Comparative Study of Automatic Techniques for Ocular Artifact Reduction in Spontaneous EEG Signals Based on Clinical Target Variables: A Simulation Case," *Computers in Biology and Medicine*, vol. 38, no. 3, pp. 348–360, 2008.

[103] T. P. Jung, S. Makeig, M. Westerfield, J. Townsend, E. Courchesne, and T. J. Sejnowski, "Analysis and Visualization of Single-trial Event-related Potentials," *Human Brain Mapping*, vol. 14, no. 3, pp. 166–185, 2001.

[104] J. Onton and S. Makeig, "Information-based Modeling of Event-related Brain Dynamics," *Progress in Brain Research*, vol. 159, pp. 99–120, 2006.

[105] M. Naeem, C. Brunner, R. Leeb, B. Graimann, and G. Pfurtscheller, "Seperability of Four-class Motor Imagery Data Using Independent Components Analysis," *Journal of Neural Engineering*, vol. 3, no. 3, pp. 208–216, 2006.

[106] H. Serby, E. Yom-Tov, and G. F. Inbar, "An Improved P300-based Brain-computer Interface," *IEEE Transactions on Neural Systems and Rehabilitation Engineering*, vol. 13, no. 1, pp. 89–98, 2005.

[107] M. E. Davies and C. J. James, "Source Separation Using Single Channel ICA," *Signal Processing*, vol. 87, no. 8, pp. 1819–1832, 2007.

[108] M. A. Klados, C. Papadelis, C. Braun, and P. D. Bamidis, "REG–ICA: A Hybrid Methodology Combining Blind Source Separation and Regression Techniques for the Rejection of Ocular Artifacts," *Biomedical Signal Processing and Control*, vol. 6, no. 3, pp. 291–300, 2011.

[109] F. Matsuo, J. F. Peters, and E. L. Reilly, "Electrical Phenomena Associated with Movements of the Eyelid," *Electroencephalography and Clinical Neurophysiology*, vol. 38, no. 5, pp. 507–511, 1975.

[110] M. A. Eisengart and D. Symmes, "Effect of Eye Blink on the Visual Evoked Response in Children," *Electroencephalography and Clinical Neurophysiology*, vol. 31, no. 1, pp. 71–75, 1971.

[111] J. Hori, K. Sakano, and Y. Saitoh, "Development of a Communication Support Device Controlled by Eye Movements and Voluntary Eye Blink," *IEICE Transactions on Information and Systems*, vol. 89, no. 6, pp. 1790–1797, 2006.

[112] R. E. Records, "Physiology of the Human Eye and Visual System," *Harper and Row. Hagerstown*, 1979.

[113] S. Hoffmann and M. Falkenstein, "The Correction of Eye Blink Artefacts in the EEG: A Comparison of Two Prominent Methods," *PLoS One*, vol. 3, no. 8, e3004, 2008.

[114] T. P. Jung, S. Makeig, C. Humphries, T. W. Lee, M. J. Mckeown, V. Iragui, and T. J. Sejnowski, "Removing Electroencephalographic Artifacts by Blind Source Separation," *Psychophysiology*, vol. 37, no. 2, pp. 163–178, 2000.

[115] H. Peng, B. Hu, Q. Shi, M. Ratcliffe, Q. Zhao, Y. Qi, and G. Gao, "Removal of Ocular Artifacts in EEG – An Improved Approach Combining DWT and ANC for Portable Applications," *IEEE Journal of Biomedical and Health Informatics*, vol. 17, no. 3, pp. 600–607, 2013.

[116] B. Mijović, M. De Vos, I. Gligorijević, J. Taelman, and S. Van Huffel, "Source Separation from Single-channel Recordings by Combining Empirical-mode Decomposition and Independent Component Analysis," *IEEE Transactions on Biomedical Engineering*, vol. 57, no. 9, pp. 2188–2196, 2010.

[117] S. Kanoga and Y. Mitsukura, "Eye-blink Artifact Reduction Using 2-step Non-negative Matrix Factorization for Single-channel Electroencephalographic Signals," *Journal of Signal Processing*, vol. 18, no. 5, pp. 251–257, 2014.

[118] G. Rebolledo-Mendez, I. Dunwell, E. A. Martínez-Mirón, M. D. Vargas-Cerdán, S. De Freitas, F. Liarokapis, and A. R. García-Gaona, "Assessing Neurosky's Usability to Detect Attention Levels in an Assessment Exercise," *Human-Computer Interaction. New Trends, Springer*, vol. 5610, pp. 149–158, 2009.

[119] G. Gratton, M. G. Coles, and E. Donchin, "A New Method for Off-line Removal of Ocular Artifact," *Electroencephalography and Clinical Neurophysiology*, vol. 55, no. 4, pp. 468–484, 1983.

[120] C. J. James and O. J. Gibson "Temporally Constrained ICA: An Application to Artifact Rejection in Electromagnetic Brain Signal Analysis," *IEEE Transactions on Biomedical Engineering*, vol. 50, no. 9, pp. 1108–1116, 2003.

[121] W. Lu and J. C. Rajapakse, "Approach and Applications of Constrained ICA," *IEEE Transactions on Neural Networks*, vol. 16, no. 1, pp. 203–212, 2005.

[122] Y. Li, Z. Ma, W. Lu, and Y. Li, "Automatic Removal of the Eye Blink Artifact from EEG Using an ICA-based Template Matching Approach," *Physiological Measurement*, vol. 27, no. 4, pp. 425–436, 2006.

[123] J. Talairach and P. Tournoux, "Co-planar Stereotaxic Atlas of the Human Brain. 3-dimensional Proportional System: An Approach to Cerebral Imaging," *Thieme Medical*, 1988.

[124] E. R. Kandel, J. H. Schwartz, and T. M. Jessell, "Principles of Neural Science," *New York: McGraw-Hill*, pp. 7–19, 2000.

[125] N. Geschwind, "Specializations of the Human Brain," *Scientific American*, vol. 241, no. 3, pp. 180–199, 1979.

[126] M. Brett, I. S. Johnsrude, and A. M. Owen, "The Problem of Functional Localization in the Human Brain," *Nature Reviews Neuroscience*, vol. 3, no. 3, pp. 243–249, 2002.

[127] M. Carter and J. C. Shieh, "Guide to Research Techniques in Neuroscience," *Academic Press*, pp. 1–37, 2015.

[128] F. A. Azevedo, L. R. Carvalho, L. T. Grinberg, J. M. Farfel, R. E. Ferretti, R. E. Leite, W. J. Filho, R. Lent, and S. Herculano–Houzel, "Equal Numbers of Neuronal and Nonneuronal Cells Make the Human Brain an Isometrically Scaled-up Primate Brain," *Journal of Comparative Neurology*, vol. 513, no. 5, pp. 532–541, 2009.

[129] M. Urbanska, M. Blazejczyk, and J. Jaworski, "Molecular Basis of Dendritic Arborization," *Acta Neurobiologiae Experimentalis*, vol. 68, no. 2, pp. 264–288, 2008.

[130] J. J. Hopfield, "Pattern Recognition Computation Using Action Potential Timing for Stimulus Representation," *Nature*, vol. 376, no. 6535, pp. 33–36, 1995.

[131] A. G. Richardson, C. C. McIntyre, and W. M. Grill, "Modelling the Effects of Electric Fields on Nerve Fibres: Influence of the Myelin Sheath," *Medical and Biological Engineering and Computing*, vol. 38, no. 4, pp. 438–446, 2000.

[132] V. M. Pickel, T. H. Joh, D. J. Reis, S. E. Leeman, and R. J. Miller, "Electron Microscopic Localization of Substance P and Enkephalin in Axon Terminals Related to Dendrites of Catecholaminergic Neurons," *Brain Research*, vol. 160, no. 3, pp. 387–400, 1979.

[133] S. R. Reiken, B. J. Van Wie, H. Sutisna, D. F. Moffett, A. R. Koch, M. Silber, and W. C. Davis, "Bispecific Antibody Modification of Nicotinic Acetylcholine Receptors for Biosensing," *Biosensors and Bioelectronics*, vol. 11, no. 1, pp. 91–102, 1996.

[134] T. R. Elliott, "The Action of Adrenalin," *The Journal of Physiology*, vol. 32, no. 5–6, pp. 401–467, 1905.

[135] M. Sheng, B. L. Sabatini, and T. C. Südhof, "Synapses and Alzheimer's Disease," *Cold Spring Harbor Perspectives in Biology*, vol. 4, no. 5, a005777, 2012.

[136] M. V. Bennett and R. S. Zukin, "Electrical Coupling and Neuronal Synchronization in the Mammalian Brain," *Neuron*, vol. 41, no. 4, pp. 495–511, 2004.

[137] D. A. Goodenough and D. L. Paul, "Gap Junctions," *Cold Spring Harbor Perspectives in Biology*, vol. 1, no. 1, a002576, 2009.

[138] K. Vervaeke, A. Lõrincz, Z. Nusser, and R. A. Silver, "Gap Junctions Compensate for Sublinear Dendritic Integration in an Inhibitory Network," *Science*, vol. 335, no. 6076, pp. 1624–1628, 2012.

[139] A. E. Pereda, "Electrical Synapses and Their Functional Interactions with Chemical Synapses," *Nature Reviews Neuroscience*, vol. 15, no. 4, pp. 250–263, 2014.

[140] S. Baillet, J. C. Mosher, and R. M. Leahy, "Electromagnetic Brain Mapping," *IEEE Signal Processing Magazine*, vol. 18, no. 6, pp. 14–30, 2001.

[141] R. Caton, "Electrical Currents of the Brain," *The Journal of Nervous and Mental Disease*, vol. 2, no. 4, pp. 610, 1875.

[142] S. Kim and A. Chiba, "Dendritic Guidance," *Trends in Neurosciences*, vol. 27, no. 4, pp. 194–202, 2004.

[143] S. P. van den Broek, F. Reinders, M. Donderwinkel, and M. J. Peters, "Volume Conduction Effects in EEG and MEG," *Electroencephalography and Clinical Neurophysiology*, vol. 106, no. 6, pp. 522–534, 1998.

[144] H. H. Jasper, "The Ten Twenty Electrode System of the International Federation," *Electroencephalography and Clinical Neurophysiology*, vol. 10, pp. 371–375, 1958.

[145] R. A. Stone and D. I. Flitcroft, "Ocular Shape and Myopia," *Annals-Academy of Medicine Singapore*, vol. 33, no. 1, pp. 7–15, 2004.

[146] J. Wallman, M. D. Gottlieb, V. Rajaram, and L. A. Fugate-Wentzek, "Local Retinal Regions Control Local Eye Growth and Myopia," *Science*, vol. 237, no. 4810, pp. 73-77, 1987.

[147] E. L. Irving, J. G. Sivak, and M. G. Callender, "Refractive Plasticity of the Developing Chick Eye," *Ophthalmic and Physiological Optics*, vol. 12, no. 4, pp. 448–456, 1992.

[148] D. R. Korb, R. C. Scaffidi, J. V. Greiner, K. R. Kenyon, J. P. Herman, C. A. Blackie, T. Glonek, C. L. Case, V. M. Finnemore, and T. Douglass, "The Effect of Two Novel Lubricant Eye Drops on Tear Film Lipid Layer Thickness in Subjects with Dry Eye Symptoms," *Optometry and Vision Science*, vol. 82, no. 7, pp. 594–601, 2005.

[149] P. D. Imesch, I. H. Wallow, and D. M. Albert, "The Color of the Human Eye: A Review of Morphologic Correlates and of Some Conditions that Affect Iridial Pigmentation," *Survey of Ophthalmology*, vol. 41, no. 2, S117–S123, 1997.

[150] M. J. Hogan, J. A. Alvarado, and J. E. Weddell, "Iris and Anterior Chamber: Histology of the Human Eye," *An Atlas and Textbook*, pp. 202–259, 1971.

[151] S. A. Strenk, L. M. Strenk, and J. F. Koretz, "The Mechanism of Presbyopia," *Progress in Retinal and Eye Research*, vol. 24, no. 3, pp. 379–393, 2005.

[152] L. C. Katz and C. J. Shatz, "Synaptic Activity and the Construction of Cortical Circuits," *Science*, vol. 274, no. 5290, pp. 1133–1138, 1996.

[153] M. B. Feller, D. P. Wellis, D. Stellwagen, F. S. Werblin, and C. J. Shatz, "Requirement for Cholinergic Synaptic Transmission in the Propagation of Spontaneous Retinal Waves," *Science*, vol. 272, no. 5265, pp. 1182–1187, 1996.

[154] International Society for Stem Cell Reserch, *A Closer Look at Stem Cells*, http://www.closerlookatstemcells.org/stem-cells-and-medicine/macular-degeneration (accessed 26-Nov-2015).

[155] C. Li, H. Guo, X. Xu, W. Weinberg, and C. X. Deng, "Fibroblast Growth Factor Receptor 2 (Fgfr2) Plays an Important Role in Eyelid and Skin Formation and Patterning," *Developmental Dynamics*, vol. 222, no. 3, pp. 471–483, 2001.

[156] eyepedia.co.uk, *Eyelids*, http://www.eyepedia.co.uk/eyes-vision/eye-anatomy/external-eye/eyelids/ (accessed 01-Dec-2015).

[157] P. J. Driver and M. A. Lemp, "Meibomian Gland Dysfunction," *Survey of Ophthalmology*, vol. 40, no. 5, pp. 343–367, 1996.

[158] J. W. Karesh, "The Evaluation and Management of Eyelid Trauma," *Clinical Ophthalmology*, vol. 5, 1996 (accessed 01-Dec-2015).

[159] J. P. Gilbard and R. L. Farris, "Tear Osmolarity and Ocular Surface Disease in Keratoconjunctivitis Sicca," *Archives of Ophthalmology*, vol. 97, no. 9, pp. 1642–1646, 1979.

[160] W. D. Mathers, J. A. Lane, J. E. Sutphin, and M. B. Zimmerman, "Model for Ocular Tear Film Function," *Cornea*, vol. 15, no. 2, pp. 110–119, 1996.

[161] R. Saxena, S. Srivastava, D. Trivedi, E. Anand, S. Joshi, and S. K. Gupta, "Impact of Environmental Pollution on the Eye," *Acta Ophthalmologica Scandinavica*, vol. 81, no. 5, pp. 491–494, 2003.

[162] P. Wolkoff, J. K. Nøjgaard, P. Troiano, and B. Piccoli, "Eye Complaints in the Office Environment: Precorneal Tear Film Integrity Influenced by Eye Blinking Efficiency," *Occupational and Environmental Medicine*, vol. 62, no. 1, pp. 4–12, 2005.

[163] OpenStax College, "Anatomy and Physiology: Chapter 14 The Brain and Cranial Nerves," *OpenStax College*, pp. 569–620, 2013.

[164] A. F. Fuchs and E. S. Luschei, "Development of Isometric Tension in Simian Extraocular Muscle," *The Journal of Physiology*, vol. 219, no. 1, pp. 155–166, 1971.

[165] R. J. Leigh and D. S. Zee, "The Neurology of Eye Movements," *Oxford University Press*, 2015.

[166] J. L. Demer, "Pivotal Role of Orbital Connective Tissues in Binocular Alignment and Strabismus the Friedenwald Lecture," *Investigative Ophthalmology and Visual Science*, vol. 45, no. 3, pp. 729–738, 2004.

[167] M. Strupp, O. Kremmyda, C. Adamczyk, N. Böttcher, C. Muth, C. W. Yip, and T. Bremova, "Central Ocular Motor Disorders, Including Gaze Palsy and Nystagmus," *Journal of Neurology*, vol. 261, no. 2, pp.542–558, 2014.

[168] T. Kuwabara, D. G. Cogan, and C. C. Johnson, "Structure of the Muscles of the Upper Eyelid," *Archives of Ophthalmology*, vol. 93, no. 11, pp. 1189–1197, 1975.

[169] P. J. Attwell, M. Ivarsson, L. Millar, and C. H. Yeo, "Cerebellar Mechanisms in Eyeblink Conditioning," *Annals of the New York Academy of Sciences*, vol. 978, no. 1, pp. 79–92, 2002.

[170] J. H. Freeman and A. B. Steinmetz, "Neural Circuitry and Plasticity Mechanisms Underlying Delay Eyeblink Conditioning," *Learning and Memory*, vol. 18, no. 10, pp. 666–677, 2011.

[171] H. Collewijn, J. Van der Steen, and R. M. Steinman, "Human Eye Movements Associated with Blinks and Prolonged Eyelid Closure," *Journal of Neurophysiology*, vol. 54, no. 1, pp. 11–27, 1985.

[172] K. R. Peshori, E. J. Schicatano, R. Gopalaswamy, E. Sahay, and C. Evinger, "Aging of the Trigeminal Blink System," *Experimental Brain Research*, vol. 136, no. 3, pp. 351–363, 2001.

[173] F. T. Ibrahimpašić, "Reflex Eyelid Blinks – On the Applicability in Psychophysiologica Researches," *Review of Psychology*, vol. 6, no. 1-2, pp. 53–78, 2000.

[174] K. A. Manning, L. A. Riggs, and J. K. Komenda, "Reflex Eyeblinks and Visual Suppression," *Perception and Psychophysics*, vol. 34, no. 3, pp. 250–256, 1983.

[175] B. Shahani, "The Human Blink Reflex," *Journal of Neurology, Neurosurgery and Psychiatry*, vol. 33, no. 6, pp. 792–800, 1970.

[176] W. Overend, "Preliminary Note on a New Cranial Reflex," *The Lancet*, vol. 147, no. 3784, pp. 619, 1896.

[177] G. Rushworth, "Observations on Blink Reflexes," *Journal of Neurology, Neurosurgery, and Psychiatry*, vol. 25, no. 2, pp. 93–108, 1962.

[178] Č. Ljubin, K. Knešaurek, and T. Ljubin, "Mathematical and Graphic Model of the Audiomotor Reflex of the Musculus Orbicularis Oculi and the Law of Energy," *Electromyography and Clinical Neurophysiology*, vol. 26, no. 4, pp. 229–240, 1985.

[179] M. L. Borowsky, "Der Blinzelabwehrreflex, Sein Biologisches Wesen und Seine Veränderungen als Neues Symptom bei Hemiplegie," *Journal of Neurology*, vol. 110, no. 1, pp. 134–150, 1929.

[180] H. Strauss, C. Landis, and W. A. Hunt, "Acoustic Motor Reactions: Especially the Cochleopalpebral Reflex," *Archives of Otolaryngology*, vol. 28, no. 6, pp. 941–945, 1938.

[181] E. E. Krauter, D. W. Leonard, and J. R. Ison, "Inhibition of Human Eye Blink by Brief Acoustic Stimulus," *Journal of Comparative and Physiological Psychology*, vol. 84, no. 2, pp. 246–251, 1973.

[182] F. K. Graham and G. M. Murray, "Discordant Effects of Weak Prestimulation on Magnitude and Latency of the Reflex Blink," *Physiological Psychology*, vol. 5, no. 1, pp. 108–114, 1977.

[183] what-when-how In Depth Tutorials and Information, *The Cranial Nerves (Organization of the Central Nervous System) Part 4*, http://what-when-how.com/neuroscience/the-cranial-nerves-organization-of-the-central-nervous-system-part-4/ (accessed 12-Dec-2015).

[184] B. S. Nashold Jr, J. P. Gills, and W. P. Wilson, "Ocular Signs of Brain Stimulation in the Human," *Stereotactic and Functional Neurosurgery*, vol. 29, no. 2–5, pp. 169–174, 1967.

[185] M. Aramideh, B. O. De Visser, P. P. Devriese, L. J. Bour, and J. D. Speelman, "Electromyographic Features of Levator Palpebrae Superioris and Orbicularis Oculi Muscles in Blepharospasm," *Brain*, vol. 117, no. 1, pp. 27–38, 1994.

[186] C. Evinger, "A Brain Stem Reflex in the Blink of an Eye," *Physiology*, vol. 10, no. 4, pp. 147–153, 1995.

[187] A. Ettl, S. Priglinger, J. Kramer, and L. Koornneef, "Functional Anatomy of the Levator Palpebrae Superioris Muscle and Its Connective Tissue System," *British Journal of Ophthalmology*, vol. 80, no. 8, pp. 702–707, 1996.

[188] C. Evinger, K. A. Manning, and P. A. Sibony, "Eyelid Movements. Mechanisms and Normal Data," *Investigative Ophthalmology and Visual Science*, vol. 32, no. 2, pp. 387–400, 1991.

[189] A. F. Fuchs, W. Becker, L. Ling, T. P. Langer, and C. R. Kaneko, "Discharge Patterns of Levator Palpebrae Superioris Motoneurons during Vertical Lid and Eye Movements in the Monkey," *Journal of Neurophysiology*, vol. 68, no. 1, pp. 233–243, 1992.

[190] F. VanderWerf, P. Brassinga, D. Reits, M. Aramideh, and B. O. de Visser, "Eyelid Movements: Behavioral Studies of Blinking in Humans under Different Stimulus Conditions," *Journal of Neurophysiology*, vol. 89, no. 5, pp. 2784–2796, 2003.

[191] A. J. Gay, M. L. Salmon, and C. E. Windsor, "Hering's Law, the Levators, and Their Relationship in Disease States," *Archives of Ophthalmology*, vol. 77, no. 2, pp. 157–160, 1967.

[192] A. Björk and E. Kugelberg, "The Electrical Activity of the Muscles of the Eye and Eyelids in Various Positions and during Movement," *Electroencephalography and Clinical Neurophysiology*, vol. 5, no. 4, pp. 595–602, 1953.

[193] Á. Esteban, A. Traba, and J. Prieto, "Eyelid Movements in Health and Disease. The Supranuclear Impairment of the Palpebral Motility," *Neurophysiologie Clinique/Clinical Neurophysiology*, vol. 34, no. 1, pp. 3–15, 2004.

[194] C. J. Bruce, M. E. Goldberg, M. C. Bushnell, and G. B. Stanton, "Primate Frontal Eye Fields. II. Physiological and Anatomical Correlates of Electrically Evoked Eye Movements," *Journal of Neurophysiology*, vol. 54, no, 3, pp. 714–734, 1985.

[195] K. Schmidtke and J. A. Büttner-Ennever, "Nervous Control of Eyelid Function," *Brain*, vol. 115, no. 1, pp. 227–247, 1992.

[196] The University of Texas Health Science Center at Houston (UTHealth), *Neuroscience Online an Electronic Textbook for the Neurosciences, Chapter 7: Ocular Motor System*, http://neuroscience.uth.tmc.edu/s3/chapter07.html (accessed 13-Dec-2015).

[197] J. A. Trigo, A. Gruart, and J. M. Delgado-Garcia, "Role of Proprioception in the Control of Lid Position during Reflex and Conditioned Blink Responses in the Alert Behaving Cat," *Neuroscience*, vol. 90, no. 4, pp. 1515–1528, 1999.

[198] R. Agostino, M. Bologna, L. Dinapoli, B. Gregori, G. Fabbrini, N. Accornero, and A. Berardelli, "Voluntary, Spontaneous, and Reflex Blinking in Parkinson's Disease," *Movement Disorders*, vol. 23, no. 5, pp. 669–675, 2008.

[199] L. J. Bour, M. Aramideh, and B. O. De Visser, "Neurophysiological Aspects of Eye and Eyelid Movements during Blinking in Humans," *Journal of Neurophysiology*, vol. 83, no. 1, pp. 166–176, 2000.

[200] D. von Cramon and U. Schuri, "Blink Frequency and Speech Motor Activity," *Neuropsychologia*, vol. 18, no. 4, pp. 603–606, 1980.

[201] P. J. De Jong and H. Merckelbach, "Eyeblink Frequency, Rehearsal Activity, and Sympathetic Arousal," *International Journal of Neuroscience*, vol. 51, no. 1-2, pp. 89–94, 1990.

[202] E. M. Jutkiewicz and J. Bergman, "Effects of Dopamine D1 Ligands on Eye Blinking in Monkeys: Efficacy, Antagonism, and D1/D2 Interactions," *Journal of Pharmacology and Experimental Therapeutics*, vol. 311, no. 3, pp. 1008–1015, 2004.

[203] L. S. Colzato, W. P. van den Wildenberg, N. C. van Wouwe, M. M. Pannebakker, and B. Hommel, "Dopamine and Inhibitory Action Control: Evidence from Spontaneous Eye Blink Rates," *Experimental Brain Research*, vol. 196, no. 3, pp. 467–474, 2009.

[204] L. F. Bacher, "Development and Manipulation of Spontaneous Eye Blinking in the First Year: Relationships to Context and Positive Affect," *Developmental Psychobiology*, vol. 56, no. 4, pp. 783–796, 2014.

[205] A. S. Powers, E. J. Schicatano, M. A. Basso, and C. Evinger, "To Blink or not to Blink: Inhibition and Facilitation of Reflex Blinks," *Experimental Brain Research*, vol. 113, no. 2, pp. 283–290, 1997.

[206] Á. Esteban, "A Neurophysiological Approach to Brainstem Reflexes. Blink Reflex," *Neurophysiologie Clinique/Clinical Neurophysiology*, vol. 29, no. 1, pp. 7–38, 1999.

[207] E. Du Bois-Reymond, "Untersuchungen uber Thierische Elektricitat," *Berlin: Verlag*, 1849.

[208] R. H. Steinberg, R. A. Linsenmeier, and E. R. Griff, "Retinal Pigment Epithelial Cell Contributions to the Electroretinogram and Electrooculogram," *Progress in Retinal Research*, vol. 4, pp. 33–66, 1985.

[209] O. Strauss, "The Retinal Pigment Epithelium in Visual Function," *Physiological Reviews*, vol. 85, no. 3, pp. 845–881, 2005.

[210] M. Brown, M. Marmor, E. Zrenner, M. Brigell, and M. Bach, "ISCEV Standard for Clinical Electro-oculography (EOG) 2006," *Documenta Ophthalmologica*, vol. 113, no. 3, pp. 205–212, 2006.

[211] A. W. North, "Accuracy and Precision of Electro-oculographic Recording," *Investigative Ophthalmology*, vol. 4, pp. 343–348, 1965.

[212] R. Barea, L. Boquete, M. Mazo, and E. López, "Wheelchair Guidance Strategies Using EOG," *Journal of Intelligent and Robotic Systems*, vol. 34, no. 3, pp. 279–299, 2002.

[213] C. G. Pinheiro, E. L. M. Naves, P. Pino, E. Losson, A. O. Andrade, and G. Bourhis, "Alternative Communication Systems for People with Severe Motor Disabilities: A Survey," *BioMedical Engineering Online*, vol. 10, no. 31, pp. 1–28, 2011.

[214] R. J. Croft and R. J. Barry, "EOG Correction of Blinks with Saccade Coefficients: A Test and Revision of the Aligned-artefact Average Solution," *Clinical Neurophysiology*, vol. 111, no. 3, pp. 444–451, 2000.

[215] J. M. Budd and Z. F. Kisvárday, "Local Lateral Connectivity of Inhibitory Clutch Cells in Layer 4 of Cat Visual Cortex (Area 17)," *Experimental Brain Research*, vol. 140, no. 2, pp. 245–250, 2001.

[216] A. Arieli, A. Sterkin, A. Grinvald, and A. Aertsen, "Dynamics of Ongoing Activity: Explanation of the Large Variability in Evoked Cortical Responses," *Science*, vol. 273, no. 5283, pp. 1868–1871, 1996.

[217] W. J. Freeman, "Origin, Structure, and Role of Background EEG Activity. Part 1. Analytic Amplitude," *Clinical Neurophysiology*, vol. 115, no. 9, pp. 2077–2088, 2004.

[218] J. Sarvas, "Basic Mathematical and Electromagnetic Concepts of the Biomagnetic Inverse Problem," *Physics in Medicine and Biology*, vol. 32, no. 1, pp. 11–22, 1987.

[219] D. Safieddine, A. Kachenoura, L. Albera, G. Birot, A. Karfoul, A. Pasnicu, A. Biraben, F. Wendling, L. Senhadji, and I. Merlet, "Removal of Muscle Artifact from EEG Data: Comparison between Stochastic (ICA and CCA) and Deterministic (EMD and Wavelet-based) Approaches," *EURASIP Journal on Advances in Signal Processing*, vol. 2012, no. 1, pp. 1–15, 2012.

[220] C. J. James and C. W. Hesse, "Independent Component Analysis for Biomedical Signals," *Physiological Measurement*, vol. 26, no. 1, R15–R39, 2005.

[221] R. Vigário and E. Oja, "BSS and ICA in Neuroinformatics: From Current Practices to Open Challenges," *IEEE Reviews in Biomedical Engineering*, vol. 1, pp. 50–61, 2008.

[222] S. Choi, A. Cichocki, H-M. Park, and S-Y. Lee, "Blind Source Separation and Independent Component Analysis: A Review," *Neural Information Processing Letters and Reviews*, vol. 6, no. 1, pp. 1–57, 2005.

[223] M. Scherg, "Fundamentals of Dipole Source Potential Analysis," *Auditory Evoked Magnetic Fields and Electric Potentials. Advances in Audiology*, vol. 6, pp. 40–69, 1990.

[224] G. Golub and W. Kahan, "Calculating the Singular Values and Pseudo-inverse of a Matrix," *Journal of the Society for Industrial and Applied Mathematics, Series B: Numerical Analysis*, vol. 2, no. 2, pp. 205–224, 1965.

[225] A. Ghodsi, "Dimensionality Reduction A Short Tutorial," *Department of Statistics and Actuarial Science, University of Waterloo, Ontario, Canada*, 2006.

[226] L. C. Shi, R. N. Duan, and B. L. Lu, "A Robust Principal Component Analysis Algorithm for EEG-based Vigilance Estimation," *35th Annual International Conference of the IEEE Engineering in Medicine and Biology Society*, pp. 6623–6626, 2013.

[227] S. Lipovetsky, "PCA and SVD with Nonnegative Loadings," *Pattern Recognition*, vol. 42, no. 1, pp. 68–76, 2009.

[228] M. E. Tipping and C. M. Bishop, "Mixtures of Probabilistic Principal Component Analyzers," *Neural Computation*, vol. 11, no. 2, pp. 443–482, 1999.

[229] N. D. Lawrence, "Gaussian Process Latent Variable Models for Visualisation of High Dimensional Data," *Advances in Neural Information Processing Systems*, vol. 16, no. 3, pp. 329–336, 2004.

[230] J. Dien, "Addressing Misallocation of Variance in Principal Components Analysis of Event-related Potentials," *Brain Topography*, vol. 11, no. 1, pp. 43–55, 1998.

[231] C. A. Joyce, I. F. Gorodnitsky, and M. Kutas, "Automatic Removal of Eye Movement and Blink Artifacts from EEG Data Using Blind Component Separation," *Psychophysiology*, vol. 41, no. 2, pp. 313–325, 2004.

[232] T. D. Lagerlund, F. W. Sharbrough, and N. E. Busacker, "Spatial Filtering of Multichannel Electroencephalographic Recordings through Principal Component Analysis by Singular Value Decomposition," *Journal of Clinical Neurophysiology*, vol. 14, no. 1, pp. 73–82, 1997.

[233] S. P. Fitzgibbon, D. M. Powers, K. J. Pope, and C. R. Clark, "Removal of EEG Noise and Artifact Using Blind Source Separation," *Journal of Clinical Neurophysiology*, vol. 24, no. 3, pp. 232–243, 2007.

[234] R. N. Vigário, "Extraction of Ocular Artefacts from EEG Using Independent Component Analysis," *Electroencephalography and Clinical Neurophysiology*, vol. 103, no. 3, pp. 395–404, 1997.

[235] A. Delorme, S. Makeig, and T. Sejnowski, "Automatic Artifact Rejection for EEG Data Using High-order Statistics and Independent Component Analysis," *In Proceedings of the Third International ICA Conference*, pp. 457–462, 2001.

[236] S. N. Jain and C. Rai, "Blind Source Separation and ICA Techniques: A Review," *International Journal of Engineering Science and Technology*, vol. 4, no. 4, pp. 1490–1503, 2012.

[237] J. A. Palmer, K. Kreutz-Delgado, and S. Makeig, "AMICA: An Adaptive Mixture of Independent Component Analyzers with Shared Components, *Swartz Center for Computatonal Neursoscience, University of California, San Diego*, 2012.

[238] A. Karfoul, L. Albera, and L. De Lathauwer, "Iterative Methods for the Canonical Decomposition of Multi-way Arrays: Application to Blind Underdetermined Mixture Identification," *Signal Processing*, vol. 91, no. 8, pp. 1789–1802, 2011.

[239] A. Hyvärinen and E. Oja, "A Fast Fixed-point Algorithm for Independent Component Analysis," *Neural Computation*, vol. 9, no. 7, pp. 1483–1492, 1997.

[240] A. Hyvärinen, J. Karhunen, and E. Oja, "Independent Component Analysis," *John Wiley and Sons*, vol. 46, 2004.

[241] A. Ferréol, L. Albera, and P. Chevalier, "Fourth-order Blind Identification of Underdetermined Mixtures of Sources (FOBIUM)," *IEEE Transactions on Signal Processing* vol. 53, no. 5, pp. 1640–1653, 2005.

[242] L. De Lathauwer, J. Castaing, and J. F. Cardoso, "Fourth-order Cumulant-based Blind Identification of Underdetermined Mixtures," *IEEE Transactions on Signal Processing*, vol. 55, no. 6, pp. 2965–2973, 2007.

[243] L. Albera, A. Ferrol, P. Chevalier, and P. Comon, "ICAR: A Tool for Blind Source Separation Using Fourth-order Statistics Only," *IEEE Transactions on Signal Processing*, vol. 53, no. 10, pp. 3633–3643, 2005.

[244] M. Girolami and C. Fyfe, "Generalised Independent Component Analysis through Unsupervised Learning with Emergent Bussgang Properties," *IEEE International Conference on Neural Networks*, vol. 3, pp. 1788–1791, 1997.

[245] J. F. Cardoso and A. Souloumiac, "Blind Beamforming for Non-Gaussian Signals," *IEE Proceedings F (Radar and Signal Processing)*, vol. 140, no. 6, pp. 362–370, 1993.

[246] D. N. Rutledge and D. J. R. Bouveresse, "Independent Components Analysis with the JADE Algorithm," *TrAC Trends in Analytical Chemistry*, vol. 50, pp. 22–32, 2013.

[247] J. Karvanen and V. Koivunen, "Blind Separation Methods Based on Pearson System and Its Extensions," *Signal Processing*, vol. 82, no. 4, pp. 663–673, 2002.

[248] A. Belouchrani, K. Abed-Meraim, J. F. Cardoso, and E. Moulines, "A Blind Source Separation Technique Using Second-order Statistics" *IEEE Transactions on Signal Processing*, vol. 45, no. 2, pp. 434–444, 1997.

[249] A. Ziehe and K. R. Müller, "TDSEP – An Efficient Algorithm for Blind Separation Using Time Structure," *International Conference on Artificial Neural Networks*, pp. 675–680, 1998.

[250] L. Albera, A. Kachenoura, P. Comon, A. Karfoul, F. Wendling, L. Senhadji, and I. Merlet, "ICA-based EEG Denoising: A Comparative Analysis of Fifteen Methods," *Bulletin of the Polish Academy of Sciences: Technical Sciences*, vol. 60, no. 3, pp. 407–418, 2012.

[251] J. A. Urigüen and B. Garcia-Zapirain, "EEG Artifact Removal – State-of-the-art and Guidelines," *Journal of Neural Engineering*, vol. 12, no. 3, 031001, 2015.

[252] A. Belouchrani, K. Abed-Meraim, J. F. Cardoso, and E. Moulines, "Second-order Blind Separation of Temporally Correlated Sources," *Proceeding of the International Conference on Digital Signal Processing*, pp. 346–351, 1993.

[253] S. I. Amari, "Natural Gradient Works Efficiently in Learning," *Neural Computation*, vol. 10, no. 2, pp. 251–276, 1998.

[254] T. W. Lee, M. Girolami, and T. J. Sejnowski, "Independent Component Analysis Using an Extended Infomax Algorithm for Mixed Subgaussian and Supergaussian Sources," *Neural Computation*, vol. 11, no. 2, pp. 417–441, 1999.

[255] F. Ghaderi, S. K. Kim, and E. A. Kirchner, "Effects of Eye Artifact Removal Methods on Single Trial P300 Detection, a Comparative Study," *Journal of Neuroscience Methods*, vol. 221, pp. 41–47, 2014.

[256] N. Ille, P. Berg, and M. Scherg, "Artifact Correction of the Ongoing EEG Using Spatial Filters Based on Artifact and Brain Signal Topographies," *Journal of Clinical Neurophysiology*, vol. 19, no. 2, pp. 113–124, 2002.

[257] A. R. Teixeira, A. M. Tome, E. W. Lang, P. Gruber, and A. M. Da Silva, "On the Use of Clustering and Local Singular Spectrum Analysis to Remove Ocular Artifacts from Electroencephalograms," *IEEE International Joint Conference on Neural Networks*, vol. 4, pp. 2514–2519, 2005.

[258] G. L. Wallstrom, R. E. Kass, A. Miller, J. F. Cohn, and N. A. Fox, "Automatic Correction of Ocular Artifacts in the EEG: A Comparison of Regression-based and Component-based Methods," *International Journal of Psychophysiology*, vol. 53, no. 2, pp. 105–119, 2004.

[259] L. Shoker, S. Sanei, and J. Chambers, "Artifact Removal from Electroencephalograms Using a Hybrid BSS–SVM Algorithm," *IEEE Signal Processing Letters*, vol. 12, no. 10, pp. 721–724, 2005.

[260] H. A. T. Nguyen, J. Musson, F. Li, W. Wang, G. Zhang, R. Xu, C. Richey, T. Schnell, F. D. Mckenzie, and J. Li, "EOG Artifact Removal Using a Wavelet Neural Network," *Neurocomputing*, vol. 97, pp. 374–389, 2012.

[261] V. Krishnaveni, S. Jayaraman, A. Gunasekaran, and K. Ramadoss, "Automatic Removal of Ocular Artifacts Using JADE Algorithm and Neural Network," *International Journal of Computer, Electrical, Automation, Control and Information Engineering*, vol. 2, no. 4, pp. 1330–1341, 2008.

[262] N. Nicolaou and S. J. Nasuto, "Automatic Artefact Removal from Event-related Potentials via Clustering," *The Journal of VLSI Signal Processing Systems for Signal, Image, and Video Technology*, vol. 48, no. 1, pp. 173–183, 2007.

[263] S. Halder, M. Bensch, J. Mellinger, M. Bogdan, A. Kübler, N. Birbaumer, and W. Rosenstiel, "Online Artifact Removal for Brain-computer Interfaces Using Support Vector Machines and Blind Source Separation," *Computational Intelligence and Neuroscience*, vol. 2007, 82069, 2007.

[264] G. Bartels, L. C. Shi, and B. L. Lu, "Automatic Artifact Removal from EEG - A Mixed Approach Based on Double Blind Source Separation and Support Vector Machine," *32nd Annual International Conference of the IEEE Engineering in Medicine and Biology Society*, pp. 5383–5386, 2010.

[265] A. Mognon, J. Jovicich, L. Bruzzone, and M. Buiatti, "ADJUST: An Automatic EEG Artifact Detector Based on the Joint Use of Spatial and Temporal Features," *Psychophysiology* vol. 48, no. 2, pp. 229–240, 2011.

[266] N. Mammone, F. L. Foresta, and F. C. Morabito, "Automatic Artifact Rejection from Multichannel Scalp EEG by Wavelet ICA," *IEEE Sensors Journal*, vol. 12, no. 3, pp. 533–542, 2012.

[267] A. Turnip and D. Esti Kusumandari, "Artifacts Removal of EEG Signals Using Adaptive Principal Component Analysis," *3rd International Conference on Computation for Science and Technology*, pp. 171–174, 2015.

[268] R. Mahajan and B. Morshed, "Unsupervised Eye Blink Artifact Denoising of EEG Data with Modified Multiscale Sample Entropy, Kurtosis, and Wavelet-ICA," *IEEE Journal of Biomedical and Health Informatics*, vol. 19, no. 1, pp. 158–165, 2015.

[269] O. G. Lins, T. W. Picton, P. Berg, and M. Scherg, "Ocular Artifacts in Recording EEGs and Event-related Potentials II: Source Dipoles and Source Components," *Brain Topography*, vol. 6, no. 1, pp. 65–78, 1993.

[270] V. Roy and S. Shukla, "Automatic Removal of Artifacts from EEG Signal based on Spatially Constrained ICA using Daubechies Wavelet," *International Journal of Modern Education and Computer Science*, vol. 6, no. 7, pp. 31–39, 2014.

[271] C. Zhang, L. Tong, Y. Zeng, J. Jiang, H. Bu, B. Yan, and J. Li, "Automatic Artifact Removal from Electroencephalogram Data Based on A Priori Artifact Information," *BioMed Research International*, 2015.

[272] Y. Kopsinis and S. McLaughlin, "Development of EMD-based Denoising Methods Inspired by Wavelet Thresholding," *IEEE Transactions on Signal Processing*, vol. 57, no. 4, pp. 1351–1362, 2009.

[273] G. L. Wallstrom, R. E. Kass, A. Miller, J. F. Cohn, and N. A. Fox, "Correction of Ocular Artifacts in the EEG Using Bayesian Adaptive Regression Splines," *Lecture Notes in Statistics– New York – Springer Verlag–*, pp. 351–366, 2002.

[274] T. T. H. Pham, R. J. Croft, and P. J. Cadusch, "Is Ocular Voltage Propagation to the Electroencephalogram Frequency Dependent?," *Psychophysiology*, vol. 46, no. 5, pp. 949–956, 2009.

[275] K. T. Sweeney, T. E. Ward, and S. F. McLoone, "Artifact Removal in Physiological Signals – Practices and Possibilities," *IEEE Transactions on Information Technology in Biomedicine*, vol. 16, no. 3, pp. 488–500, 2012.

[276] J. Gao, H. Sultan, J. Hu, and W. W. Tung, "Denoising Nonlinear Time Series by Adaptive Filtering and Wavelet Shrinkage: A Comparison," *IEEE Signal Processing Letters*, vol. 17, no. 3, pp. 237–240, 2010.

[277] P. L. Feintuch, "An Adaptive Recursive LMS Filter," *Proceedings of the IEEE*, vol. 64, no. 11, pp. 1622–1624, 1976.

[278] M. Rupp, "A Family of Adaptive Filter Algorithms with Decorrelating Properties," *IEEE Transactions on Signal Processing*, vol. 46, no. 3, pp. 771–775, 1998.

[279] J. Benesty and T. Gänsler, "New Insights into the RLS Algorithm," *EURASIP Journal on Applied Signal Processing*, vol. 2004, pp. 331–339, 2004.

[280] F. Abd Rahman, M. F. Othman, and N. A. Shaharuddin, "A Review on the Current State of Artifact Removal Methods for Electroencephalogram Signals," *The 10th Asian Control Conference 2015*, pp. 1–6, 2015.

[281] K. Mayyas, "Performance Analysis of the Deficient Length LMS Adaptive Algorithm," *IEEE Transactions on Signal Processing*, vol. 53, no. 8, pp. 2727–2734, 2005.

[282] P. He, M. Kahle, G. Wilson, and C. Russell, "Removal of Ocular Artifacts from EEG: A Comparison of Adaptive Filtering Method and Regression Method Using Simulated Data," *27th Annual International Conference of the IEEE Engineering in Medicine and Biology Society*, pp. 1110–1113, 2006.

[283] J. P. Lindsen and J. Bhattacharya, "Correction of Blink Artifacts Using Independent Component Analysis and Empirical Mode Decomposition," *Psychophysiology*, vol. 47, no. 5, pp. 955–960, 2010.

[284] S. Khatun, R. Mahajan, and B. I. Morshed, "Comparative Analysis of Wavelet Based Approaches for Reliable Removal of Ocular Artifacts from Single Channel EEG," *IEEE International Conference on Electro/Information Technology*, pp. 335-340, 2015.

[285] J. Lin and A. Zhang, "Fault Feature Separation Using Wavelet-ICA Filter," *NDT and E International*, vol. 38, no. 6, pp. 421–427, 2005.

[286] B. Azzerboni, M. Carpentieri, F. La Foresta, and F. C. Morabito, "Neural-ICA and Wavelet Transform for Artifacts Removal in Surface EMG," *IEEE International Joint Conference on Neural Networks*, vol. 4, pp. 3223–3228, 2004.

[287] N. E. Huang, Z. Shen, S. R. Long, M. C. Wu, H. H. Shih, Q. Zheng, N. C. Yen, C. C. Tung, and H. H. Liu, "The Empirical Mode Decomposition and the Hilbert Spectrum for Nonlinear and Non-stationary Time Series Analysis," *Proceedings of the Royal Society of London A: Mathematical, Physical and Engineering Sciences*, vol. 454, no. 1971, pp. 903–995, 1998.

[288] P. Flandrin and P. Goncalves, "Empirical Mode Decompositions as Data-driven Wavelet-like Expansions," *International Journal of Wavelets, Multiresolution and Information Processing*, vol.2, no. 4, pp. 477–496, 2004.

[289] M. Feldman, "Analytical Basics of the EMD: Two Harmonics Decomposition," *Mechanical Systems and Signal Processing*, vol. 23, no. 7, pp. 2059–2071, 2009.

[290] S. D. Wu, J. C. Chiou, and E. Goldman, "Solution for Mode Mixing Phenomenon of the Empirical Mode Decomposition," *IEEE 3rd International Conference on Advanced Computer Theory and Engineering*, vol. 2, pp. 500–504, 2010.

[291] Z. Wu and N. E. Huang, "Ensemble Empirical Mode Decomposition: A Noise-assisted Data Analysis Method," *Advances in Adaptive Data Analysis*, vol. 1, no. 1, pp. 1-41, 2009.

[292] M. E. Torres, M. A. Colominas, G. Schlotthauer, and P. Flandrin, "A Complete Ensemble Empirical Mode Decomposition with Adaptive Noise," *IEEE International Conference on Acoustics, Speech and Signal Processing*, pp. 4144-4147, 2011.

[293] S. Kanoga and Y. Mitsukura, "Eye Blink Artifact Rejection in Single-channel Electroencephalographic Signals by Complete Ensemble Empirical Mode Decomposition and Independent Component Analysis," *37th Annual International Conference of the IEEE Engineering in Medicine and Biology Society*, pp. 121–124, 2015.

[294] H. Nolan, R. Whelan, and R. B. Reilly, "FASTER: Fully Automated Statistical Thresholding for EEG Artifact Rejection," *Journal of Neuroscience Methods*, vol. 192, no. 1, pp. 152–162, 2010.

[295] I. Daly, F. Pichiorri, J. Faller, V. Kaiser, A. Kreilinger, R. Scherer, and G. Müller-Putz, "What Does Clean EEG Look Like?," *34th Annual International Conference of the IEEE Engineering in Medicine and Biology Society*, pp. 3963–3966, 2012.

[296] D. D. Lee and H. S. Seung, "Learning the Parts of Objects by Non-negative Matrix Factorization," *Nature*, vol. 401, pp. 788–791, 1999.

[297] D. D. Lee and H. S. Seung, "Algorithms for Non-negative Matrix Factorization," *In Advances in Neural Information Processing System*, vol. 13, pp. 556–562, 2001.

[298] M. W. Berry, M. Browne, A. N. Langville, V. P. Pauca, and R. J. Plemmons, "Algorithms and Applications for Approximate Nonnegative Matrix Factorization," *Computational Statistics and Data Analysis*, vol. 52, no. 1, pp. 155–173, 2007.

[299] P. Smaragdis and J. C. Brown, "Non-negative Matrix Factorization for Polyphonic Music Transcription," *IEEE Workshop on Applications of Signal Processing to Audio and Acoustics*, pp. 177–180, 2003.

[300] P. Smaragdis, B. Raj, and M. V. Shashanka, "Supervised and Semi-supervised Separation of Sounds from Single-channel Mixtures," *Independent Component Analysis and Signal Separation*, vol. 4666, pp. 414–421, 2007.

[301] P. Smaragdis and B. Raj, "Example-driven Bandwidth Expansion," *IEEE Workshop on Applications of Signal Processing to Audio and Acoustics*, pp. 135–138, 2007.

[302] H. Lee and S. Choi, "Group Nonnegative Matrix Factorization for EEG Classification," *In Proceeding of the International Conference on Artificial Intelligence and Statics*, vol. 5, pp. 320–327, 2009.

[303] C. Févotte, N. Bertin, and J. L. Durrieu, "Nonnegative Matrix Factorization with the Itakura-Saito Divergence: With Application to Music Analysis," *Neural Computation*, vol. 21, no. 3, pp. 793–830, 2009.

[304] C. Damon, A. Liutkus, A. Gramfort, and S. Essid, "Non-negative Matrix Factorization for Single-channel EEG Artifact Rejection," *IEEE International Conference on Acoustics, Speech and Signal Processing*, pp. 1177–1181, 2013.

[305] C. A. Majmudar, R. Mahajan, and B. I. Morshed, "Real-time Hybrid Ocular Artifact Detection and Removal for Single Channel EEG," *IEEE International Conference on Electro/Information Technology*, pp. 330–334, 2015.

[306] W. D. Chang, H. S. Cha, K. Kim, and C. H. Im, "Detection of Eye Blink Artifacts from Single Prefrontal Channel Electroencephalogram," *Computer Methods and Programs in Biomedicine*, vol. 124, pp. 19–30, 2015.

[307] P. O. Hoyer, "Non-negative Matrix Factorization with Sparseness Constraints," *The Journal of Machine Learning Research*, vol. 5, pp. 1457–1469, 2004.

[308] I. S. Dhillon and S. Sra, "Generalized Nonnegative Matrix Approximations with Bregman Divergences," *In Advances in Neural Information Processing Systems*, pp. 283–290, 2005.

[309] T. Virtanen and A. Klapuri, "Analysis of Polyphonic Audio Using Source-filter Model and Non-negative Matrix Factorization," *In Advances in Models for Acoustic Processing, Neural Information Processing Systems Workshop*, 2006.

[310] R. Kompass, "A Generalized Divergence Measure for Nonnegative Matrix Factorization," *Neural Computation*, vol. 19, no. 3, pp. 780–791, 2007.

[311] A. T. Cemgil, "Bayesian Inference for Nonnegative Matrix Factorisation Models," *Computational Intelligence and Neuroscience*, 785152, 2009.

[312] M. Nakano, H. Kameoka, J. Le Roux, Y. Kitano, N. Ono, and S. Sagayama, "Convergence-guaranteed Multiplicative Algorithms for Nonnegative Matrix Factorization with Beta-divergence," *Proceedings of IEEE International Workshop on Machine Learning for Signal Processing*, pp. 283–288, 2010.

[313] M. D. Hoffman, D. M. Blei, and P. R. Cook, "Bayesian nonparametric Matrix Factorization for Recorded Music, *Proceedings of the 27th International Conference on Machine Learning*, pp. 439–446, 2010.

[314] A. Liutkus and R. Badeau, "Generalized Wiener Filtering with Fractional Power Spectrograms", *IEEE International Conference on Acoustics, Speech and Signal Processing*, pp. 266–270, 2015.

[315] A. Liutkus, D. Fitzgerald, and R. Badeau. "Cauchy Nonnegative Matrix Factorization," *IEEE Workshop on Applications of Signal Processing to Audio and Acoustics*, 2015.

[316] H. Kameoka, N. Ono, K. Kashino, and S. Sagayama, "Complex NMF: A New Sparse Representation for Acoustic Signals," *IEEE International Conference on Acoustics, Speech and Signal Processing*, pp. 3437–3440, 2009.

[317] K. Yoshii, R. Tomioka, D. Mochihashi, and M. Goto, "Beyond NMF: Time-domain Audio Source Separation without Phase Reconstruction," *14th International Society for Music Information Retrieval Conference*, pp. 369–374, 2013.

[318] K. Yoshii, R. Tomioka, D. Mochihashi, and M. Goto, "Infinite Positive Semidefinite Tensor Factorization for Source Separation of Mixture Signals," *Proceedings of the 30th International Conference on Machine Learning*, vol. 28, pp. 576–584, 2013.

[319] N. P. Castellanos and V. A. Makarov, "Recovering EEG Brain Signals: Artifact Suppression with Wavelet Enhanced Independent Component Analysis," *Journal of Neuroscience Methods*, vol. 158, no. 2, pp. 300–312, 2006.

[320] K. J. Friston, A. P. Holmes, and K. J. Worsley, "How Many Subjects Constitute a Study?," *Neuroimage*, vol. 10, no. 1, pp. 1–5, 1999.

[321] B. Giraudeau and J. Y. Mary, "Planning a Reproducibility Study: How Many Subjects and How Many Replicates per Subject for an Expected Width of the 95 per cent Confidence Interval of the Intraclass Correlation Coefficient," *Statistics in Medicine*, vol. 20, no. 21, pp. 3205–3214, 2001.

[322] D. H. Brainard, "The Psychophysics Toolbox," *Spatial Vision*, vol. 10, pp. 433–436, 1997.

[323] D. G. Pelli, "The VideoToolbox Software for Visual Psychophysics: Transforming Numbers into Movies," *Spatial Vision*, vol. 10, no. 4, pp. 437–442, 1997.

[324] M. Kleiner, D. Brainard, D. Pelli, A. Ingling, R. Murray, and C. Broussard, "What's New in Psychtoolbox-3," *Perception*, vol.36, no.14, 2007.

[325] P. Berg and M. B. Davies, "Eyeblink-related Potentials," *Electroencephalography and Clinical Neurophysiology*, vol. 69, no. 1, pp. 1–5, 1988.

[326] A. Yagi, "Visual Signal Detection and Lambda Responses," *Electroencephalography and Clinical Neurophysiology*, vol. 52, no. 6, pp. 604–610, 1981.

[327] D. I. McCloskey, "Corollary Discharges: Motor Commands and Perception," *In Books VB (ed) Handbook of Physiology: The Nervous System*, vol. 2, pp. 1415–1447, 1981.

[328] D. E. Lake, J. S. Richman, M. P. Griffin, and J. R. Moorman, "Sample Entropy Analysis of Neonatal Heart Rate Variability," *American Journal of Physiology-Regulatory, Integrative and Comparative Physiology*, vol. 283, no. 3, R789–R797, 2002.

[329] J. S. Richman and J. R. Moorman, "Physiological Time-series Analysis Using Approximate Entropy and Sample Entropy," *American Journal of Physiology-Heart and Circulatory Physiology*, vol. 278, no. 6, H2039–H2049, 2000.

[330] H. B. Xie, W. X. He, and H. Liu, "Measuring Time Series Regularity Using Nonlinear Similarity-based Sample Entropy," *Physics Letters A*, vol. 372, no. 48, pp. 7140–7146, 2008.

[331] A. Delorme, T. Sejnowski, and S. Makeig, "Enhanced Detection of Artifacts in EEG Data Using Higher-order Statistics and Independent Component Analysis," *Neuroimage*, vol. 34, no. 4, pp. 1443–1449, 2007.

[332] O. G. Lins, T. W. Picton, P. Berg, and M. Scherg, "Ocular Artifacts in Recording EEGs and Event-related Potentials II: Source Dipoles and Source Components," *Brain Topography*, vol. 6, no. 1, pp. 65–78, 1993.

[333] P. D. Welch, "The Use of Fast Fourier Transform for the Estimation of Power Spectra: A Method Based on Time Averaging Over Short Modied Periodograms," *IEEE Transactions on Audio and Electroacoustics*, vol. 15, no. 2, pp. 70–73, 1967.

[334] D. A. Overton and C. Shagass, "Distribution of Eye Movement and Eyeblink Potentials Over the Scalp," *Electroencephalography and Clinical Neurophysiology*, vol. 27, no. 5, pp. 546 (abstr.), 1969.

[335] J. C. Corby and B. S. Kopell, "Differential Contributions of Blinks and Vertical Eye Movements as Artifacts in EEG Recording," *Psychophysiology*, vol. 9, no. 6, pp. 640–644, 1972.

[336] D. G. Girton and J. Kamiya, "A Simple On-line Technique for Removing Eye Movement Artifacts from the EEG," *Electroencephalography and Clinical Neurophysiology*, vol. 34, no. 2, pp. 212–216, 1973.

[337] J. Möcks and T. Gasser, "How to Select Epochs of the EEG at Rest for Quantitative Analysis," *Electroencephalography and Clinical Neurophysiology*, vol. 58, no. 1, pp. 89–92, 1984.

[338] P. L. Nunez and R. Srinivasan, "Electric Fields of the Brain: The Neurophysics of EEG," *Oxford University Press, New York*, 2006.

[339] M. M. C. Van den Berg-Lenssen, C. H. M. Brunia, and J. A. Blom, "Correction of Ocular Artifacts in EEGs Using an Autoregressive Model to Describe the EEG; A Pilot Study," *Electroencephalography and Clinical Neurophysiology*, vol. 73, no. 1, pp. 72–83, 1989.

[340] B. N. Cuffin and D. Cohen, "Comparison of the Magnetoencephalogram and Electroencephalogram," *Electroencephalography and Clinical Neurophysiology*, vol. 47, no. 2, pp. 132–146, 1979.

[341] G. R. Müller-Putz, R. Scherer, C. Brauneis, and G. Pfurtscheller, "Steady-state Visual Evoked Potential (SSVEP)-based Communication: Impact of Harmonic Frequency Components," *Journal of Neural Engineering*, vol. 2, no. 4, pp. 123–130, 2005.

[342] D. Zhu, J. Bieger, G. G. Molina, and R. M. Aarts, "A Survey of Stimulation Methods Used in SSVEP-based BCIs," *Computational Intelligence and Neuroscience*, vol. 2010, no. 1, 2010.

[343] J. Ma, S. Bayram, P. Tao, and V. Svetnik,"High-throughput Ocular Artifact Reduction in Multichannel Electroencephalography (EEG) Using Component Subspace Projection," *Journal of Neuroscience Methods*, vol. 196, no. 1, pp. 131–140, 2011.

[344] Q. Zhao, B. Hu, Y. Shi, Y. Li, P. Moore, M. Sun, and H. Peng, "Automatic Identification and Removal of Ocular Artifacts in EEG – Improved Adaptive Predictor Filtering for Portable Applications," *IEEE Transactions on NanoBioscience*, vol. 13, no. 2, pp. 109–117, 2014.

[345] B. S. Nashold Jr, W. P. Wilson, and D. G. Slaughter, "Sensations Evoked by Stimulation in the Midbrain of Man," *Journal of Neurosurgery*, vol. 30, no. 1, pp. 14–24, 1969.

[346] J. M. Van Buren, "Confusion and Disturbance of Speech from Stimulation in Vicinity of the Head of the Caudate Nucleus," *Journal of Neurosurgery*, vol. 20, no. 2, pp. 148–157,1963.

[347] B. S. Nashold Jr and J. P. Gills, "Ocular Signs from Brain Stimulation and Lesions," *Archives of Ophthalmology*, vol. 77, no. 5, pp. 609–618, 1967.

[348] E. T. Detorakis, R. E. Engstrom, B. R. Straatsma, and J. L. Demer, "Functional Anatomy of the Anophthalmic Socket: Insights from Magnetic Resonance Imaging," *Investigative Ophthalmology and Visual Science*, vol. 44, no. 10, pp. 4307–4313, 2003.

[349] E. Tolosa and M. J. Marti, "Blepharospasm-oromandibular Dystonia Syndrome (Meige's Syndrome): Clinical Aspects," *Advances in Neurology*, vol. 49, pp. 73–84, 1987.

[350] F. Grandas, J. Elston, N. Quinn, and C. D. Marsden, "Blepharospasm: A Review of 264 Patients," *Journal of Neurology, Neurosurgery and Psychiatry*, vol. 51, no. 6, pp. 767–772, 1988.

[351] B. Eppinger, J. Kray, B. Mock, and A. Mecklinger, "Better or Worse than Expected? Aging, Learning, and the ERN," *Neuropsychologia*, vol. 46, no. 2, pp. 521–539, 2008.

[352] P. Seeman, N. H. Bzowej, H. C. Guan, C. Bergeron, L. E. Becker, G. P. Reynolds, E.D. Bird, P. Riederer, K. Lellinger, S. Watanabe, and W. W. Tourtellotte, "Human Brain Dopamine Receptors in Children and Aging Adults," *Synapse*, vol. 1, no. 5, pp. 399–404, 1987.

[353] J. O. Rinne, P. Lönnberg, and P. Marjamäki, "Age-dependent Decline in Human Brain Dopamine D1 and D2 Receptors," *Brain Research*, vol. 508, no. 2, pp. 349–352, 1990.

[354] P. Allard and J. O. Marcusson, "Age-correlated Loss of Dopamine Uptake Sites Labeled with [3 H] GBR-12935 in Human Putamen," *Neurobiology of Aging*, vol. 10, no. 6, pp. 661–664, 1989.

[355] S. Y. Ma, B. J. Ciliax, G. Stebbins, S. Jaffar, J. N. Joyce, E. J. Cochran, J. H. Kordower, D. C. Mash, A. I. Levey, and E. J. Mufson, "Dopamine Transporter-immunoreactive Neurons Decrease with Age in the Human Substantia Nigra," *Journal of Comparative Neurology*, vol. 409, no. 1, pp. 25–37, 1999.

[356] L. Bäckman, L. Nyberg, U. Lindenberger, S. C. Li, and L. Farde, "The Correlative Triad among Aging, Dopamine, and Cognition: Current Status and Future Prospects," *Neuroscience and Biobehavioral Reviews*, vol. 30, no. 6, pp. 791–807, 2006.

[357] Y. Yasui, "A Brainwave Signal Measurement and Data Processing Technique for Daily Life Applications," *Journal of Physiological Anthropology*, vol. 28, no. 3, pp. 145–150, 2009.

[358] B. Kulis, M. A. Sustik, and I. S. Dhillon, "Low-rank Kernel Learning with Bregman Matrix Divergences," *The Journal of Machine Learning Research*, vol. 10, pp. 341–376, 2009.

[359] L. M. Bregman, "The Relaxation Method of Finding the Common Point of Convex Sets and Its Application to the Solution of Problems in Convex Programming," *USSR Computational Mathematics and Mathematical Physics*, vol. 7, no. 3, pp. 200–217, 1967.

[360] S. Kanoga and Y. Mitsukura, "ICA-based Positive Semidefinite Matrix Templates for Eye-blink Artifact Removal from EEG Signal with Single-electrode," *The 10th Asian Control Conference 2015*, pp. 1535–1540, 2015.

[361] E. Marg, "Development of Electro-oculography: Standing Potential of the Eye in Registration of Eye Movement," *AMA Archives of Ophthalmology*, vol.45, no.2, pp.169-185, 1951.

[362] L. Xiong, X. Chen, T. K. Huang, J. G. Schneider, and J. G. Carbonell, "Temporal Collaborative Filtering with Bayesian Probabilistic Tensor Factorization," *Proceedings of the 2010 SIAM International Conference on Data Mining*, vol. 10, pp. 211–222, 2010.

[363] P. Rai, Y. Wang, S. Guo, G. Chen, D. Dunson, and L. Carin, "Scalable Bayesian Low-rank Decomposition of Incomplete Multiway Tensors," *In Proceedings of the 31st International Conference on Machine Learning*, pp. 1800–1808, 2014.

[364] A. Liutkus, R. Badeau, and G. Richard, "Gaussian Processes for Underdetermined Source Separation," *IEEE Transactions on Signal Processing*, vol. 59, no. 7, pp. 3155–3167, 2011.

[365] N. Guan, D. Tao, Z. Luo, and B. Yuan, "NeNMF: An Optimal Gradient Method for Nonnegative Matrix Factorization," *IEEE Transactions on Signal Processing*, vol. 60, no. 6, pp. 2882–2898, 2012.

[366] E. Richard, P. A. Savalle, and N. Vayatis, "Estimation of Simultaneously Sparse and Low Rank Matrices," *In Proceedings of the 29th International Conference on Machine Learning*, 2012.

[367] P. Sprechmann, A. M. Bronstein, and G. Sapiro, "Learning Efficient Sparse and Low Rank Models," *IEEE Transactions on Pattern Analysis and Machine Intelligence*, vol. 37, no. 9, pp. 1821–1833, 2015.

[368] G. Wang, A. V. Kossenkov, and M. F. Ochs, "LS-NMF: A Modified Non-negative Matrix Factorization Algorithm Utilizing Uncertainty Estimates," *BMC Bioinformatics*, vol. 7, no. 1, 2006.

[369] Z. Zhang and K. Zhao, "Low-rank Matrix Approximation with Manifold Regularization," *IEEE Transactions on Pattern Analysis and Machine Intelligence*, vol. 35, no. 7, pp. 1717–1729, 2013.

[370] Y. D. Kim and S. Choi, "Nonnegative Tucker Decomposition," *IEEE Conference on Computer Vision and Pattern Recognition*, pp. 1–8, 2007.

[371] A. Cichocki, R. Zdunek, and S. I. Amari, "Nonnegative Matrix and Tensor Factorization [Lecture Notes]," *IEEE Signal Processing Magazine*, vol. 25, no. 1, pp. 142–145, 2008.

[372] C. Boutsidis and E. Gallopoulos, "SVD Based Initialization: A Head Start for Nonnegative Matrix Factorization," *Pattern Recognition*, vol. 41, no. 4, pp. 1350–1362, 2008.

[373] L. Zhao, G. Zhuang, and X. Xu, "Facial Expression Recognition Based on PCA and NMF," *IEEE 7th World Congress on Intelligent Control and Automation*, pp. 6826–6829, 2008.

[374] A. K. Jain, "Data Clustering: 50 Years beyond K-means," *Pattern Recognition Letters*, vol. 31, no. 8, pp. 651–666, 2010.

[375] M. Belkin and P. Niyogi, "Laplacian Eigenmaps for Dimensionality Reduction and Data Representation," *Neural Computation*, vol. 15, no. 6, pp. 1373–1396, 2003.

[376] S. D. Kamvar, D. Klein, and C. D. Manning, "Interpreting and Extending Classical Agglomerative Clustering Algorithms Using a Model-based Approach," *In Proceedings of the 19th International Conference on Machine Learning*, 2002.

[377] W. Caudill and H. Weinstein, "Maternal Care and Infant Behavior in Japan and America," *Psychiatry*, vol. 32, no. 1, pp. 12–43, 1969.

[378] V. F. Panaccione and R. G. Wahler, "Child Behavior, Maternal Depression, and Social Coercion as Factors in the Quality of Child Care," *Journal of Abnormal Child Psychology*, vol. 14, no. 2, pp. 263–278, 1986.

[379] K. Paul, J. Dittrichová, and H. Papoušek, "Infant Feeding Behavior: Development in Patterns and Motivation," *Developmental Psychobiology*, vol. 29, no. 7, pp. 563–576, 1996.

[380] N. A. Fox, H. A. Henderson, K. H. Rubin, S. D. Calkins, and L. A. Schmidt, "Continuity and Discontinuity of Behavioral Inhibition and Exuberance: Psychophysiological and Behavioral Influences Across the First Four Years of Life," *Child Development*, vol. 72, no. 1, pp. 1–21, 2001.

[381] T. A. Dennis, M. Hong, and B. Solomon, "Do the Associations between Exuberance and Emotion Regulation Depend on Effortful Control?," *International Journal of Behavioral Development*, vol. 34, no. 5, pp. 462–472, 2010.

[382] H. H. Goldsmith, "Studying Temperament via Construction of the Toddler Behavior Assessment Questionnaire," *Child Development*, vol. 67, no. 1, pp. 218–235, 1996.

[383] M. B. Pontifex, B. J. Saliba, L. B. Raine, D. L. Picchietti, and C. H. Hillman, "Exercise Improves Behavioral, Neurocognitive, and Scholastic Performance in Children with Attention-deficit/hyperactivity Disorder," *The Journal of Pediatrics*, vol. 162, no. 3, pp. 543–551, 2013.

[384] L. J. Weitzman, D. Eifler, E. Hokada, and C. Ross, "Sex-role Socialization in Picture Books for Preschool Children," *American Journal of Sociology*, pp. 1125–1150, 1972.

[385] A. Wigfield and J. T. Guthrie, "Engagement and Motivation in Reading," *Handbook of Reading Research*, vol. 3, pp. 403–422, 2000.

[386] J. A. Coan and J. J. Allen, "Frontal EEG Asymmetry as a Moderator and Mediator of Emotion," *Biological Psychology*, vol. 67, no. 1, pp. 7–50, 2004.

[387] R. N. Goodman, J. C. Rietschel, L. C. Lo, M. E. Costanzo, and B. D. Hatfield, "Stress, Emotion Regulation and Cognitive Performance: The Predictive Contributions of Trait and State Relative Frontal EEG Alpha Asymmetry," *International Journal of Psychophysiology*, vol. 87, no. 2, pp. 115–123, 2013.

[388] S. Wikström, I. H. Pupp, I. Rosén, E. Norman, V. Fellman, D. Ley, and L. Hellström-Westas, "Early Single-channel aEEG/EEG Predicts Outcome in Very Preterm Infants," *Acta Paediatrica*, vol. 101, no. 7, pp. 719–726, 2012.

[389] P. J. Marshall, Y. Bar-Haim, and N. A. Fox, "Development of the EEG from 5 Months to 4 Years of Age," *Clinical Neurophysiology*, vol. 113, no. 8, pp. 1199–1208, 2002.

[390] J. Claassen, S. A. Mayer, R. G. Kowalski, R. G. Emerson, and L. J. Hirsch, "Detection of Electrographic Seizures with Continuous EEG Monitoring in Critically Ill Patients," *Neurology*, vol. 62, no. 10, pp. 1743–1748, 2004.

[391] F. Moeller, H. R. Siebner, S. Wolff, H. Muhle, O. Granert, O. Jansen, U. Stephani, and M. Siniatchkin, "Simultaneous EEG-fMRI in Drug-naive Children with Newly Diagnosed Absence Epilepsy," *Epilepsia*, vol. 49, no. 9, pp. 1510–1519, 2008.

[392] A. R. Clarke, R. J. Barry, R. McCarthy, and M. Selikowitz, "EEG-defined Subtypes of Children with Attention-deficit/hyperactivity Disorder," *Clinical Neurophysiology*, vol. 112, no. 11, pp. 2098–2105, 2001.

[393] J. F. Lubar, "Discourse on the Development of EEG Diagnostics and Biofeedback for Attention-deficit/hyperactivity Disorders," *Biofeedback and Self-regulation*, vol. 16, no.3, pp.201–225, 1991.

[394] A. R. Clarke, R. J. Barry, R. McCarthy, and M. Selikowitz, "EEG Analysis in Attention-deficit/hyperactivity Disorder: A Comparative Study of Two Subtypes," *Psychiatry Research*, vol. 81, no. 1, pp. 19–29, 1998.

[395] S. N. Light, J. A. Coan, C. Zahn-Waxler, C. Frye, H. H. Goldsmith, and R. J. Davidson, "Empathy Is Associated with Dynamic Change in Prefrontal Brain Electrical Activity during Positive Emotion in Children," *Child Development*, vol. 80, no. 4, pp. 1210–1231, 2009.

[396] M. D. Lewis, I. Granic, and C. Lamm, "Behavioral Differences in Aggressive Children Linked with Neural Mechanisms of Emotion Regulation," *Annals of the New York Academy of Sciences*, vol. 1094, no. 1, pp. 164–177, 2006.

[397] E. Rognoni, D. Galati, T. Costa, and M. Crini, "Relationship between Adult Attachment Patterns, Emotional Experience and EEG Frontal Asymmetry," *Personality and Individual Differences*, vol. 44, no. 4, pp. 909–920, 2008.

[398] E. O. Brigham, "The Fast Fourier Transform and Its Applications," *Erlbaum, Englewood Cliffs, NJ*, 1988.

[399] A. Subasi, "EEG Signal Classification Using Wavelet Feature Extraction and a Mixture of Expert Model," *Expert Systems with Applications*, vol. 32, no. 4, pp. 1084–1093, 2007.

[400] S. J. Schiff, A. Aldroubi, M. Unser, and S. Sato, "Fast Wavelet Transformation of EEG," *Electroencephalography and Clinical Neurophysiology*, vol. 91, no. 6, pp. 442–455, 1994.

[401] I. Daubechies, "Orthonormal Bases of Compactly Supported Wavelets," *Communications on Pure and Applied Mathematics*, vol. 41, no. 7, pp. 909–996, 1988.

[402] W. Y. Hsu, "Assembling A Multi-feature EEG Classifier for Left-right Motor Imagery Data Using Wavelet-based Fuzzy Approximate Entropy for Improved Accuracy," *International Journal of Neural Systems*, vol. 25, no. 8, 1550037, 2015.

[403] D. W. Hosmer and S. Lemeshow, "Applied Logistic Regression," *Wiley, New York*, 1989.

[404] R. Tibshirani, "Regression Shrinkage and Selection via the Lasso," *Journal of the Royal Statistical Society. Series B (Methodological)*, vol. 58, pp. 267–288, 1996.

[405] B. Krishnapuram, L. Carin, M. A. Figueiredo, and A. J. Hartemink, "Sparse Multinomial Logistic Regression: Fast Algorithms and Generalization Bounds," *IEEE Transactions on Pattern Analysis and Machine Intelligence*, vol. 27, no. 6, pp. 957–968, 2005.

[406] S. K. Shevade and S. S. Keerthi, "A Simple and Efficient Algorithm for Gene Selection Using Sparse Logistic Regression," *Bioinformatics*, vol. 19, no. 17, pp. 2246–2253, 2003.

[407] H. Zou and T. Hastie, "Regularization and Variable Selection via the Elastic Net," *Journal of the Royal Statistical Society: Series B (Statistical Methodology)*, vol. 67, no. 2, pp. 301–320, 2005.

[408] J. Friedman, T. Hastie, and R. Tibshirani, "Regularization Paths for Generalized Linear Models via Coordinate Descent," *Journal of Statistical Software*, vol. 33, no. 1, pp. 1-22, 2010.

[409] J. A. Hanley and B. J. McNeil, "The Meaning and Use of the Area under a Receiver Operating Characteristic (ROC) Curve," *Radiology*, vol. 143, no. 1, pp. 29–36, 1982.

[410] A. Cichocki, H. Lee, Y. D. Kim, and S. Choi, "Non-negative Matrix Factorization with α-divergence," *Pattern Recognition Letters*, vol. 29, no. 9, pp. 1433–1440, 2008.

[411] N. Lu, T. Li, J. Pan, X. Ren, Z. Feng, and H. Miao, "Structure Constrained Semi-nonnegative Matrix Factorization for EEG-based Motor Imagery Classification," *Computers in Biology and Medicine*, vol. 60, pp. 32–39, 2015.

[412] S. Sun and J. Zhou, "A Review of Adaptive Feature Extraction and Classification Methods for EEG-based Brain-computer Interfaces," *2014 International Joint Conference on Neural Networks*, pp. 1746–1753, 2014.

[413] N. Lu and T. Yin, "Motor Imagery Classification via Combinatory Decomposition of ERP and ERSP Using Sparse Nonnegative Matrix Factorization," *Journal of Neuroscience Methods*, vol. 249, pp. 41–49, 2015.

[414] H. Tsubakida, T. Shiratori, A. Ishiyama, and Y. Ono, "Nonnegative Matrix Factorization Common Spatial Pattern in Brain Machine Interface," *2015 3rd International Winter Conference on Brain-Computer Interface*, pp. 1–4, 2015.

[415] M. A. Morgan, L. M. Romanski, and J. E. LeDoux, "Extinction of Emotional Learning: Contribution of Medial Prefrontal Cortex," *Neuroscience Letters*, vol. 163, no. 1, pp. 109–113, 1993.

[416] M. R. Milad and G. J. Quirk, "Neurons in Medial Prefrontal Cortex Signal Memory for Fear Extinction," *Nature*, vol. 420, no. 6911, pp. 70–74, 2002.

[417] A. J. McDonald, F. Mascagni, and L. Guo, "Projections of the Medial and Lateral Prefrontal Cortices to the Amygdala: A Phaseolus Vulgaris Leucoagglutinin Study in the Rat," *Neuroscience*, vol. 71, no. 1, pp. 55–75, 1996.

[418] K. M. Hurley, H. Herbert, M. M. Moga, and C. B. Saper, "Efferent Projections of the Infralimbic Cortex of the Rat," *Journal of Comparative Neurology*, vol. 308, no. 2, pp. 249–276, 1991.

[419] G. D. Fisk and J. M. Wyss, "Descending Projections of Infralimbic Cortex that Mediate Stimulation-evoked Changes in Arterial Pressure," *Brain Research*, vol. 859, no. 1, pp. 83–95, 2000.

[420] N. S. Floyd, J. L. Price, A. T. Ferry, K. A. Keay, and R. Bandler, "Orbitomedial Prefrontal Cortical Projections to Distinct Longitudinal Columns of the Periaqueductal Gray in the Rat," *Journal of Comparative Neurology*, vol. 422, no. 4, pp. 556–578, 2000.

[421] J. C. Gewirtz, W. A. Falls, and M. Davis, "Normal Conditioning Inhibition and Extinction of Freezing and Fear-potentiated Startle Following Electrolytic Lesions of Medial Prefrontal Cortex in Rats," *Behavioral Neuroscience*, vol. 111, no. 4, pp. 712–726, 1997.

[422] G. J. Quirk, E. Likhtik, J. G. Pelletier, and D. Paré, "Stimulation of Medial Prefrontal Cortex Decreases the Responsiveness of Central Amygdala Output Neurons," *The Journal of Neuroscience*, vol. 23, no. 25, pp. 8800–8807, 2003.

[423] K. N. Ochsner, S. A. Bunge, J. J. Gross, and J. D. Gabrieli, "Rethinking Feelings: An fMRI Study of the Cognitive Regulation of Emotion," *Journal of Cognitive Neuroscience*, vol. 14, no. 8, pp. 1215–1229, 2002.

PUBLICATIONS

Journal papers (related to thesis)

[1] S. Kanoga and Y. Mitsukura, "Eye-blink Artifact Rejection Using 2-step Non-negative Matrix Factorization for Single-channel Electroencephalographic Signals," *Journal of Signal Processing*, vol. 18, no. 5, pp. 251–257, September 2014.

[2] S. Kanoga and Y. Mitsukura, "Proposing an Eye Blink Artifact Rejection Technique from Single-channel EEG Signals Using Positive Semi-definite Tensor Factorization," *IEEJ Transactions on Electronics, Information and Systems*, vol. 135, no. 7, pp. 848–855, July 2015.

[3] S. Kanoga, M Nakanishi, and Y. Mitsukura,"Assessing the Effects of Voluntary and Involuntary Eyeblinks in Independent Components of Electroencephalogram," *Neurocomputing*, vol. 193, pp. 20–32, June 2016.

[4] S. Kanoga and Y. Mitsukura, "A Study of Pattern Recognition in Children Using Single-channel Electroencephalogram for Specialized Electroencephalographic Devices," *IEEJ Transactions on Electronics, Information and Systems*, accepted.

International conference papers

[1] S. Kanoga and Y. Mitsukura, "Analysis of Relationship between Intention and Behavior Using EEG-EMG Coherence during Isotonic Exercise," *2013 RISP International Workshop on Nonlinear Circuits, Communications and Signal Processing*, pp. 604–607, Hawaii (USA), March 2013.

[2] S. Kanoga and Y. Mitsukura, "Construction of the Interest Prediction Models for Nursery School Child Using a Single-channel Electroencephalograph," *2013 IEEE Conference on Systems, Process and Control*, pp. 129–134, Kuala Lumpur (Malaysia), December 2013.

[3] A. Negishi, S. Kanoga, and Y. Mitsukura, "EEG Difference Extraction with Pure Tone Stimulation of Different Frequencies," *2014 RISP International Workshop on Nonlinear Circuits, Communications and Signal Processing*, pp. 673–676, Hawaii (USA), March 2014.

[4] S. Kanoga and Y. Mitsukura, "GA-SVM for Pattern Recognition of Single-channel Electroencephalographic Recordings from Nursery School Child under Resting and

Feeling Interest States," *2014 RISP International Workshop on Nonlinear Circuits, Communications and Signal Processing*, pp. 665–668, Hawaii (USA), March 2014.

[5] S. Kanoga and Y. Mitsukura, "Proposed Blink Artifacts Rejection Method Mixing with Electroencephalographic Recordings Using Single-channel Electroencephalographic Recordings and Non-negative Matrix Factorization," *The 13th International Workshop on Advanced Motion Control*, pp. 536–541, Kanagawa (Japan), March 2014.

[6] S. Kanoga and Y. Mitsukura, "An Eye Blinking Artifact Rejection Method Using Single-channel Electroencephalographic Signals and 2 Step Non-negative Matrix Factorization," *5th International Symposium on Advanced Control of Industrial Processes*, pp. 120–125, Hiroshima (Japan), May 2014.

[7] S. Kanoga and Y. Mitsukura, "A Time-domain Eye Blink Artifacts Rejection Technique for Single-channel EEG Signals," *2014 International Symposium on Nonlinear Theory and Its Applications*, pp. 124–127, Luzern (Switzerland), September 2014.

[8] S. Kanoga and Y. Mitsukura, "Classification of EEG Signals from Nursery School Children in an Immersion or not in the Feeling for Portable Applications," *2015 RISP International Workshop on Nonlinear Circuits, Communications and Signal Processing*, pp. 555–558, Kuala Lumpur (Malaysia), March 2015.

[9] S. Kanoga and Y. Mitsukura, "Removal of Eye Blink Artifact from Single-channel EEG Signal Using Positive Semi-definite Tensor Factorization," *The 1st IEEJ International Workshop on Sensing, Actuation, and Motion Control*, pp. 1–6, Nagoya (Japan), March 2015.

[10] S. Kanoga and Y. Mitsukura, "ICA-based Positive Semidefinite Matrix Templates for Eye-Blink Artifact Removal from EEG with Single-electrode," *The 10th Asian Control Conference 2015*, pp. 1585–1590, Kota Kinabalu (Malaysia), May 2015.

[11] S. Kanoga and Y. Mitsukura, "Eye Blink Artifact Rejection in Single-channel Electroencephalographic Signals by Complete Ensemble Empirical Mode Decomposition and Independent Component Analysis," *37th Annual International Conference of the IEEE Engineering in Medicine and Biology Society*, pp. 121–124, Milano (Italy), August 2015.

[12] N. Toyoshima, S. Kanoga, and Y. Mitsukura, "Construction of Predictive Models for Bicycle Riding Comfort Evaluation Using Electromyogram and Electroencephalogram," *2016 IEEE 12th International Colloquium on Signal Processing and Its Applications*, pp. 100–104, Melaka (Malaysia), March 2016.

Domestic conference papers and reports

[1] S. Kanoga, T. Fuji, and Y. Mitsukura, "Correlation of EMG and EEG Acquisition during Kinematics," *IEEJ 2012 Annual Conference of Electronics, Information and Systems Society*, pp. 1035–1039, Aomori (Japan), September 2012.

[2] S. Kanoga, T. Fuji, and Y. Mitsukura, "Analysis of Degree of Absorption Using Biological Signals," *Workshop on Institute of Systems, Control and Information Engineers*, pp.1265–1269, Kyoto (Japan), November 2012.

[3] S. Kanoga and Y. Mitsukura, "Relationship Analysis of Intention and Movement Using EEG-EMG Coherence during Isotonic Exercise," *IEEJ Technical Meeting on Perception Information*, pp. 1–6, Tokyo (Japan), April 2013.

[4] S. Kanoga and Y. Mitsukura, "EEG Analysis for Detection of Nursery School Children's Interest Using Evolutionary PLS Regression," *IEEJ 2013 Annual Conference of Electronics, Information and Systems Society*, pp. 938–943, Hokkaido (Japan), September 2013.

[5] S. Kanoga and Y. Mitsukura, "A Study of State Estimation for Nursery School Children's Interest Using Single Channel EEG," *The 23th Fuzzy, Artificial Intelligence, Neural Networks and Computational Intelligence*, pp. 243–248, Fukuoka (Japan), September 2013.

[6] Y. Kimura, S. Kanoga, K. Tamura, H. Kataoka, Y. Mitsukura, and Y. Aoki, "表情及び姿勢変動に着目したTV視聴者の視聴状態推定 (This title is only written in Japanese)," *Dynamic Image Processing for Real Application Workshop 2015*, pp. 200–205, Kumamoto (Japan), March 2014.

[7] S. Kanoga and Y. Mitsukura, "An Application of Non-negative Matrix Factorization Based on Hybrid Learning Method for Single-channel Electroencephalographic Signals Mixed with Eye-blink Artifacts," *IEEJ Technical Meeting on Perception Information*, pp. 63–68, Aichi (Japan), March 2014.

[8] S. Kanoga and Y. Mitsukura, "A Model for Predicting Child's Emotions in Playing Card Game Using Single-channel Electroencephalographic Signals," *IEEJ Technical Meeting on Perception Information*, pp. 117–120, Kanagawa (Japan), September 2014.

[9] S. Kanoga, Y. Mitsukura, "Proposing a Time Domain Eye Blink Artifacts Rejection Technique with Positive Semi-definite Tensor Factorization," *IEEJ 2014 Annual Conference of Electronics, Information and Systems Society*, pp. 936–941, Shimane (Japan), September 2014.

[10] S. Kanoga, N. Toyoshima, and Y. Mitsukura, "Comparison of Interest Prediction Medels of Children Using Time-frequency Analysis," *The 20th Intelligent Mechatronics Workshop*, pp. 160–163, Tokyo (Japan), July 2015.

Awards

[1] Best presenter, *2013 IEEE Conference on Systems, Process and Control*, December 2013.

[2] IEEJ excellent presenation award, *The Institute of Electrical Engineers of Japan*, September 2014.

[3] Repayment exemption for students who have achieved an especially excellent record, *Japan Student Services Organization*, March 2015.